



Department of Applied Science and Technology
(DISAT)

POLITECNICO DI TORINO

Conductive photopolymers: In situ synthesis of metal nanoparticles

A thesis submitted in partial fulfillment of the requirement of degree of
Doctorate in Materials Science and Technology

by

Rabia Nazar

XXVII Cycle (2012- 2015)

Supervisor

Prof. Roberta Bongiovanni

Co-Supervisor

Prof. Marco Sangermano

ABSTRACT

A prologue to the field of noble metal nanoparticles is presented with a brief commentary on the basic synthesis techniques to manufacture these metal nanoparticles and to exploit the full use of their unique properties. In recent years scientific interest in embedding the metal nanoparticles in a host polymer has been increased significantly. A great advancement in the field of conductive polymers by embedding metal nanoparticles in them has been witnessed because they are likely to be an alternative to the conventional conductors. There are different available techniques in use these days to prepare these polymer-metal nanocomposites. However, photopolymerization is gaining a lot more attention mainly because of some extra ordinary advantages. This is one of the most effective ways to convert liquid monomers into polymer materials upon irradiation of UV light. Furthermore, embedding of nanoscopic metal particles in polymer matrices is with the help of free radical photopolymerization technique is one of the easiest and fastest ways. Photocured polymeric films are a promising candidate for the realization of flexible electronics, due to their easy processability, low cost, and availability. The objective of this thesis is to synthesize and stabilize two different kinds of noble metal nanoparticles i.e. silver and copper nanoparticles in an acrylic resin. In order to carry out this research, the quality of obtained nanoparticles was examined with respect to the nature of substrates, irradiation time, and monomer/salt ratio.

In the first half of this research, electrically conductive UV-cured films have been prepared by irradiating an acrylic difunctional monomer in the presence of silver nitrate, pyrrole, and a photoinitiator. Homogeneously dispersed silver nanoparticles (size range 50–80nm) embedded by polypyrrole formed throughout the acrylic matrix. Interestingly, the electrical conductivity of the acrylic films increased a hundred times after the formation of the Ag polypyrrole nanoparticles. Evaluation of the irradiation process was conducted by UV–Vis spectroscopy using model systems where the acrylic monomer was substituted by a solvent. It has been shown that as a function of composition and irradiation time there is a simultaneous reduction of

silver nitrate and pyrrole polymerization forming silver nanoparticles covered by the conductive polymer. The effect of PVP concentration on the different properties of silver nanoparticles was investigated. It was ascertained that there is a significant influence on the morphology of silver nanoparticles.

The second half of this research is to synthesize copper nanoparticles. Synthesis of the less stable copper nanoparticles is more difficult and challenging because copper nanoparticles are easily oxidized. Different stabilizing agents like poly(N-vinylpyrrolidone) (PVP), pyrrole, sodium L-ascorbate are used as capping agents to prevent the aggregation and to stabilize the obtained copper nanoparticles against oxidation. The copper nanoparticles obtained were characterized by UV-vis absorption spectra, dynamic light scattering, scanning transmission electron microscopy and FESEM. It has been observed that the particle size and particle size distribution influenced significantly in the presence of PVP. However, there is no substantial effect observed by adding pyrrole as a stabilizer.

Acknowledgements

First and foremost I owe gratitude and praise to ALLAH for endowing me with health, patience, knowledge and all the means to complete my work. My words cannot express my love and gratitude for my father. This achievement in my life is undoubtedly because of his prayers, support and encouragement

I would like to express my sincere appreciation to my supervisor Prof. Roberta Bongiovanni and, for her constant support and guidance throughout this tenure. I have learned so much from her in so many ways, especially how to be a free thinker and an independent scientist. I will always remember the kind nature, care and love she showed to me in all difficult times I have been through in. I would also like to acknowledge Prof. Marco Sangermano for his support and guidance. I truly appreciate his help and constant support. I would also like to thank Dr. Silvia ronchetto for taking the time out of her busy schedule to teach me the use of XRD analysis. I would like to extend my gratitude to the faculty and staff of the DISAT Department during my studies. I enjoyed working with all of them and learned from all of them a lot. I would like to express my special thanks to my senior fellow Dr. Ignazio roppolo. I would also like to extend my deepest thanks and good wishes to Dr. Giovanna Colucci, she is the one who guided me for the very first time in the lab. And because of her guidance and support I became familiar with the lab and the lab equipments in a very short time.

There are also a lot of people without their help, the work presented in thesis would not have been possible Thanks to Alessandra, Monica, Sophie, Florence, Atif, Naguib, Federico, Erika, Elena,

Apart from all my labmates, I would like to say my special thanks to my office mate and my friend Monica. She has always been very kind and friendly with me. The last few months of my stay in Italy, will always be very special and memorable for me because of her.

I would like to extend my gratitude to the faculty and staff of the DISAT Department during my graduate studies.

I would like to express my sincere gratitude to the Higher education commission (HEC) of Pakistan for providing me generously the financial support for carrying out my research

A special acknowledgement to University of Engineering and technology Lahore, (UET) for granting me leave to pursue my higher studies.

Last, but not least, I wish to express my sincere thanks to my father, who has loved me unconditionally. Through every hardship or accomplishment, he has been behind me every step of the way and this work is a direct result of that. Very special thanks to my sisters and my brother, for being very patient and understanding. Their love and continuous support was there with me throughout my life especially these three years of my life. I know that you all have made a lot of sacrifices to help me achieve my goals and I am looking forward to less frantic schedules and spending more time with you. I feel myself really lucky to have great friends during this time, My special thanks go to all my friends: Iffat, Saima, Hira, Veena, Asia, Sanam, Mishay, who made my time really enjoyable.

Finally, I am deply grateful to my best friend and my sister "Iffat". I have been extremely lucky to have her as my friend. I shared each and every moment of my life with her. Besides the fact, that I was far away from my family, her love and care was constantly with me.

Dedicated to the memory of my

Beloved Mother

Who passed away

on june 2013

May Allah rest her soul in eternal peace

To Allah we belong and to HIM we have to return

She sacrificed her life best moments for me

*She was always waiting for this day and wishing to live and
to share this moment with me*

But, Allah did what He ordained to do.

And I am sure she is smiling and looking at me from Heavens

Table of contents

ABSTRACT	i
Acknowledgements.....	i
List of Figures.....	i
List of Tables	i
List of Acronyms.....	i
List of Symbols.....	i
CHAPTER 1	2
1.1 Prologue.....	3
1.2 The beauty of Photochemistry.....	4
1.3 Aims and Scope.....	4
1.4 Organization of thesis	5
CHAPTER 2	7
2.1 Introduction	8
2.2 A brief History.....	9
2.3 Importance of Nanotechnology	10
2.4 Synthesis Techniques.....	14
2.4.1 Photochemical strategies	16
2.5 Polymer-metal nanocomposite synthesis.....	24

2.5.1	Nanoparticles precursors in polymer	25
2.5.2	Nanoparticles precursors in polymer precursor	27
2.5.3	Nanoparticles preforms in polymer	28
2.5.4	Nanoparticles preforms in polymer precursor	29
2.6	Stabilization of metal nanoparticles	31
2.7	Properties & Applications.....	36
CHAPTER 3.....	42
3.1	Introduction.....	43
3.2	Photochemical synthesis of Ag NPs.....	43
3.3	Photochemical synthesis of Cu NPs.....	49
3.4	Polymer-metal nanocomposites.....	55
3.4.1	Polymer nanocomposites embedded by Ag particles.....	55
3.4.2	Polymer nanocomposites embedded by Cu NPs	62
CHAPTER 4.....	65
4.1	Objective.....	66
4.2	Experimental Setup	66
4.3	Materials and Synthesis of Silver nanoparticles	67
4.3.1	Materials.....	67
4.3.2	Synthesis of Ag NPs from ethanol solutions.....	67
4.3.3	Synthesis of polymeric composites embedding Ag NPs	68
4.4	Materials and synthesis of Copper nanoparticles	69
4.4.1	Materials.....	69
4.4.2	Synthesis of CuNPs from solution.....	69
4.4.3	Synthesis of polymeric composites embedding CuNPs.....	71
4.5	Characterization techniques	72

CHAPTER 5	76
5.1 Objective	77
5.2 Characterization of solutions containing silver salt: monitoring the reduction process with and without pyrrole	78
5.2.1 Optical characterization	78
5.2.2 XRD Analysis	85
5.2.3 DLS Analysis	87
5.2.4 TEM Analysis	90
5.3 Photopolymerization of acrylic oligomers in the presence of silver salt and pyrrole	91
5.3.1 FTIR Analysis	91
5.3.2 Optical characterization of UV-cured films	92
5.3.3 FE-SEM Analysis of UV-cured films	93
5.3.4 Electrical Characterization	95
5.3.5 TGA Analysis	97
5.4 Protection of Silver nanoparticles	98
5.4.1 Optical characterization of ethanol solution containing silver particles in the presence of PVP	99
5.4.2 DLS Analysis	103
5.4.3 SEM Analysis	105
5.4.4 XRD Analysis	107
5.4.5 FE-SEM Analysis	109
5.4.6 Optical Characterization of solution containing Cu salt	111
5.4.7 Stabilization of Cu-NPs against aggregation	121
5.4.8 Stabilization of Cu-NPs against oxidation	128
5.4.9 DLS Analysis	133
5.5 Photopolymerization of acrylic oligomers in the presence of CuCl₂ and diethanol amine	134
5.5.1 DSC Analysis	140

5.5.2	Optical characterization of UV-cured films embedding Cu particles.....	141
5.5.3	Stabilization of UV-cross linked films against oxidation	145
CHAPTER 6	152
6.1	Conclusions	152
6.2	Future work	154

List of Figures

Figure 1 Lycurgus Cup (British Museum AD 4th century) ²⁶	10
Figure 2 Bibliographic analysis based on the search of “nanoparticles” in Scifinder Scholar. Blue represents scientific publications (e.g. books, articles, reviews) and green represents patents. ²⁵	11
Figure 3 Sizes, shapes and composition of metal nanoparticles can be systematically varied to produce materials with distinct light-scattering properties ²⁷ .	13
Figure 4 Evolution of Nanotechnology with the span of time (years).	14
Figure 5 Schematic view of Top-Down and Bottom-up technique	15
Figure 6 Schematic system of photo-induced synthesis of metal nanoparticles ⁶³	17
Figure 7 Photochemical strategies for the generation of ketyl radicals from organic precursors. The asterisk (*) denotes the excited state of a molecule, frequently a triplet state in the examples used in this contribution, while “hv” indicates exposure to light ⁶⁷ .	19
Figure 8 Photolysis to produce benzoyl ketyl radical ⁷⁰	20
Figure 9 Photoreduction of Benzophenone followed by electron transfer to the metal ion M^{n+} ⁶⁷	21
Figure 10 Schematic illustration of photopolymerization process	22
Figure 11 Mechanism of photopolymerization	23
Figure 12 Schematic presentation of the preparation methods of polymer-metal nanocomposites	25
Figure 13 Schematic description of grafting-to and grafting-from approaches ⁹⁰	29
Figure 14 Schematic presentation of steric stabilization mechanism	33
Figure 15 Structure of the repeat unit of PVP	34
Figure 16 Schematic illustration of Cu-Ag core shell NP ¹⁸³	35
Figure 17 Effect of optical field on the electron cloud in a spherical metal nanoparticle ¹⁹¹	37
Figure 18 Example of LSPR modulation through different NP compositions. The LSPR absorption band of gold/silver alloy NPs increases to longer wavelengths with increasing amounts of gold.	38

Figure 19 Growth of absorbance band by UV-irradiating silver trifluoroacetate in the presence of cyclohexylamine and hexadecylamine ²³¹	46
Figure 20 Photoreduction of silver bromide in the presence of ascorbic acid ²³²	47
Figure 21 UV-vis spectra of silver nanoparticles by changing molar ratios of AgBr/ascorbic acid ²³²	47
Figure 22 UV-vis spectra of stabilized silver nanoparticles after 48 hours and after 48 days ²³²	48
Figure 23 TEM image of silver/polypyrrole core shell nanoparticles ²²	49
Figure 24 Change in the UV-vis absorption spectra of $(\text{Cu}(\text{ClO}_4)_2)$ in an ethanol solution irradiated for 60 mins ²³⁰	52
Figure 25 Photolysis of photoinitiator under UV-irradiation ⁵⁰	53
Figure (26-a) UV-vis spectra of copper nanoparticles in the presence of 5×10^{-3} M CuSO_4 , 2×10^{-1} N 2-propanol, in different concentrations of PVA, (a) 0.79, (b) 1.5, (c) 2.3, (d) 3.4×10^{-2} M. (23-b) Histogram of Cu particles in the presence of 5×10^{-3} M CuSO_4 , 2×10^{-1} N 2-propanol, 3.4×10^{-2} M PVA ^{211-a}	54
Figure 27 Dielectric properties of Al/epoxy and Al/Ag-epoxy composites with different Al filler loading ⁹⁵	57
Figure 28 Evolution of dielectric constant, $\tan\delta$ and AC conductivity with nanoparticle content at room temperature and several frequencies ranging from 1kHz to 1 MHz ²⁷⁵	58
Figure 29 Conductivities of different materials (conductors, semi-conductors, insulators and superconductors) with comparison with the conducting polymers. ^{96-c}	60
Figure 30 Conduction mechanism in Polypyrrole ^{97-b}	61
Figure 31 Direct pattern formation on the polyester film by UV-irradiation (b) Microscopic image of the copper pattern ⁵⁰	63
Figure 32 XRD pattern of the copper pattern on the polyester films ⁵⁰	63
Figure 33 Block Diagram of the UV-curing process	68
Figure 34 Color change observed after a) 1 min, b) 3 min, c) 5 min d) 10min of UV-irradiation. [$10\% \text{AgNO}_3 + 2\% \text{Py} + 0.002\% \text{PI}$].	79
Figure 35 UV-Vis spectra of the ethanol solution containing 5 wt% (a), 10 wt% (b) and 20 wt% (c) of AgNO_3 . All the solutions contained 2 wt% of pyrrole and the radical photoinitiator 0.002%PI.	81

Figure 36. UV-vis spectra of 2%Py and 0.002%PI in Ethanol at different irradiation times.	82
Figure37 UV-Vis spectra of the ethanol solution containing 5 wt% (a), 10 wt% (b) and 20 wt% (c) of AgNO ₃ and the radical photoinitiator.	84
Figure 38 XRD analyses of the ethanol solution containing 5 wt% of AgNO ₃ and 2 wt% of pyrrole, after 10 minutes of UV-irradiation	86
Figure 39 DLS-images of diameter distribution by intensity of nanosized silver colloids (a) with 5wt% , 10wt%, 20wt%AgNO ₃ w/o (Py)pyrrole (b) with 5wt%,10wt%,20wt%AgNO ₃ with 2% (Py) after 10mins UV-irradiation.	89
Figure 40 TEM analysis of the ethanol solution containing 5 wt% of AgNO ₃ and 2 wt% of pyrrole, after 10 minutes of UV-irradiation.	90
Figure 41 Real time FTIR acrylic group conversion as a function of irradiation time for the PEGDA formulations containing increasing amount of AgNO ₃ in the range between 5 -20wt%.	92
Figure 42 UV-Vis absorption of the crosslinked film containing (5-20 wt%) of AgNO ₃ and 2 wt% of pyrrole are reported.	93
Figure43 FESEM image of the fracture surface of the crosslinked films a) 10wt% AgNO ₃ b) 20%AgNO ₃	94
Figure44 Electrical conductivity of the UV-cured films. (a) with the increase in AgNO ₃ content (b) with and without the presence of Py.	96
Figure 45 Thermograms of Samples: Sample-a (PEGDA+2wt%PI), Sample-b(PEGDA+10wt%AgNO ₃ +2wt%PI), Sample-c(PEGDA+20wt%AgNO ₃ +2wt%PI)	98
Figure 46 UV-Vis spectra of the ethanol solution containing 10 wt% of AgNO ₃ +2 wt% of pyrrole and the radical photoinitiator 0.002%PI. (12a) 1%PVP (b)2%PVP and (c) 4%PVP (d) 6%PVP (e) 8%PVP (f) 10% PVP	102
Figure 47 DLS-images of diameter distribution by intensity of nanosized silver colloids with different PVP concentrations after 10mins UV-irradiation.	104
Figure 48 SEM analysis of the ethanol solution containing 10 wt% of AgNO ₃ and 2 wt% of pyrrole, (a) with 1%PVP (b) with 2%PVP after 10 minutes of UV-irradiation	106
Figure 49 XRD Analysis of ethanol solution containing 10wt%AgNO ₃ , 2wt%pyrrole, 0.002%PI and (a) 6wt% PVP (b)4wt%PVP UV-irradiated for 10 mins.	108

Figure 50 FESEM image of the fracture surface of the crosslinked films (a) 0wt% PVP	111
Figure 51 Color change observation of CuCl ₂ -ethanol solution a) before UV, (b) 1mins, (c)3mins, (d)5mins, (e)after 10mins of UV-irradiation.	113
Figure 52 UV-vis spectra of CuCl ₂ ethanol solution under different irradiation times.	114
Figure 53 Color change observation: a) CuCl ₂ -ethanolsolution, b) CuCl ₂ -amine coordination complex, c) CuCl ₂ -amine coordination complex after 10 mins UV-irradiation.	116
Figure 54 UV-visible spectra of copper chloride-amine coordination complex under UV-irradiation at different times.	118
Figure 55 Color change observation: a) CuSO ₄ -amine coordination complex bf UV, b) CuSO ₄ -amine coordination complex after 10 mins UV-irradiation.	120
Figure 56 UV-visible spectra of CuSO ₄ -amine coordination complex under UV-irradiation at different times.	121
Figure 57 UV-visible spectra of CuCl ₂ -amine coordination complex in the presence of 0.2%(w/v) pyrrole under UV-irradiation at different times of irradiation.	123
Figure 58 DLS images of diameter distribution by intensity of copper colloids (a) CuCl ₂ -amine coordination complex (b) CuCl ₂ -amine coordination complex in the presence of 0.2%(w/v) pyrrole	125
Figure 59 UV-visible spectra of CuCl ₂ -amine coordination complex in the presence of 0.5%(w/v) PVP under UV-irradiation at different times of irradiation	126
Figure 60 DLS images of diameter distribution by intensity of copper colloids (a) CuCl ₂ -amine coordination complex (c)CuCl ₂ -amine coordination complex in the presence of 0.5%(w/v) PVP	127
Figure 61 Color change observed after different times of UV-irradiation.	130
Figure 62 UV-vis spectra of CuCl ₂ -diethanol amine coordination complex in the presence of 0.02MSodium L-ascorbate and 0.5%(w/v) PVP.	131
Figure 63 DLS images of diameter distribution by intensity of copper colloids (a) CuCl ₂ -amine coordination complex (d) CuCl ₂ -amine coordination complex in the presence of 0.02M Sodium L-ascorbate and 0.5%(w/v) PVP	132
Figure 64 Particle size distribution from DLS (a) CuCl ₂ -amine coordination complex (b) CuCl ₂ -amine coordination complex in presence of 0.2wt%Py (c) CuCl ₂ -amine	

coordination complex in presence of 0.5wt%PVP.(d). CuCl ₂ -amine coordination complex in presence of 0.5wt%PVP in the presence of 0.4% Na-ascorbate	134
Figure 65 UV-vis absorption spectra of CuCl ₂ -amine complex before UV-irradiation	136
Figure 66 DSC curves of samples without CuCl ₂ and the samples containing 1wt% and 5wt% CuCl ₂ .	141
Figure 67 Color change observed in a freshly prepared film containing a) 0.5wt%CuCl ₂ , b) 1wt%CuCl ₂	142
Figure 68 UV-Vis absorption spectra of the crosslinked film freshly prepared containing 0.5wt% and 1wt%CuCl ₂ , 5wt%PI, 2wt%DEA	143
Figure 69 Color change observed in a film after 2 hrs containing a) 1wt%CuCl ₂ , b) 0.5wt%CuCl ₂	144
Figure 70 UV-Vis absorption spectra of the crosslinked film containing 1%CuCl ₂ and 0.5wt% CuCl ₂ , 5%PI, 2%DEA after 2 hrs in an open atmosphere	145
Figure 71 Change in color observed (a) CuCl ₂ -amine coordination complex in PEGDA, (b) in the presence of 0.2%(w/w) pyrrole, (c) Freshly prepared crosslinked film in the presence of 0.2%(w/w) pyrrole	146
Figure 72 UV-vis spectra of the cross linked films containing 1%CuCl ₂ , 5%PI, 2%DEA in the presence of 0.2%pyrrole after regular intervals of time	147
Figure 73 Change in color observed (a) CuCl ₂ -amine coordination complex in PEGDA, (b) in the presence of 0.5%(w/w) PVP, (c) Crosslinked film in the presence of 0.5%(w/w) PVP,	149
Figure 74. UV-vis spectra of the cross linked films containing 1%CuCl ₂ , 5%PI, 2%DEA in the presence of 0.5% PVP after regular intervals of time	149

List of Tables

Table 2.1 Dependence of No. of particles per given mass on its diameter	12
Table 3.1 Dependence on Cu size particles with the PVP concentration	50
Table 5.1 Simple peak indexing	87
Table 5.2 Electrical Characteristics of UV-cured films	97
Table 5.3 Simple peak indexing	108
Table 5.4 List of photoinitiators with their UV-vis absorption peaks	137
Table 5.5 Amounts of photoinitiators used	138
Table 5.6 Amounts of photoinitiators used in wt%	139

List of Acronyms

UV-vis absorption	Ultra violet vis absorption
TEM	Transmission electron microscopy
DLS	Dynamic Light Scattering
XRD	X-Ray Diffraction
FTIR	Fourier Transform Infrared Spectroscopy
TGA	Thermogravimetric Analysis
DSC	Differential Scanning Calorimetry
FE-SEM	Field Emission Scanning Electron Microscopy
PI	photoinitiator
NPs	nanoparticles
MNPs	Metal nanopaticles
Ag	Silver
AgNO₃	Silver nitrate
Cu	Copper
CuSO₄	Copper sulphate
CuCl₂	Copper chloride
PVP	Poly vinyl pyrrolidone
Ppy	Polypyrrole
Py	Pyrrole

EtOH	Ethanol
Na-Asc	Sodium ascorbate
Ag-NPs	Silver nanoparticles
Cu-NPs	Copper nanoparticles
DEA	Diethanol amine
BP	Benzophenone
PEGDA	Poly (ethylene glycol) diacrylate

List of Symbols

Q_{ext} =total extinction efficiency for a homogenous sphere

Q_{sca} =total scattering efficiency for a homogenous sphere

ϵ =refractive index of the metal

ϵ_m =refractive index of the surrounding medium

m =ratio of the refractive index of the sphere and the surrounding medium ($m=\epsilon/\epsilon_m$)

R =radius of the sphere of the particles

λ =wavelength of light

x =size parameter ($x = 2\pi n m R/\lambda$),

ψ_n and ξ_n =Riccati-Bessel functions

V =volume of the nanoparticle

ϵ_m =dielectric constant of the surrounding medium

λ =wavelength of light and the dielectric constant of the metal is expressed in the complex form as a function of the wavelength of light, where $\epsilon(\lambda) = \epsilon_1(\lambda) + i\epsilon_2(\lambda)$.

D_f = *Translational diffusion coefficient*

k_B = Boltzmann constant

T = temperature of the suspension

η = viscosity of the surrounding media

R_H = Hydrodynamic radius

nm = nanometer

μm = micrometer

θ = diffraction angle

V = Voltage

% = percentage

Wt%= weight percentage

ρ =resistivity

Chapter 1

Introduction

1.1 Prologue

Since the last two decades, the world has been fascinated by extraordinary features of metals. And this credit goes to a lot of scientists who actually dig deep insights in this particular field i.e. Nanotechnology. Nanotechnology deals with processes that take place on the nanometer scale, that is, from approximately 1 to 100 nm.¹ And because of this special dimensions metal nanoparticles exhibit some special properties which cannot be exhibited by the same molecules in their bulk form.² The reason behind this fact is: with the reduction in the metal size, the surface-volume ratio increases and due to which one can see an incredible change in the final properties of the metal particles.³ As particles size decrease, the number of surface atoms becomes equal to or even exceeds the number of inner-core atoms and surface of the bulk material is negligibly small in comparison to the total volume. From the time of their discovery till this date there has been tremendous efforts being made to synthesize these metals and to tune their properties in a desired way. Metal nanoparticles specially, gold, silver and copper are the main focus of research because of their unique optical properties.

Generally there are two types of synthesis techniques to synthesize metal nanoparticles i.e. Bottom-up and Top-down to synthesize these metal nanoparticles (MNPs).⁴ Having their own pros and cons, both techniques are in use depending upon the application areas of the resulting MNPs. In this research work, we mainly deal with the bottom up technique and more specifically to the photochemical reduction of metal nanoparticles with the help of UV-light; details are given in Section 2.4 of Chapter 2. In-situ radical photoinduced polymerization was carried out to generate metal nanoparticles embedded in polymer films. This process is chosen in this work because of different reasons, a few of them are: this process is a very quick, and there is no need to use solvents, so it is a clean process, can be carried out at room temperature.

1.2 The beauty of Photochemistry

Giacomo Ciamician at the beginning of the 20th century laid the foundations for a large part of present day-used key paths in organic synthesis based on the work done in the last decades of 19th century ⁵. Addressing the French Chemical Society on June 8, 1908^{5-a} he made the following historic remarks,

'It has often been a reproach to the great successes of modern organic chemistry that victory has been obtained with too great a show of strength. Indeed, one has to admit that such an objection is not deprived of some ground. Using aggressive reagents and high temperatures is almost always unavoidable when carrying out an organic synthesis in the laboratory. Deploying energy would, on the other hand, not be so frustrating for modern organic chemistry, were it not that the living world, in particular plants, gives us the marvelous example of great results obtained, at least from what appears, by using minimal means.'

1.3 Aims and Scope

The aims to carry out prospective research can be divided into two major goals:

1. The synthesis and study of colloidal silver and copper metal particles in an ethanol solution via one step photochemical reduction method.
 - The effect of time of irradiation on the kinetics of the reaction will be carried out.
 - After confirming the photochemical reduction of both the metal particles in solution form, the next step will be to achieve their stability.
 - In contrast to silver particles, the synthesis of copper metal particles is much more challenging. The surface of these particles is extremely reactive, when exposed to air, surface oxidation occurs immediately.
 - Silver particles are stable in air against oxidation, while the problem is to achieve stability against aggregation. To serve the purpose of

- stabilization against aggregation, effect of the addition of polymer capping agent i.e. PVP will be explored in the case of Ag particles
 - Copper particles are prone towards oxidation and aggregation. There is a need to protect them against oxidation as well as against aggregation. We will determine the effect of different stabilizers on the stability of obtained Cu particles.
2. The next step will be to in-situ photo reduce silver and copper metal particles along with the acrylic resin crosslinking with the help of photochemical reduction technique.
- The main goal in embedding Ag and Cu nanoparticles in a polymer matrix is to develop a simple yet efficient method to develop conductive polymer composites.
 - In case of silver particles embedded in polymeric films, addition of conjugated conductive monomer (pyrrole) on the reduction mechanism of silver salt and on the crosslinking reaction of the polymer will be studied.
 - The effect of the addition of different concentrations of silver salt and addition of pyrrole on the particle size and conductivity behavior of the obtained UV-crosslinked films will be studied.
 - With addition to conducting monomer, the effect on the particle size of the Ag particles with the addition of polymeric capping agent i.e. PVP will also be checked.
 - On the other hand, we will try to optimize the dispersion and stabilization of copper particles embedded in a polymer matrix to stabilize against oxidation. And to achieve a conductive behavior.

1.4 Organization of thesis

Chapter 2 provides a basic and short historical overview and the importance of the field nanotechnology. Different techniques which can be employed to synthesize nanoparticles are given. However, a sound and contingent discussion about the

photochemical reduction process and the role of different photoinitiators is also presented.

Some work related to stabilization of the metal NPs and to avoid their aggregation is discussed. Afterwards, different techniques (*in-situ* and *ex-situ*) to prepare polymer-metal nanocomposites are discussed briefly. At the end of this chapter are stated different properties and applications of noble metal nanoparticles.

A comprehensive literature review of the work done in the field of the photochemical synthesis of silver and copper nanoparticles is discussed in Chapter 3. The work done by various scientists to photosynthesize silver and copper nanoparticles in an ethanol solution and in a polymeric resin is briefly discussed. And a sound foundation is developed for the work done in this thesis.

Chapter 4 devotes to the experimental setup and materials needed to prepare silver and copper nanoparticles both in a solvent as well as in the polymer matrix. Materials and synthesis technique for silver NPs and for Cu NPs are given separately. Also, the details about the setup required for the stabilization to achieve for these MNPs is also given. After that, details of the equipments used for characterization of obtained metal nanoparticles in solvent and in polymer matrix are stated at the end of this chapter.

The kinetics of the reaction is studied with the help of UV-vis spectra. The morphology and structure of the obtained metal nanoparticles are characterized with the help of, DLS, XRD, TEM, FESEM, while the thermal properties are taken under consideration by employing TGA and DSC analysis. The electrical conductivity of the polymer matrix containing silver particles is also found out. Results of all the experiments done are presented in Chap. 5.

In the last Chapter, brief conclusion and remarks of the work done is stated. Also the future perspectives are listed down.

A comprehensive glossary is given at the beginning of this document, containing a list of all important symbols, acronyms, figures and tables. The reference cited in this work are given at the end of this thesis.

Chapter 2

Literature Survey

2.1 Introduction

Electrically conductive polymer composites fabricated by employing an insulating polymer and conductive filler is one of the most important discovery of the 20th century.⁶

Nanomaterials can be defined in principle materials of having at least one dimension within a nanometer range, i.e. in a range between 1nm to several hundred nanometers⁷. The mounting interest in the study of metal nanoparticles is attributed mainly to the potential technological applications that differ a lot from their own bulk properties⁸⁻¹⁹. A lot of research is being carried out from the last two decades because of the potential advantages like ease of fabrication, low cost and proficient stability offered by these nanomaterials.²⁰ Esumi *et al.*²¹ stated that nano particles own remarkable chemical and physical properties as compared to bulk metals because of their high surface area to volume ratio and size dependant properties. Metal nanoparticles, particularly silver, gold and copper have been the focus of vigorous research from the last few decades because of the vast potential they possess to be employed in different application areas. They exhibit unique optical properties²², and may be employed in different fields like biomedical²³, electronic²⁴, and in catalytic materials.²⁵

In this chapter, we will briefly discuss the history and origination of the metal nanoparticles. The nano-objects in general are not new; the new thing is that the properties of these materials can be characterized easily on a very small scale, which not only helps in their handling but also replacing conventional materials in different applications. The discussion extends to the different photochemical methodologies to synthesis metal nanoparticles particularly noble metal nanoparticles. Metal nanoparticles embedded in a host polymer have gained significant interest in recent years. There are a variety of attempts available in literature carried out to disperse these metal nanoparticles in polymer matrix. Generally, two different approaches used to serve the purpose of fabricating polymer-metal nanocomposites i.e. *ex-situ* and *in-situ*. A brief overview of the work done in the past to fabricate polymer-metal

nanocomposites is given in the end of this chapter. The discussion on the use of these metal nanoparticles in different applications because of their interesting properties will conclude the discussion.

2.2 A brief History

From the ancient times gold nanoparticles (gold colloids) are in use to color glass (ruby glass) but there was no scientific understanding behind the use of it. Romans were using colloidal gold and silver to color glass of intense colors depending on the concentrations of metals being used. One of the earliest examples of the use of colloidal metal particles to make beautiful colored glass is the famous Lycurgus cup²⁶ of the 4th century (shown in Figure 1).

However, Michael Faraday²⁹ was the first person who scientifically investigated gold colloid formation in the middle of nineteenth century. He reduced a solution of HAuCl_4 with elemental phosphorus resulting in the formation of ruby-red gold sols. Barber *et al*²⁷⁻²⁸ investigated the reason for the color of these glasses with the help of transmission electron microscopy and explains the reason for this color, he explained in his findings that the color change is due to the interaction of visible light with surface electrons of the gold nanoparticles. As we know today, the color depends on size, shape and surrounding medium. Faraday's original gold solution contained sub-30 nm gold particles with a rather broad size distribution.²⁹



Figure 1 Lycurgus Cup (British Museum AD 4th century)²⁶

2.3 Importance of Nanotechnology

A lot of attention has been received by the nano sized materials during the last two decades. The fundamentals of nanotechnology rest on the fact that the properties of resulting substance change dramatically when the size is reduced to the nanometer range. Figure 2 shows the amount of publications in this field,²⁵ where it is shown a profound increase in the number of publications due to their widespread potential applications in different fields such as Medicine, Chemistry, Physics and so on. Moreover, not only scientific publications have been growing, but also a huge number of patents have been issued since the last decade. This attraction by scientific community is not only because of their special properties but also because of the great technological applications which they can offer. So, a new field has been stimulated in order to better understand and to make the best possible use of these nano scale materials, which is now known as Nanoscience. Another term for this field is also in use i.e. nanotechnology which relates to the ability of developing functional devices by exploiting the full use of these nanometer ranged materials for different technological

applications. This term nanotechnology was not always used so broadly. Norio Taniguchi was the first person who introduced this term “Nanotechnology” dates back in 1974.³⁰

The size dependant affects on the properties of these materials stems the interest in this field; as the radical property changes with the reduction in particle size from micro to nano scale is observed. An increase in the surface area to volume ratio gives an increase in the total surface area; which alters the physical and chemical properties of these materials. Changes in the electronic structure of these nanoparticles make it possible to change the associations of the entities forming the nanoparticles and presence of defects.

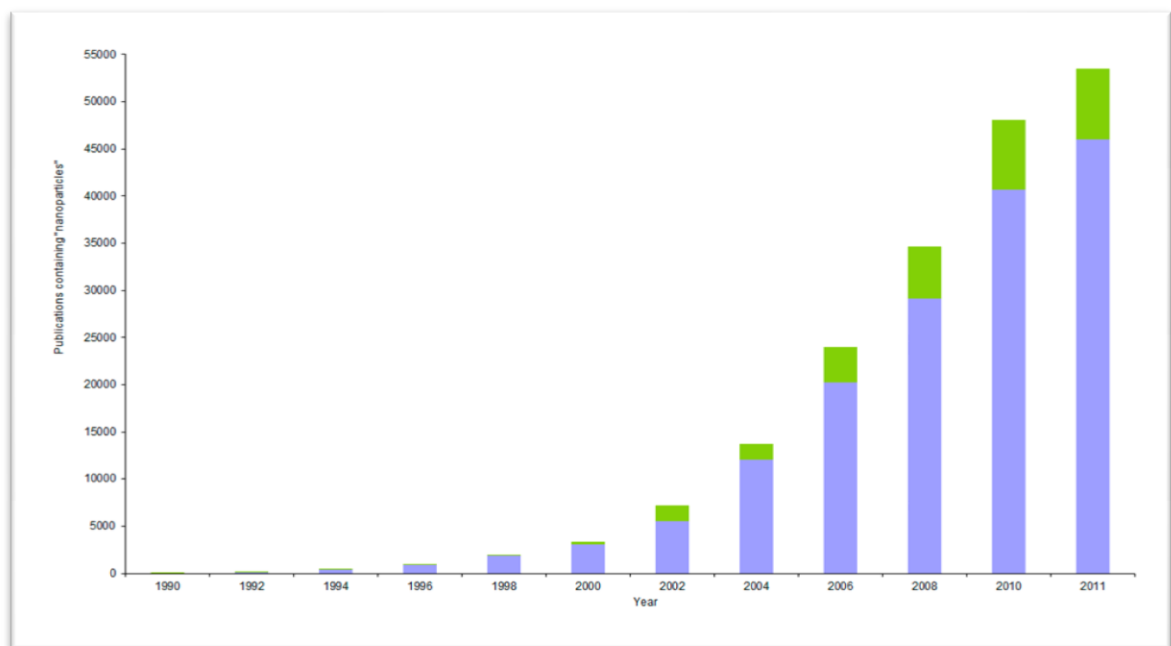


Figure 2 Bibliographic analysis based on the search of “nanoparticles” in Scifinder Scholar. Blue represents scientific publications (e.g. books, articles, reviews) and green represents patents.²⁵

Nanoparticles have lower melting point compared to their bulk materials because of their higher surface-volume ratio, due to which bonds between neighboring particles form at lower temperature³¹. In 2004, European commission (EC)^{31-b} reported in their study that when the particles' size get very small, there are more atoms present on the surface than in the inside of the particles, and those atoms on the surface may exhibit different properties than the atoms inside the particles.

Similarly, in 2006 Berger,³² demonstrated in his findings that the chemical reaction can take place on the surface of the particles as they possess a higher surface area, in contrast to the macro particles of the same material. Nass *et al.*³³ stated that a particle with a 10nm diameter has approximately 20% of its atoms forming the surface, whereas a particle of 1 nm diameter has 90% of atoms present on its surface. The dependence of the number of particles on its diameter is tremendous (shown in Table 2.1)³⁴. This is the reason that these nano materials differ fundamentally from the particles of same matter but larger in size. And numerous applications and benefits have been revealed till now and still a vigorous research is going on.

Table 2.1 Dependence of No. of particles per given mass on its diameter

Particle diameter (nm)	No. of particles (per cm ³)	Particle surface area (μm ³ /cm ³)
5	153,000,000	12,000
20	2,400,000	3,016
250	1,200	240
5,000	0.15	12

Furthermore, there are some physical phenomenon that do not exist in materials with larger grain sizes. The general quantum-size effect for optical transitions in semiconductor nanocrystals which occurs in very small nanoparticles (<10 nm) due to the quantum confinement effects inherent in particles of that size³⁵. A typical

example of size dependant properties of these metal particles can be illustrated as shown in Figure 3.

Research in his field has a vast spectrum of areas to be covered because nanotechnology has the potential to revolutionize almost all the industries ranging from health, biomedical, information technology, semi conductors etc

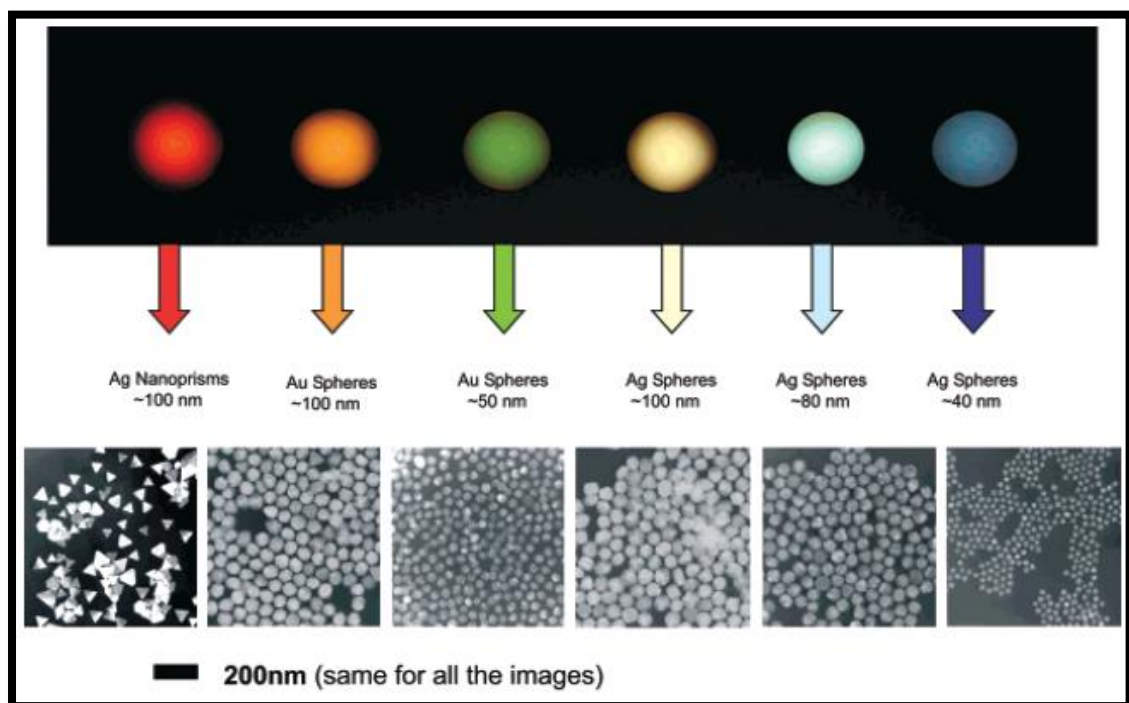


Figure 3 Sizes, shapes and composition of metal nanoparticles can be systematically varied to produce materials with distinct light-scattering properties²⁷.

Several breakthroughs and advances are expected in this field in the coming years (shown in Figure 4) which will impact a lot of advantages in material sciences, optical communications, self assembling products and systems and reaching the size barrier of microprocessor. An innovation is expected in the self-adapting fabrics, in medical treatments and in exploration of space which would be much cheaper as well.^{31-b}

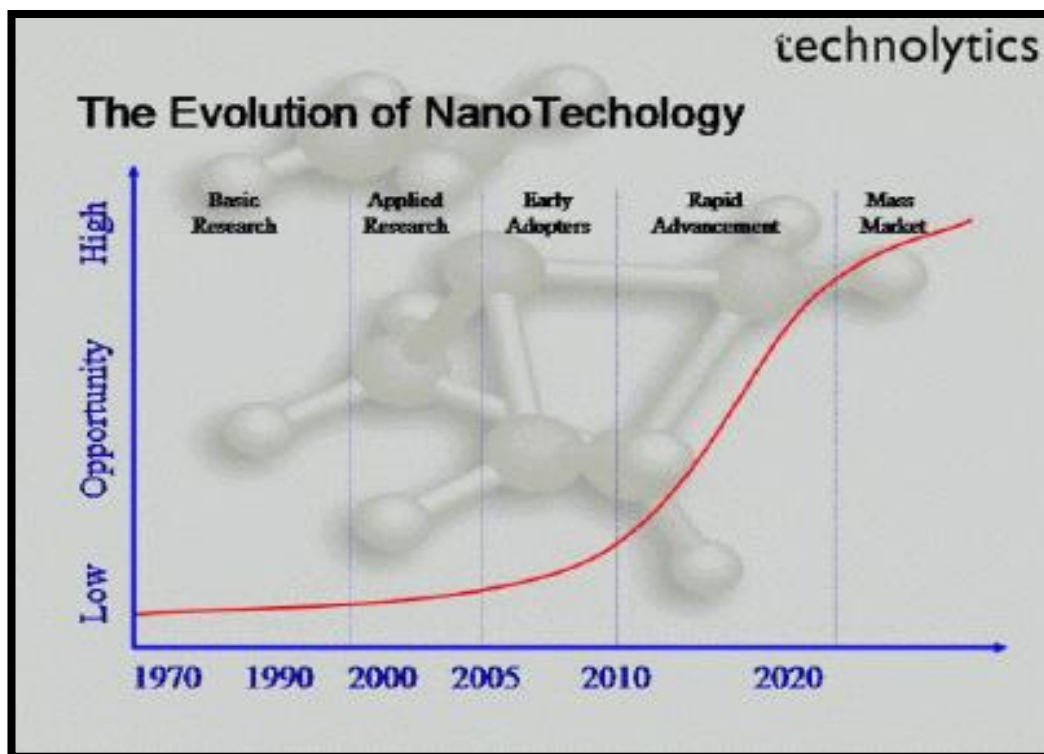


Figure 4 Evolution of Nanotechnology with the span of time (years).

2.4 Synthesis Techniques

The synthesis techniques of metal nanoparticles are gaining more and more attention and have become the subject of many studies in recent years.³⁶ Despite the fact that this special branch of materials devotes different technological advantages, their synthesis is also a very sensitive issue. Over recent years, a whole bunch of synthesis techniques of metal nanoparticles have been developed. And a lot of research is going on in this field till up to this date. Among the various methods developed for the synthesis of these metal nanoparticles (MNPs) they can be generally classified into Top-down³⁷ and Bottom-up³⁸ strategies. The term “top-down” refers to the mechanical crushing of source material using a milling process and reducing those source materials to the desired size and shape. In the “bottom-up” strategy, molecular or atomic structures are

built up by into more complex nanoscale assemblies by using different chemical processes (Figure5). The selection of the respective process depends on the chemical composition and the desired features specified for the nanoparticles.³⁹ **Top down** approaches generally include Pattern transfer (lithography), Deposition (or film growth), Etching (removal of material) and Physical vapor deposition (sputtering) etc. While there is still an important role to be played by top-down methods, there are some underlying limitations associated with this technique. These techniques are slow, requiring prohibitively expensive equipment to produce small scale and, often uniquely, two-dimensional structures.

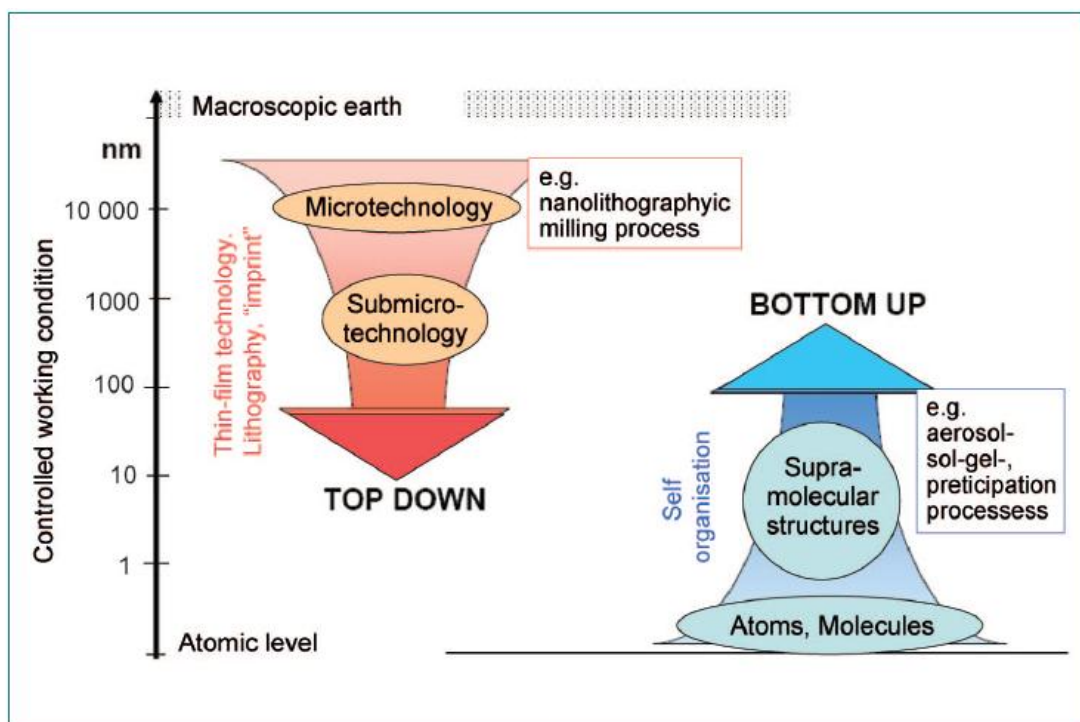


Figure5 Schematic view of Top-Down and Bottom-up technique

None of these disadvantages, on the other hand, are suffered by the more novel and versatile bottom-up techniques which are increasingly being employed to produce structures of even smaller scale and more complex architecture than has previously

been achievable. Despite the fact that it allows large-scale synthesis of the nanoparticles, but an obvious disadvantage is that the nanoparticles are usually of non-uniform size and shape compared to those produced by a top-down method. **Bottom-up** approach involves the fabrication of structures from smaller units, using the properties that they possess to induce their self-assembly in the desired manner. This approach includes chemical vapor growth. Compared to top-down lithographic methods, the bottom-up self-assembly approach is cheaper and enables the fabrication of large area two-dimensional or three-dimensional samples, making it attractive for different applications.⁴ Evidence for the efficacy of these techniques can be gathered through the observation of nature, which is also seen to follow a bottom-up approach. The organization of molecules to form progressively larger structures, from cells and DNA, and including, meter scale biological organisms, in a hierarchical manner show the effectiveness that such approaches can provide. Indeed the entire field of biomimetics seeks to take advantage of structures found in nature which have evolved over a long period of time and, as the name suggests, use them as models or blue-prints which can then be reproduced using innovative chemical methods.

Different bottom-up techniques have been developed and reported in the literature such as sol-gel process⁴⁰⁻⁴⁴, chemical reduction and electrochemical reduction of metal salts⁴⁵⁻⁴⁶, photochemical reduction⁴⁷⁻⁵⁶ etc

In this research we synthesize polymer-metal nanocomposite with the help of free radical photopolymerization. So a brief overview of the use of different photochemical strategies is presented here.

2.4.1 Photochemical strategies

The beginning of the photochemistry of metal nanoparticles goes back to the discovery made by a German physicist and a medical professor Johann Heinrich Schulze⁵⁷ in 1700s when he observed the change in color of the silver solution upon the application of light. Whereas in 1857, Faraday described the synthesis of deep-red solutions of colloidal gold and also investigated the optical properties of gold nanoparticles⁵⁸.

Giacomo Ciamician^{5-a} at the beginning of the 20th century laid the foundations for a large part of present day used key work in organic synthesis, based on the work done in the last decades of 19th century.

Although the photochemical method comes under the category of bottom up approach, but the advantages and its centering applications are critically different from other available bottom up techniques. For example, photochemical synthesis has been applied to photography (photographically sensitive materials say silver salt) and lithography, mainly because of the reason that photochemical synthesis is suitable for the selective fabrication of metal NPs with high spatial resolution^{53, 59-62}. However most of the other bottoms up techniques for the synthesis of the metal NPs do not have this feature.

The basic principle of photochemical synthetic method lies in the generation of metal atom (M^0) through the direct photoreduction of a metal source (metal salt or complex), or the reduction of metal ions using photochemically generated intermediates such as excited molecules and radicals (photosensitization) as shown in Figure 6.

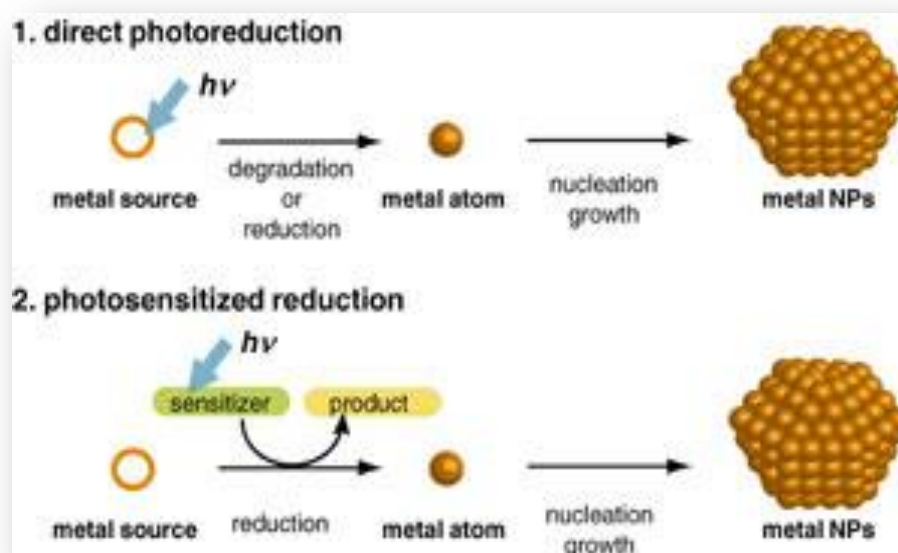
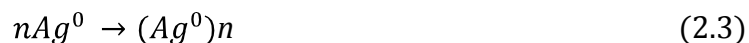
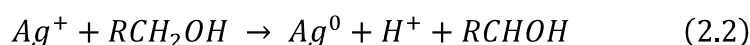
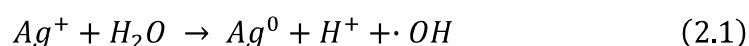


Figure 6 Schematic system of photo-induced synthesis of metal nanoparticles⁶³

Metal nanoparticles can be formed by **direct excitation** of a metal precursor by light. The advantage in this technique lies in the fact that it does not require a chemical reducing agent and because of this reason, it can be employed in different mediums including oxides, glasses, polymer films, cells, etc. Hada *et al.*⁶⁴ reported the mechanism of photochemical formation of silver nanoparticles in aqueous and alcoholic medium.

In their study, they proposed that the electron transference to silver ion from solvent molecule is the main reaction of photolysis.



As shown in the above first two reactions that Ag^+ goes to Ag^0 state by transferring an electron from the solvent molecule when UV light is subjected to them. And then that Ag^0 associates with other silver atoms to form silver nanoparticles.

Another approach for the photochemical synthesis is **photosensitization**. In this technique photoactive agents are in use mainly because of their property that they generate intermediates, when light is being incident on them. These intermediates reduce the existing metal to form the M^0 state⁶³

The oxidative radical formation by photochemical process is the most widely used technique. This is more beneficial in terms of speed and efficiency of the reaction as compared to direct photoreduction to produce metal particles. Flexibility of the excitation wavelength is an additional benefit because it depends not only on the metal source, but also on the sensitizer.⁶¹

Based on their formation mechanism, radical precursors can be divided into two categories hydrogen bond cleavage (I) and abstraction (II). As the name suggests, the first one is due to the abstraction of hydrogen by excited organic molecules from co-existing hydrogen donors. A typical radical precursor/hydrogen donor couple is

the ketone derivatives/ α -alcohol system such as acetone ketyl reduction⁵⁵, acetone⁴⁸, acetophenone⁶⁵, benzophenone^{56,66}. The significant point of the ketone derivatives/ α -alcohol system is the role of the α -alcohol. The singlet excited state decays to the triplet excited state through intersystem crossing.

The ketone derivatives in the triplet excited state abstract hydrogen from the hydrogen donor to generate the ketyl radical and radicals derived from the alcohol. These radicals reduce metal ions to generate the metal NPs.⁶⁷

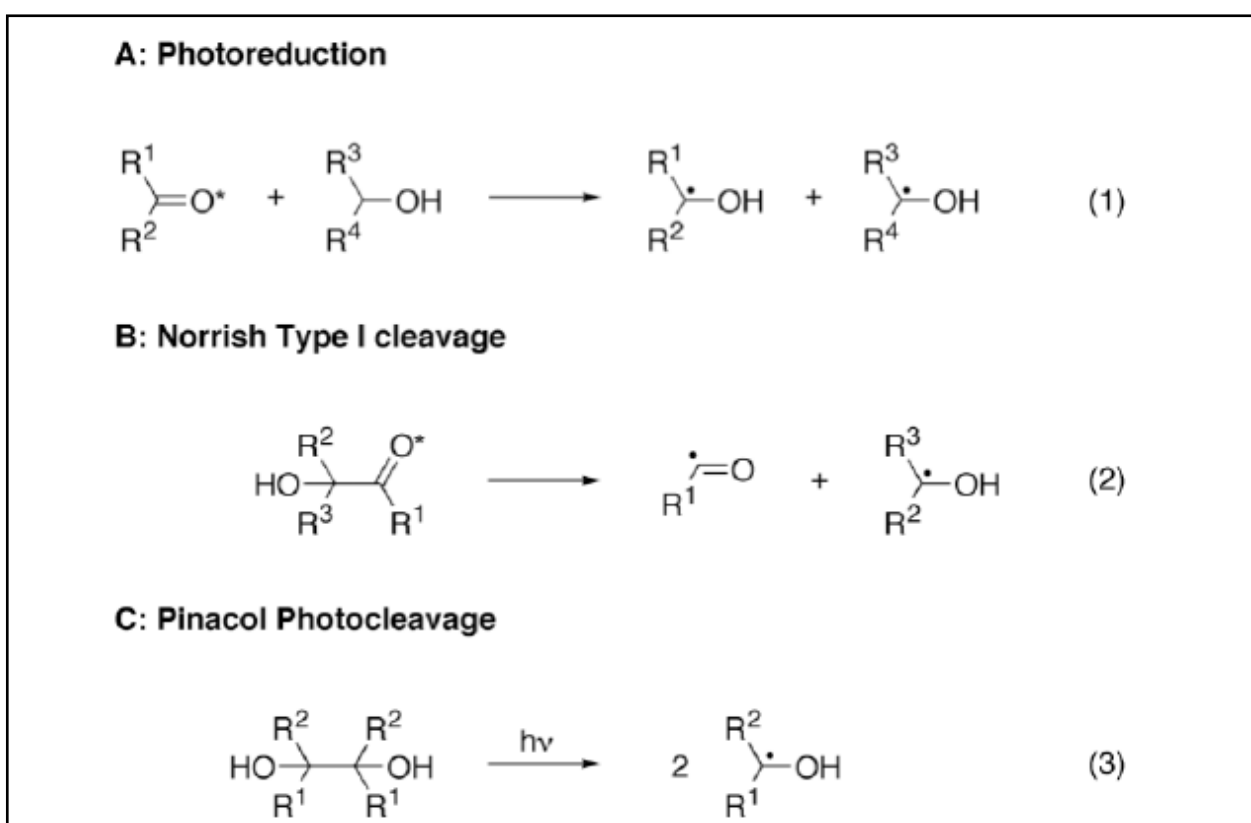


Figure 7 Photochemical strategies for the generation of ketyl radicals from organic precursors. The asterisk (*) denotes the excited state of a molecule, frequently a triplet state in the examples used in this contribution, while "h ν " indicates exposure to light⁶⁷.

The α -alcohol works as a solvent, hydrogen donor and oxidative radical precursor. Bond cleavage is one of the important fundamental photochemical processes. To generate radicals for the photochemical synthesis of metal NPs a number of photo-induced bond cleavages are there. Figure 7 shows three of those photoreactions that can be employed for the generation of ketyl radicals from the organic molecules.⁶⁷

The Norrish type I reaction can occur from both singlet and triplet excited state, but according to Encina *et al.*⁶⁸ aromatic ketones is dominated by triplet state reactions. 2-Hydroxy-2-methyl-1-phenyl propanone and its derivatives have been used widely as photo-initiators for free radical polymerization⁶⁹. Eichler *et al.*⁷⁰ in 1980 described that upon irradiation, it undergoes classical type I cleavage to produce a benzoyl ketyl radical pair with a high rate constant and good efficiency as shown in Figure 8.

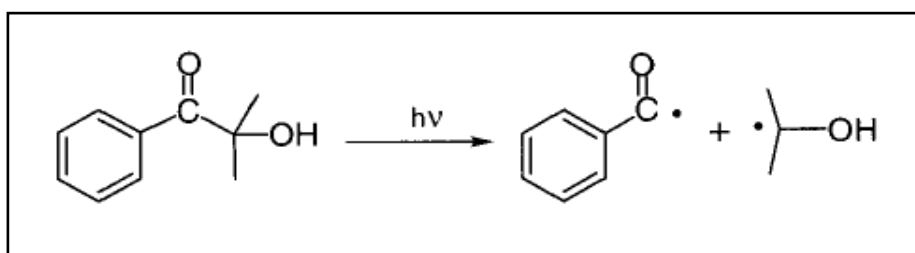


Figure 8 Photolysis to produce benzoyl ketyl radical⁷⁰

Unfortunately, this structure has a low absorption above 300 nm. A bathochromic shifted absorption can be achieved through modification by using different substituents. S. Jockusch *et al.*⁶⁸ carried out a detailed study on this matter, and according to them a biggest bathochromic shift was observed by substituting dimethylamino group. If we take into account the case of benzophenone, its triplet state has n,π^* character, and due to this property it is an excellent hydrogen abstractor from appropriate donors (such as alcohols, some hydrocarbons, benzylic and allylic hydrogens, among others)⁶⁷, as illustrated in Figure 9. It is to emphasize the catalytic nature of this process; benzophenone is regenerated in contrast to the systems containing Benzoin where the starting ketone is not regenerated in the process.

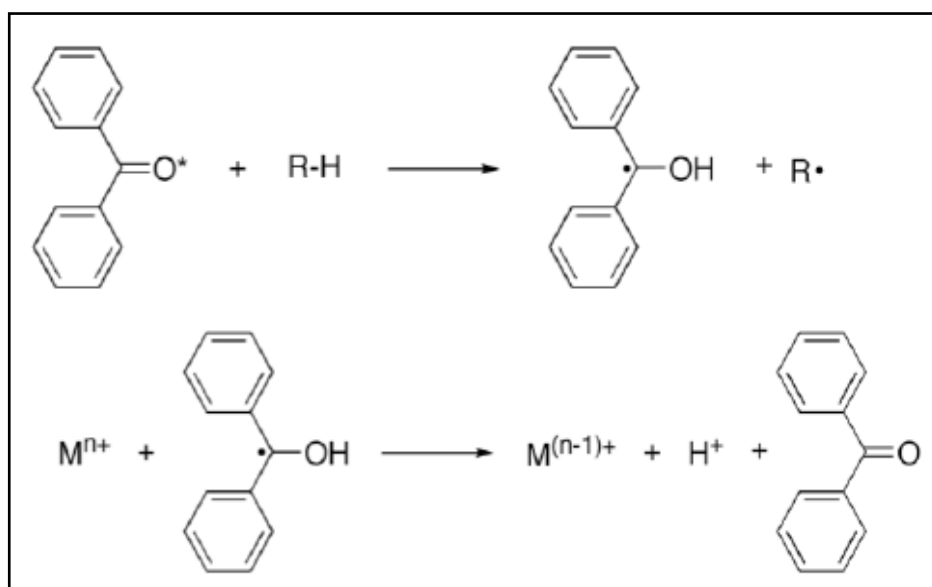


Figure 9 Photoreduction of Benzophenone followed by electron transfer to the metal ion M^{n+}

67

The photochemical synthesis differs from other methods solely because of the character of light, which controls photochemical reactions and hence it is a clean process.

The main advantages of photochemical synthesis are grouped as:

- I. As observed in photography and lithography, light induced processing has high spatial resolution⁵⁹⁻⁶². And due to this advantage one can fabricate metal NPs in a selective region. And also the direct 3-D writing of metal NPs in a transparent matrix or free standing metal structures has been accomplished by using multiphoton absorption with an ultrashort-pulse laser, or through stepwise excitation using two laser beams of different wavelengths⁷¹⁻⁷⁷.
- II. The first law of photochemistry states that *light must be absorbed by a chemical substance in order for a photochemical reaction to take place*. Due to this law, light can simulate an objective reaction without affecting the external circumstances⁴⁹. This advantage is useful for the in-situ fabrication of metal NPs in transparent matrices, as well as the template synthesis of metal NPs using micelles, zeolites, dendrimers etc ^{21, 78-79}.

- III. Light is the exclusive trigger of a photochemical reaction and this characteristic allows us to start the formation of metal NPs through photochemical reaction at any given point in time.

2.4.1.1 Radical Photopolymerization

Photopolymerization involves the conversion of liquid monomers into a glassy or rubbery polymer structure with the help of irradiation of UV-light at room temperature; it also implies an increase of molecular weight by light⁸⁰. The scheme of the process is shown in Figure 10.

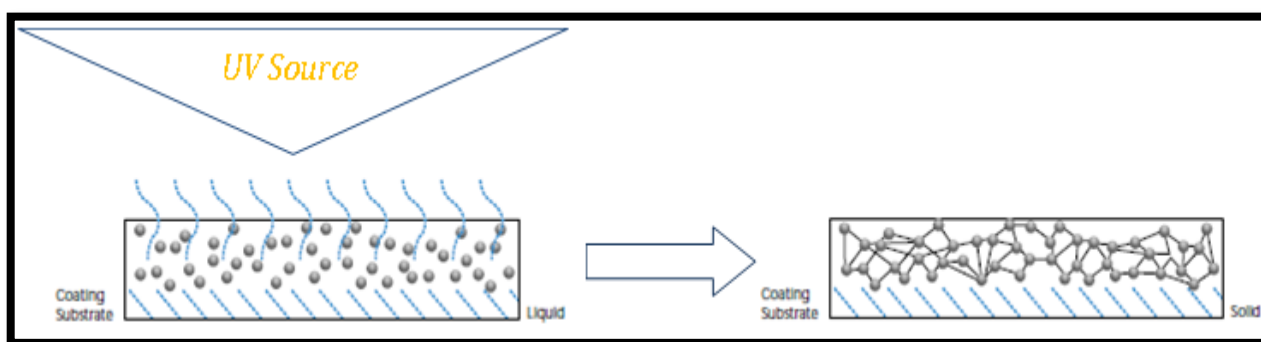


Figure 10 Schematic illustration of photopolymerization process

Monomers employed in this technique can be mono or multifunctional molecules depending on the number of reactive groups. The photoinitiators absorb UV-light being incident on them, and results into the fragmentation into reactive species. As a result of this fragmentation, species generated can be free radical or cationic in nature as shown in Figure 11.

In case of free radical polymerization, photoinitiator after being subjected to UV-irradiation spontaneously decompose itself into free radicals

and hence initiates a chain reaction for the polymerization.⁸¹ Photoinitiators for radical polymerization are classified as cleavage (type I) and H-abstraction type (type II) initiators. These radicals react with the double bond of monomer (which is mostly acrylic) which results in the further growth of radicals. Then a quickly growing chain is produced with the addition of radical to the carbon-carbon double bond generating a new radical at the end of the polymer chain. This fast growing chain is stopped by a chain breaking reaction, which is basically a bimolecular reaction. On the other hand, initiator used in cationic polymerization is either Lewis acid or Bronsted acid. The strong acid releases H^+ which adds to the monomer. This cationic species then reacts with the functional groups to propagate the reaction. In the cationic reaction, chain transfer can occur and alcohols can be used for this purpose. There are several pros and cons attached to both mechanisms; like oxygen may interfere in the reaction in case of free radical based photopolymerization but complete oxygen inhibition can be achieved in cationic one. Free radical photoinitiators can be used for acrylic system as well as for other unsaturated polyester resins. Whereas, cationic systems are dependent on the use of epoxy or vinyl ether functional resins. Despite all the different problems related to both mechanisms, free radical photopolymerization constitute a major part of the industry as it is the most efficient way. They have this ability to convert the liquid monomer into highly cross-linked functional polymeric materials rapidly.

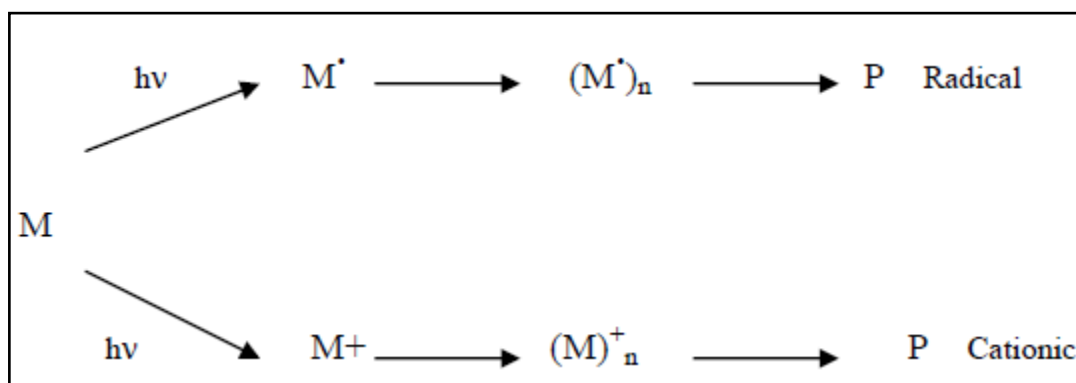


Figure 11 Mechanism of photopolymerization

We can say that photochemistry is a powerful tool for investigating the formation and growth processes of metal NPs.

2.5 Polymer-metal nanocomposite synthesis

A polymer matrix in which nanoparticles are embedded to enhance some particular properties of parent matrix is called polymer nanocomposite.⁸² These nanocomposites basically constitute polymer matrix and fillers of at least one dimension in the range of 1-100 nm.¹ By combining the special properties of nano-sized materials with the flexible, easy to process, high modulus polymers: high performance novel materials can be developed for sophisticated industrial applications. Noble metal nanoparticles embedded in a host polymer gained significant interest in recent years due to the incredible properties they offer i.e. electrical properties⁸³, optical properties⁸⁴ etc which makes their use possible in different areas like in sensors and biosensors^{85,86}, electronic devices⁸³, catalysis⁸⁷, antibacterial⁸⁸ and antifouling coatings⁸⁹ etc. The embedding of metal nanoparticles in polymer matrices is one of another easy way to stabilize these particles against aggregation. There are different inorganic nanofillers which can be employed based on the different properties which one want to incorporate into the final polymeric composite, may include metal (like Au, Ag, Pt, C, Fe and metal alloys CoPt), semiconductors (e.g. PbS, CdS, ZnO) different oxides (TiO₂, SiO₂, ferric oxide) and carbon based materials (like CNTs, graphene, carbon nanofibre)⁹⁰. Synthesis of NPs in a polymeric media has been anticipated to be more useful due to their ease of processing, solubility, low toxicity and also because of the possibility of controlling the growth and size of the nanoparticles.⁹¹ There are a lot of attempts being made to fabricate metal nanoparticles-polymer composites. In a broad spectrum, there are two approaches which can be used to synthesize nanoparticles in a polymer matrix i.e. *in-situ* and *ex-situ* techniques.

A brief description of these approaches is given in the following sections. It is shown symbolically in Figure 12, the different paths to synthesize polymer nanocomposites.

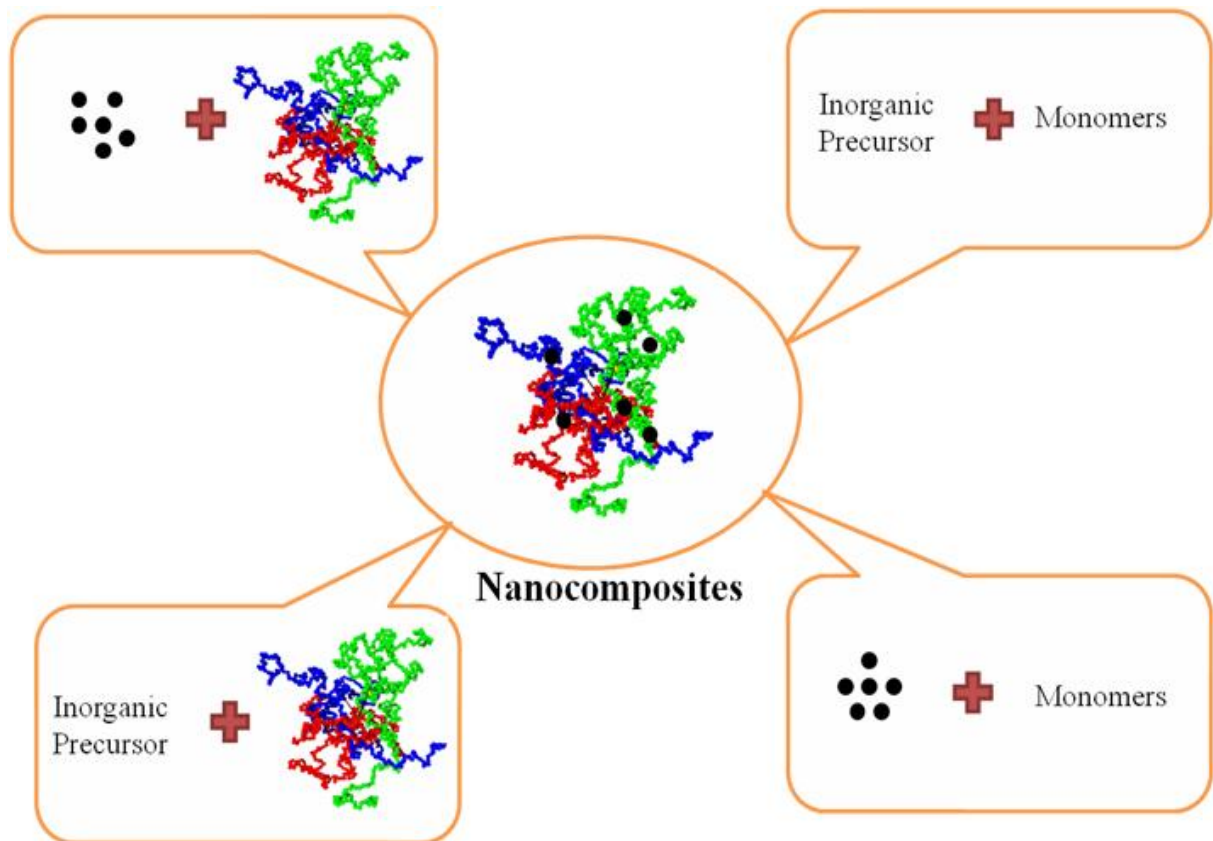


Figure 12 Schematic presentation of the preparation methods of polymer-metal nanocomposites

2.5.1 Nanoparticles precursors in polymer

In this method, metal ions are being reduced inside a polymeric matrix. This technique results in a homogenous dispersion of metal nanoparticles in the polymeric matrix. There has been a lot of work done by different scientists to achieve this specific type of polymer nanocomposite.

Metal salts have been reduced in an already formed polymer (PANI) by different scientists in an aqueous solution or by using any other suitable solvent, and it was

observed that the rate of reaction and the size of the particles formed are strongly dependant on the medium of reaction⁹²⁻⁹⁴.

In-situ photochemical method is also being employed very efficiently to fabricate nanoparticles inside the polymer matrix. Silver particles were synthesized in the epoxy resin by exposing them to UV light⁹⁵. Furthermore, a lot of literature has been published on this technique as it is very efficient, easy and less expensive than the other available techniques^{57,96}. Noble metal nanoparticles like Ag, Au, Cu etc can be in-situ synthesized in a one step photochemical method^{47,49-50,53-56,97}.

Wang *et al.*^{98, 99} prepared nano composites in PANI and PVP by electrospinning method. This has been reported in their work that the size of particles obtained through this method was efficiently very small i.e. less than 50 nm^{98, 99}.

Reports have been published on the preparation of core shell particles in the co-block micelles¹⁰⁰⁻¹⁰⁴. Because the particles are formed within the core of the micelles of the diblock copolymer, macroscopic segregation of the metal particles can be avoided very efficiently¹⁰⁵.

Nanoparticles of very small size and homogenously distributed in the polymer matrix can also be prepared by reverse micelle method. Zhang *et al.*¹⁰⁶ developed a novel method by using compressed CO₂ to prepare Ag nanoparticles in polystyrene (PS) by using surfactant i.e. sodium bis (2-ethylhexyl) sulfosuccinate (AOT). The main advantage of this process is that very small sized nanoparticles can be obtained¹⁰⁷; compressed CO₂ can drive the Ag nanoparticles out of the reverse micelles¹⁰⁸⁻¹⁰⁹, while the surfactant AOT remains in the solution. Also the particle morphology and size can be controlled by controlling the pressure of CO₂. Silver particles in an epoxy resin have been prepared by an in-situ reduction for the capacitive applications.⁸³

2.5.2 Nanoparticles precursors in polymer precursor

In this method, monomer is directly oxidized in the presence of metal ions precursor. In this case, the metal ion precursor oxidizes itself to metal particles and hence polymerizes the monomer.¹¹⁰. Conventionally, polymerization of organic monomer and formation of metal particles were executing separately and then subsequently mixing both entities which results in the aggregation of the metal particles and ultimately leading to the non-homogeneous mixing. Also in some techniques extreme temperature and pressure values have to be kept which in return give rise to a complex and high cost phenomena. Only few techniques are present in the literature which describes the simultaneous one step reaction in which metal precursor oxidizes themselves to metal ions and polymerize the monomer. For instance, the γ -irradiation method and the ultraviolet irradiation techniques were applied to synthesize polymer metal nanocomposites, in which the reduction of metal ions and the polymerization of the monomer were simultaneous^{110(a-b)}. A reliable method i.e. microwave assisted synthesis of polymer nanocomposites in one step is reported in 1986 for the first time. Polyacrylamide-silver nanocomposites were prepared by γ -irradiation technique in non-aqueous solution for the first time by Zhu *et al*¹¹¹. In this method, AgNO_3 was dissolved in ethanol and acrylamide was added as a monomer, without the addition of any surfactant and by irradiating this solution silver particles were formed. From the TEM images it was shown that the particles were well distributed in the polymer matrix¹¹¹.

This technique has opened up new doors for the further research and development of the polymer composites in a single step and in a short time. Another report on the polyacrylamide-silver nanocomposite by using the same technique in the presence of ethylene glycol was published¹¹². This method leads to a homogeneous distribution of metal nanoparticles in polyacrylamide matrix. Ethylene glycol acts as both reducing reagent and as a solvent, means no other reducing agent is needed. Also, there is no need to use any initiator to polymerize acrylamide polymerization and there is no need to use surfactant for stabilization of metal nanoparticles. All these factors make it possible to avoid subsequent complicated workup procedures

for removal of these additives, finally leading to fast, simple, and low-cost process in the preparation of polymer metal nanocomposites¹¹².

2.5.3 Nanoparticles preforms in polymer

In this technique, already formed nanoparticles are incorporated in the polymer matrix. The main advantage of this procedure is that the particles incorporated would be of high quality. But a major problem while dealing with this method is the incompatibility of these particles with the polymer matrix, which therefore results in the non-homogenous distribution of these particles in the matrix¹¹³. As a result of this, large clusters of nanoparticles form and the required properties are not achieved. So, in order to avoid this problem compatibility has to be achieved by stabilizing the nanoparticle dispersions¹¹⁴.

Another approach to disperse NPs homogenously in a polymer matrix is by surface-initiated polymerization (grafting from) and tethering (grafting to) techniques^{115, 116}. These techniques are proven to be very useful for synthesizing homogenous polymeric nanocomposites. A schematic diagram describing these approaches is shown in Figure 13.

In the *grafting-to* method, a preformed and end-functionalized polymer is attached to the surface. Besides the fact that this method is a simple and modular approach, there are some drawbacks as well. Steric repulsion between polymer chains already attached and a chain diffusing to the surface limits the available graft density.

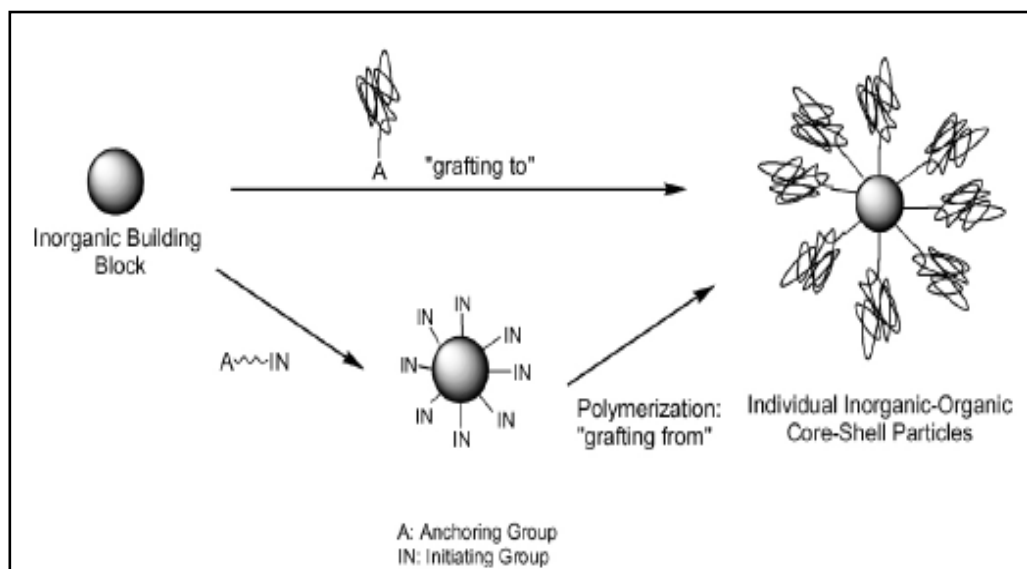


Figure 13 Schematic description of grafting-to and grafting-from approaches⁹⁰

In the *grafting-from* method, the surface is functionalized with an initiator or chain transfer agent and the polymer is grown from the surface. The diffusion of a relatively small monomer to the surface does not suffer from the same steric repulsion as a diffusing polymer chain.

2.5.4 Nanoparticles preforms in polymer precursor

This procedure involves dispersing inorganic nanoparticles directly into the monomer solution, prior to its polymerization. But in this procedure particles may separate out and starts to settle down quickly at the bottom. It is difficult to disperse these particles homogenously in the polymer matrix. So, a good linkage has to be assured at the interface, different stabilizers may be employed to serve the purpose.

Oliveira *et al.*¹¹⁷ developed a two phase polymerization route, by following the technique of Burst *et. al.*¹¹⁸, in their work aniline was dissolved in a silver nanoparticles toluene solution; polymerization took place at the water-toluene interface. It was observed that silver nanoparticles were homogeneously dispersed in the resulting polymer.

Emulsion polymerization is another common route to carry out the synthesis of polymers. Polymerization of ethylacrylate has been carried out in the presence of silica to synthesize Polyethylacrylate and it was demonstrated in the work carried out by J.E. Mark *et al.*,¹¹⁹ that the nature of interface between the monomer and particles is dependent on the type of silica used. Different nanocomposites with monomers like styrene and methyl methacrylate intercalated with clay are also reported in the literature¹²⁰⁻¹²¹. Polymerization occurs mainly at the surface of the unmodified particles, and polymerization of monomer initiated in the same adsorbed layer on which the monomer got absorbed¹²²⁻¹²⁴. The hydrophobic polymers were in-situ fabricated within the hydrophilic inorganic layered materials. A lot of literature on oxides, semiconducting and non-metal nanoparticles is available in literature¹²⁵⁻¹³⁰.

As already mentioned, the main challenge in employing this technique is to obtain well-dispersed particles with a narrow size distribution. Different techniques have been devised to achieve this goal, and the most effective is to polymerize in the presence of amphiphilic molecules. Amphiphilic molecules or surfactants like, carboxylic acid¹³¹, alcohols¹²⁵, thiols¹³²⁻¹³⁴, and amines can be chemisorbed on the surface of the nanoparticles and therefore form a hydrophobic interface and in result prevents the agglomeration of these particles.

These surfactants do not play any role in the polymerization process; they disperse the nanoparticles more efficiently in the growing polymer during the polymerization¹³⁵⁻¹³⁶. Luca *et al.*¹³¹ reported the encapsulation of silver particles by polymerizing styrene-methacrylic acid in the presence of oleic acid.

And it was demonstrated that oleic acid is essential to obtain silver particles encapsulation, and it increases the compatibility of the particles with the polymer matrix; when polymerization was done in the absence of oleic acid, only polymer particles without metal core were produced and there was no polymer shell observed around the particles. There is another technique i.e. microemulsion in use to prepare polymer nanocomposites. This is a very similar dispersion based approach which can be used to prepare small, homogeneous droplets of monomer or polymer precursors, and then changing them to the final polymer composites¹³⁷. Different reports to prepare nanocomposites by microemulsion polymerization

based on some inorganic particles like titania¹³⁸⁻¹⁴⁰, calcium carbonate¹⁴¹, magnetite¹⁴² etc are already present in the literature. But, gold and silver nanocomposites have been synthesized by Kim *et al.*¹⁴³ for the first time by using microemulsion technique. In this method, metal nanoparticles were first prepared and then grafted with small hydrophobic polymer chains which lead to the dispersion of the particles in the organic solvent. And then these particles were dispersed in a suitable monomer to initiate microemulsion polymerization in the presence of a surfactant and a free radical initiator.¹⁴³

2.6 Stabilization of metal nanoparticles

A very important feature which hinders the use of these nanoparticles is their high tendency to self aggregate. Because of the large surface area, they possess high surface energy due to which they have a great chance of aggregation. Owing to this reason, MNPs are so reactive that when they touch each other fuse together and results in a loss of the nanometric size and hence special properties.¹⁴⁴ A problem arises to the fabrication and use of these MNPs in different applications¹⁴⁵ because of this feature. Overcoming this problem to stabilize the nanoparticles is one of the greatest challenges in their handling.¹⁴⁶ Nanoparticles can be synthesized successfully by three steps: nucleation, growth, and termination by a capping agent or ligand (or stabilizing agent) through colloidal forces.¹⁴⁷ These colloidal forces can be classified into three main types: Van der Waals interactions, electrical double-layer interactions, and steric interactions. In addition, hydrophobic and solvation forces can also play an important role¹⁴⁸. MNPs can be stabilized by using different strategies. In the ex-situ synthesis, polymeric shell is formed by dispersing the NPs in a polymeric solution by using different mechanochemical approaches.

Particles coated by polymer consider being more stable against aggregation because of a profound decrease of their surface energy. The problem in this technique is that the success of the stabilization is limited by the possibility of re-aggregation of the MNPs along the time.

On the other hand, in-situ process to prepare and stabilize nanoparticles can be combined in one step. And this process gives an opportunity of quick and easy way to synthesize stabilized NPs. Because of this reason, in-situ techniques to prepare and stabilize MNPs are getting much attention. The most commonly used substances for the stabilization purpose are ligands and polymers.¹⁴⁹ Especially those natural or synthetic polymers which have an affinity towards the metal nanoparticles. These substances not only control the aggregation but can also affect the reduction rate of the metal particles¹⁴⁹. Synthesis of polymer-stabilized nanoparticles basically involves two steps: first to reduce the metal ions into neutral atoms and then coordinating these MNPs to the polymer¹⁵⁰. In order to determine the size and shape of the resultant MNPs there are different parameters to control: choice of the synthesis technique (as bottom-up technique usually use an agent i.e. *capping materials* to protect and stabilize NPs against aggregation), the metal salt used, the reaction time etc. To prevent the aggregation of silver nanoparticles, there are different stabilizers available for this purpose. These stabilizers (capping agents) employed to provide the stability through the common colloidal stabilization mechanism: electrostatic (Citrate-AgNPs), steric (PVP-AgNPs) and electrosteric (BPEI-AgNPs)¹⁵¹. Stable Ag NPs can be produced by using citrate capping effect as was synthesized by Henglein and Giersig¹⁵². El-Badawy *et. al*¹⁵¹ in their study showed that the citrate molecules being adsorbed on the surface of AgNPs results in stabilizing them. And it was shown in their studies the silver particles formed aggregates in the absence of citrate. The BPEI-AgNPs are electrosterically stabilized through the adsorption of the polyelectrolyte (BPEI) containing amine groups which ionize as a function of the solution pH¹⁵³. Some other stabilizing agents such as SDS (Sodium dodecyl sulphate)¹⁵⁴ and CTAB (Cetyl trimethyl ammonium bromide)¹⁵⁵ can also be used to stabilize the AgNPs against aggregation and precipitation. Apart from these different chemical stabilizing agents, polymers are most commonly used as stabilizers and protective agents. Polymers like PVP (Polyvinyl pyrrolidone)¹⁵⁶⁻¹⁶⁰, PVA, (Polyvinyl alcohol)¹⁶¹, etc can be utilized to serve this purpose. The schematic presentation of the steric stabilization can be achieved with the help of polymers (PVP) is shown in Figure 14. However, among all these polymer stabilizers PVP (steric stabilizer) is considered to be an excellent capping agent as it attributes

special protecting properties owing to its unique structure. PVP is a homopolymer with a polyvinyl backbone and its repeating units shown in Figure 14, it is composed of a highly polar amide group that confers hydrophilic and polar-attracting properties, and also non-polar methylene groups both in the backbone and in the ring that confer hydrophobic properties.¹⁶² The N and O in the polar groups have a strong affinity for silver nanoparticles. PVP because of its certain features is used in a wide range of applications in medicine (e.g. as a drug carrier, a component of plasma substitute or wound dressing) and technological domains (e.g. in aerosol hair sprays, pigment dispersions, cosmetics)¹⁶². The PVP protective mechanism of silver nanoparticles formation has been currently described by many researchers.

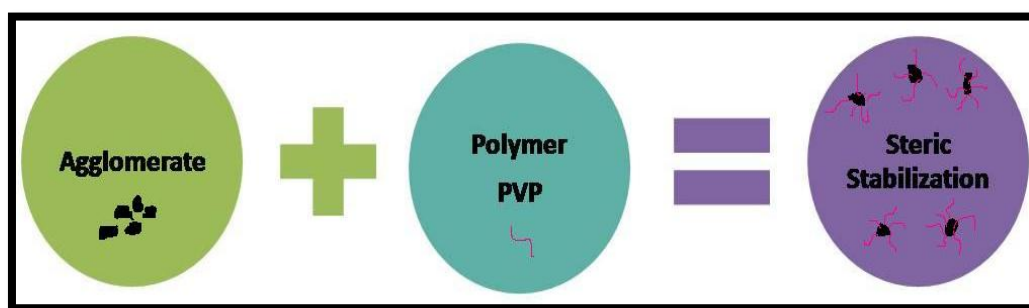


Figure 14 Schematic presentation of steric stabilization mechanism

There are three steps of PVP mechanism carried out to hinder the aggregation of AgNPs. First stage involves the bond formation between the stabilizer and silver ions, and then PVP donates lone pair, electrons of oxygen and nitrogen atoms to *sp* orbitals of silver ions, and thus the coordinative complex of Ag ions and PVP forms in aqueous solution. Second, PVP promotes the nucleation of the metallic silver which thus leads to the aggregation of Ag atoms. Third, these primary nanoparticles then coalesce with each other or interact with PVP to form larger aggregates known to be secondary aggregates.¹⁵⁸ PVP prohibits silver particle aggregation and grain growth as a result of its steric effect.

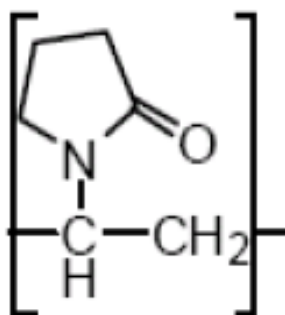


Figure 15 Structure of the repeat unit of PVP

On the other hand, the real major problem in utilizing copper nanoparticles in different applications is their inherent tendency to oxidize in ambient conditions.¹⁶³ There are few attempts reported to protect the metal particles from oxidation by minimizing the contact of oxygen to the surface of copper nanoparticles by providing a protective layer. Different other efforts are also being made to prevent agglomeration and coagulation process in order to obtain uniform sized homogenous particles. A protective thin layer of silica has been in use to avoid the interaction of oxygen molecules with the nanoparticle surface and to prevent the nanoparticles from aggregating and contacting each other. A lot of work has been done to protect the gold and silver metal particles by coating their surfaces with silica layer.¹⁶⁴⁻¹⁶⁸ However, only one attempt has been made by Kobayashi *et al.*²⁵³ who prepared Cu nanoparticles in an aqueous solution and reported their stability for at least one month with the help of silica coating. A more commonly employed technique to stabilize the metal particles is with the help of surfactants, they may avoid the aggregation of the particles by binding themselves to their surface. Size and shape of the copper NPs may be controlled by using different surfactants like oleic acid¹⁷⁰, alkanethiols¹⁷¹, sodium dodecyl sulphate¹⁷², CTAB¹⁷³ etc. Another promising approach to stabilize the copper NPs is to use polymers as capping agents. Among these polymers, polyvinyl pyrrolidone (PVP) has been widely used as a capping agent for the stabilization of nanoparticles¹⁷⁴⁻¹⁷⁷. Jeong *et al.*¹⁷⁸ demonstrated the effect of the molecular weight of PVP on the size of the copper NPs, and thereby confirmed that there is a direct relation between the mol. wt. of PVP and the particle size of NPs, which in turn determines the electrical conductivity

of the film formed. Kobayashi *et al.*¹⁷⁹ employed a conductive polymer i.e. polypyrrole to chemically stabilize copper nanoparticles, and hence these nanoparticles coated with polypyrrole proved to be chemically stable for at least 50 days even in an open air atmosphere. A very common way to achieve stabilization of copper NPs is through the preparation of bimetallic nanoparticles from various combinations of noble metals. And in case of the protection of copper particles, different techniques like electrodeposition¹⁸⁰ and thermal evaporation under ultrahigh vacuum¹⁸¹ have been in use to prepare copper-silver core shell nanostructures. However, another different approach to synthesize copper-silver core shell structure has been carried out by Lee *et al.*¹⁸² This is a two step process in which firstly core particles are produced and then those core particles acts as a reducer for the reduction of shell atoms present on the core surface. Although it is a bit difficult to control this process but is a good way to obtain high conductivity. The schematic illustration of the process is shown in Figure 16¹⁸³

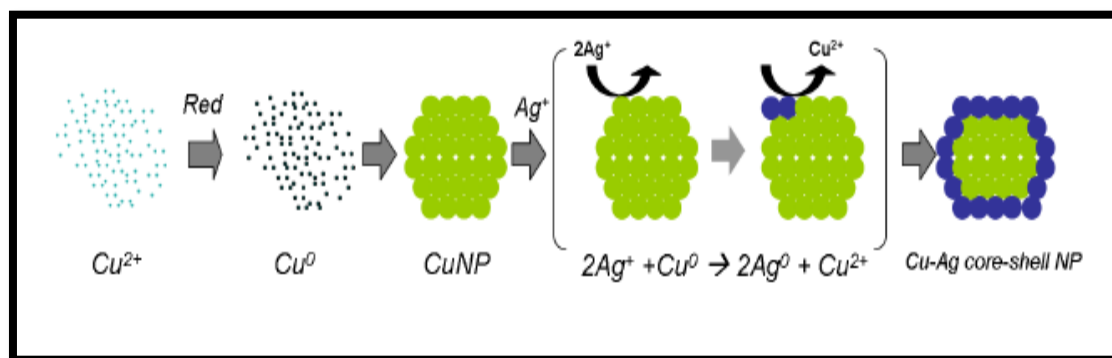


Figure 16 Schematic illustration of Cu-Ag core shell NP¹⁸³

However, a very few attempts to stabilize copper nanoparticles against aggregation formed through the photochemical reduction. And there is no such attempt to protect the copper NPs against oxidation. However, Zhu *et al.*¹⁸⁴ tried to improve the particle size distribution of the Cu NPs by adding polymeric capping agent i.e. PVP. And they showed in their results that particles prepared in the presence of PVP are smaller and the size distribution is narrower than those prepared without the presence of PVP. And the reason for this may be the attachment of the PVP on the

surface of the copper particles resulting in the prevention of further aggregation as was shown in case of silver particles in Figure 14. In the same way, Giuffrida et al.⁷⁴ found out the effect of the amount of PVP on the size of the Cu particles and in their observation they concluded that the higher concentration of PVP is needed to obtain very small particles size i.e. less than 10 nm. S. Kapoor *et al.*^{175, 185} proposed a mechanism to photo reduce copper salt in the presence of benzophenone by using PVP and gelatin as a stabilizing agents.

In recent years there have been significant progresses in controlling the size, shape and composition in order to tailor the desired properties to be used in different fields.¹⁸⁷⁻¹⁸⁸.Some of the mechanisms regarding the stabilization forces have been thoroughly revised in the literature¹⁸⁹⁻¹⁹⁰.

2.7 Properties & Applications

Noble metal NPs, particularly gold and silver NPs, have been extensively studied from the time of their discovery up to this date. These NPs have contributed a lot to the development of variety of the techniques and methods for molecular diagnostics, therapy, imaging, catalysis, drug delivery etc. A lot of data can be found on the specific bio-applications for noble metal NPs, e.g. molecular diagnostics and therapy¹⁹⁰⁻¹⁹³ or cancer treatment applications.¹⁹⁴⁻¹⁹⁷

Because of some remarkable properties of noble metal nanoparticles, they are continually employing in different applications. Optical properties of these MNPs is one of the most important among all the other properties, mainly due to their size and shape dependence and particularly due to the significant property i.e. surface plasmon resonance. Surface plasmons are electromagnetic modes localized on an interface between a metal and a dielectric. It is a well-known fact now that surface plasmon resonance strongly depends on the dielectric properties of nanoparticles, and also on the solvent, substrate and adsorbate^{84, 223-226}.

Free electrons present in the metal oscillate when the light in resonance with the surface plasmon oscillation occurs. As the light passes, polarization of the electron

density of the particles to one surface occurs and oscillates in resonance with the frequency of the light causing a standing oscillation. This is referred to as the surface plasmon resonance, since it is located at the surface. This feature of MNPs makes possible their use to develop optical biosensors with the help of immobilization of bio molecules on the surface of noble metal nanoparticles.

These biosensors employed different techniques like fluorescence spectroscopy, interferometry and localized Surface plasmon Resonance (LSPR) to activate.²⁰²⁻²⁰³ One of the most researched area for biosensing of noble metal NPs is the LSPR, and the main underlying advantage that it does not need any electrical contact to operate and depends on the morphology and physical properties of the matrix. It basically arises from the electromagnetic waves that propagate along the surface of the conductive metal and because of this reason by varying the size of the metal particles the corresponding properties may be altered.²⁰⁴ In LSPR, the size of the metal particles is smaller than the wavelength of light, the plasmon wave shows a dipole character due to the combined oscillation of the conduction electrons against the immobile ions.²⁰⁵⁻²⁰⁶ And this is the reason that almost all of the noble metal nanoparticles produce a strong absorption when excited with an electromagnetic wave, such as light, due to this collective oscillation of the conduction electrons located at the surface of these particles as shown in Figure 17.

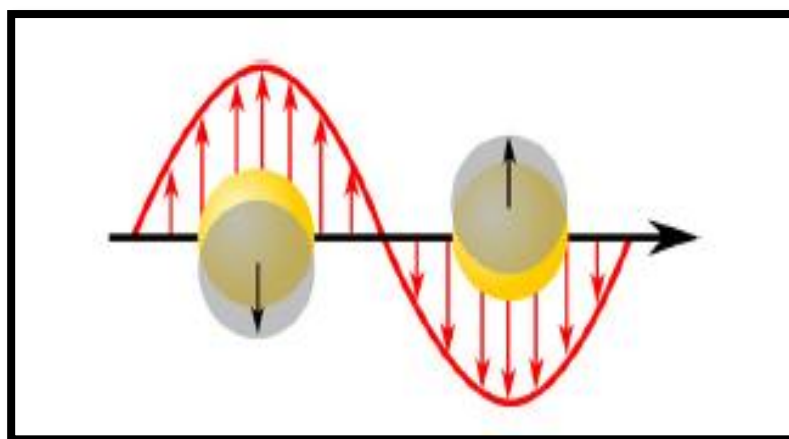


Figure 17 Effect of optical field on the electron cloud in a spherical metal nanoparticle¹⁹¹

The LSPR yields for silver and gold NPs gives an exceptionally high absorption coefficients and scattering properties within the UV/visible wavelength range and due to this reason these metal particles have a higher sensitivity in optical detection

methods than conventional organic dyes, making them the perfect candidates for colorimetric biosensing applications²⁰⁷⁻²⁰⁸.

Because of the dependence of their LSPR properties on the size, shape and composition of these metal particles, one can easily play with these parameters to change the LSPR properties²⁰⁹⁻²¹⁰ Figure 18 illustrates the effect of nanoparticle composition in LSPR that has been already demonstrated beneficial for the development of new and highly sensitive biosensing methods.²¹¹⁻²¹²

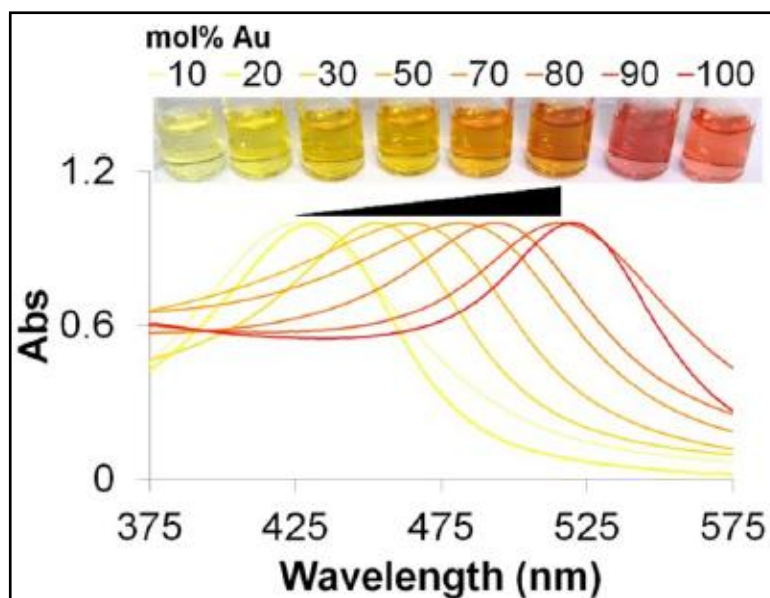


Figure 18 Example of LSPR modulation through different NP compositions. The LSPR absorption band of gold/silver alloy NPs increases to longer wavelengths with increasing amounts of gold.

Mie^{177-b} solved a set of Maxwell equations for spherical particles which can be used to study the interaction of the MNPs. The total extinction and scattering efficiency Q_{ext} and Q_{sca} for a homogenous sphere are stated in the following infinite series:

$$Q_{ext} = \frac{2}{x^2} \sum_{n=1}^{\infty} (2\varepsilon + 1) \text{Re}[a_n + b_n] \quad (2.4)$$

$$Q_{sca} = \frac{2}{x^2} \sum_{n=1}^{\infty} (2\varepsilon + 1) [a_n^2 + b_n^2] \quad (2.5)$$

$$Q_{abs} = Q_{ext} - Q_{sca} \quad (2.6)$$

$$a_n = \frac{m \psi_n(mx) \psi_n'(x) - \psi_n(x) \psi_n'(mx)}{m \psi_n(mx) \xi_n'(x) - m \xi_n(x) \psi_n'(mx)} \quad (2.7)$$

$$b_n = \frac{\psi_n(mx) \psi_n'(x) - m \psi_n(x) \psi_n'(mx)}{\psi_n(mx) \xi_n'(x) - m \xi_n(x) \psi_n'(mx)} \quad (2.8)$$

Where,

ε =refractive index of the metal

ε_m =refractive index of the surrounding medium

m =ratio of the refractive index of the sphere and the surrounding medium ($m = \varepsilon/\varepsilon_m$)

R =radius of the sphere

λ =wavelength of light

x =size parameter ($x = 2\pi n m R/\lambda$),

ψ_n and ξ_n are the Riccati-Bessel functions and the prime represents first differentiation with respect to the argument in parentheses.

These expressions have been solved in the dipole approximation for spherical nanoparticles much smaller than the wavelength of light (<20nm) where only the dipole contributes to the absorption by the nanoparticle.²¹³⁻²¹⁵

$$Q_{abs} = \frac{18\pi V \varepsilon_m^{3/2}}{\lambda} \times \frac{\varepsilon_2(\lambda)}{[\varepsilon_1(\lambda) + 2\varepsilon_m]^2 + \varepsilon_2(\lambda)^2} \quad (2.9)$$

Where,

V =volume of the nanoparticle

ε_m =dielectric constant of the surrounding medium

λ =wavelength of light and the dielectric constant of the metal is expressed in the complex form as a function of the wavelength of light, where $\varepsilon(\lambda) = \varepsilon_1(\lambda) + i\varepsilon_2(\lambda)$.

This allows the calculation of the expected absorption and scattering spectra of small spherical metal nanoparticles.

It has been observed that with the change in the dielectric constant of the surrounding material there is an effect on the oscillation frequency mainly due to the varying ability of the surface to accommodate electron charge density from the nanoparticles.²¹⁶ One can employ equation 2.9 to calculate the expected shift in the absorption spectrum with the change in dielectric constant (ϵ_m) of the medium. As already stated, the dielectric constant can be varied by varying the solvent, but the capping material is most important in determining the shift of the plasmon resonance due to the local nature of its effect on the surface of the nanoparticle.

The basic idea behind the use of the noble metal nanoparticles in the field of sensors lies on the fact that the detection of the chemically bonded molecules is possible by observing a change induce in the electron density on their surface, which results in a shift in the surface plasmon absorption maximum. Mie basically calculated the surface plasmon resonance of small spherical particles by solving Maxwell's equations. However, Gan⁵⁰⁻⁵¹ further extended this theory and applied it to ellipsoidal geometries. The particles are usually characterized by their aspect ratio, and the plasmon resonance for nanorods split into two bands. If the electrons oscillate perpendicular to the major axis, a high energy band refers to the transverse Plasmon absorption. On the other hand if the band is shifted to the lower energy and the electrons oscillate along the major axis, is known as the longitudinal surface Plasmon absorption. There are different methods which can be used to calculate Plasmon resonance for these arbitrary shaped particles by using discrete dipole approximation (DDA).^{84,217-218}

With the better understanding of the properties of these metal particles, their use in different fields has been increased tremendously. One other important area is their use in catalysis. Their use as catalysts has increased enormously in a variety of organic and inorganic reactions. It has been shown that the properties of transition metals nanoparticles like high surface energy and high surface to volume ratio make them an attractive candidate for their use as catalysts. As we know this fact that it is highly desirable to increase the rate of reaction and to subsequently increase the yield of the desired products, and catalysis can serve this purpose very well. There

are mainly two major types of available catalysts, i.e. homogenous²¹⁹⁻²²⁰, where the catalyst is in the same phase as the reactants (colloidal) or inhomogenous²²¹⁻²²² (supported) catalyst systems, where the catalyst is in the solid phase with the reaction occurring on the surface. Both systems have their own advantages. For instance, inhomogeneous catalysts are not mixed in the system and can be readily separated but on the other hand the reaction rate is very slow because of the restricted surface area. Meanwhile, homogeneous catalysts have the ability to fasten the reaction to a great extent and therefore provide a good conversion rate per molecule of the catalyst, but as they are miscible in the reaction mixture, it would be difficult to remove them after the reaction. The difficulty in removing homogenous catalysts from the reaction medium leads to problems in retaining the catalyst for reuse. The separation and recycling of the catalyst is highly favorable since catalysts are often very expensive.

Narayanan and El-Sayed²²³ showed in their work that in the case of homogenous catalysis, shape of the nanoparticles has a crucial effect on the reactivity; they showed that the particles having shapes with more corners and edges have high reactivity as compared to those having less corners or edges. Metals which are not at all reactive in bulk form may have very high reactivity when their size reduced to a great extent. For example gold is one of the noble metals available and is not reactive when in bulk form, but the small particles of gold are catalytically more active^{222, 224}.

Chapter 3

Photochemical

Synthesis

of

Ag and Cu

Nanoparticles

3.1 Introduction

Photochemistry is an effective tool for the preparation of metal nanoparticles primarily because of the spatial and temporal control of the light and being really fast in converting the liquid monomers to polymer materials in a desired shape at room temperature under the irradiation of UV-light source. Apart from the utilization of UV-light to create reactive species and to initiate a reaction, a photoinitiator is necessary to add in a system which should be capable enough to absorb enough of the incident light to produce free radicals. With this technique, not only the initiation of reaction can be controlled effectively, also reaction can be stopped easily just by switching off the light²²⁵. Photopolymerization played a very important role in developing polymer chemistry.

This work deals with the photochemical techniques for the synthesis of different noble metal nanoparticles particularly Ag and Cu NPs.

In this work, we followed bottom-up photochemical reduction approach to synthesize in-situ silver and copper nanoparticles in an acrylic resin. We have tried to optimize this process in order to obtain UV-cured conductive films containing these metal nanoparticles.

This chapter provides a brief summary of the photochemical synthesis of noble metal nanoparticles particularly silver and copper. A comprehensive discussion on the work done in order to fabricate and stabilize in-situ generated metal nanoparticles in different solvents and polymeric mediums is described.

3.2 Photochemical synthesis of Ag NPs

The photochemical synthesis of silver nanoparticles in the presence of photoactive agents under UV-light has gained significant interest and attention over the last two decades. ^{22, 47, 96, 226}

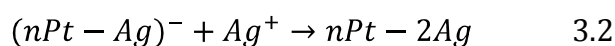
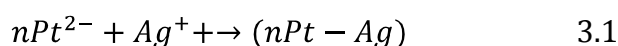
The photoreduction mechanism of silver nanoparticles has been studied by Hada *et. al.*⁶⁴, they proposed the formation mechanism of direct excitation of AgClO_4 in aqueous and alcoholic solution. They determined the quantum yield of reaction in the presence of different alcohols and aqueous solutions. The quantum yield of the reaction in their study increases tremendously in the α -alcohols as compared to the other alcohols.

Y.Yonezawa *et.al.*²²⁷ on the other hand measured the quantum yield of the colloidal silver in the presence of different stabilizers like sodium dodecylsulphate, sodium alginate and colloidal silica, an increase in quantum yield was found in the presence of all the protective agents except for the AgClO_4 -sodium alginate solution.

Silver nanoparticles can also be produced by photoreducing AgNO_3 in the presence of PVP, and citrate-capped Pt seeds was used as a catalyst.²²⁸ The photochemical reaction of citrate in the presence of Pt-nanoparticle seeds is proposed in the following way,

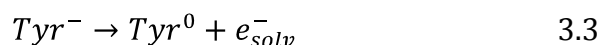


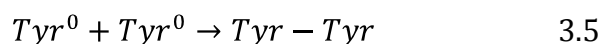
Ag^+ ions upon encountering the Pt nanoparticle seeds react in a following way,



However, by the repetition of the process described in these two reactions, Ag particles can grow on the surface of Pt seeds.

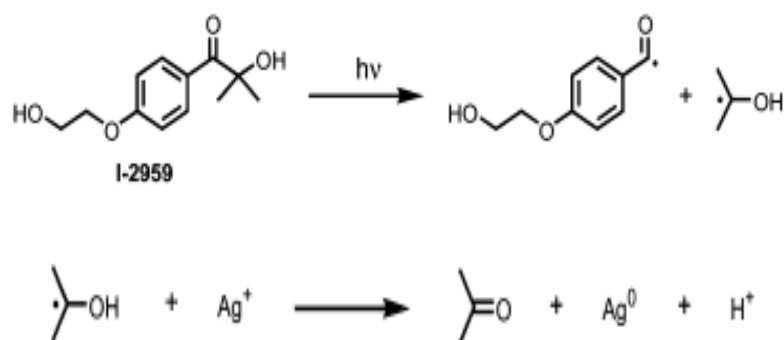
Highly fluorescent silver nanoparticles were photochemically produced by reducing Ag_2SO_4 utilizing water as a solvent with the help of tyrosin which works both as a photoinitiator and as a stabilizer.²²⁹ The formation mechanism of Ag^0 was proposed by P.Kashirsagar *et. al.*²²⁹ with the probability of formation of dityrosine (reaction 3.3) under UV irradiation.

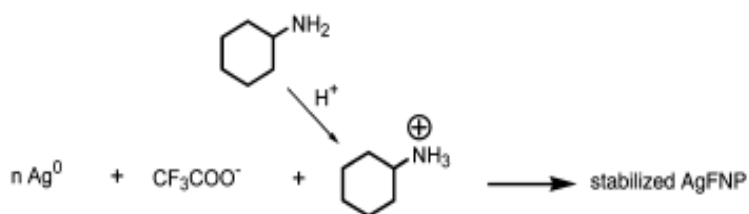




As shown in reaction 3.3, tyrosine radical formed with the release of solvated electrons. These solvated electrons have high probability to photoreduce silver ions to silver metals. The stability was achieved with the help of photo-oxidation products of tyrosine such as dityrosine etc, Ultrafine silver metal particles in the presence of PVP and benzoin was prepared and characterized by T.Ikature et.al.²³⁰ In their study, they determined the effect of the benzoin concentration on the absorption band of silver particles, which shifts greatly to shorter wavelength i.e. from 420 nm to 400 nm with the increase in benzoin concentration. However, with the help of TEM micrographs it was shown that the particle size decrease with increasing benzoin concentration. This result was interpreted by the fact that benzoyl and benzyl radical inject electrons into Ag particles, and the strong repulsion forces can be obtained with the increase in the benzoin concentration.

Highly fluorescent silver nanoparticles (AgFNPs) have also been prepared by facile photochemical method by using ketyl radical i.e. I-2959, and the formation and stabilization of photoreduced AgFNPs was tested in the presence of different amines.²³¹ They proposed mechanism of the formation of silver nanoparticles is shown below.





The formation and stabilization of Ag particles was tested with and without the presence of different amines like cyclohexylamine, hexadecylamine, triethylamine, butylamine. However, the best results obtained were in the presence of cyclohexylamine and hexadecylamine (shown in Figure 19).²³¹

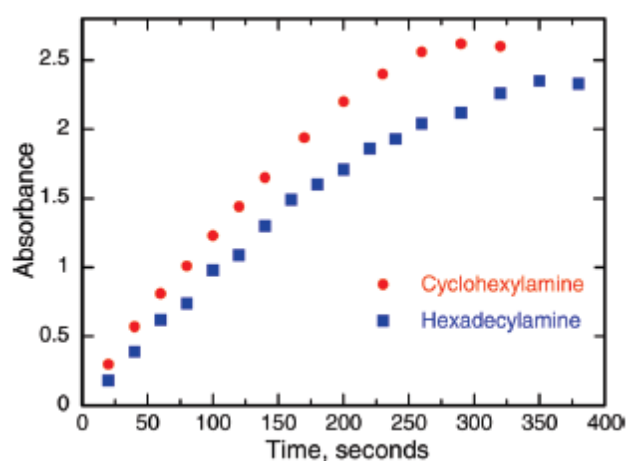


Figure 19 Growth of absorbance band by UV-irradiating silver trifluoroacetate in the presence of cyclohexylamine and hexadecylamine²³¹

Absorbance spectra in the presence of cyclohexylamine and hexadecylamine in toluene as a solvent are shown in Figure 19.

Silver nanoparticles were prepared by photoreducing the AgBr solution by using ascorbic acid as a reductant.²³² Effect of the different concentrations of ascorbic acid on the Plasmon absorption of the obtained silver nanoparticles was studied with the help of UV-vis spectra. Photoreduction of silver bromide in the presence of ascorbic acid is shown in Figure 20

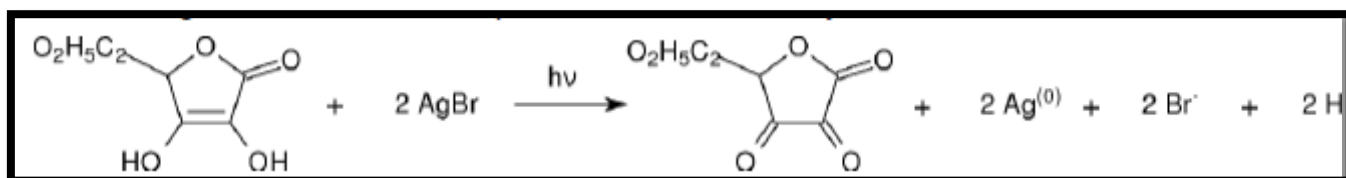


Figure 20 Photoreduction of silver bromide in the presence of ascorbic acid²³²

The absorption peaks of the obtained silver nanoparticles with the different molar ratios of AgBr:reductant i.e. 1:1.5, 1:3, 1:4.5, 1:9 are at 429 nm, 428 nm, 419 nm, and 389 nm. The decrease in the wavelength of the absorption peaks with the increase in the molar ratio of AgBr:reductant may be due to the decrease in the particle size of the silver particles. An additional absorption in the wavelength with the increase in the molar ratios of silver bromide to ascorbic acid may be due to the very large aggregates of the silver particles.

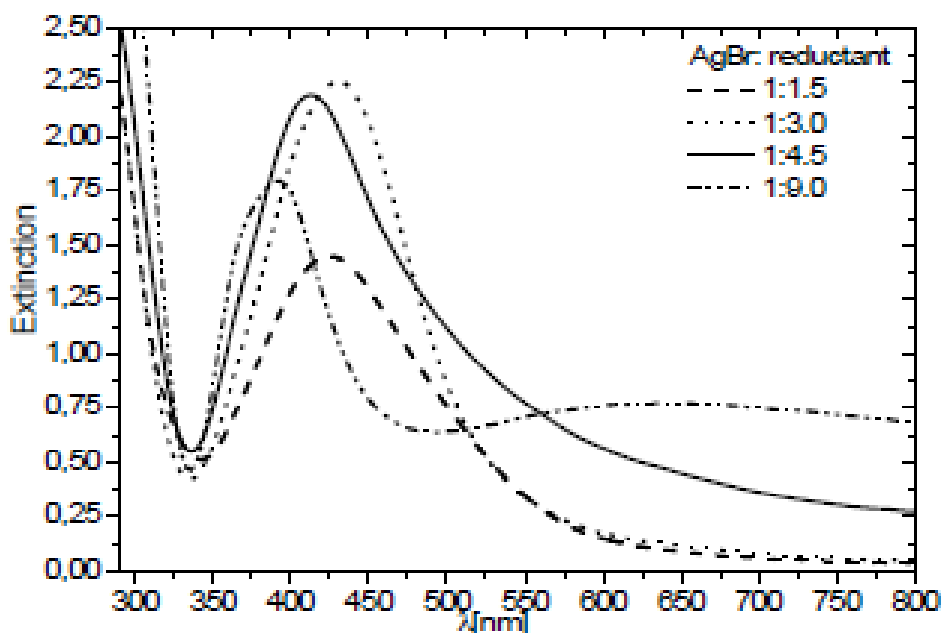


Figure 21 UV-vis spectra of silver nanoparticles by changing molar ratios of AgBr/ascorbic acid²³²

The silver particles were stabilized by adding gelatin, and the stability of the obtained particles was monitored with the help of UV-vis spectra. UV-Vis spectra of

the stored solutions were performed three times, at different times: after finishing of synthesis, after 48 hours and after 48 days following the finish of silver nanoparticles synthesis.

As can be seen from Figure 22, there is no change in the absorption wavelength of the particles even after 48 days since their formation. It implies that the size of particles remains constant. According to literature,²³² the shift in the absorption peak with the passage of time show an increment in the size of the particles. Hence, it can be stated that gelatin used as a protective agent in the dispersion systems containing silver colloids feature a sufficiently high stability.

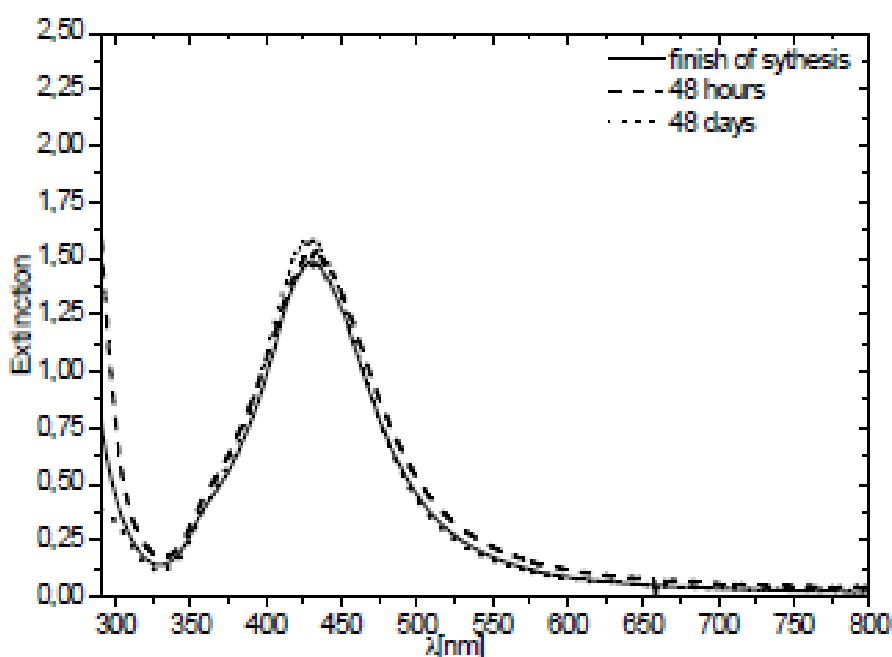
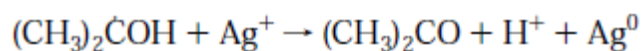
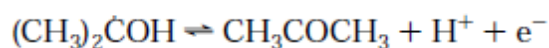
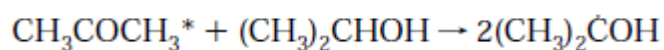


Figure 22 UV-vis spectra of stabilized silver nanoparticles after 48 hours and after 48 days²³²

A simple photochemical reduction technique to synthesize silver metal particles and the effect of the various polymer stabilizers was observed by A. Henglein.⁴⁸ With the help of UV-irradiation, ketyl radicals were generated with the excitation of acetone and subsequent abstraction of hydrogen from 2-propanol (shown in reaction). These generated ketyl radicals are strong reductants, and they react further with Ag^+ ions.



The effect of the addition of different polymeric stabilizers (polyethyleneimine, sodium polyphosphate, sodium polyacrylate, and polyvinyl pyrrolidone) was checked. The narrowest size distribution with the best optical properties was obtained using polyethyleneimine.

Silver/polypyrrole core shell nanoparticles in the presence of PVP were produced by one step UV-induced polymerization.²²

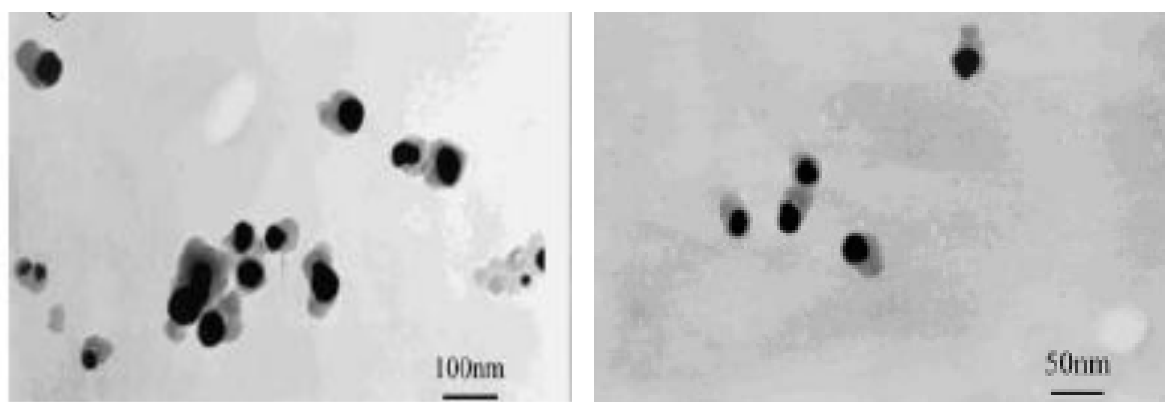


Figure 23 TEM image of silver/polypyrrole core shell nanoparticles²²

With the addition of PVP, it was observed that the core shell structure of silver/polypyrrole formed instead of silver/polypyrrole mixture as shown in Figure 23. Silver nanoparticles in the range of 10-40 nm were produced.

3.3 Photochemical synthesis of Cu NPs

As compared to other noble metal nanoparticles, synthesis of copper nanoparticles is the most challenging task since copper nanoparticles are fairly unstable in ambient conditions. However, copper is much cheaper than other available noble

metal nanoparticles including silver, also possesses reasonable conductivity²³³ (6% less than that of Ag), therefore, it is economically attractive. It is an inexpensive metal²³⁴ but like other noble metals, it possesses electronic²³⁵, catalytic²³⁶, antimicrobial²³⁷ and optical properties²³⁸. Apart from its useful properties the main challenge to use them in practical applications lies in their inherent tendency to oxidize when exposed to air²³⁹⁻²⁴⁰ and aggregation of nanoparticles which may give rise to unwanted properties of the particles²⁴¹. The formation of oxides on the surface of the nanoparticles give rise to a major problem i.e. the reduction in electrical conductivity and therefore restricts their use in conductive printing applications²³³. There are different techniques reported since 1990s to synthesize copper nanoparticles; including chemical reduction in solution by using hydrazine²³⁸, sodium citrate²⁴², polyol²⁴³ and sodium borohydride²⁴⁴, electrochemical deposition²⁴⁵, and photochemical reduction^{56, 230,246}. There are different approaches to protect the metal particles by hindering the oxygen penetration to the surface of these particles, and to prevent agglomeration and coagulation processes. A protective thin layer of silica has been in use to avoid the interaction of oxygen molecules with the nanoparticle surface and to prevent the nanoparticles from aggregating and contacting each other. A lot of work has been done to protect the noble metal particles by coating their surfaces with silica layer²⁴⁷⁻²⁵¹. However, Kobayashi *et al.*²⁵³ prepared Cu nanoparticles in aqueous solution by chemical reduction method and reported the stability of copper nanoparticles in an open atmosphere for at least one month with the help of silica coating. A more commonly employed technique to stabilize the metal particles is with the help of surfactants, they may avoid the aggregation of the particles by binding themselves to their surface. Size and shape of the Cu NPs may be controlled by using different surfactants like oleic acid²⁴⁰, alkanthiols²⁵³, sodium dodecyl sulphate²⁵⁴, CTAB²³⁹ etc.

Another promising approach to stabilize the Cu NPs is to use polymers as capping agents. Among these polymers, poly (N-vinylpyrrolidone) (PVP) has been widely used as a capping agent for the stabilization of nanoparticles^{56, 241,255}. Jeong *et al.*²⁵⁶ demonstrated the effect of the weight of PVP on the size of the Cu NPs, and thereby

confirmed that there is a direct relation between the mol. wt. of PVP and the particle size of NPs, which in turn determines the electrical conductivity of the film formed. Kobayashi *et al.*²³⁴ employed a conductive polymer i.e. polypyrrole to chemically stabilize copper nanoparticles, and hence those particles coated with polypyrrole proved to be chemically stable even in the air for at least 50 days.

The simplest and more economical among all the above mentioned techniques is the use of UV-irradiation to reduce metal salts in the presence of any suitable photoinitiator. Only a limited data is available on this technique to synthesize and to stabilize copper nanoparticles.

S.Kapoor *et al.*⁵⁶ reported for the first time the photochemical fabrication of copper nanoparticles by using PVP as a capping agent. S.Kapoor *et al.*^{56,257} photosynthesized copper nanoparticles with the help of CuSO₄ by using the free radicals produced by the photoinitiator (Benzophenone), in the presence of stabilizers PVP and gelatin respectively. They studied the effect of the presence of Benzophenone (BP) on the formation of Cu nanoparticles, and the size of Cu nanoparticles obtained was shown to be 15 nm. The experimental results show there is no effect on the size of copper particles, with the change in the CuSO₄ concentration. However, with the change in PVP concentration a change in the particle size of the copper particles was observed as shown in Table 3.2

Table 3.1 Dependence on Cu size particles with the PVP concentration

PVP (wt %)	Absorption band (nm)	D (nm)	σ
0.1	565	20	7.2
0.25	565	18	4.5
0.5	565	15	4.0

Ikatura *et al.*²³⁰ determined the suitable conditions for the photoreduction of (Cu (ClO₄)₂) in an ethanol solution. The photoreduction from copper ion to copper metal was only observed both in the presence of benzoin and UV-light, a distinct peak of

copper colloid was observed at 570 nm. Absence of any one of this variable would not result in the photoreduction of the copper ion. The effect of the different concentrations of benzoin on the absorption spectra of the obtained copper particles (shown in Figure 24) shows an increase in the absorption peak at 570 nm with the increase in benzoin concentration. In the absence of benzoin no peak is observed.

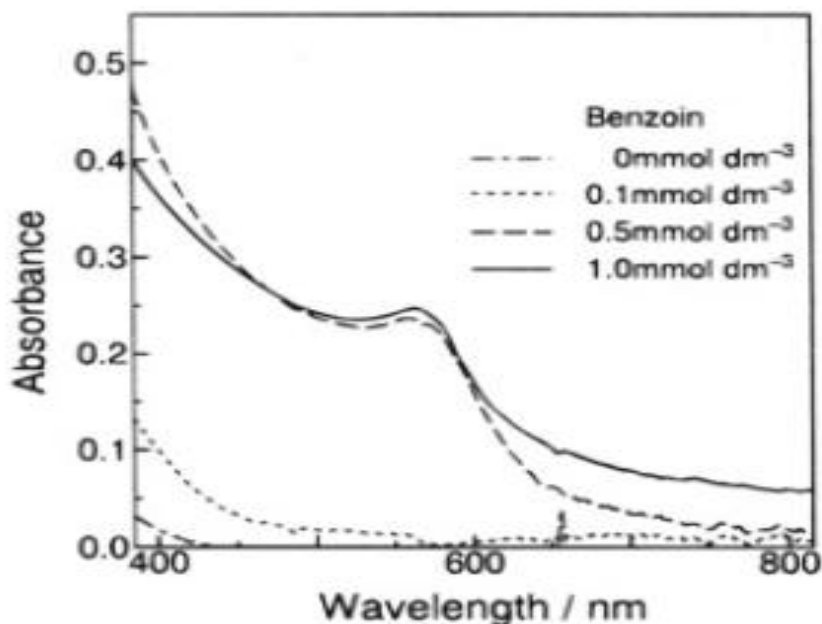
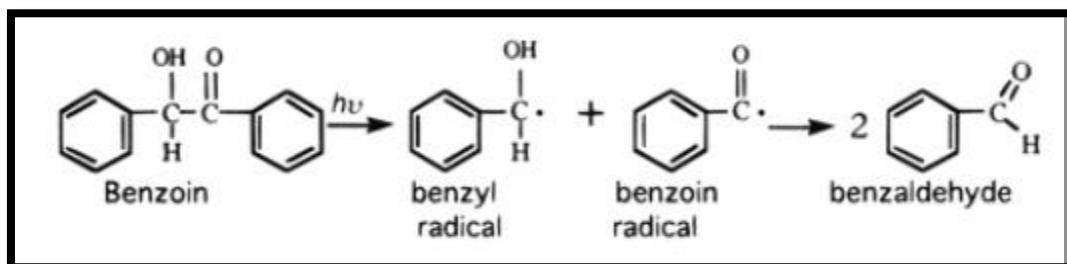


Figure 24 Change in the UV-vis absorption spectra of $(\text{Cu}(\text{ClO}_4)_2)$ in an ethanol solution irradiated for 60 mins²³⁰

The above results imply that benzoin works efficiently for promoting the photoreduction of copper ions via photolytically produced benzoyl and benzyl radicals or benzaldehyde. The α -cleavage of benzoin is as follows:



Giuffrida *et al.*²⁴⁶, reported two step photochemical route to fabricate colloidal copper in an ethanol solution. The photoreduction of copper complex $\text{Cu}(\text{acac})_2$ in their report underwent photoreduction in two steps. First the complex $\text{Cu}(\text{acac})_2$ absorbs UV light, Hacac released and copper(1) alkoxides formed, then with the release of acetylacetone with an electron transfer, colloidal copper obtained. The photoreduction of copper complex was investigated in the presence of PVP, and the data collected by characterizing the obtained copper nanoparticles show that the added PVP can play two roles i.e. of a sensitizer and can act as a surfactant, and 0.05M concentration of PVP was enough to obtained particles in the range of 4nm.

Zhu *et al.*⁵⁰ used $\text{CuCl}_2 \cdot 2\text{H}_2\text{O}$ to prepare Cu nanoparticles and Cu patterned surfaces in the presence of amine by using the free radicals produced by the photolysis of photoinitiator Irgacure 184 under UV-irradiation.

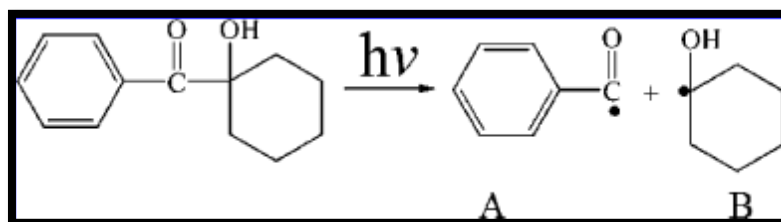


Figure 25 Photolysis of photoinitiator under UV-irradiation⁵⁰

They studied the photoreduction phenomena by UV-vis spectroscopy and gas-chromatography–mass spectrometry. In order to improve the size of the obtained particles, polymeric capping agent i.e. PVP was added to the solution which not only helps in reducing the particle size but also assists in narrowing the particle size distribution of the copper nanoparticles obtained in an ethanol solution.

Copper nanoparticles obtained by radiation induced synthesis technique in the presence of PVA (Poly-vinyl alcohol) as a stabilizing agent, were characterized by UV-vis absorption spectra. The absorption peak shifted towards higher wavelength (i.e. to 590 nm from 575 nm) with the decrease in the PVA concentration. This shift in absorption wavelength relates to the increase in particle size with the decrease in the PVA concentration.^{211-a}

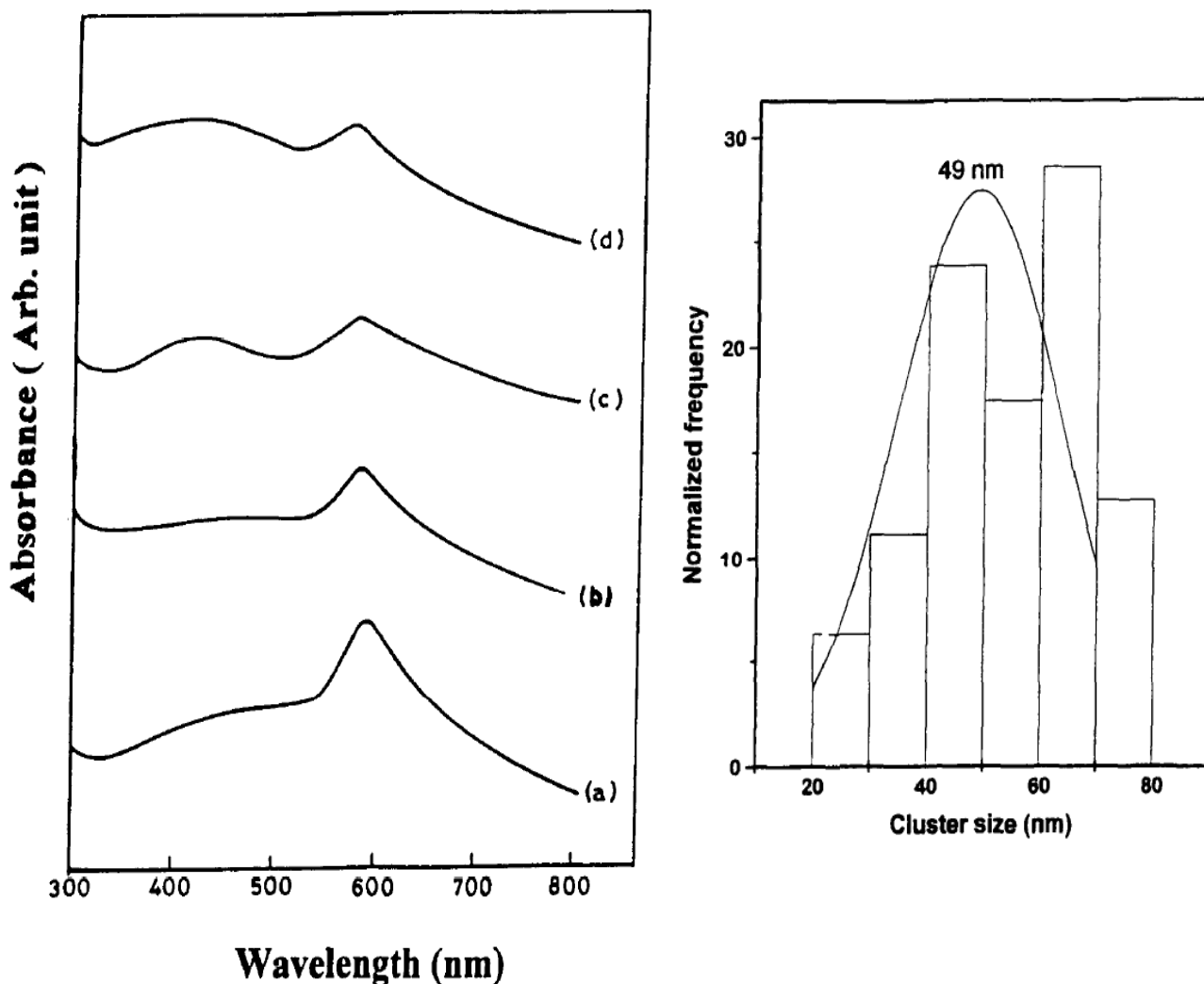


Figure (26-a) UV-vis spectra of copper nanoparticles in the presence of 5×10^{-3} M CuSO_4 , 2×10^{-1} N 2-propanol, in different concentrations of PVA, (a) 0.79, (b) 1.5, (c) 2.3, (d) 3.4×10^{-2} M. (26-b) Histogram of Cu particles in the presence of 5×10^{-3} M CuSO_4 , 2×10^{-1} N 2-propanol, 3.4×10^{-2} M PVA^{211-a}

In their experimental work, S.S. Joshi *et al.*^{211-a} proved with the help of TEM and XRD analysis, which with the addition of PVA as a capping agent, stabilized copper nanoparticles in the range of 49nm were obtained.

3.4 Polymer-metal nanocomposites

The polymer nanocomposites are one kind of composite materials comprising mainly of nanometer-sized inorganic nanoparticles, in the range of 1-100nm²⁵⁸⁻²⁵⁹. The first reported polymer nanocomposite in the literature is by Lüdersdorff^{5-a}. A gold salt was reduced in the presence of gum arabic, and as a result nanocomposite in the form of purple solid was obtained, by co-precipitating gum arabic and gold together in ethanol.

A substantial rise in the fabrication of polymer-metal nanocomposite is observed from the last two decades. A dramatic increase in the interest of the preparation of Polymer matrix composites is due to their unique optical, catalytic, electric and magnetic properties^{260-262, 83-86}.

Considerable change in properties can be observed with the reduction in size and by carefully designing metals with important cooperative physical phenomena such as superparamagnetism, size-dependent band-gap⁹⁰, but the limitation in their use is a high manufacture expense.¹¹⁴ However, polymers are known to be flexible, lightweight materials and can be produced at a low cost. They are also known to allow easy processing and can be shaped into thin films by various techniques such as dip-coating, spin-coating, film-casting, and printing.⁹⁰

Generally, there are two approaches which can be used to synthesize nanoparticles in a polymer matrix i.e. *in-situ* and *ex-situ* techniques (as discussed in Section 2.4 of Chapter 2)

However, because of the objective of this work, the discussion will be entirely devoted to the *in-situ* photochemical synthesis of silver and copper nanoparticles embedded in a polymer matrix.

3.4.1 Polymer nanocomposites embedded by Ag particles

The main goal in carrying out this research was *in-situ* photo synthesis of silver NPs in an acrylic resin in order to increase the electrical conductivity of the resultant polymer nanocomposite. Two main strategies can be followed to enhance the

electrical conductivity of a photo cured material: by a top-down approach conductive filler is homogeneously dispersed within the polymeric matrix reaching a percolation threshold and therefore a low surface resistivity²⁶³⁻²⁶⁸ alternatively a bottom-up approach can be pursued, where metallic conductive nanoparticles are generated in-situ during the photopolymerization process.^{269-270,97,88} In the bottom-up process, while metal nanoparticles are formed by electron transfer from the photochemically generated free radical to the salts, polymerizations are initiated by free radicals or carbocations thus formed depending on the type of monomers and photoinitiating system used in the formulation. However, despite the success of the process, it is possible to reach conductive behavior only for large metal particles precursor contents, which would affect strongly the processability and cost of the formulations.^{264-265,271}.

Another way to gain electrical conduction is the use of conducting conjugated polymers: their preparation by photochemical means has scarcely been investigated although, in particular those based on pyrrole and derivatives, are extensively used in the fabrication of electronics and electro-optic devices due to the characteristic electronic and optical properties.²⁷² Yagci and co-workers²⁷³ demonstrated that polythiophene can be obtained by UV-irradiation using onium salt as light absorbing compound. Sangermano *et al.*²⁷⁴ described a novel methodology for fabricating conductive epoxy-polythiophene network films by simultaneous photoinduced step-growth and cationic ring opening polymerization processes.

The dielectric constant of in-situ photochemically synthesized Aluminum/epoxy composites was measured by J.Lu *et al.*⁹⁵ with and without the presence of Ag particles. The results show an increase of 50% of dielectric constant for the composites containing Ag particles (shown in Figure 27).

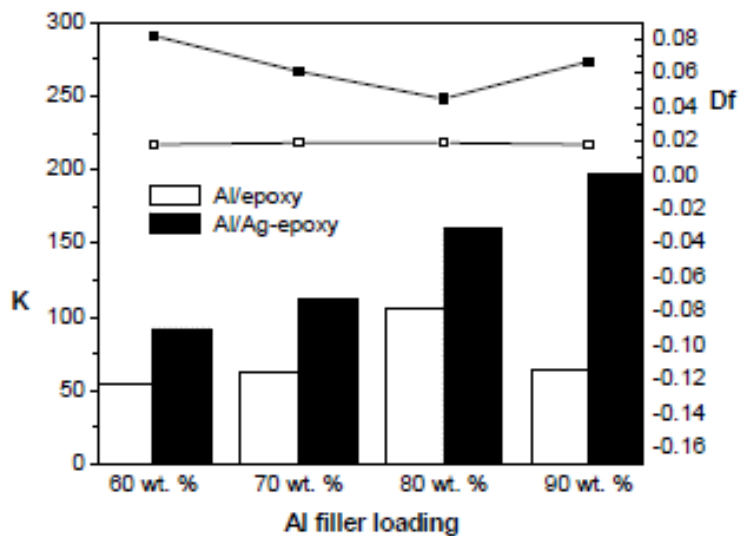


Figure 27 Dielectric properties of Al/epoxy and Al/Ag-epoxy composites with different Al filler loading⁹⁵

Based on the results, it was suggested that Ag-polymer nanocomposites prepared via photochemical approach can be employed as a high-K polymer matrix to host various fillers such as conductive metal or high dielectric constant ceramic filler

Ijjeri *et al.*⁴⁷ proposed the preparation of conductive films by an in-situ reduction of a silver salt in the presence of pyrrole and a UV-curable monomer. They obtained the polymer matrix free radical photopolymerization, while simultaneously, under UV exposure, the silver nitrate oxidized pyrrole to polypyrrole and reduced itself to metallic state. With this technique a high surface conducting polymer composite could be achieved thanks to the conductive conjugated polymer (polypyrrole) and the uniform distribution of silver metal particles. In this study, we demonstrated the effect of the presence of the pyrrole concentration on the preparation of silver nanoparticles.

Silver particles were synthesized in the epoxy resin by exposing them to UV light.⁹⁵ Furthermore, a lot of literature has been published on this technique as it is very

efficient, easy and less expensive than the other available techniques^{57,96}. The effect of the silver particles content on the dynamics and relaxations of the polymeric chain and on the electrical properties of the epoxy/silver nanocomposites was observed by G.Kortaberria et.al.²⁷⁵ With the increase in silver precursor, a decrease in the glass transition temperature was observed, the reason behind this may be due to the presence of solvent which acts as a plasticizing agent. The evolution of the parameters shows that the percolation threshold was not achieved even for the maximum amount of silver precursor i.e. 20%. The evolution of dielectric constant, $\tan\delta$ and AC conductivity with nanoparticle content at room temperature and several frequencies ranging from 1 kHz to 1 MHz is shown in Figure 28

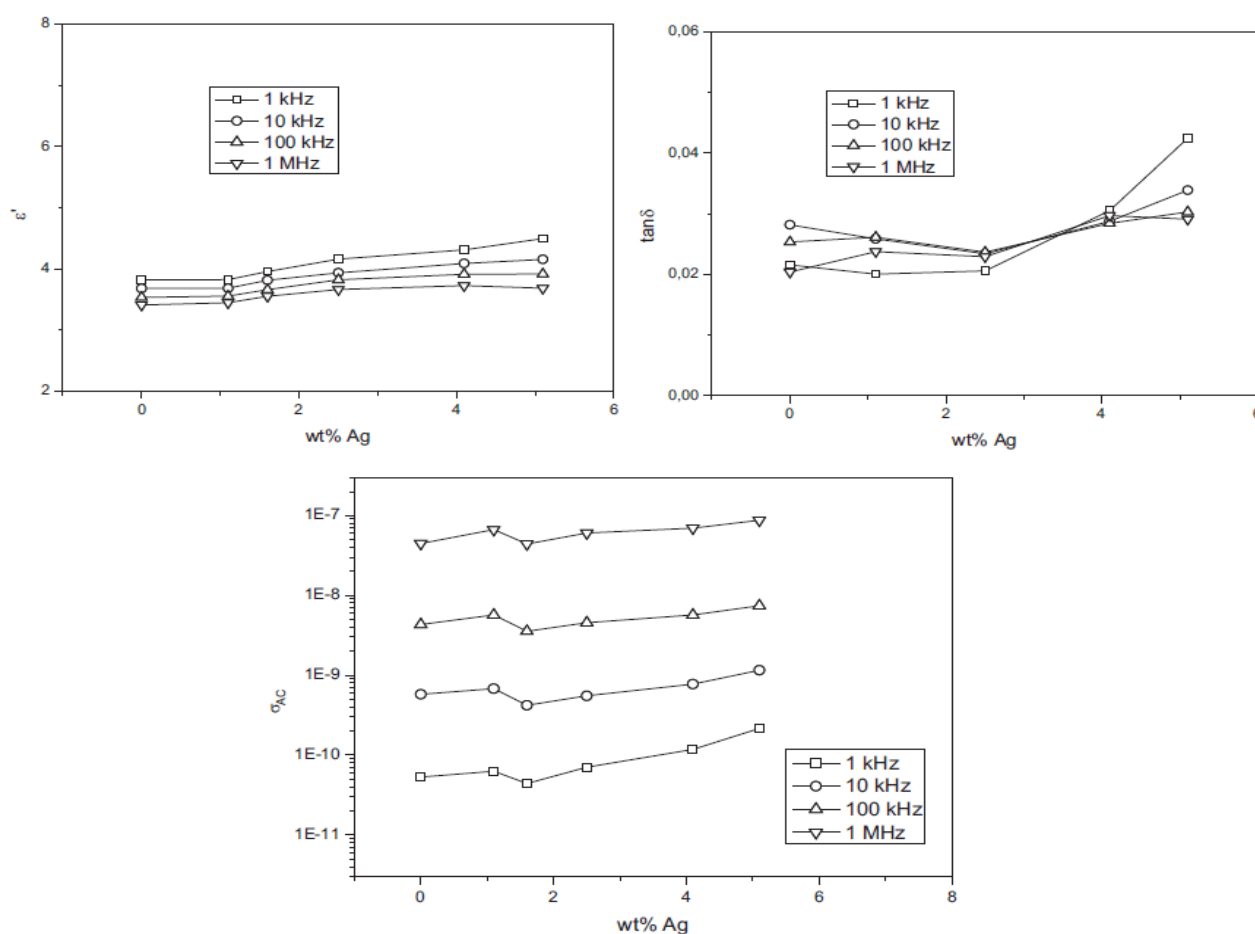
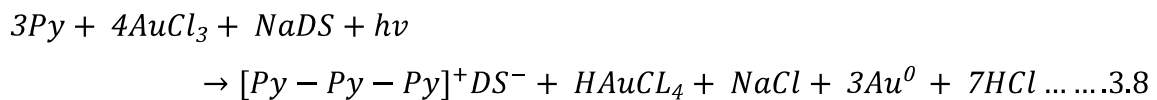
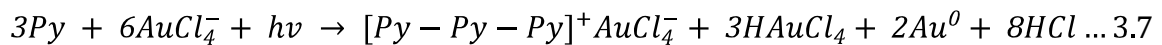


Figure 28 Evolution of dielectric constant, $\tan\delta$ and AC conductivity with nanoparticle content at room temperature and several frequencies ranging from 1 kHz to 1 MHz²⁷⁵

Noble metal nanoparticles like Ag, Au, Cu etc can be in-situ synthesized in a one step photochemical method.^{47, 49-50, 53-54, 56, 97} to incorporate electrical conductivity in insulating polymers.

A good amount of information is available on this subject. For example, the function of silver nanoparticles incorporated in a photo chemically produced polymeric films i.e. polypyrrole was observed in terms of electrical conductivity by M. A. Breimer *et. al.*⁹⁶ They found the electrical conductivity of the silver nanoparticles dispersed in polypyrrole films to be 3×10^{-2} S/cm², which appears to be quite in good agreement with the value available in literature.



The aim of this work was to produce electrically conductive UV-cured films by irradiating an acrylic difunctional monomer in the presence of silver nitrate, pyrrole, and a photoinitiator.

Among different available conducting polymers, polypyrrole is one of the most promising as it offers different effective properties like conductivity, chemical stability and some other^{96-a}. The conductive behavior of polymers in general is attributed to their conjugated structures, which may help in transporting the charge electrons. In the last century, discovery of conducting polymer (polyacetylene) has changed the face of the science and therefore role of the polymers have changed drastically. Akamatu et al.^{96-b} discovered the electrical conductivity in molecular charge transfer complexes which is a cause to promote the development of conducting polymers.

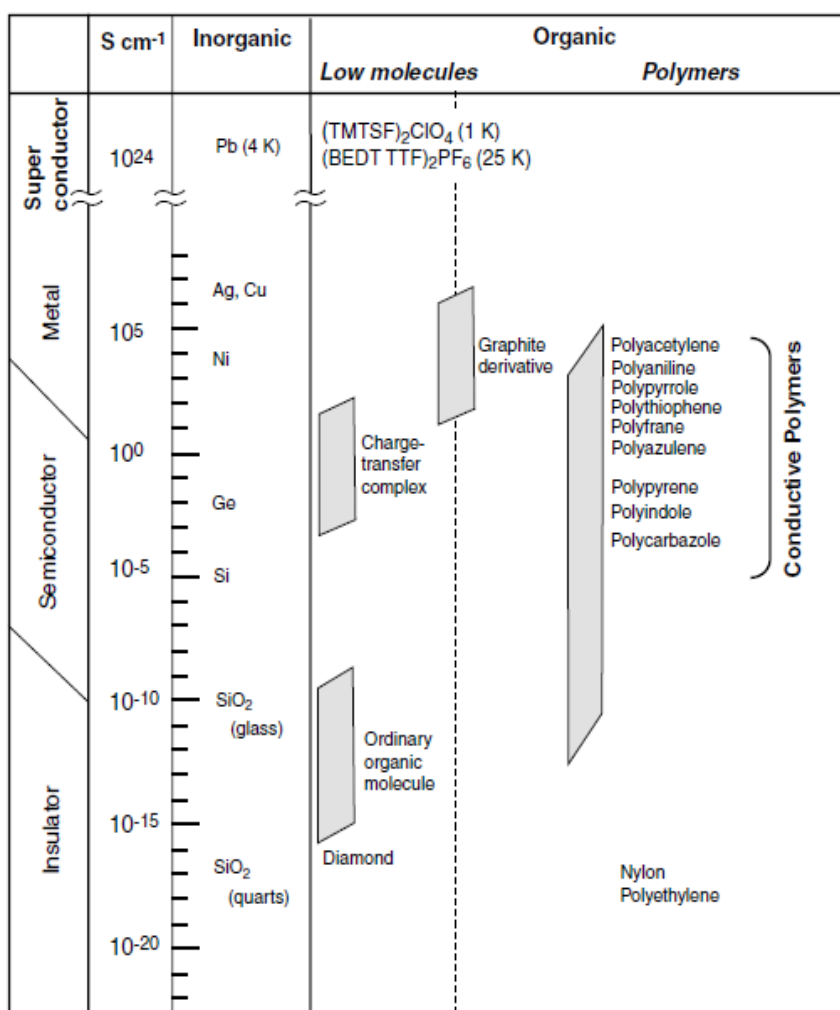


Figure 29 Conductivities of different materials (conductors, semi-conductors, insulators and superconductors) with comparison with the conducting polymers.^{96-c}

This breakthrough opens up the possibility of utilizing these lightweight and flexible polymers in different electronic devices. A lot of different other conjugated conducting polymers have been synthesized since then, and work in this field is still very dynamic. These conjugated conducting polymers have conductivities in the range of 10^{-10} to 10^5 S/cm as shown in Figure 29.

The charge associated with the oxidized state of the polypyrrole is delocalized over pyrrole units and form a radical cation (polaron) or a dication^{97-a} as shown in Figure 30. A polaron may be a radical cation (oxidation) or a radical anion (reduction). Theoretical studies show that the polaron states of polypyrrole are located about 0.5eV from the band edges. A polymeric chain having a polaron when subjected to further oxidation, an electron may be removed from the polaron or from the rest of the chain. In the former case, a polaron radical is removed and two new positive charges form. While in the second case, two polarons are formed.

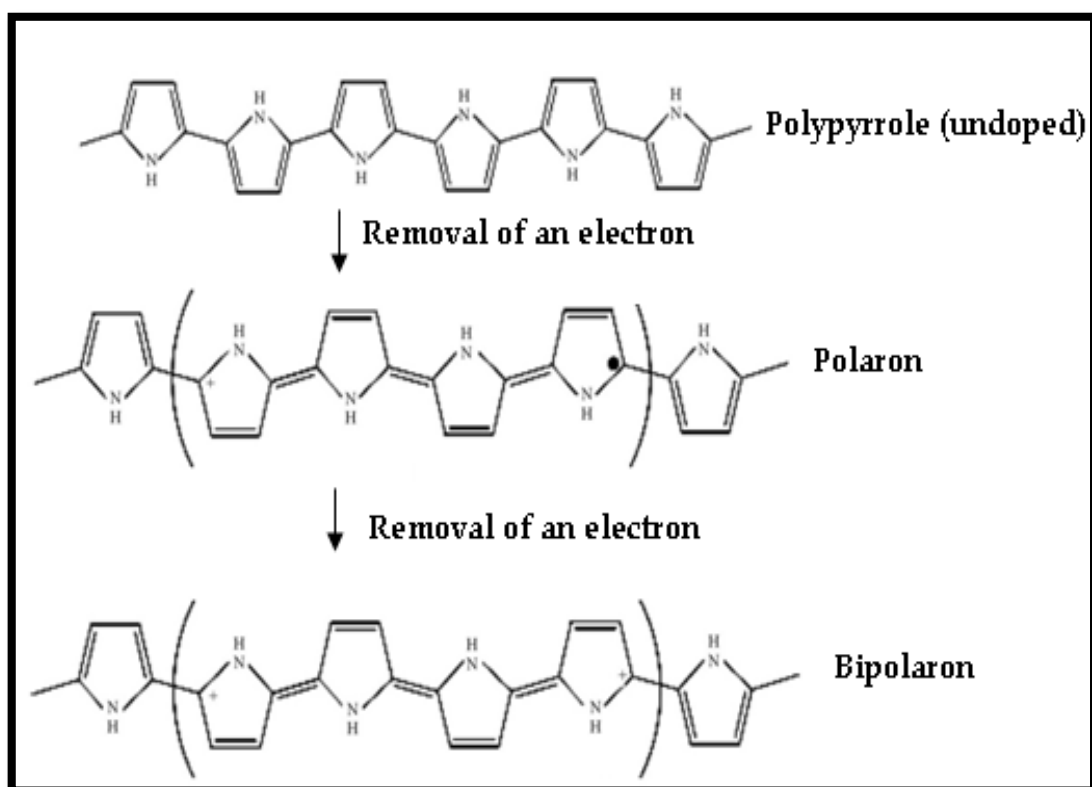


Figure 30 Conduction mechanisms in Polypyrrole^{97-b}

The formation of bipolaron causes the further reduction in ionization compared to two polarons, hence proving that formation of bipolaron is thermodynamically more favorable. The quantum chemical calculations showed the lesser value of bipolaron energies i.e. 0.4eV.^{97-b}

In this work we have tried to optimize the process of producing a conductive UV-cured film containing polypyrrole and silver particles. First of all, we investigated the reduction of the silver salt dissolved in a solvent as a function of the irradiation time, presence of pyrrole, and monomer/salt ratio. The size and morphology of the particles was studied. We repeated the process using a difunctional acrylic monomer, thus forming films whose conductivity was significantly increased. (will be discussed in Section 5.3)

3.4.2 Polymer nanocomposites embedded by Cu NPs

Giuffrida *et al*²⁷⁶ devised a novel technique to prepare nanoparticles and films, both were prepared from a bis (2, 4-pentanedionato) copper (II) [Cu-(acac)₂] ethanol solution under UV irradiation at 254 nm by controlling the homogeneous versus the heterogeneous nature of the formation process. This reaction depends primarily on the UV absorption of Cu (acac)₂. The hemolytic cleavage of the Cu–O bond is caused by the irradiation of the ligand-to-metal charge-transfer band. The photoreaction was completed after more than 4.5 h when the concentration of the Cu (acac)₂ ethanol solutions was 10⁻⁴M.

Zhu *et. al.*⁵⁰ prepared copper film and copper patterns directly on the transparent substrate. In their test, copper particles were grown directly on the surface of polyester film by contacting the film with the CuCl₂-amine coordination complex when it is irradiated.

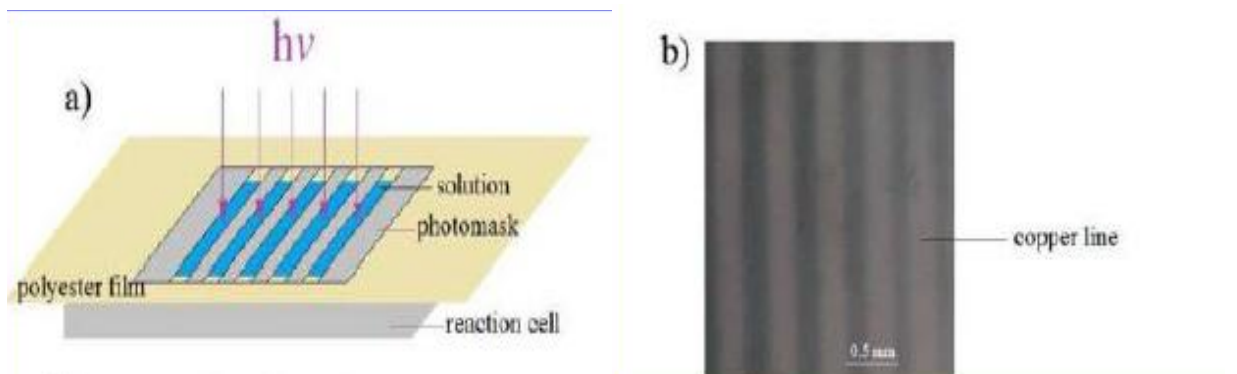


Figure 31 Direct pattern formation on the polyester film by UV-irradiation (b) Microscopic image of the copper pattern⁵⁰

The copper pattern formed directly on the surface of the film by UV-irradiating for 10 minutes. The image of the copper stripes was obtained by optical microscopic image as shown in Figure 31.

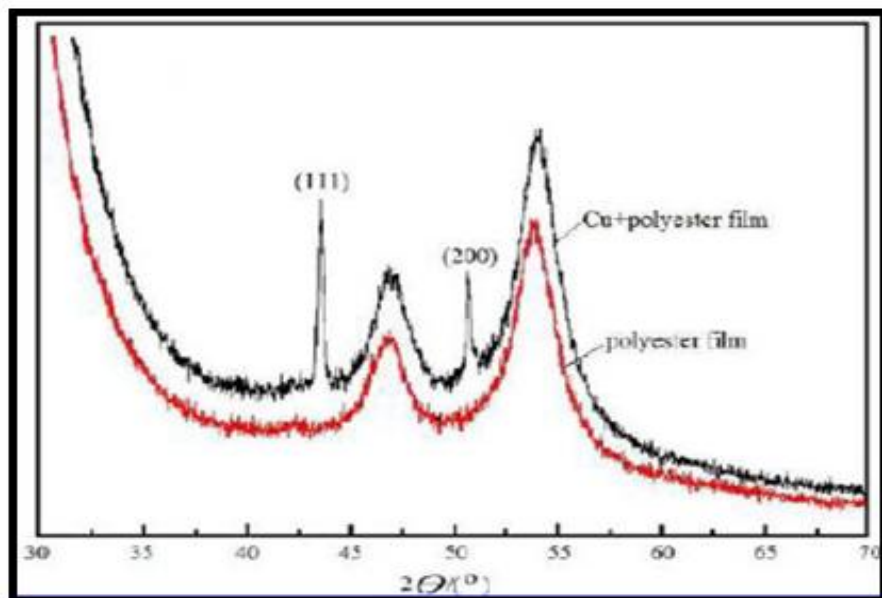


Figure 32 XRD pattern of the copper pattern on the polyester films⁵⁰

The first work reported by K. Mallick^{50-a} describing a single step synthetic way to prepare polymer-copper based nanocomposite by using copper sulphate as a salt, whereas o-toluidine used as a precursor. In their work, during the reaction o-

toluidine was oxidized and forms poly (o-toluidine), while on the other hand cupric sulfate gets reduced and forms copper nanoparticle. The conductivity of Cu-poly (o-toluidine) was found to be 10^{-3} S/cm⁻¹, measured by four probe method.

Chapter 4

Materials And Characterization Techniques

4.1 Objective

The aim of this work is to fabricate electrically conductive polymers by using noble metal nanoparticles with the help of one step free radical photopolymerization technique. In a systematic way, first the effect of UV-irradiation was observed on the silver and copper based ethanol solutions. After synthesizing and characterizing these MNPs based solutions; the next step carried out was to investigate the contemporary acrylic resin crosslinking reaction and consequently in-situ generation of these nanoparticles.

The protocol of the work done here to obtain UV-cured conductive polymeric films is same for both type of metal salts used: initially photoreduction of the ethanol solution containing silver and copper salt under UV irradiation was carried out. The production of metal nanoparticles in ethanol was confirmed with the help of different characterization techniques like UV-vis spectroscopy, XRD and TEM analysis after this, the same process was repeated in an acrylic media i.e. difunctional acrylic monomer, thus obtained the metal embedded UV-cross linked polymeric films. The structural and morphological properties of incorporated metal nanoparticles were examined with respect to the role of the metal ions, time of UV-irradiation, monomer/salt ratio.

4.2 Experimental Setup

In this chapter, materials and instruments used to carry out this research are presented. The materials used for synthesis of silver and copper nanoparticles, the detailed procedure of the synthesis technique are given in separate sections (4.3, 4.4). Finally the equipments used for their characterization is listed at the end.

4.3 Materials and Synthesis of Silver nanoparticles

4.3.1 Materials

Polyethylene glycol di acrylate (PEGDA) having an average molecular weight of 700 was purchased from Aldrich. Silver Nitrate (AgNO_3) (99.5%), Pyrrole ($\text{C}_4\text{H}_5\text{N}$, 98%), Polyvinyl pyrrolidone (PVP) ($M_w = 40,000$ g/mol), Ethanol ($\text{C}_2\text{H}_5\text{OH}$) were obtained from Aldrich. The free radical photoinitiator used was 2-hydroxy-2-methyl-1-phenylpropan-1-one (Darocur 1173) provided by BASF. All of the chemicals were used as such without any further purification.

4.3.2 Synthesis of Ag NPs from ethanol solutions

Solution of AgNO_3 in ethanol were prepared by mixing different concentrations of silver salt (5wt%, 10wt%, 20wt %) in the presence of photoinitiator (0.002%w/v) with and without the addition of pyrrole (2wt %). Each resulting solution was irradiated for different intervals of time (1min, 3min, 5min and 10min) under UV light at a radiation intensity of $45\text{mW}/\text{cm}^2$ under nitrogen.

After confirming the formation of silver particles with and without the presence of 2wt% pyrrole in the presence of different concentration of silver salt. We tried to stabilize the obtained silver particles against aggregation and nucleation.

We demonstrated the effect of the PVP concentration on the preparation of stabilized, homogenously dispersed silver nanoparticles in ethanol. For this reason, solution of 10wt% AgNO_3 in ethanol was prepared in the presence of photoinitiator (0.002%w/v) with and without the addition of pyrrole (2wt %). And at the end, different concentrations of PVP (1wt%, 2wt%, 4wt%, 6wt%, 8wt%, 10wt %) were added respectively in order to characterize the obtained particles in terms of their stability. Each solution was UV-irradiated at an intensity of $45\text{mW}/\text{cm}^2$ under nitrogen for different irradiation times i.e. (1min, 3min, 5min and 10min).

4.3.3 Synthesis of polymeric composites embedding Ag NPs

Polymer composites were prepared by dissolving different concentrations of AgNO_3 (5wt%, 10wt%, 20wt %), pyrrole (2wt %) and photoinitiator (2wt %) in the PEGDA oligomer. The resulting formulation was coated on glass substrates (film thickness 100 μm) and exposed to UV light at a radiation intensity of 45mW/cm² under nitrogen for the necessary time to assure curing as depicted in Figure 33.

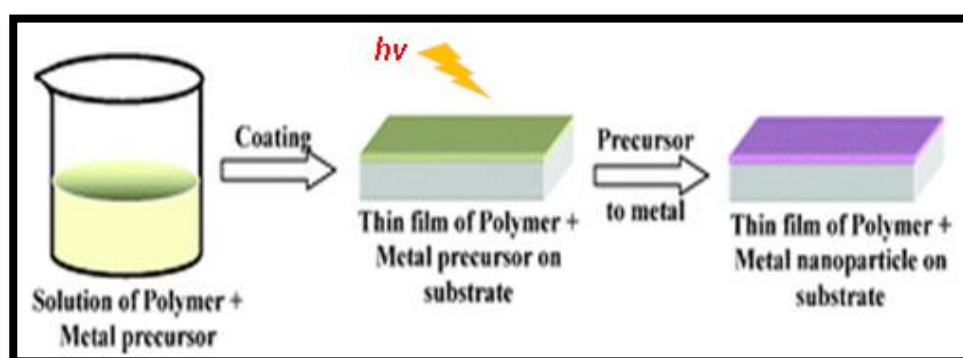


Figure 33 Block Diagram of the UV-curing process

In order to stabilize and to observe the effect of adding PVP on the particle size and size distribution of the silver particles obtained in an acrylic resin.

Based on the experimental results obtained by adding different concentrations of PVP in an ethanol solution containing silver particles. We chose to work with the two different concentrations of PVP i.e. (1wt % and 2wt %). The polymeric formulation was prepared by adding AgNO_3 (10wt %), pyrrole (2wt %) in the PEGDA oligomer. After this, 1wt% and 2wt% PVP was added and mixed in the same formulation with the help of ultraturax by mixing them for 2 minutes respectively. At the end photoinitiator (2wt %) was added. The resulting formulation was coated on glass substrates (film thickness 100 μm) and exposed to UV light at a radiation intensity of 45mW/cm² under nitrogen for the necessary time to assure curing.

4.4 Materials and synthesis of Copper nanoparticles

4.4.1 Materials

Polyethylene glycol di acrylate (PEGDA) having an average molecular weight of 700 was purchased from Aldrich. Copper chloride dihydrate ($\text{CuCl}_2 \cdot 2\text{H}_2\text{O}$) and Copper Sulphate ($\text{CuSO}_4 \cdot 5\text{H}_2\text{O}$) were used as copper precursors; Diethanol amine (DEA), methanol and ethanol were purchased from Aldrich. Benzophenone (BP) was supplied by BASF. PVP ($M_w=40,000$ g/mol) and Pyrrole ($\text{C}_4\text{H}_5\text{N}$, 98%) were purchased from Aldrich. Sodium ascorbate was purchased from Aldrich. Different photoinitiators used i.e. Camphorquinone (4,7,7-trimethylbicyclo[2.2.1]heptane-2,3-dione), Darocur TPO (Diphenyl (2,4,6-trimethylbenzoyl)- phosphine oxide), Darocur 1173 (2-Hydroxy-2-methyl-1 phenyl-1-propanone), Irgacure 784 (Bis (eta 5-2,4-cyclopentadien-1-y) Bis [2,6-difluoro-3-(1H-pyrrol-1-yl)phenyl] titanium), Irgacure 2959 (2-Hydroxy-1-[4-(2-hydroxyethoxy) phenyl]-2-methyl-1-propanone), Irgacure 907 (2-Methyl-1-[4-(methylthiol)phenyl]- 2-(4-morpholinyl)-1-propanone), Irgacure 819 (Phosphine oxide, phenyl bi 2,4,6-trimethyl benzoyl) , ITX (Thioxanthen-9-one) were provided by BASF. All these chemicals were used as received without any further purification.

4.4.2 Synthesis of CuNPs from solution

In order to prepare ethanol solution of copper salt, 0.01M CuCl_2 was dissolved in 10ml ethanol in the presence of 0.02M photoinitiator (benzophenone) and then mixed them for 3 minutes in an ultrasonic bath. The solution was purged by bubbling nitrogen in the cuvette containing solution for 10 minutes, and then the cuvette was sealed to avoid the contact with oxygen. The solution was irradiated for different intervals of time (1min, 3min, 5min, 10min) under UV light at a radiation intensity of $45\text{mW}/\text{cm}^2$.

However, in order to prepare copper amine coordination complex 0.01M CuCl_2 was dissolved in 10ml ethanol in the presence of 0.02M photoinitiator (benzophenone)

and then mixed them for 3 minutes in the ultrasonic bath. After adding all these contents, 0.04M diethanol amine was added in the same solution to make an amine complex.

The resultant copper-amine complex was diluted as per requirement and deaerated in UV cuvette by bubbling nitrogen for ten minutes and then sealed that cuvette to inhibit the oxygen contact. The solution was irradiated for different intervals of time (1min, 3min, 5min, 10min) under UV light at a radiation intensity of 45mW/cm².

To check the effect of UV-irradiation on any other copper salt, CuSO₄ was chosen to study the behavior upon irradiating the solution for different intervals of time. In this case, 0.01M CuSO₄ was dissolved in 10ml methanol (copper sulphate being highly polar in nature is not soluble in ethanol) in the presence of 0.02M photoinitiator (benzophenone) and then mixed them for 3 minutes in ultrasonic bath, after this 0.04M diethanol amine was added to make copper-amine complex. In a very similar manner, the resultant copper-amine complex was diluted as per requirement and deaerated in UV cuvette by bubbling nitrogen for ten minutes and then sealed that cuvette to inhibit the oxygen contact. The solution was irradiated for different intervals of time (1min, 3min, 5min, 10min) under UV light at a radiation intensity of 45mW/cm².

4.4.2.1 Stabilization of CuNPs in solution

In order to stabilize the obtained copper nanoparticles, two polymer capping agents were used i.e. PVP and pyrrole. First of all, CuCl₂-amine was prepared by dissolving 0.01M CuCl₂ in 10ml ethanol, and then 0.02M photoinitiator (benzophenone) was added and mixed them for 3 minutes in an ultrasonic bath, 0.04M diethanol amine (DEA) was added to the CuCl₂-ethanol solution. At the end, 0.2% (w/v) pyrrole was added in the CuCl₂-amine coordination complex. Afterwards the solution was deaerated in a quartz cuvette by bubbling nitrogen for 10 minutes, and then the cuvette was sealed with a rubber plug. UV-vis spectra were recorded after different

intervals of irradiation time (1min, 3min, 5min, and 10min).

In order to stabilize with the help of PVP, CuCl₂-amine coordination complex was first formed by dissolving 0.01M CuCl₂ in 10ml ethanol in the presence of 0.02M photoinitiator(benzophenone) and mixing them for 3 minutes in an ultrasonic bath and at the end 0.04M diethanol amine (DEA) was added. 0.5% (w/v) PVP was added in the CuCl₂-amine coordination complex which serves as a polymer capping agent. Afterwards, the obtained solution was deaerated in a UV cuvette by bubbling nitrogen for 10 minutes. The changes in absorbance were measured with the help of UV-vis absorption spectra by irradiating the solution for different intervals of time (1min, 3min, 5min, and 10min).

All the copper-amine complexes and the also the copper-ethanol solution prepare and UV-irradiated for different intervals of time were stored in the air tight cuvettes.

Sodium ascorbate was also used to achieve stability of Cu nanoparticles in solution form against oxidation. To serve the purpose, solution of 0.01M CuCl₂, 0.02M sodium ascorbate (Na-asc.) was prepared in 10 ml H₂O, as Na-asc is not soluble in ethanol. In this solution Darocur 1173 is used (0.02M) and 0.04M DEA is added in the presence of (0.5w/v) % of PVP. The solution was irradiated for different intervals of time (1min, 3min, 5min, and 10min) in the presence of nitrogen at an intensity of 45mW.cm⁻². And the resulting solutions after irradiation were not stored in the air tight cuvettes, as were used in all the other solutions containing copper salt. The formation of Cu-NPs and their stability was checked with the help of UV-vis spectra.

4.4.3 Synthesis of polymeric composites embedding CuNPs

Polymer composites were prepared by dissolving different concentrations of copper salt: 0.5wt% and 1wt% CuCl₂ and 5wt% photoinitiator (benzophenone) in a few drops of ethanol, PEGDA oligomer 1g was added in this formulation and finally 2wt% diethanol amine was added. The resulting formulation was coated onto glass substrates (film thickness 100 μm) and exposed to UV light at a radiation intensity of

45mW/cm², under nitrogen for the necessary time to assure curing as depicted in Figure 33.

In order to stabilize the polymeric films against oxidation containing copper nanoparticles. Two polymeric capping agents were employed i.e. PVP and pyrrole.

The polymeric formulations containing copper salt in the presence of these capping agents were prepared as given below,

1. 1wt% CuCl₂, 5wt% photoinitiator (benzophenone) were mixed in a few drops of ethanol, PEGDA oligomer was added in this formulation and finally 2wt% diethanol amine was added. In this case, for stabilization to be achieved, 0.2wt%Pyrrole was added in the polymeric formulation.
2. 1wt% CuCl₂, 5wt% photoinitiator (benzophenone) were mixed in a few drops of ethanol, PEGDA oligomer was added in this formulation and 2wt% diethanol amine was added. In order to achieve stabilization 0.5wt%PVP was added in the same copper amine formulation, and mixed with the help of ultraturax for 5 minutes.

These resulting formulations were UV irradiated by coating them on to glass substrates with a thickness of 100 μm as shown in Figure 4.2 at a radiation intensity of 45mW/cm² under nitrogen for the necessary time.

4.5 Characterization techniques

Ultraviolet visible spectra (UV-vis). The UV-vis spectra was recorded by using double beam UNICAM UV2 (ATI Unicam, Cambridge, UK) spectrophotometer in a spectral range of 190–1100nm. The UV-vis spectra can be obtained for the solutions as well as for the cure polymeric film.

Transmission Electron Microscopy (TEM) The morphological characterization of the silver particles in this work was done by transmission electron microscopy (TEM) in a 300 keV transmission electron microscope Philips CM30. TEM

micrographs were processed with a slow scan CCD camera and analyzed with the Digital Micrograph program.

Dynamic Light Scattering (DLS) The particles size distribution was measured by using DLS Zetasizer Nanoseries ZS90 instrument purchased from Malvern Instrument (UK). This can measure the size of particles in the range from 2 nm to 3 μm . Before measurement, all samples were diluted 1:100 (to optimize the measurement) in water. Each measurement was repeated three times.

The hydrodynamics radius of the particles was calculated by using Stokes equation,

$$D_f = k_B T / 6\pi\eta R_H \quad (4.1)$$

Where,

D_f = Translational diffusion coefficient

k_B = Boltzmann constant

T = temperature of the suspension

η = viscosity of the surrounding media

R_H = Hydrodynamic radius

X-Ray Diffraction Diffraction measurements was carried out by using an X'Pert Phillips diffractometer CuK α radiation; 2θ range: 2–30 $^\circ$; 2θ step: 0.02 $^\circ$; step time: 2 s), with fixed specimen and moving X-ray source and detector simultaneously of a θ angle).

XRD analysis is based on Bragg's law

$$n\lambda = 2d \sin \theta \quad (4.2)$$

Here, n is an integer, λ is the X-ray wavelength, d is the distance between crystal lattice planes, and θ is the diffraction angle. This law gives the relationship between the wavelength of electromagnetic radiation to the diffraction angle and the lattice spacing in a crystalline sample. These diffracted X-rays are then detected, processed and counted. By scanning the sample through a range of 2θ angles, all possible diffraction directions of the lattice should be attained due to the random orientation of the powdered material.

Fourier Transform Infrared Spectroscopy FTIR spectra were recorded by using FTIR spectrometer (Thermo-Nicolet 5700 instrument) on thin samples, polymerized with different exposure times under nitrogen. Conversion was calculated by monitoring the decrease of the area of the absorption band of the reactive functionality ((meth) acrylate C=C peak at around 1620 cm^{-1}) with time.

Thermogravimetric Analysis (TGA)

Thermograms of our sample were performed by using Mettler Toledo TGA/SDTA 851 apparatus. The samples were analyzed under nitrogen flow of 60ml/min from 25°C to 800°C, with a heating rate of 10°C /min.

Differential Scanning Calorimetry (DSC) DSC measurements were performed under nitrogen flux, at 60°C for 2 hours with a DSCQ 1000 of TA Instruments equipped with a low temperature probe. The kinetics of the process was studied by using STARe software.

Field Emission Scanning Electron Microscopy (FESEM) The morphology of the cured films was investigated by employing field-emission scanning electron microscopy (FESEM) taken with a high resolution FE-SEM analyses. Using LEO (ex LEICA, ex CAMBRIDGE) S260 equipped with a system of microanalysis-X. Accelerating voltage of 300 V to 3 kV (accelerating rate of 100 V) and 4 kV to 30 kV (accelerating rate of 1 kV) was applied. Samples were put into liquid nitrogen to be cryofractured, the cross section was analyzed. Samples were metalized with carbon, under vacuum.

Electrical characterization was performed by means of a two-point probe method. Conductivity of the cured films was measured between two copper plates used as electrodes (electrode surface 0, 4 cm^2). Electrical measurements were performed by using a Keithley-238 High Current Source Measure Unit as high voltage source and

nano-amperometer, multiple measurements in air at room temperature were performed, in the range $[-5, 5]$ V.

Chapter 5

Results and Discussion

5.1 Objective

The focus of this project is to synthesize noble metal nanoparticles and study of the development of UV-cured conductive polymeric films by an in-situ generation of noble metal nanoparticles.

UV-cured polymeric films are a promising candidate for the realization of flexible electronics, due to their easy processability, low cost and availability.¹ This polymerization technique allows a fast transformation of a liquid monomer into a crosslinked polymer with tailored physical-chemical and mechanical properties. The main limit in their application for realization of electronic devices or in ink-jet technology is related to the very high surface resistivity of the typical acrylic or epoxy resins employed in UV-curing technology. And to overcome this particular problem, we have devised a facile and quick method by using two noble metal nanoparticles.

In this research work, we have tried to synthesize and stabilize silver and copper nanoparticles embedded in polymer matrices. The first choice is to use silver nanoparticles along with a conducting monomer i.e. pyrrole. First of all, we investigated the photo reduction of the silver salt dissolved in a suitable solvent as a function of the irradiation time, presence of pyrrole, and monomer/salt ratio. The size and morphology of the particles obtained was studied. We repeated the process using a photocurable difunctional acrylic photocurable monomer, thus forming a crosslinked polymer in the form of a film. The particle size embedded in the polymer resin as well as the conductivity of the resulting films was measured.

In contrast to silver nanoparticles, the synthesis of copper nanoparticles is much more challenging, since copper nanoparticles are fairly unstable and undergo oxidation instantly. However, copper costs significantly less than silver, therefore, it is economically attractive. When copper nanoparticles are exposed to air, surface oxidation occurs and ultimately aggregation appears in a very short time. We have tried to achieve the stabilization of Cu nanoparticles. By following the same path, copper nanoparticles were synthesized both in the solvent and in the polymer.

We have divided this chapter in two sections; first section describes systems with silver nanoparticles and the second section describes the results obtained while characterizing systems with copper nanoparticles.

5.2 Characterization of solutions containing silver salt: monitoring the reduction process with and without pyrrole

As a preliminary study we investigated the effect of UV irradiation on silver salt dissolved in ethanol with and without the presence of pyrrole. The concentration of silver precursor was kept in the range between 5-20wt%, in the presence of 0.002% photoinitiator i.e. Darocur 1173, with and without the presence of 2wt%pyrrole.

The details of different formulations prepared to analyze with the help of UV-vis spectra are given in Section 4.3.2.

5.2.1 Optical characterization

As a preliminary study we investigated the effect of UV irradiation on silver salt dissolved in ethanol together with pyrrole. The different formulations were prepared adding increasing silver salt content in the range between 5 to 20 wt%, while the pyrrole was kept constant at 2 wt% and the photoinitiator (PI) was 0.002%. In Figure 34 are reported the cuvettes containing, as an example, the formulation with 10wt% of AgNO_3 and 2wt% of pyrrole (Py) before and after irradiation for different times under inert atmosphere. It is evident a clear color change since the transparent solutions turned brown.

Similar color changes were observed for all the investigated formulations containing different silver salt concentration. The process was then monitored, during irradiation, with UV-Vis spectra analyses.

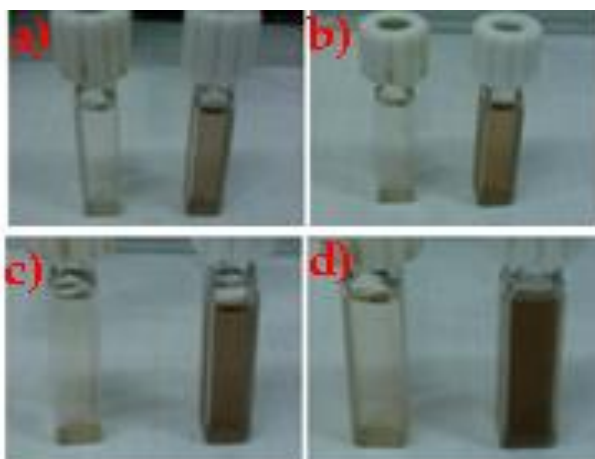


Figure 34 Color change observed after a) 1 min, b) 3 min, c) 5 min d) 10min of UV-irradiation. [10%AgNO₃+ 2%Py+ 0.002%PI].

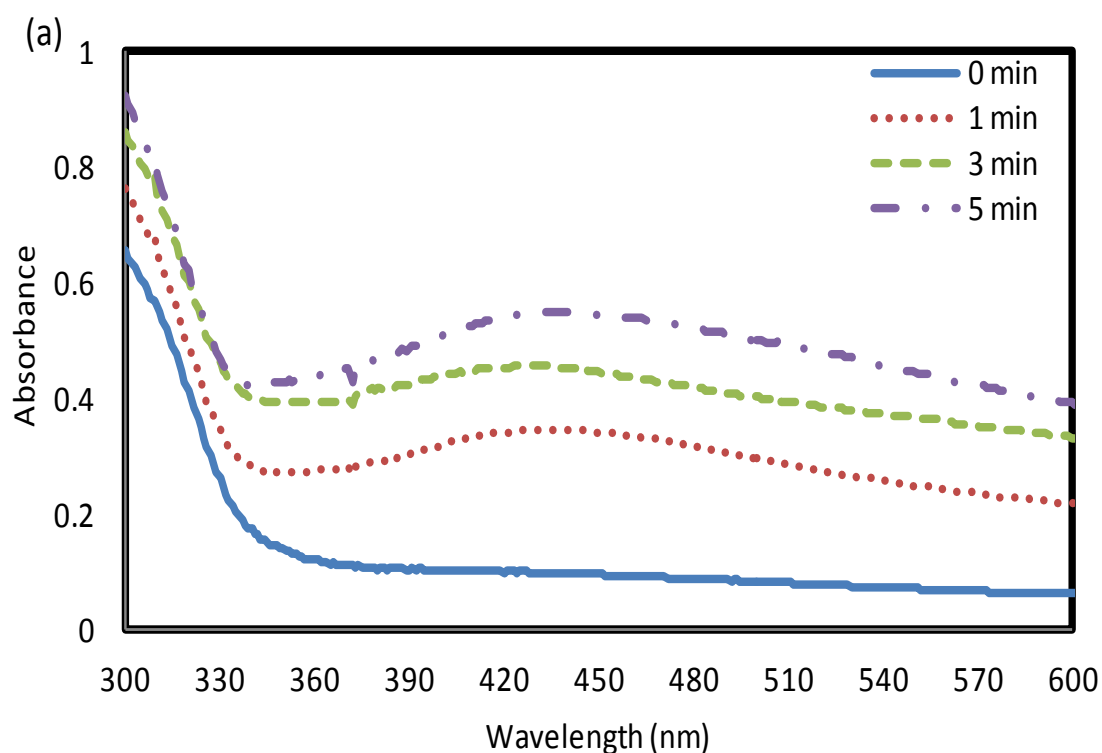
In Figure 35(a-c) the UV-Vis spectra of different solutions before and after irradiation are reported. The solutions were diluted enough to get the UV-vis spectra in a desired range (5wt% was not diluted; 10wt% and 20wt% were diluted 1:20 and 1:30 times respectively). In the spectra, a strong absorption below 330 nm is observed which is mainly due to the photoinitiator and a broad band centered at around 440 nm formed whose intensity increases as a function of irradiation time. The growth of this band as a function of irradiation time could be related to the chemical reactions involving the metal salt and the pyrrole monomer.

On the absorption of light, spontaneous reduction of silver salt from solution occurs to form silver metal particles. Meanwhile, pyrrole gets oxidized and forms a pyrrole radical cation through excitation of electrons in the π -orbital.⁹⁶

In order to better interpret the spectra and understand the reaction, pyrrole and silver ion solutions were studied separately.

UV-Vis spectra were recorded on solutions containing only pyrrole or only silver salt after irradiation for different irradiation times. In Figure 36 the spectra show the

presence of a shoulder centered at around 310 nm when pyrrole is dissolved into ethanol and irradiated: no other absorption is present at higher wavelength in agreement with the absence of any visible color change during irradiation. The shoulder is certainly due to the photoinitiator; however it is increased by increasing irradiation time. Therefore it could also be attributed to the formation of polypyrrole, in accordance with the previous literature data²² which demonstrated the UV-induced polymerization of pyrrole, in the presence of radical photoinitiators.



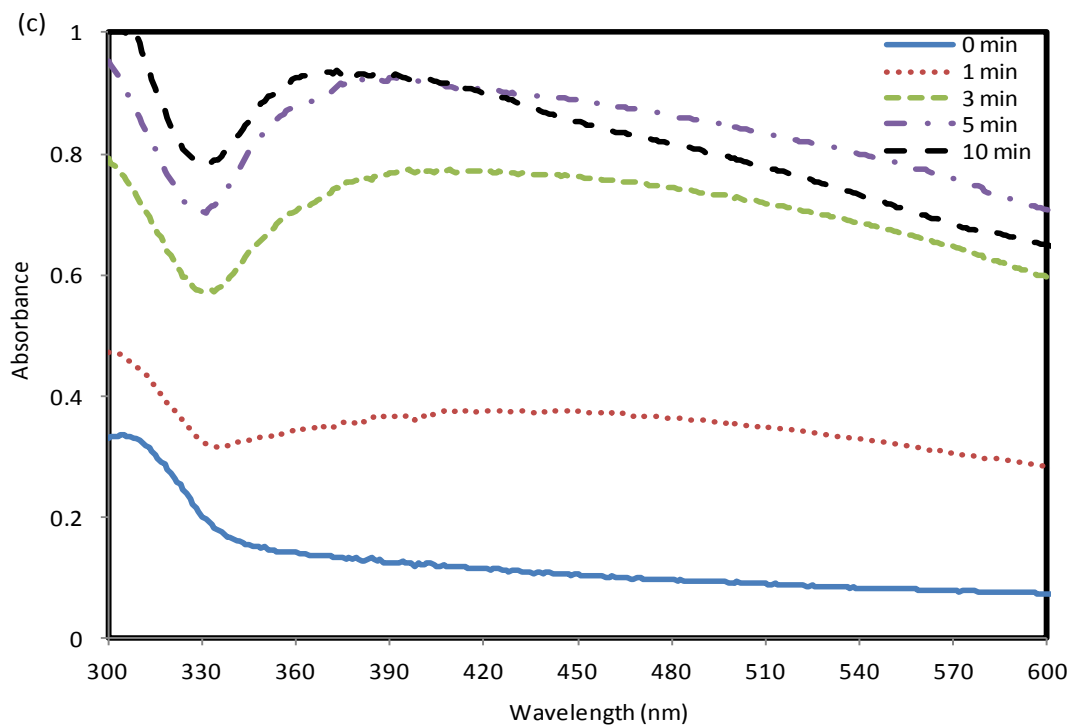
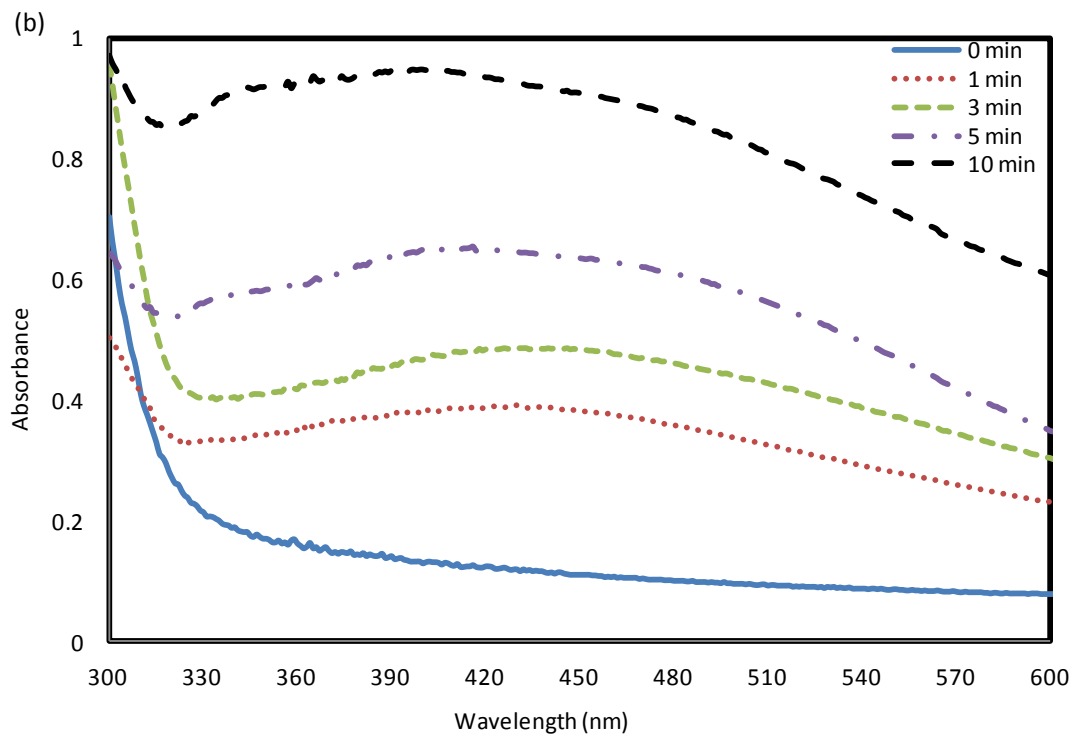


Figure 35 UV-Vis spectra of the ethanol solution containing 5 wt% (a), 10 wt% (b) and 20 wt% (c) of AgNO_3 . All the solutions contained 2 wt% of pyrrole and the radical photoinitiator 0.002%PI.

In Figure 37(a-c) we report the UV-Vis spectra of the ethanol solutions containing 5 wt% (Figure 31-a), 10 wt% (Figure 31-b) and 20 wt% (Figure 31-c) of silver salt, in the presence of the radical photoinitiator, before irradiation and after different irradiation times.

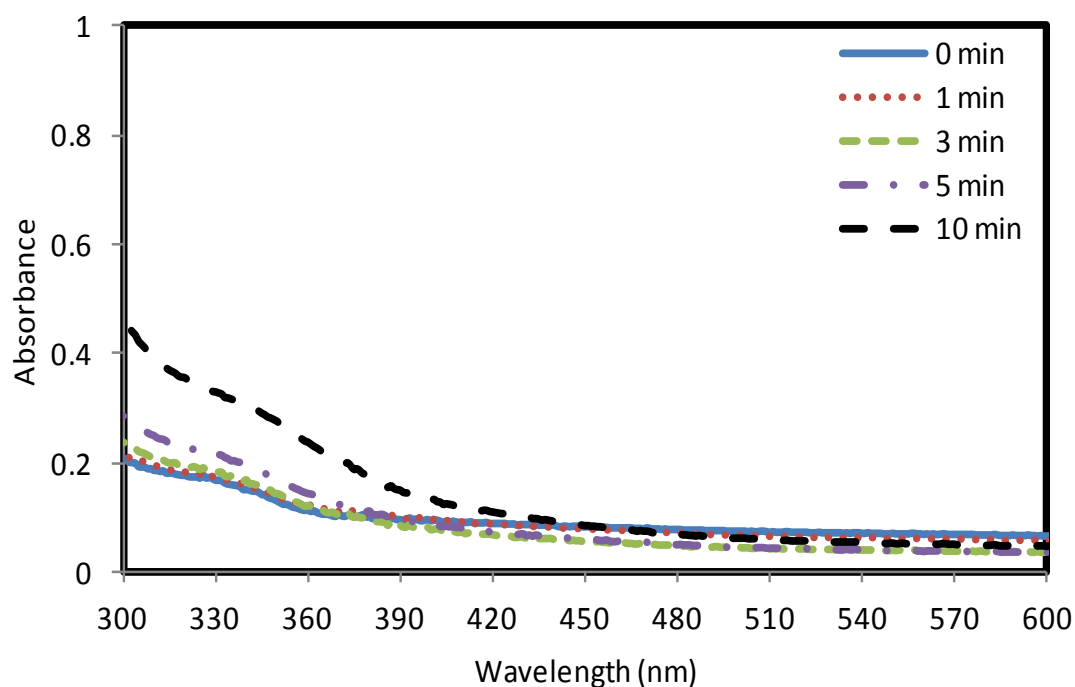


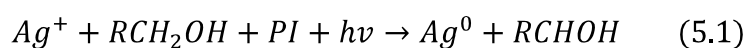
Figure 36 UV-vis spectra of 2%Py and 0.002%PI in Ethanol at different irradiation times.

One can see that when AgNO_3 is dissolved in ethanol, before irradiation there is no absorption peak in the visible region. When the solutions are UV-irradiated, a peak evidenced at around 430 nm.

This absorption can be attributed to the plasmon resonance effect²²⁶ arising from the appearance of metal particles, suggesting the formation of silver nanoparticles.

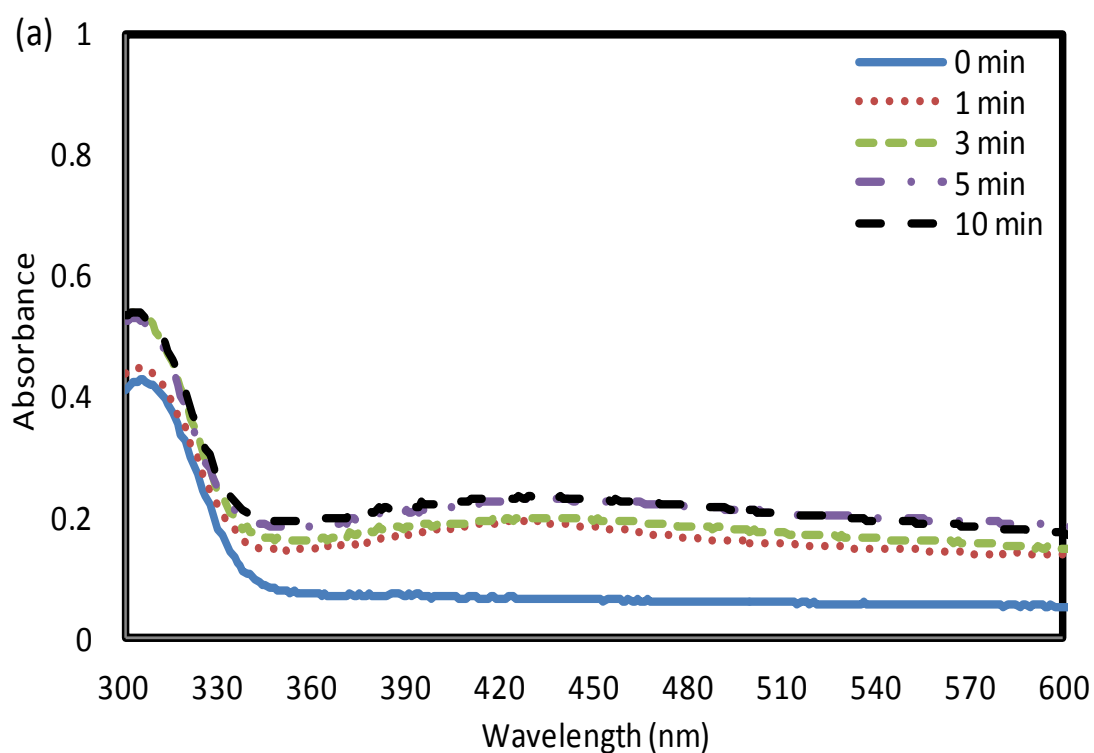
It is accompanied by a visible color change of all the investigated solutions: they turn from transparent to brown after irradiation (already shown in Figure 34).

The mechanism through which the silver nanoparticles form by electron transference to silver ions from solvent may proceeds like,



Equation (5.1) shows that Ag^+ goes to Ag^0 by transferring an electron from the solvent molecule when UV light subjected to them. And then that Ag^0 associates with other silver atoms to form silver nanoparticles as shown in Equation (5.2).

This accurate investigation clearly suggests that, during UV-irradiation, we have at the same time reduction of silver ions with the formation of silver metal nanoparticles and polymerization of pyrrole to form polypyrrole.



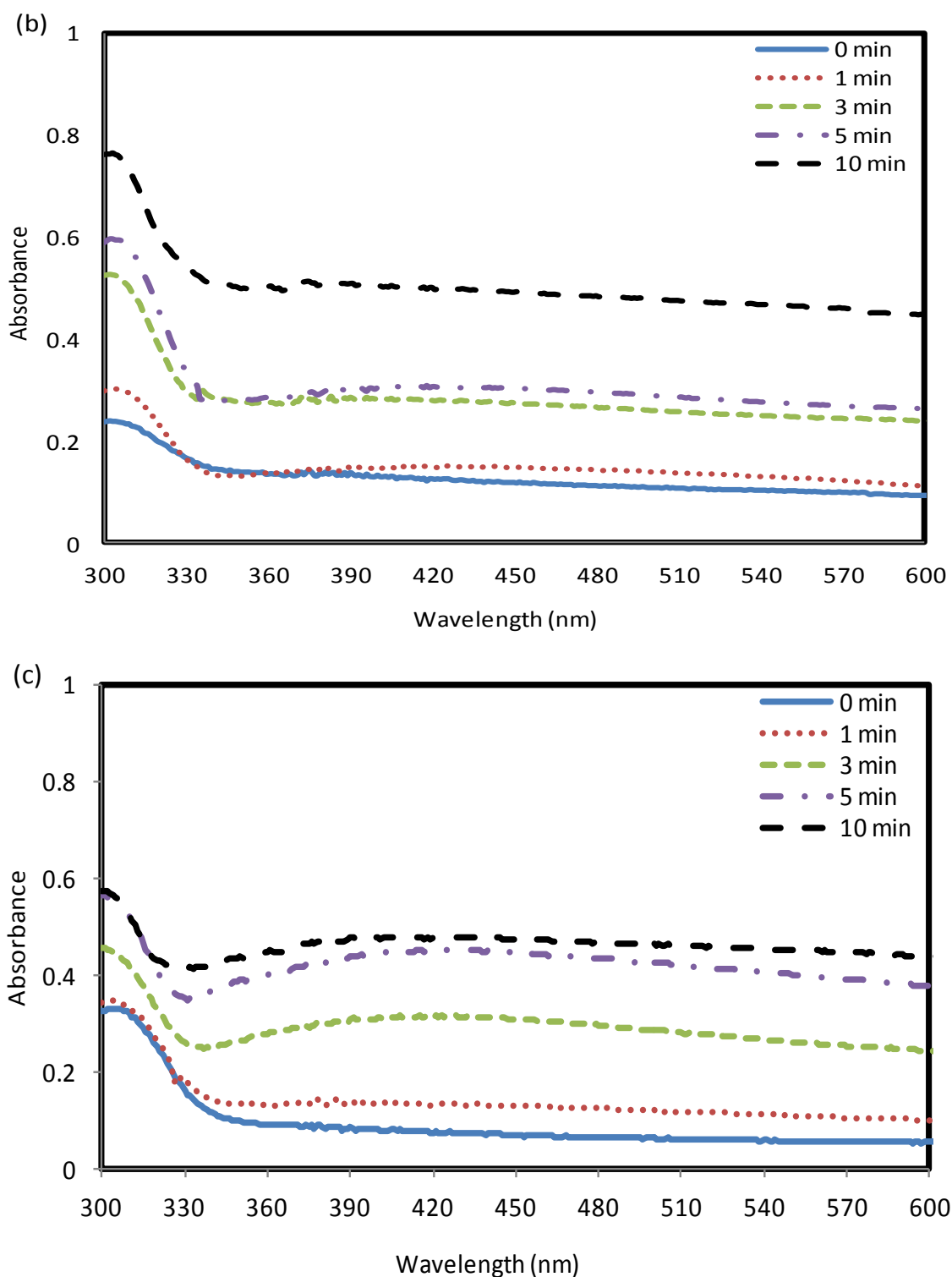


Figure 37 UV-Vis spectra of the ethanol solution containing 5 wt% (a), 10 wt% (b) and 20 wt% (c) of AgNO_3 and the radical photoinitiator.

We investigated the photoreduction of ethanol solution containing silver nitrate and pyrrole in the absence of photoinitiator. The results show that this solution cannot

be photoreduced. No visible changes were observed by the UV-vis spectra, which therefore indicate that no photoreduction under UV-light is possible without using photoinitiator. Nevertheless the presence of the photoinitiator is essential for the polymer formation, both for acrylic and for polypyrrole. In an experiment, the solution containing silver salt and pyrrole was UV-irradiated for different times i.e. 1min, 3min, 5min, and 10min without the presence of photoinitiator. Visible changes in the color of the solution after irradiation were observed but the UV-vis spectra shows that the particles are not formed as a huge noise was observed instead of any particular absorption peak. In a similar manner, polymer formulation containing silver salt and pyrrole was tried to UV-crosslinked without the photoinitiator, but no crosslinking was achieved under the same conditions as were used previously.

5.2.2 XRD Analysis

The powder X-ray diffraction (XRD) pattern performed on the sample after evaporating the solvent confirms that the particles generated were effectively silver nanoparticles. The recorded spectrum on the composition of 5 wt% of AgNO_3 and 2 wt% of pyrrole, after 10 minutes of UV-irradiation is shown in the Figure 38. The recorded peaks confirmed the presence of silver metal particles. The peaks related to silver NPs are reported in literature to be: 38.7° , 44.1° , 64.6° and 78.3° [JCPDS No 03-0931].

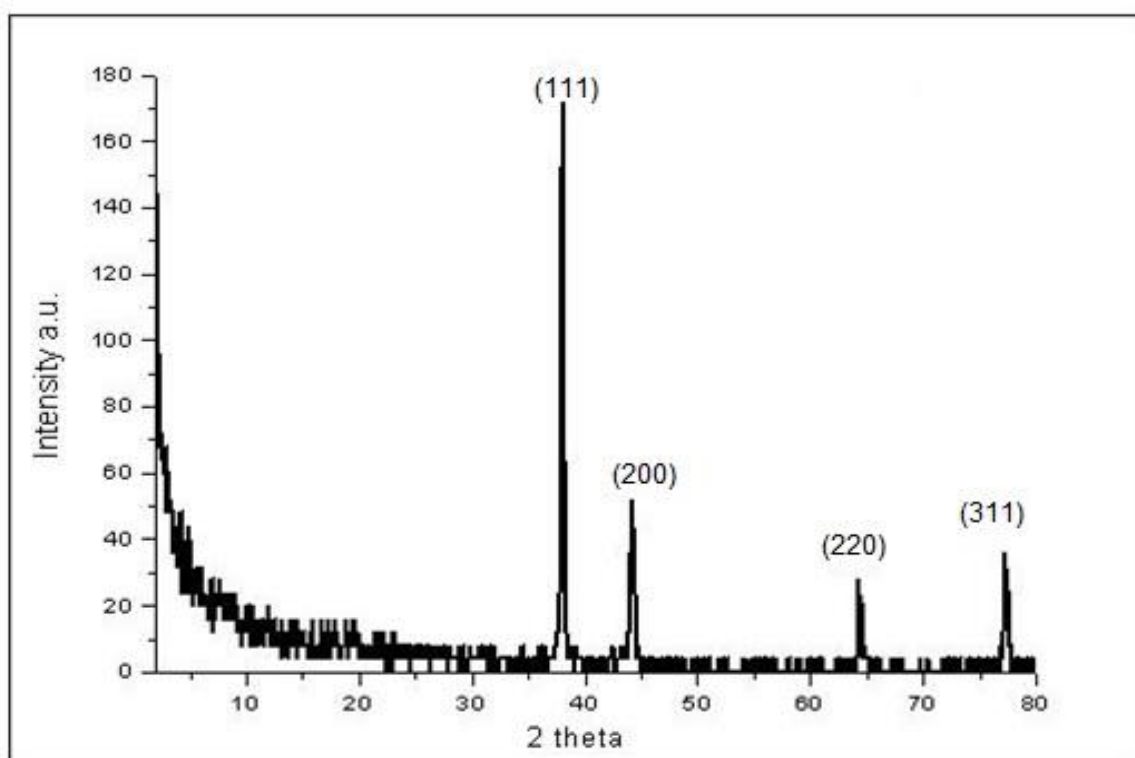


Figure 38 XRD analyses of the ethanol solution containing 5 wt% of AgNO_3 and 2 wt% of pyrrole, after 10 minutes of UV-irradiation

These data points correspond to cubic crystalline structure of silver and assigned to (111), (200), (220) and (311) plans of silver respectively²⁷⁷. The recorded peaks at 2θ angle for our sample were: 38° , 44° , 64° and 78° . The possible reason for the slight decrease with respect to the data reported in literature could be attributed to the polypyrrole coating formed around silver cores.

To calculate the crystallite size of the particle size obtained, we used Scherrer's formula. Identification of unit cells of the obtained silver particles can be done with the help of the given data. Indexing is a process which can be used to determine the unit cell dimensions with the help of peak positions. First, miller indices (h k l) should be assigned in order to index a diffraction pattern.

Table 5.1 Simple peak indexing

Peak position, 2θ	$1000 \times \sin^2\theta$	$1000 \times \sin^2\theta / 35$	Reflection	Remarks
38	105.99	3	(1 1 1)	$1^2+1^2+1^2=3$
44.	140	4	(2 0 0)	$2^2+0^2+0^2=4$
64	280.8	8	(2 2 0)	$2^2+2^2+0^2=8$
78	379.88	11	(3 1 1)	$3^2+1^2+1^2=11$

Scherrer's formula to estimate the crystallite size is given,

$$D = \frac{K\pi}{\beta \cos\theta} \quad (5.3)$$

Whereas, $K=0.9$, π =wavelength of x-ray (0.1541 nm), β = FWHM (full width at half maximum), θ = the Bragg's diffraction angle and 'D' is particle diameter size. The crystallite size of the silver nanoparticles has found to be in the range of 100 nm.

5.2.3 DLS Analysis

Particle size distribution was estimated with the help of DLS technique. In order to achieve a thorough understanding of the presence of pyrrole and effect of the irradiation time on the size of the particles, DLS analysis was performed on the ethanol solution containing different percentages of silver salt i.e. 5, 10 and 20 wt% of silver nitrate with and without the presence of 2wt% pyrrole, 0.002wt% PI after subjected to UV-irradiation for 1, 3, 5 and 10 mins.

The DLS curves for different concentrations of silver content w/o and with the presence of pyrrole for the maximum irradiation time i.e. 10mins is shown in Figure 5.6(a-b). It can be observed by looking the Figure 39-a) that when there is no pyrrole particle size has a

broad distribution ranging from almost 100 to 800 nm; and there is no particular effect of the increase in silver content. The mean particle size of 5wt% AgNO_3 is reported to be 370 nm, 10wt% AgNO_3 is 320nm, and for 20wt% AgNO_3 is 350nm. There is no profound effect on the mean particle size of the particles obtained, however the size distribution becomes narrower with the increase in metal content. But, in all the cases with different UV-irradiation times there is not any remarkable difference in the size and size distribution of the particles.

Whereas with the addition of pyrrole (2wt%) in the sample containing increasing amount of silver content, not much difference in particle size distribution was observed.

In the presence of 2wt%pyrrole, the mean particle size of 5wt% AgNO_3 solution obtained is 270nm, 10wt% AgNO_3 is 310 nm, with the 20wt% AgNO_3 mean particle size is 307nm. (Figure 39-b) In all cases of different silver salt concentration and the addition of pyrrole in the ethanol solutions subjected to different UV-irradiation times, did not exhibit any remarkable difference in the size and size distribution of the particles. So, after looking at all these curves we can conclude that particle size of the silver particles in ethanol solution ranges approximately in the range of 300-350nm, which indeed agrees with the result obtained from TEM analysis.

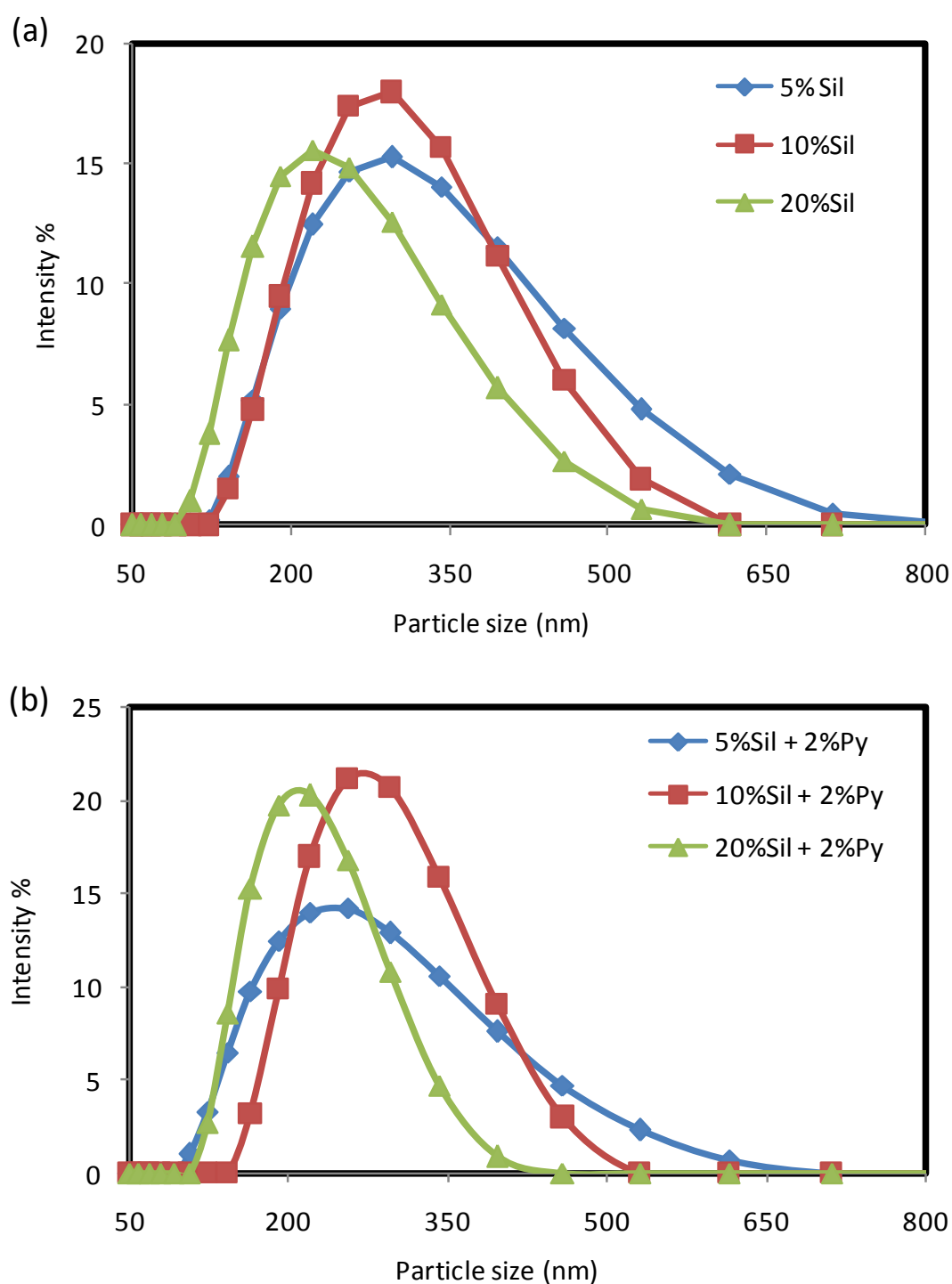


Figure 39 DLS-images of diameter distribution by intensity of nanosized silver colloids (a) with 5wt% , 10wt%, 20wt%AgNO₃ w/o (Py)pyrrole (b) with 5wt%,10wt%,20wt%AgNO₃ with 2% (Py) after 10mins UV-irradiation

5.2.4 TEM Analysis

With the objective of looking into the morphology of these obtained particles, TEM analysis was performed after UV-irradiating the ethanol solutions. The same solution chosen to perform XRD was investigated with the TEM as well, i.e. 5wt%AgNO₃ and 2wt% pyrrole after 10mins UV irradiation. Quite large aggregates are evident due to particle-particle interactions and to the high vacuum conditions of the TEM analyses (shown in Figure 40). It is interesting to remark that the particles have core-shell morphology: one can suppose that the metal core is covered by a polypyrrole matrix. And this assumption has already been proved through the XRD analysis. It can also be noticed that particles have great tendency to aggregate. The average dimensions of the particles are in the range of 200-300 nm which is in a reasonable agreement with the values recorded by DLS.

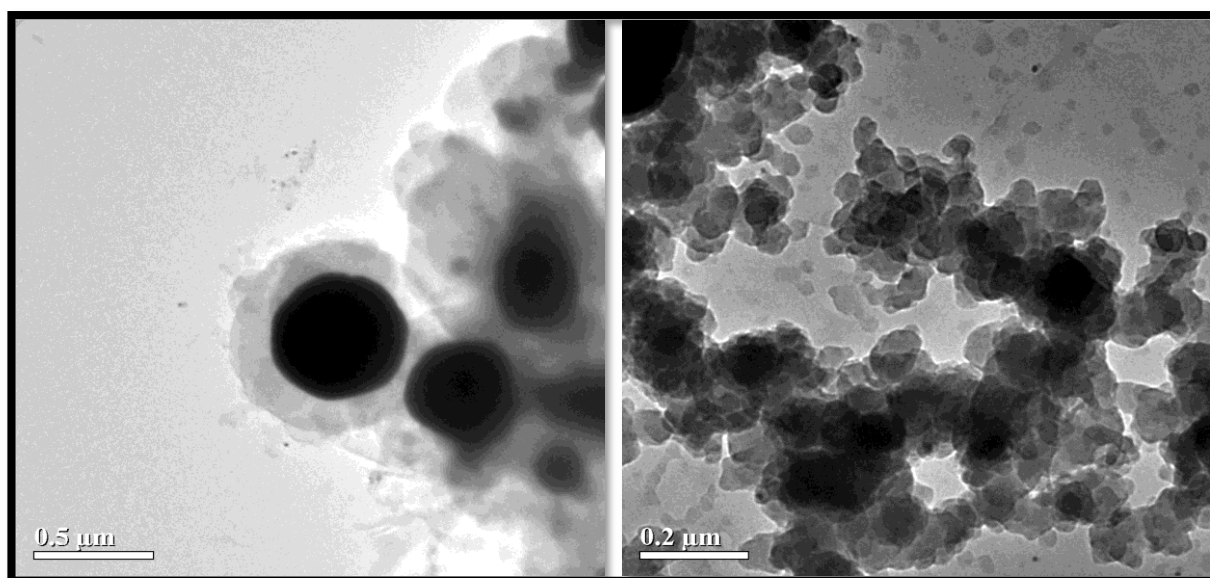


Figure 40 TEM analysis of the ethanol solution containing 5 wt% of AgNO₃ and 2 wt% of pyrrole, after 10 minutes of UV-irradiation.

5.3 Photopolymerization of acrylic oligomers in the presence of silver salt and pyrrole

After studying the irradiation of the silver salt with and without pyrrole in ethanol, the next step was the investigation of the contemporary acrylic resin crosslinking reaction and in-situ formation of silver metal particles and polypyrrole. In order to obtain UV-cured acrylic crosslinked films different concentrations of silver salt (5wt%, 10wt% and 20wt %) and pyrrole (2wt %) were dissolved into PEGDA, the PI was added in a higher amount (2wt %). The resulting formulations were UV-irradiated after coating onto glass substrates at a radiation intensity of $45\text{mW}\cdot\text{cm}^{-2}$ under nitrogen for the necessary time to assure curing. Details of the whole procedure are discussed already in Section 4.3.3.

5.3.1 FTIR Analysis

At first FTIR analyses were conducted to monitor the curing of PEGDA in the presence of different concentrations of silver salt (5-20wt %), pyrrole (2wt %) and PI (2wt %), UV-cured under nitrogen for necessary time to get cured. The analysis showed that after 30 sec of UV-irradiation one reaches the complete conversion of the PEGDA acrylic double bond (as shown in Figure 41), with a complete disappearance of the C=C band centered at around 1620 cm^{-1} . This is in agreement with the previous investigations²⁶⁷ and attributable to the high reactivity of PEGDA acrylic resin. When silver salt and pyrrole were added to the monomer, respectively in the range between 5 to 20 wt% of silver salt and 2 wt% of pyrrole, not any significant effect was evidenced in the rate of photopolymerization or final acrylic double bond conversion. Nevertheless, from the previous investigations, we were aware that a longer irradiation time is needed in order to obtain in-situ reduction of silver salt and UV-induced polymerization of pyrrole. For this reason the complex formulations, made of PEGDA, silver salt, pyrrole and radical photoinitiator, were irradiated for 3 minutes.

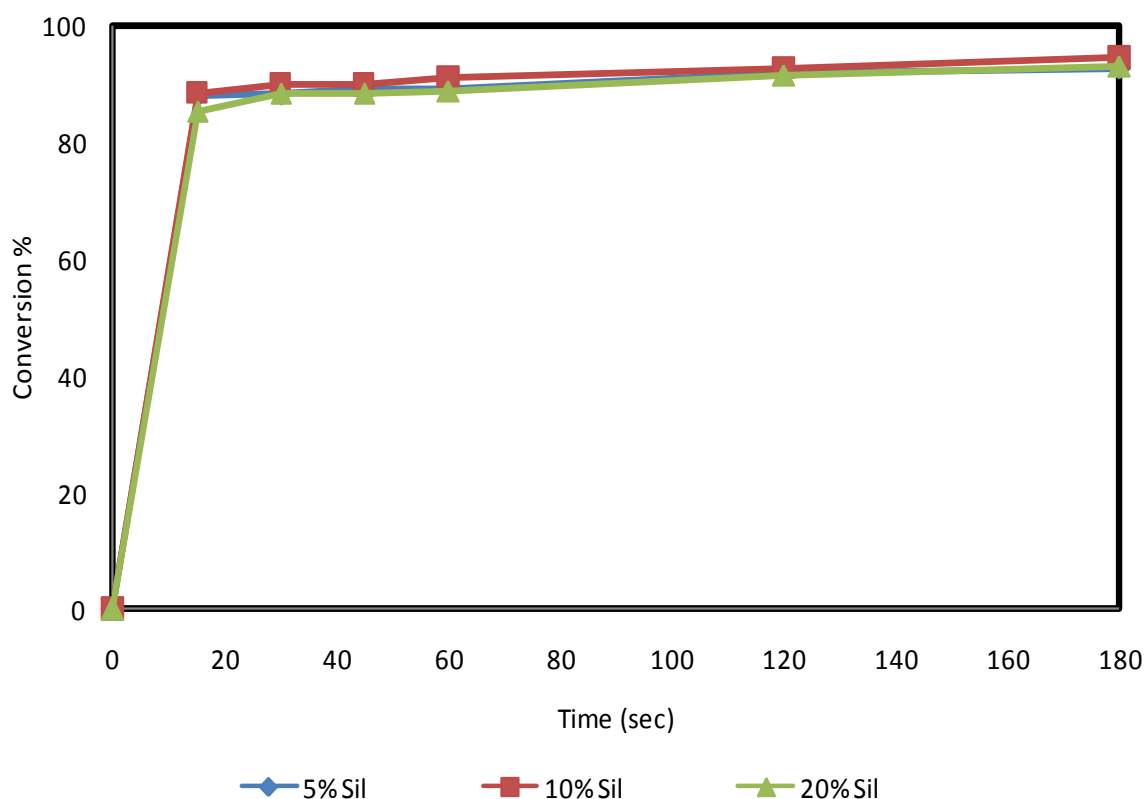


Figure 41 Real time FTIR acrylic group conversion as a function of irradiation time for the PEGDA formulations containing increasing amount of AgNO_3 in the range between 5 - 20wt%.

5.3.2 Optical characterization of UV-cured films

The UV-crosslinked films irradiated for 3 minutes under nitrogen were subjected to UV-vis spectroscopy analyses. Spectra in Figure 42 show a clear and strong absorption band centered at around 430 nm and a shoulder below 330 nm, as it happened for the ethanol solutions in the spectra of Figure 35. The intensity of the band is stronger than in the spectra of Figure 35 as the solutions were diluted; the intensity is increasing by increasing the silver salt concentration in the photocurable formulation. The strong absorption peak at 430 nm can be attributed to the formation of silver particles plasmon resonance, as previously recorded for the UV-irradiation of ethanol solution containing the silver precursor. The signal below

330nm is related to the PI and the formation of polypyrrole, as discussed for the ethanol solutions.

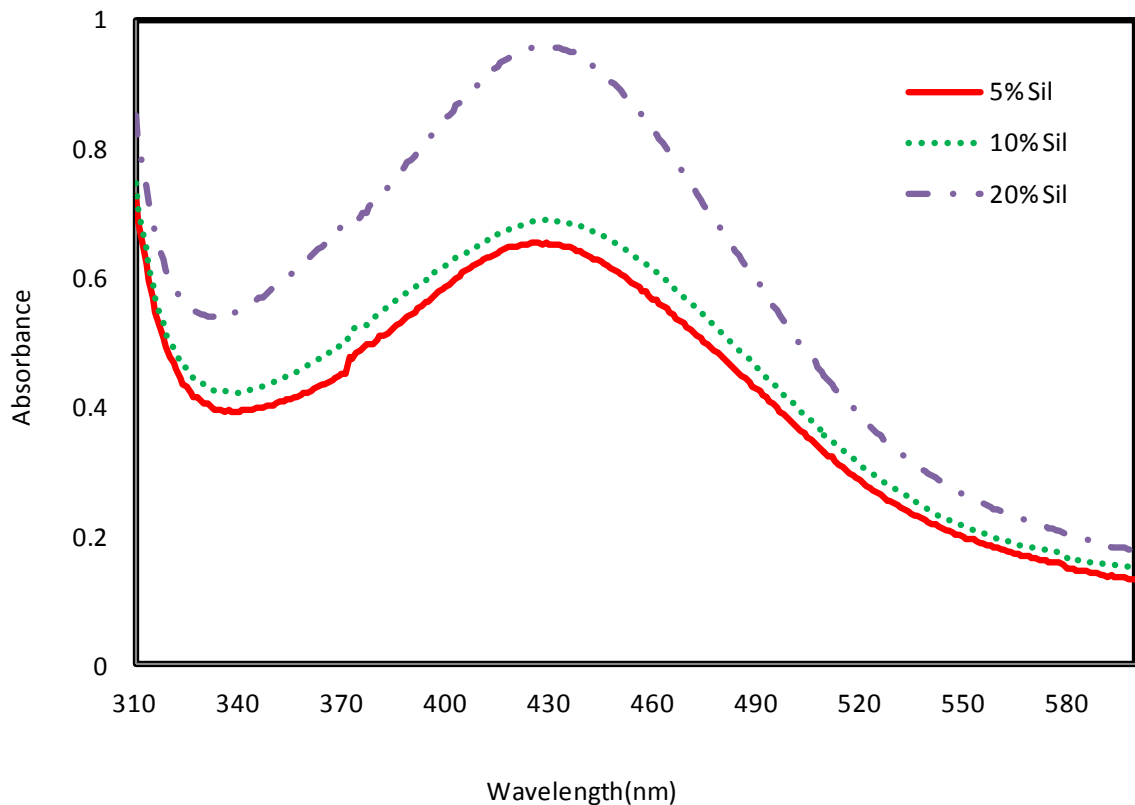


Figure 42 UV-Vis absorption of the crosslinked film containing (5-20 wt %) of AgNO_3 and 2 wt% of pyrrole are reported.

5.3.3 FE-SEM Analysis of UV-cured films

FE-SEM analyses were performed on the cryofractured surface of the crosslinked films. Images of the surface fracture of the cured film obtained in the presence of 10wt% and 20wt% of silver precursor are shown in Figure 43.

The metal particles are very well distributed within the polymeric matrix with a quite narrow particle size distribution between 50nm to 80nm. Lower particles size dimensions are obtained with respect to the ethanol solution UV-irradiation. This could be due to the quick polymer network formation which hindered further diffusion of the metal particles generated in-situ, avoiding further growing of the nucleated silver metal germs and agglomeration.

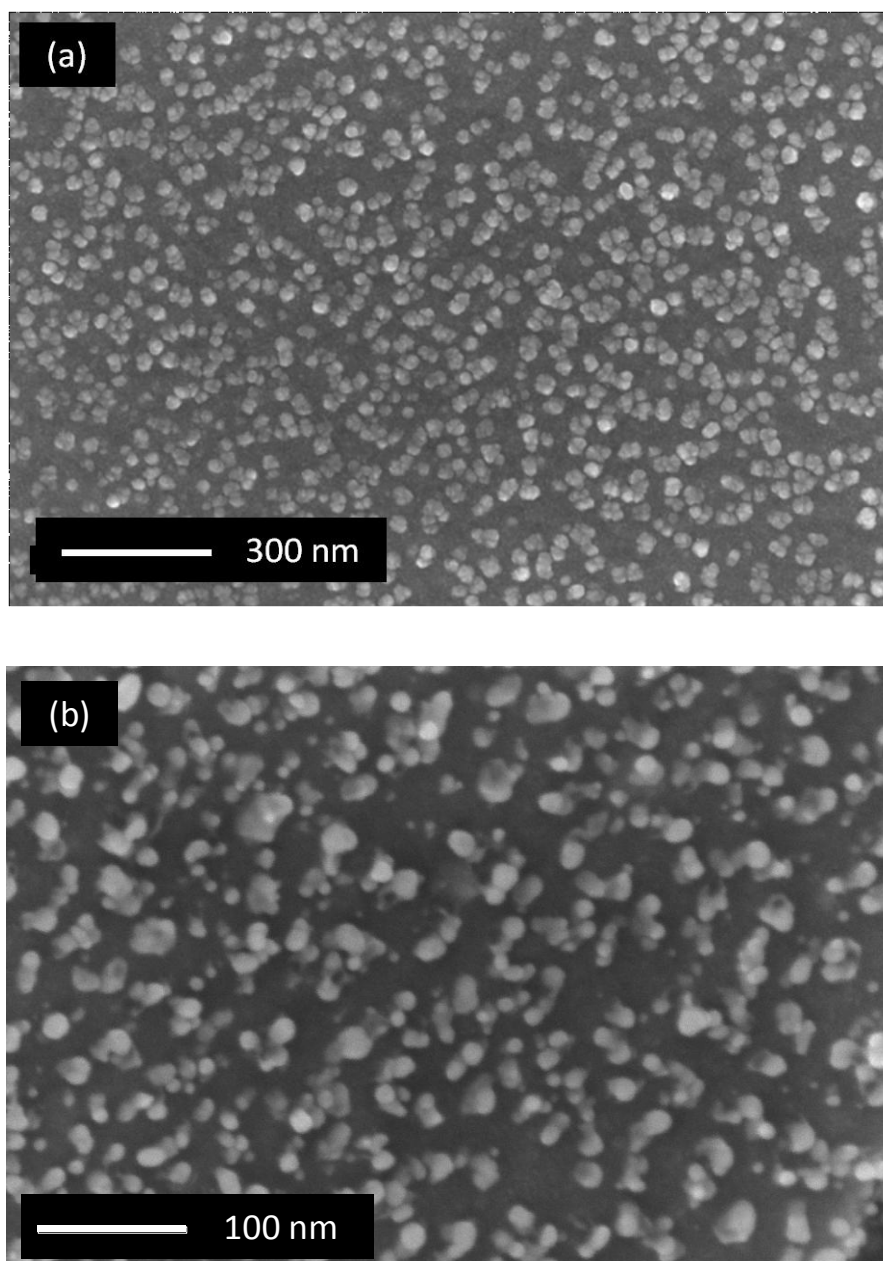


Figure43 FESEM image of the fracture surface of the crosslinked films a) 10wt% AgNO_3 b) 20% AgNO_3

5.3.4 Electrical Characterization

Electrical characterization was performed on cross-linked films. The I-V curves are reported in Figure (44-a) for the PEGDA films containing 5 wt%, 10 wt% and 20 wt% of AgNO₃; all the samples showed a linear ohmic behavior. As expected, a strong increase of conductance was observed by increasing the amount of silver precursor in the photocured film. By observing FESEM images (Figure 43), it is possible to ascribe this effect to the formation of a conductive percolative path through the polymer network induced by the presence of the well distributed silver nanoparticles. The presence of pyrrole further decreases the resistivity as evidenced in Figure (44-b). The electrical characteristics demonstrating the resistivity as a function of silver nitrate content are collected in Table 5.2. The pristine cross-linked PEGDA showed a value of ρ of nearly 20 M Ω cm, when 5 wt% of AgNO₃ is dissolved into the monomer the surface resistivity decreased of two order of magnitude and reached the lowest value of 45,5 k Ω cm when 20 wt% of silver precursor was dissolved into PEGDA. This decrease in resistivity of the UV-crosslinked films is promising for using such materials in applications where higher resistivity is required like strain gauges and pressure sensors. This value makes this material good candidate for resistor materials²⁷⁸.

The further addition of 2 wt% of pyrrole to the formulations always induced a further decrease of resistivity in comparison with the films obtained only in the presence of silver salt. This indicates that polypyrrole formed with the proposed mechanism effectively contribute to current conduction improving electrons flow through the film.

This improvement may be attributed to the conjugated structure of polymer which may help in transporting the charge from one silver nanoparticle to the other.^{278-b}

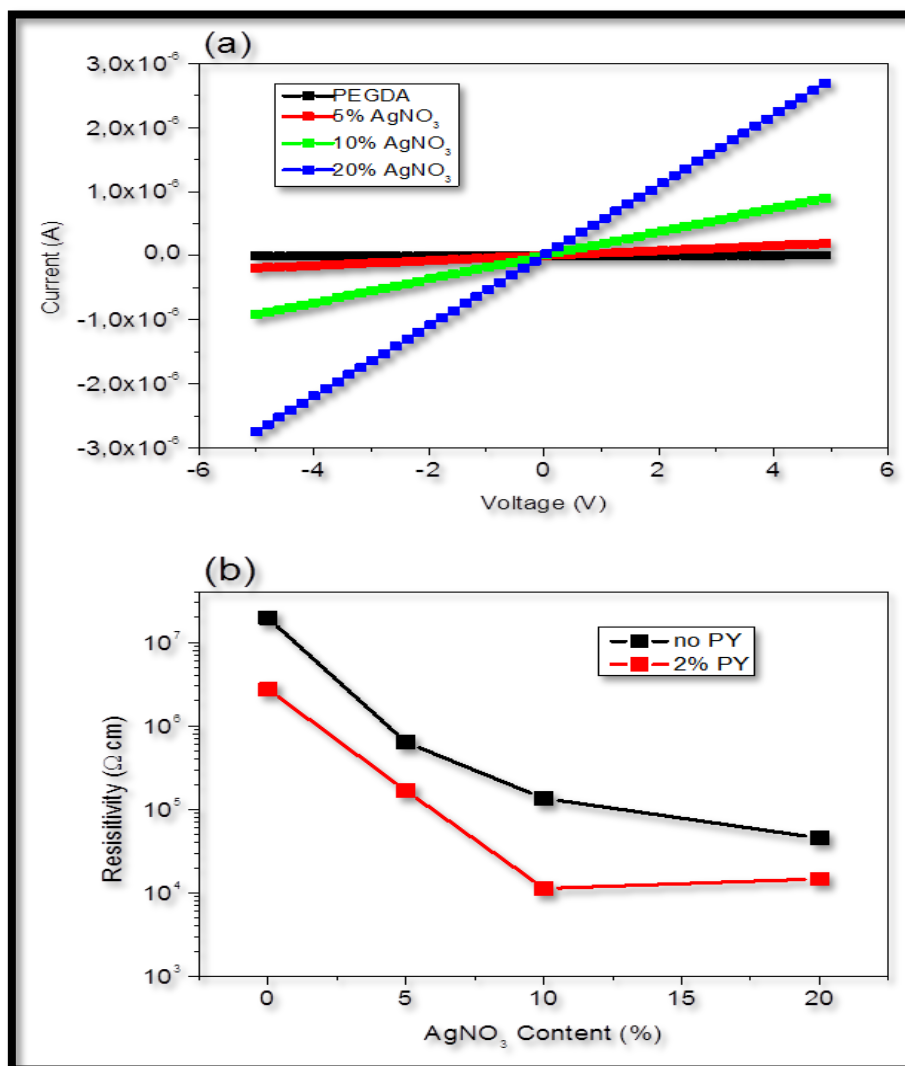


Figure 44 Electrical conductivity of the UV-cured films. (a) with the increase in AgNO₃ content (b) with and without the presence of Py.

Table 5.2 Electrical Characteristics of UV-cured films

Sample	G(S)	ρ (Ω .cm)
PEGDA	1,27E-9	1,96 E7
+ 5 wt% AgNO ₃	3,91E-8	6,40 E5
+ 10 wt% AgNO ₃	1,84E-7	1,36 E5
+ 20 wt% AgNO ₃	5,50E-7	4,55 E4
+ 2wt% Pyrrole	9,09E-9	2,75E6
+ 5 wt% AgNO ₃ + 2 wt% Pyrrole	1,48E-7	1,69 E5
+ 10 wt% AgNO ₃ + 2 wt% Pyrrole	2,20E-6	1,13 E4
+ 20 wt% AgNO ₃ + 2 wt% Pyrrole	1,69E-6	1,47 E4

5.3.5 TGA Analysis

This is a technique which involves the measurement of the weight of the sample as a function of temperature in the scanning mode or as a function of time in the isothermal mode. So, it is used to characterize the polymer-metal nanocomposites as it provides information on the thermal stability of the nanocomposite relative to the polymers.²⁴⁴

Decomposition profiles for our samples were obtained while heating at a rate of 10°C/min in nitrogen from room temperature to 600°C. The relation between the temperature and weight loss can be observed from Figure 45. It can be observed easily that there is no profound effect on the thermal decomposition of the polymer with the increase in silver content. The degradation starts from almost 360°C for all the samples. The weight percentage of the residual silver content is higher for the Sample c as compared to the other sample b because of the reason that Sample c contains more silver content 20wt% as compared to the Sample b (containing 10% AgNO₃). However, (sample-a) is PEGDA in the presence of 2wt% photoinitiator. We can conclude that addition of different concentrations of silver content does not affect the thermal stability of the polymer

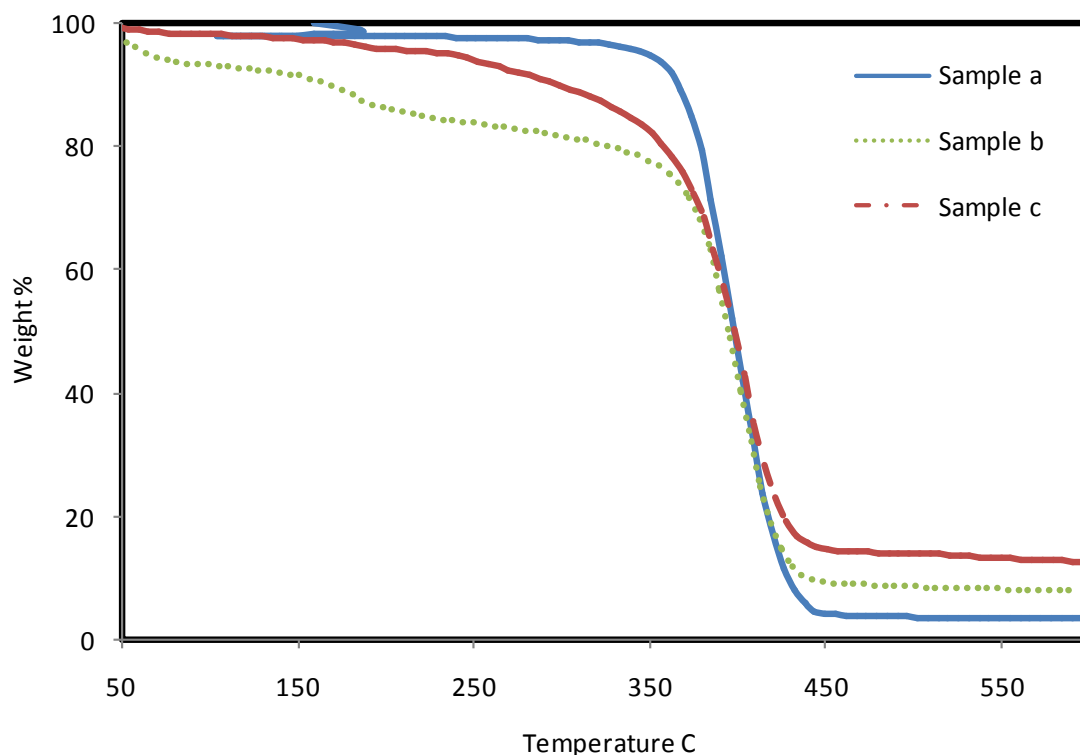


Figure 45 Thermograms of Samples: Sample-a (PEGDA+2wt%PI), Sample-b (PEGDA+10wt%AgNO₃+2wt%PI), Sample-c (PEGDA+20wt%AgNO₃+2wt%PI)

5.4 Protection of Silver nanoparticles

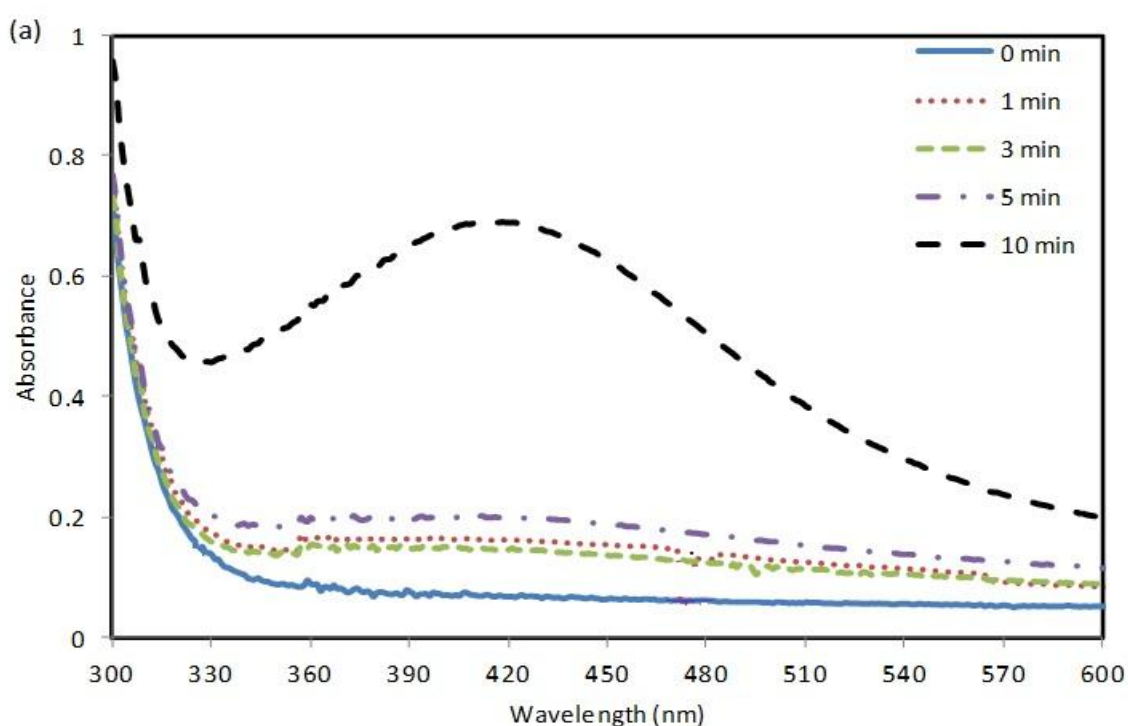
The details of the preparation of ethanol solution containing PVP is given in detail in Section 4.3.2. Different concentrations of PVP were added in the ethanol solution containing 10wt%AgNO₃, 2wt%Py and 0.002% PI, in order to achieve the stability of silver particles in the ethanol solution. The aim was to obtain finely dispersed smaller particles having narrower size distribution. However, the better results in terms of the reduced particle size without much aggregation were achieved for 1wt%, 2wt%, 4wt%

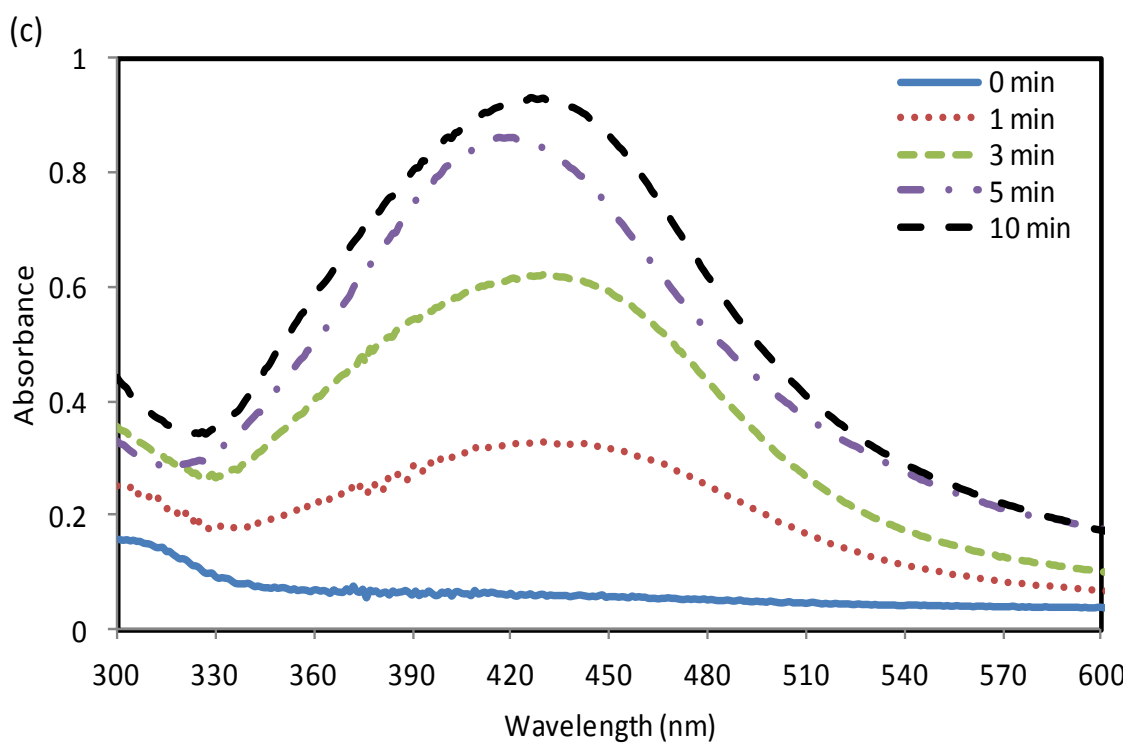
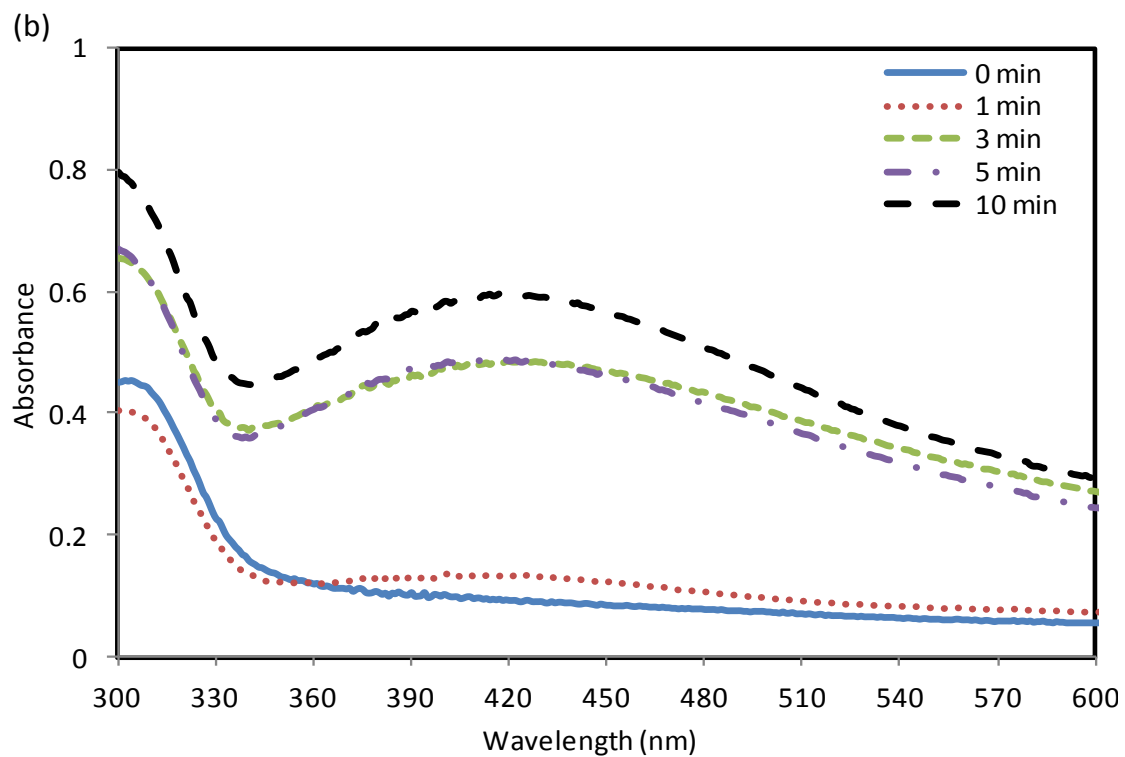
and 6wt% PVP. The broad peak of UV-vis spectrum as was shown in Figure 37 indicates the wide range of particle size distribution. Also DLS (Figure 39-b) and TEM analysis (Figure 40) confirmed this fact that the silver particles obtained have a very broad particle size distribution especially in the ethanol solution.

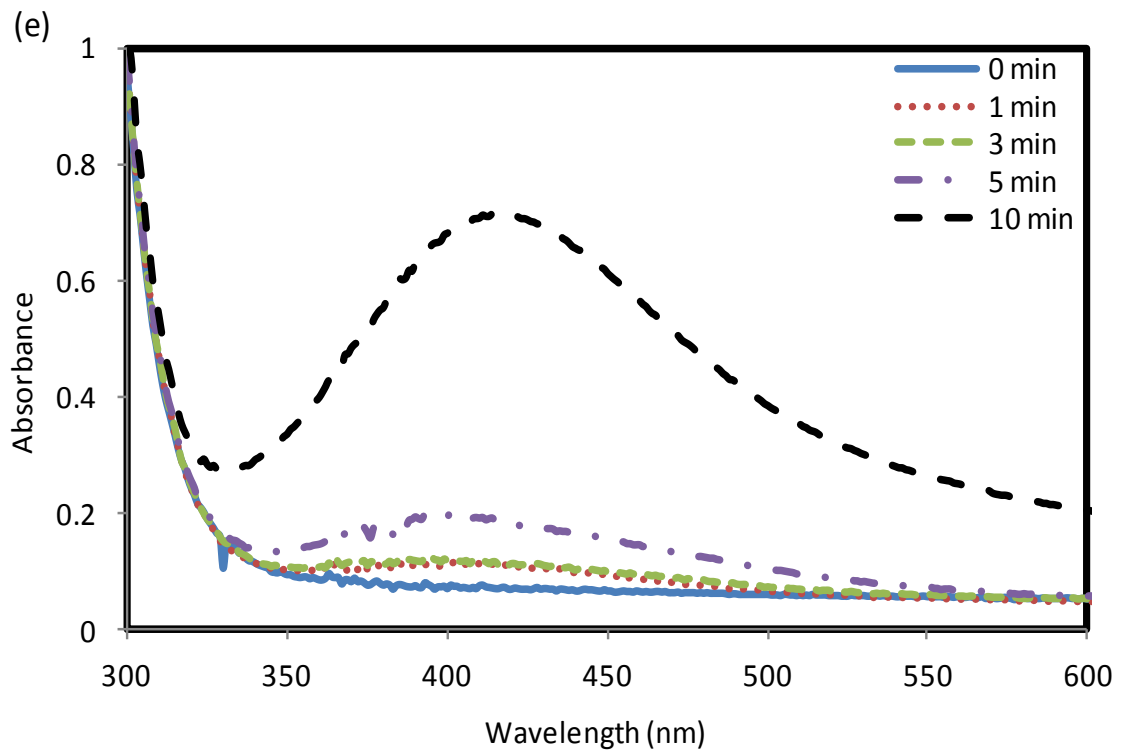
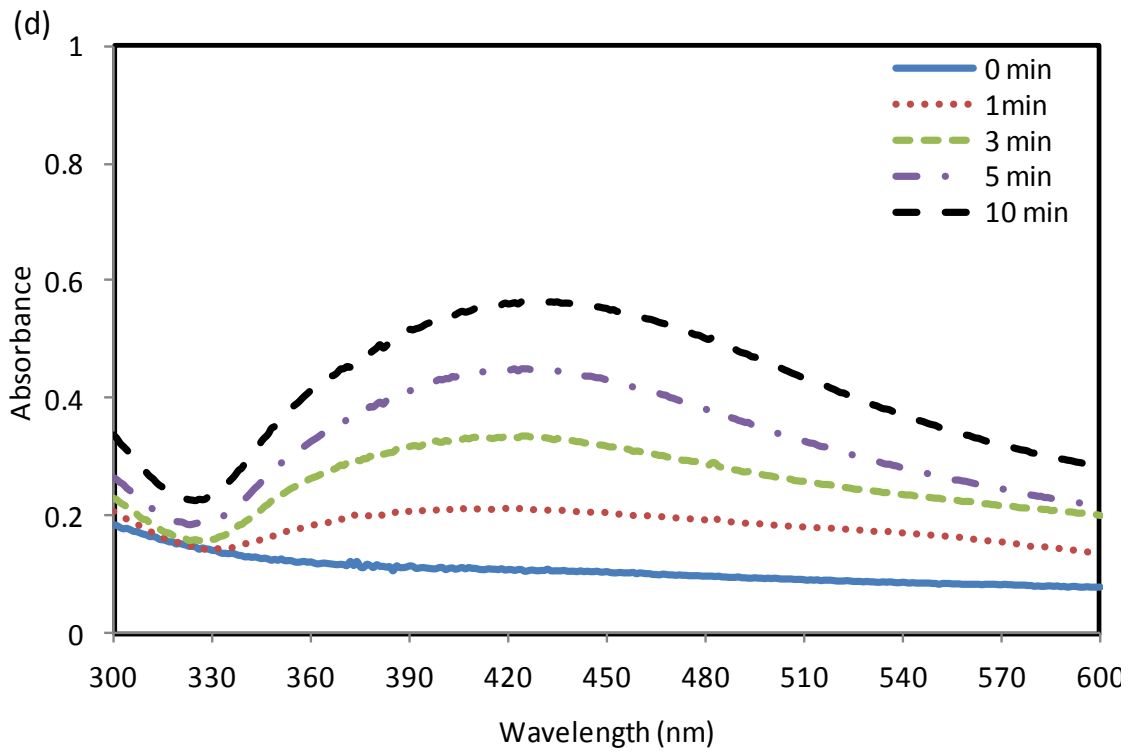
5.4.1 Optical characterization of ethanol solution containing silver particles in the presence of PVP

To make it sure that the silver nanoparticles are distributed finely and there is no aggregation of the particles, we tried to obtain UV-vis spectra of the ethanol solution containing suspended silver nanoparticles.

The ethanol solution of 10%AgNO₃,2% pyrrole in the presence of 0.002%PI was chosen to check the effect of the addition of a stabilizer i.e. PVP. The different concentrations of PVP (1%, 2%, 4%, 6%, 8%, 10%) were added in the solution. In a similar manner as done before, these solutions were photoreduced these solutions under UV light in the presence of N₂ by varying the time of irradiation i.e. (1min, 3min, 5min, and 10min). All these solutions were diluted enough to get the UV-vis spectra in a desired range.







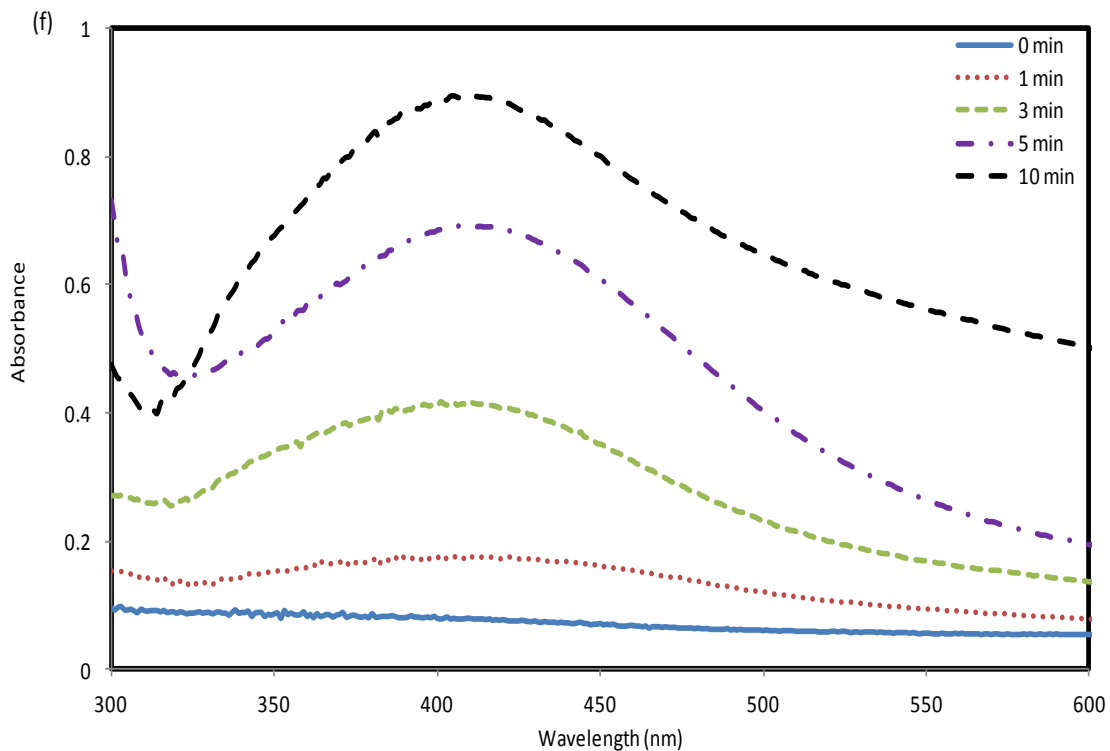


Figure 46 UV-Vis spectra of the ethanol solution containing 10 wt% of AgNO_3 +2 wt% of pyrrole and the radical photoinitiator 0.002%PI. (12a) 1%PVP (b) 2%PVP and (c) 4%PVP (d) 6%PVP (e) 8%PVP (f) 10% PVP

The peaks containing PVP concentration more than 4% PVP are very broad as compared to the ones having lesser percentage of PVP. Absorbance spectra (shown in Figure 46 a-f) collected for all these solutions showed the protective mechanism with the help of PVP as compared to those spectra in the absence of PVP. However, it has already been proved in Figure 35 (a-c) and in Figure 37 (a-c) that silver nanoparticles can be formed in the presence of photoinitiator and UV light, independent of PVP concentration. However, the addition of this stabilizing agent (PVP) helps in reducing the size distribution of the particles. But, the amount of PVP added in order to achieve more uniform sized nanoparticles is also crucial.

Solutions containing lesser amount of PVP have very narrow peaks as compared to the ones having higher amount of PVP. It can be clearly observed that colloids with PVP concentration 1wt% and 2wt% show a very strong plasmon band at around 420nm. However, with the increase in PVP concentration to 4wt%-10wt% PVP

consequently show relatively very broader peaks which can be seen clearly from the Figure 46 (c-f)

It is observed that the band position of the spectra depends on the particle size and on the amount of the stabilizer added. The dependence of the particle size on the UV-vis absorption peak was first studied by Mie^{8-a} and then by Wang *et al.*^{245-b}. According to their findings, with the shift of the absorption peak towards the longer wavelength, particle size becomes bigger.

Based on the UV-vis spectra it can be concluded that in all samples silver nanoparticles are formed independently of the PVP concentration. But, with the addition of stabilizer, peaks with a very strong plasmon resonance can be obtained. However, with the increase in the concentration of PVP the position of maximum absorption wavelength is shifted to a larger wavelength. It is observed that silver nanoparticles with the PVP concentration of 1wt% and 2wt% have the narrowest peak having tightest size distribution but increase in PVP concentration results in broader peaks i.e. large size distribution of the particles.

5.4.2 DLS Analysis

DLS analysis was carried out in order to understand the effect of PVP on the particle size distribution of silver nanoparticles. DLS analysis was performed on the ethanol solution containing 10wt% of AgNO₃ in the presence of 2wt% pyrrole, 0.002wt% PI and different concentrations of PVP ranging from 1wt%, 2wt%-10wt% after subjected to UV-irradiation for 1, 3, 5 and 10 mins.

The DLS curves for different concentrations of PVP content in the presence of pyrrole irradiated for maximum time i.e. 10 mins is shown in Figure 47. It can be observed clearly by looking the Figure 47 that in the presence of lowest amount of PVP i.e. 1%, the particle size ranges from 80-300nm while the mean particle size is about 150nm, but by increasing the concentration to 2% PVP the narrowest particle size distribution ranging from almost 50 to 190 nm is obtained: and the mean particle size is about 90 nm. If we compare it with the value of particle size distribution obtained when there was no PVP (was shown in Figure 39-b) this value reduced almost more than three times. This confirms the theoretical implication

about the dependence of particle size on the absorption spectrum of the particles. So, it can be concluded that the band position depends on the size of the particles obtained. However, if we study the curves constituting the greater amount of PVP it is evident that with the increase in its concentration particle size distribution broadened and the Z-average diameter size of the silver nanoparticles containing 4% PVP is 197 nm and for 6%PVP is 254 nm respectively, which is still less than those solutions containing no PVP at all.

With the further increase in the stabilizer amount to 8% and 10% even larger nanoparticle clusters are formed. As can be seen from Figure 47 a broad range of particle size distribution is obtained. The average diameter size in the presence of 8% PVP is 325 nm, while in the presence of 10% PVP the average Z-diameter size is calculated to be 350 nm. This phenomenon of increase in the particle size in the presence of stabilizer may be attributed to the dense polymer network coating on the silver particles

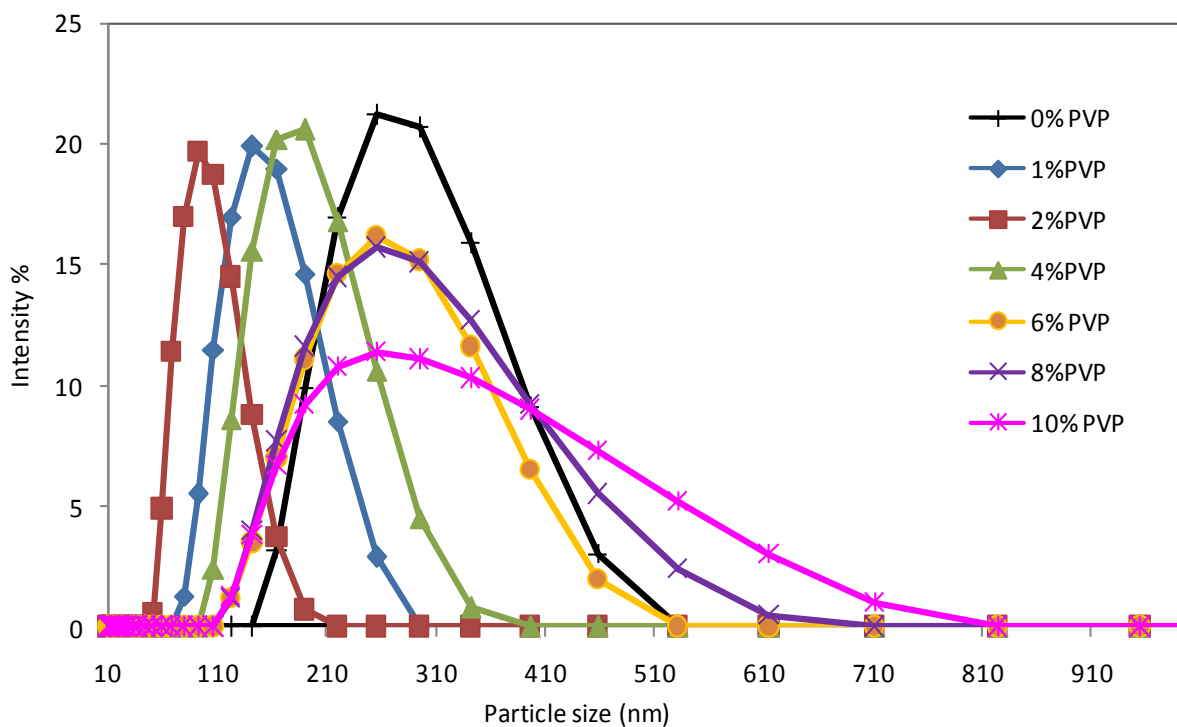


Figure 47 DLS-images of diameter distribution by intensity of nanosized silver colloids with different PVP concentrations after 10mins UV-irradiation.

Summarizing the results obtained by DLS, one can conclude that average size of silver nanoparticles and size distribution is broader in comparison with the silver particles with smaller amount of PVP. The PVP concentration less than 2% may be too less to prevent the agglomeration of all of the prepared particles, although the concentration of PVP till 6% provides a means of reducing the particle size of the prepared silver particles as compared to those prepared without PVP. With further increase in the PVP concentration, mean particle size and size distribution is broadened in comparison with silver nanoparticles having no or lower amount of PVP, which may be due to the thick coating of the polymer around the silver particles.

Based on the results obtained by UV-vis absorption spectra and DLS analysis of all the samples containing different PVP concentration, samples with PVP concentration 2% show the narrowest particle size and size distribution, other samples with higher PVP concentration have very broad peaks and large size distribution.

5.4.3 SEM Analysis

Keeping in view the results obtained by UV-vis spectra and DLS analysis, SEM Analysis was performed on the ethanol solutions containing 1% and 2% PVP after UV irradiating them for 10 minutes. This study was carried out in order to confirm the presence of silver particles and to see the effect of PVP on their particle size. Due to the high vacuum conditions of the SEM analyses, quite large aggregates are formed and are visible in Figure 48 (a-b). Figure 48 (a) shows the SEM image: in the presence of 1% PVP the particle size is in the range of 100-200 nm. While in the presence of 2% PVP, small particles in the range of approximately 24-107nm are obtained. The values obtained by this analysis correspond with the ones obtained with the help of DLS. Therefore, it can be concluded with the help of DLS and SEM analysis that PVP concentration as low as 2% leads to the synthesis of Ag-NPs with a narrowest size range with the small amount of large clusters.

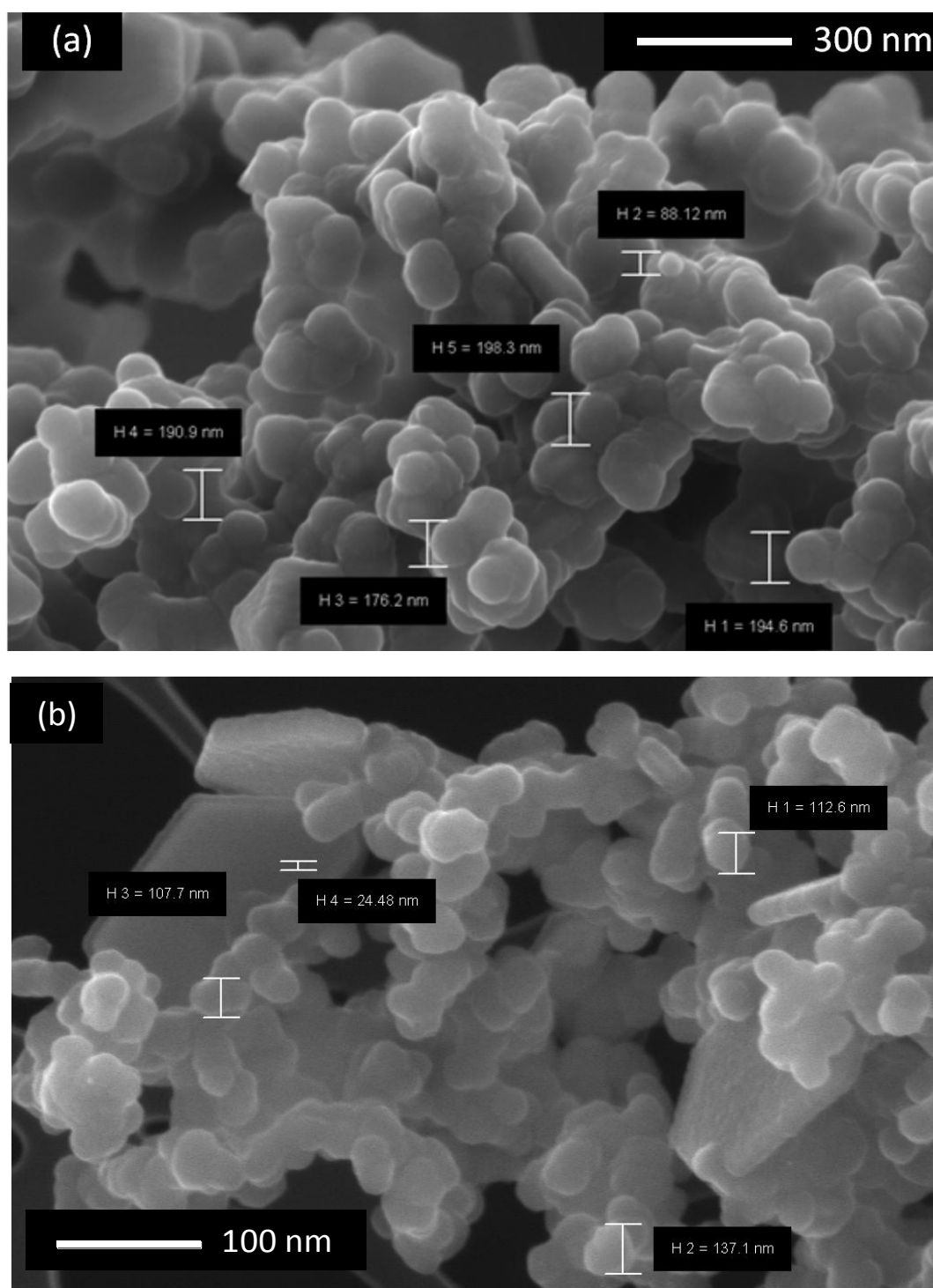


Figure 48 SEM analysis of the ethanol solution containing 10 wt% of AgNO_3 and 2 wt% of pyrrole, (a) with 1%PVP (b) with 2%PVP after 10 minutes of UV-irradiation

5.4.4 XRD Analysis

XRD analysis of the ethanol solution containing 10wt%AgNO₃, 2wt%pyrrole, 0.002%PI along with the different concentrations of PVP i.e. 1wt%, 2wt%, 4wt%, 6wt% was done to assure the dispersion of nanoparticles in the solution. XRD analysis performed on the powder obtained after evaporating the solvent is shown in Figure 38, and the peaks obtained thereby confirmed the presence of silver nanoparticles. However, in order to confirm that the particles are finely dispersed throughout the solution and there will be no aggregation of the particles with the help of the addition of stabilizer. We carried out the XRD analysis, and calculated the data for the 2 θ range of 10 to 70 degrees with a step of 0.02 degree.

We were not able to collect some good defined peaks for the ethanol solution containing 1wt% and 2wt%PVP. It can be assumed that this concentration may not be enough to give very strong signals to be recorded. However, the XRD analysis of ethanol solution containing 10wt % AgNO₃, 2wt % pyrrole, 0.002 % PI, PVP i.e. 4wt % and 6wt% has been carried out and is shown in Figure 49(a-b).

With the help of this diffractogram, one can state clearly that the peaks obtained are of silver particles. This data can be used for the identification of unit cell for any compound. Indexing is the process which can be employed to determine the unit cell dimensions with the help of peak positions. First, miller indices ($h k l$) should be assigned in order to index a diffraction pattern. The crystallite size of silver particles is estimated with the help of curve a shown in Figure 49.

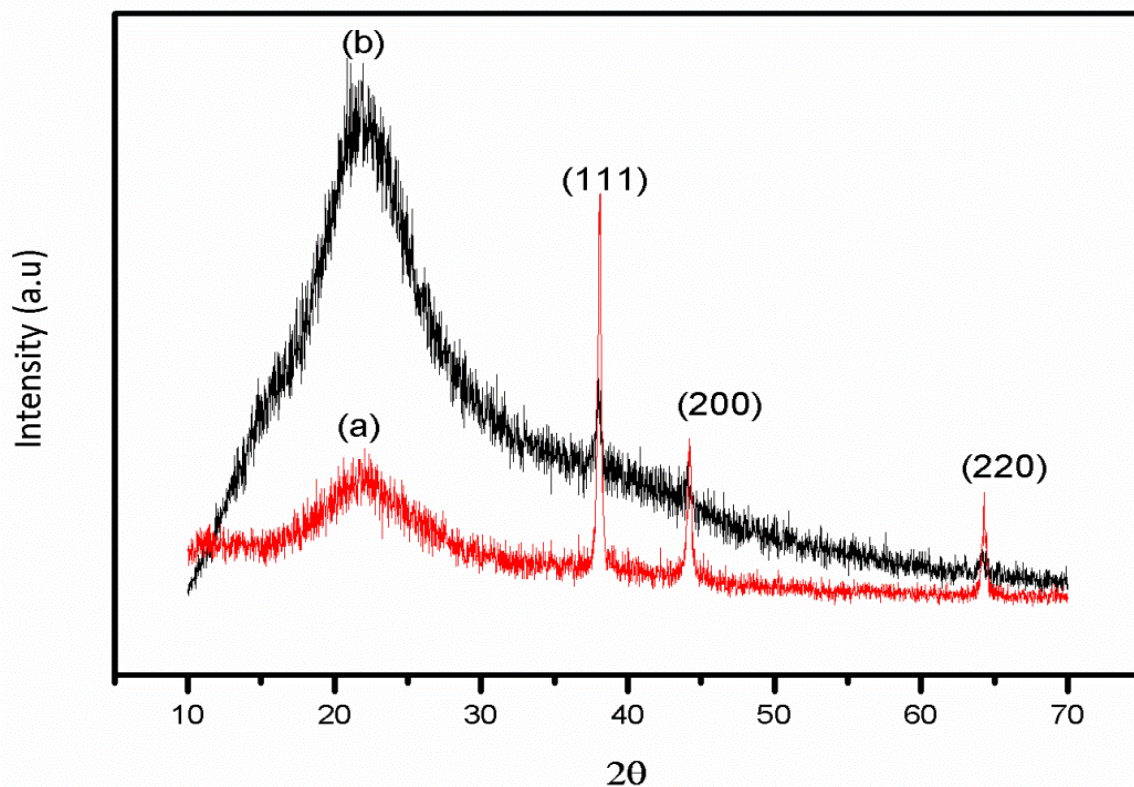


Figure 49 XRD Analysis of ethanol solution containing 10wt%AgNO₃, 2wt%pyrrole, 0.002%PI and (a) 6wt% PVP (b)4wt%PVP UV-irradiated for 10 mins.

Table 5.3 Simple peak indexing

Peak position, 2θ	$1000 \times \sin^2\theta$	$1000 \times \sin^2\theta / 35$	Reflection	Remarks
37.91	105.5	3	(1 1 1)	$1^2+1^2+1^2=3$
44.05	140.63	4	(2 0 0)	$2^2+0^2+0^2=4$
64.1	281.5	8	(2 2 0)	$2^2+2^2+0^2=8$

The crystallite size of the particles can be estimated with the help of same Scherrer's formula (Equation 5.3) used previously,

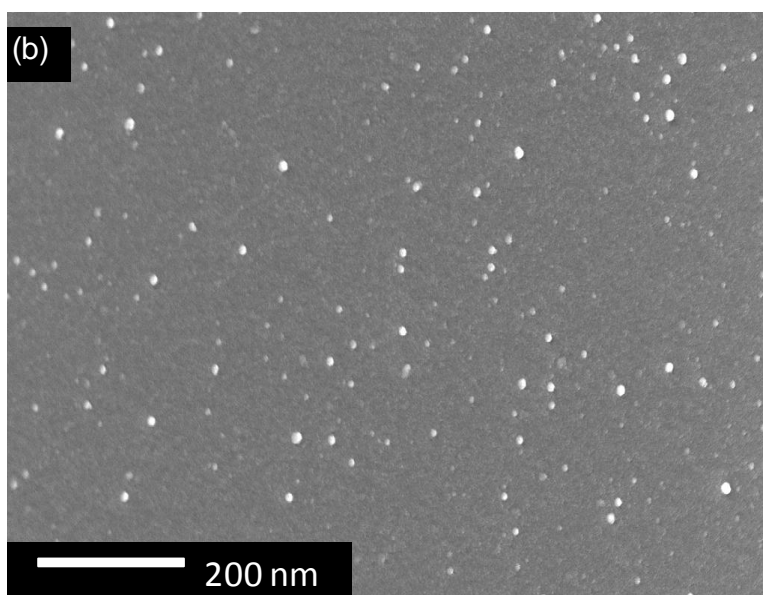
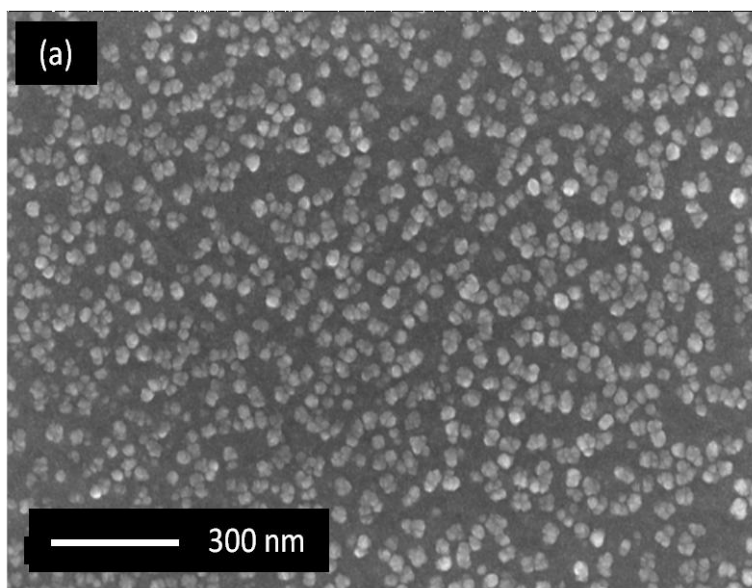
$$D = \frac{K\pi}{\beta \cos\theta} \quad (5.3)$$

Whereas, $K=0.9$, π =wavelength of x-ray (0.1541 nm), β = FWHM (full width at half maximum), θ = the Bragg's diffraction angle and 'D' is particle diameter size. The crystallite size of the silver nanoparticles calculated as an example for the sample containing 4% PVP is found to be in the range of 170 nm.

5.4.5 FE-SEM Analysis

To carry out the morphological studies of the silver particles embedded in a polymer matrix in the presence of a stabilizing agent i.e. PVP. The narrow particle size of the silver particles was obtained in the presence of 1wt% and 2wt% PVP. So, the same concentrations of the stabilizing agent were added in a polymeric formulation to see its effect on the particle size of the silver particles. UV-cured cross linked films were obtained by curing together 10wt%AgNO₃, 2wt%pyrrole, 2wt%PI in the presence of 1wt% and 2wt% PVP respectively under nitrogen for 3 minutes each. FE-SEM analyses were performed on the cryofractured surface of the obtained crosslinked films. Images of the surface fracture of the cured film obtained in the presence of 10wt% silver precursor in the presence of different concentrations of PVP (1% and 2% are shown in Figure 50). Very well distributed particles are obtained within the polymeric matrix with a quite narrow particle size distribution. Lower particle size distribution is obtained in polymer matrix with contrast to the ethanol solution. Hereby, it confirms the reason we assumed at first place that this is change in particle size may be due to the quick polymer network formation which hindered further diffusion of the metal particles generated in-situ, avoiding further growing of the nucleated silver metal germs. Figure 50(b) shows the FESEM images: in the presence of 1%PVP the particle size is in the range of 70-80 nm.

While in (c) the presence of 2%PVP, very small particles are obtained i.e. in the range of 45-65 nm.



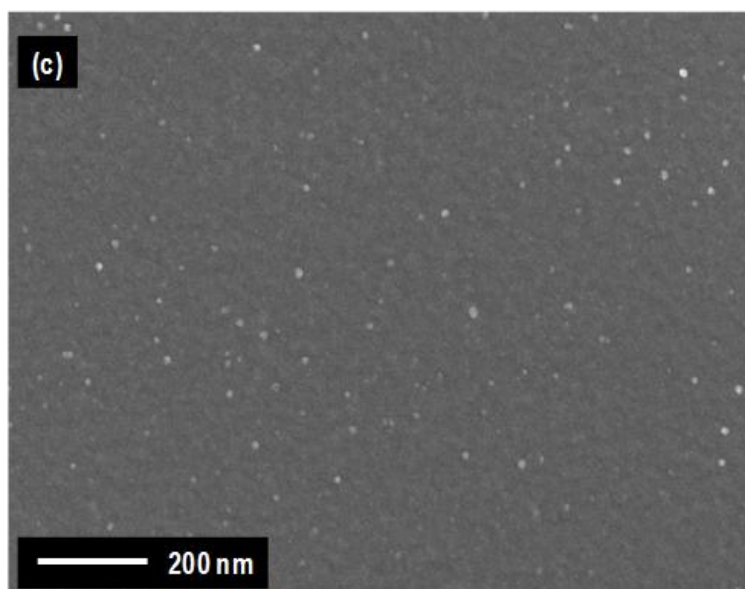


Figure 50 FESEM image of the fracture surface of the crosslinked films (a) 0wt% PVP
(b) 1%PVP (c) 2wt% PVP

After carrying out all the characterization, it is worth to note that the size of silver particles after being stabilized by PVP calculated with the help of different techniques is in a reasonable agreement.

5.4.6 Optical Characterization of solution containing Cu salt

Previous studies^{56,241,246,257} have shown that copper ions can be photoreduced to copper nanoparticles. Thus, as a preliminary study we investigated the effect of photoreduction on the ethanol solution of CuCl_2 under UV-irradiation.

5.4.6.1 *Optical Characterization of CuCl_2 -ethanol solution*

The ethanol solution of CuCl_2 was prepared by dissolving 0.01M CuCl_2 in 10ml ethanol, then added 0.02M photoinitiator (benzophenone) and mixed it in ethanol for 3 minutes in an ultrasonic bath.

Afterwards the solution was deaerated in a quartz cuvette by bubbling nitrogen for 10 minutes, and then the cuvette was sealed with a rubber plug. Section 4.4.2 can be referred for the further details on the details of the synthesis.

The CuCl_2 -ethanol solution was diluted enough (1:5 times to get the UV-vis spectra in a desired range) to observe the photoreduction mechanism after different irradiation times (1min, 3min, 5min, 10min) at a radiation intensity of $45\text{mW}\cdot\text{cm}^{-2}$. The green color of the CuCl_2 -ethanol solution was diluted a little after 1 min. of UV-irradiation.

But, a clear change in color with the further increase in irradiation time is manifested. The color of the CuCl_2 ethanol solution changes from green to transparent after 3 minutes of UV-irradiation, the solution turns light black after 5 minutes of irradiation and after the maximum irradiation time i.e. 10 minutes black precipitates formed on the wall of the cuvette (shown in Figure 51). The results of time dependant UV-vis spectra are shown in Figure 52 where clear visible changes in the spectra can be observed with the change in time of irradiation. Prior to irradiation, the absorption band of CuCl_2 -ethanol solution appears to be in the range of 650-900 nm. According to literature⁵⁰, the visible band is attributed to the UV-vis absorption spectra of CuCl_2 .

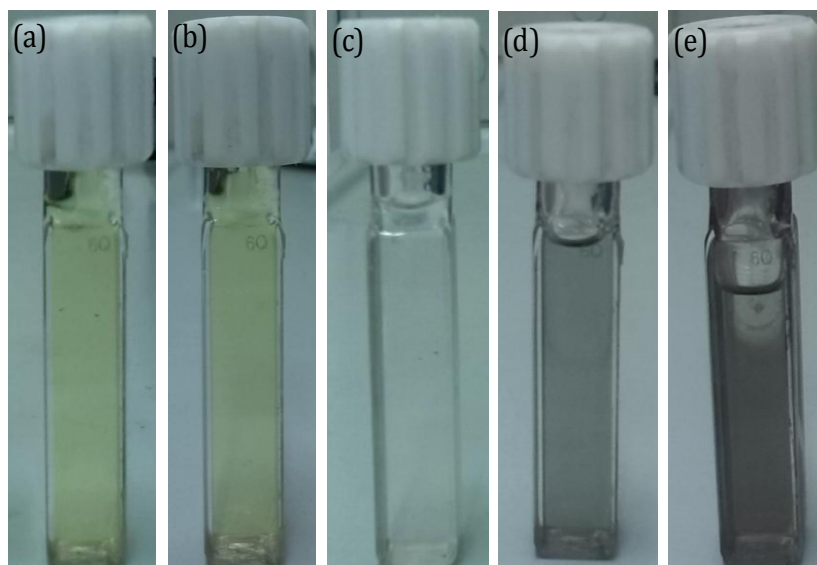


Figure 51 Color change observation of CuCl_2 -ethanol solution a) before UV, (b) 1mins, (c) 3mins, (d) 5mins, (e) after 10mins of UV-irradiation.

While the band below 400 nm corresponds to the absorption of photoinitiator. The UV-vis spectra after 1 min of UV-irradiation is identical to the one before irradiation, accordingly there was no color change recorded after 1 min of irradiation. However, with the further increase in the irradiation time to 3 mins, the CuCl_2 -ethanol solution became nearly colorless (*shown in Figure 51*) subsequently the absorption peak in the range of 650-900 nm completely disappears, which shows the conversion of Cu^{2+} state to Cu^+ . After 5 minutes of UV-irradiation an absorption band appears in the range 560-630 nm, centered at around 600 nm. The absorption increases with the further increase in irradiation time to 10 mins and the absorption band became more wide ranging from 560-720 nm.

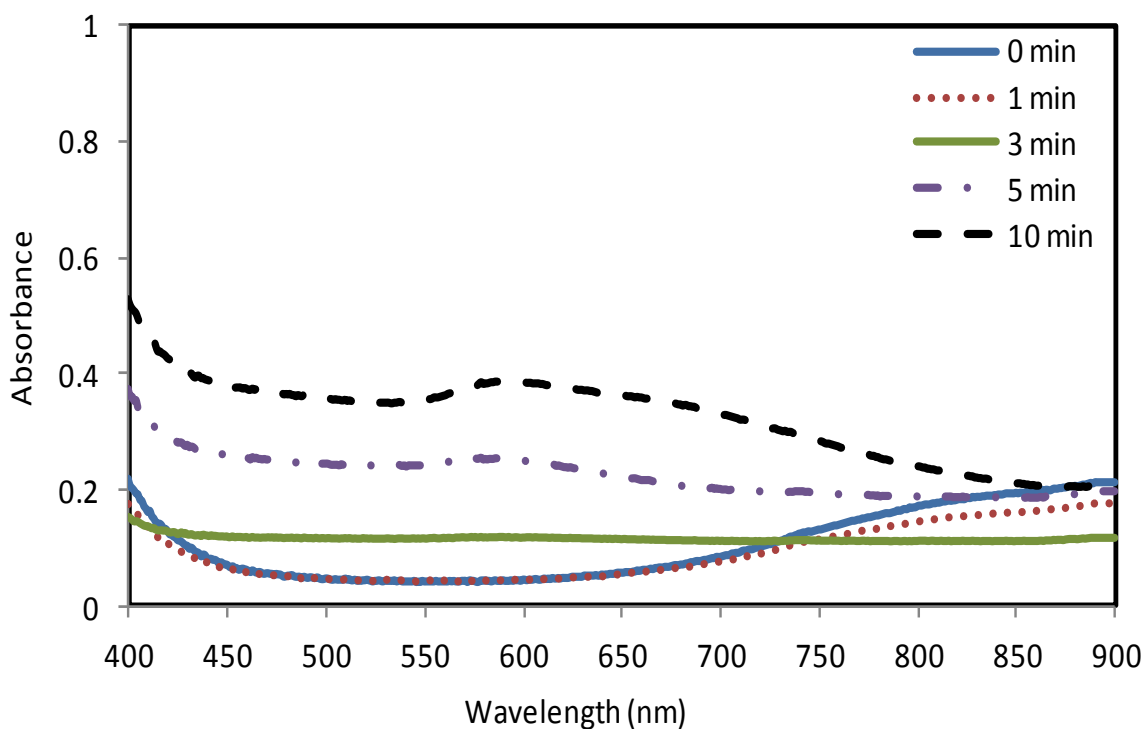


Figure 52 UV-vis spectra of CuCl_2 ethanol solution under different irradiation times.

Generally, it is accepted that the copper nanoparticles show absorbance peak in the range of 575-600 nm²⁴⁶, as the exact position of absorption band is still not known for copper nanoparticles, but rather is a function of several parameters, like solvent, stabilizing agents if used any and the size and shape of the particles.²⁴⁰ Based on the data available in the literature, it appears that with the photoreduction of CuCl_2 -ethanol solution, we can obtain Cu NPs. However, these peaks are not as defined as found in the literature.^{234, 241, 254}. The change in the color of the solution containing copper particles usually defines the oxidation state of the respective copper nanoparticles²⁸² and is related to the reaction taking place. According to the literature²⁸³⁻²⁸⁴, the color of the solution containing Cu-NPs believes to be brick red or pinkish red in color. But, in this case, we observed black precipitates on the wall of the cuvette. So, we can conclude our discussion that even if complete photoreduction of CuCl_2 -ethanol solution in the presence of BP as a photoinitiator takes place, an immediate oxidation of copper particles occurs after their formation.

According to literature,²⁸⁵ copper nanoparticles cannot be synthesized easily by merely photoreducing copper precursors in solution form like other noble metals i.e. gold and silver, since the surface of these nanoparticles is extremely reactive showing a greater tendency to generate cupric oxide (CuO) and cuprous oxide (Cu_2O).

5.4.6.2 *Optical Characterization of CuCl_2 -amine coordination complex*

The most challenging task in the preparation of copper nanoparticles is to get rid of aggregation or precipitation and oxidation during the preparation and storage of colloidal copper particles.²⁸⁶

In order to achieve efficient photoreduction of Cu^{2+} to Cu^0 state and to avoid the propensity towards oxidation: a considerable amount of work has been done to explore the effect of adding different types of amines i.e. saturated amines like ammonia, ethylenediamine, diethylenetriamine and triethylenetetramine²⁸⁷ and unsaturated amines like oleyl amines²⁴⁰, 1-hexadecyl amine.²⁸⁸

The complexes of monoethanol amine (MEA), diethanol amine (DEA) and tertiary ethanol amine (TEA) with cupric ions have been studied by C.W.Davis and B.N.Patel²⁸⁹ in 1968 with the help of potentiometric, conductometric and spectrophotometric techniques. They described in their studies that the hydroxyl group of diethanol amine coordinates with copper to form an uncharged complex, which further reacts to form an anion after losing hydrogen atom. Based on the studies, diethanol amine is the most optimum ligand to use in conjunction with CuCl_2 in an ethanol solution to form copper-amine coordination complex.

Moreover, to identify the best set of conditions to prepare Cu NPs with the help of one step photoreduction technique, two different copper precursors were tried which are $\text{CuCl}_2 \cdot 2\text{H}_2\text{O}$ and $\text{CuSO}_4 \cdot 5\text{H}_2\text{O}$.

The CuCl_2 -amine coordination complex by employing diethanol amine was prepared and the change in the complex before and after irradiation was monitored with the help of UV-vis spectra. The CuCl_2 -amine complex was prepared by dissolving 0.01M CuCl_2 in 10ml ethanol, then added 0.02M photoinitiator (benzophenone) and mixed it for 3 minutes in an ultrasonic bath, 0.04M diethanol amine (DEA) was added to the CuCl_2 -ethanol solution. As soon as diethanol amine was added to the CuCl_2 -ethanol solution, color of the solution turns blue from green as shown in Figure 53. Afterwards the solution was deaerated in a quartz cuvette by bubbling nitrogen for 10 minutes, and then the cuvette was sealed with a rubber plug. The further details on the synthesis are given in Section 4.4.2

The change in color upon adding diethanol amine to CuCl_2 -ethanol solution demonstrates the formation of complex between copper chloride and diethanol amine (DEA). UV-vis spectra analysis was carried out to confirm the formation of CuCl_2 -amine coordination complex and to investigate the effect of different intervals of UV-irradiation time.

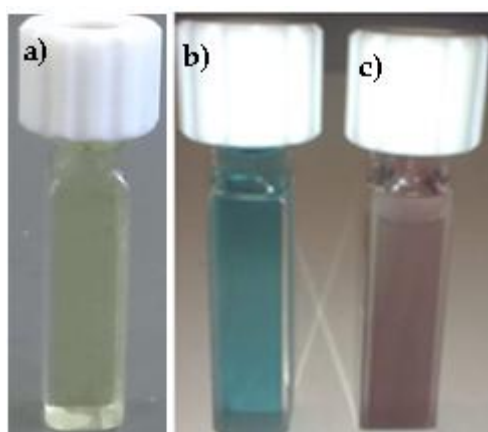


Figure 53 Color change observation: a) CuCl_2 -ethanol solution, b) CuCl_2 -amine coordination complex, c) CuCl_2 -amine coordination complex after 10 mins UV-irradiation.

The copper-amine coordination complex was diluted enough (1:5 times) to record the spectra in a desired range. The UV-vis absorption spectra of CuCl₂-amine complex prior to irradiation show a net absorption peak at around 700 nm. According to the literature,²⁵⁵ this peak is assigned to the copper-diethanol amine coordination complex. The change in color and the absorption spectra appeared to be quite different than those observed in the photoreduction of the CuCl₂-ethanol solution (*shown in Figure 51 and 52*). The absorption peak at 700nm completely disappeared after 1 min UV-irradiation, since the color of the solution turns from blue to completely colorless. This phenomenon shows the photoreduction of Cu²⁺ to Cu⁺ state. With the further increase in irradiation time i.e. to 3 and 5 mins, the solution changes its color from transparent to red and the absorption spectra shows an absorption peak at around 590 nm which is due to the formation of Cu NPs, along with an additional absorption at around 750-800nm, which is the identification of presence of CuO on the surface of the obtained particles.²⁹¹ However, with the maximum UV-irradiation time i.e. 10 mins, the solution turned into deep red color(Figure 53-c), a very sharp absorption peak appears at around 590nm: which confirms the formation of copper particles^{246,254}. The absorbance peak obtained after 10 mins of irradiation corresponds to the formation of Cu⁰ from Cu⁺ state, diethanol amine makes it possible as it serves to solubilize the Cu⁺ ion in an ethanol solution, and avoids the precipitation of cuprous compound, as observed for the systems which do not contain the complexing agent as was shown in Figure 52.

Nevertheless, the intensity of absorption decreases after 10mins of UV-irradiation. The decrease in absorbance observed after the maximum UV-irradiation time is due to the aggregation and precipitation of the particles. A film of copper colloids was also clearly observed on the wall of the quartz cuvette.

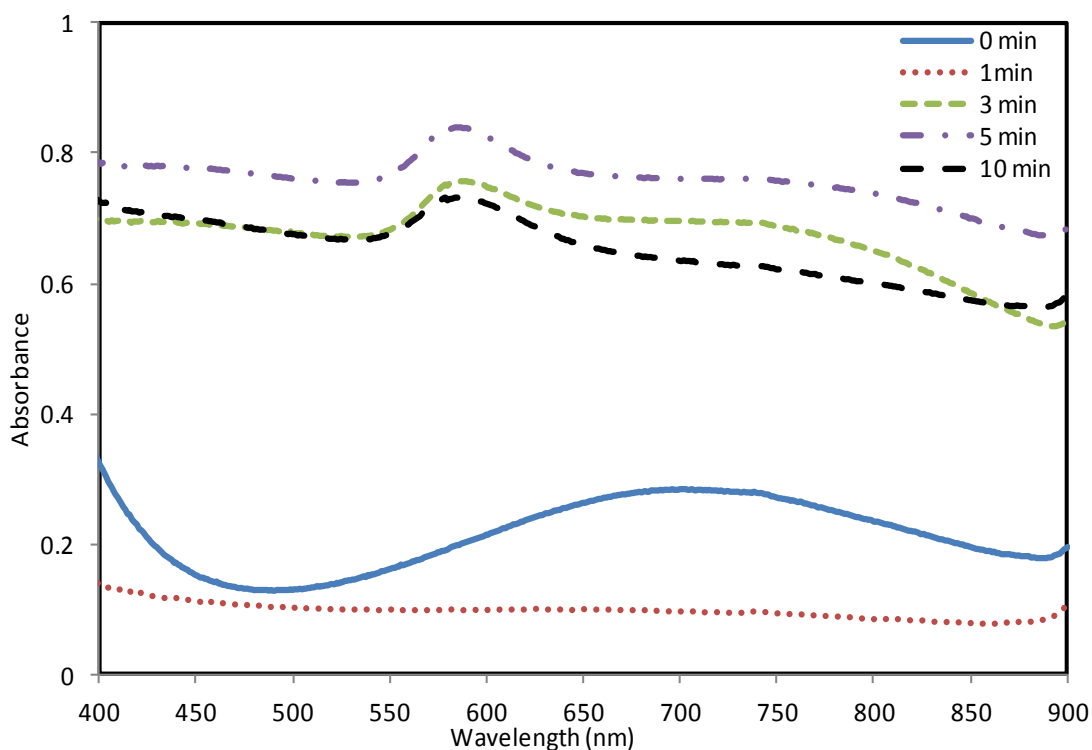


Figure 54 UV-visible spectra of copper chloride-amine coordination complex under UV-irradiation at different times.

The experimental results show that copper nanoparticles can be formed by photoreducing CuCl_2 salt in the presence of a radical photoinitiator (benzophenone) and using diethanol amine as a ligand. Based on the literature^{26, 50,287} and on the basis of experimental results obtained in our laboratory we may resolve that in order to prepare copper nanoparticles by photoreduction mechanism of copper chloride, it is necessary to use nitrogen based coordination ligands.

5.4.6.3 *Optical Characterization of CuSO_4 -amine coordination complex*

After confirming the synthesis of copper particles with the help of copper chloride in the presence of diethanol amine as a ligand, we employed the same technique to investigate the effect of UV-irradiation on another salt of copper i.e. $\text{CuSO}_4 \cdot 5\text{H}_2\text{O}$.

In a very similar systematic way, 0.01M CuSO_4 was dissolved in 10ml methanol (*The solvent was changed because of the strong polar nature of CuSO_4 as it is not soluble in ethanol*) in the presence of 0.02M photoinitiator (benzophenone) and mixed them together for 3 minutes in an ultrasonic bath. After mixing them well in methanol, 0.04M diethanol amine was added. At the end, the solution was deaerated in a UV cuvette by bubbling nitrogen for 10 minutes. The change in color of the CuSO_4 -amine coordination complex after irradiating for different intervals of time (Figure 55) and the absorption spectra recorded for each value (Figure 56) appeared to be quite different than those observed in the photoreduction of the CuCl_2 -amine coordination complex (*already shown in Figure 53 and 54*). However, the color of the CuSO_4 ethanol solution turns to blue from green as soon as 0.04M diethanol amine (DEA) was added in the solution which confirms the formation of coordination complex between copper salt and the diethanol amine. The solution was diluted enough to get the UV-vis spectra in a desired range(1:5 times).Before irradiating CuSO_4 -amine complex, absorption in the range of 600-700 nm can be clearly observed which is same as was observed for the CuCl_2 -amine coordination complex before irradiation. Thus, appearance of this peak confirms the formation of copper-amine coordination complex.²⁹⁰



Figure 55 Color change observation: a) CuSO_4 -amine coordination complex before UV, b) CuSO_4 -amine coordination complex after 10 mins UV-irradiation.

After the maximum time of irradiation blue color of the CuSO_4 amine coordination complex turned to black as shown in Figure 55. The absorption peak after 10 mins irradiation is very broad with a maximum absorption peak at around 650 nm.

According to literature,²⁹²⁻²⁹³ the peak at around 650 nm shows the presence of oxide layer on the surface of copper particles.

From the UV-vis spectra analysis carried out under different set of conditions, we were able to photochemically synthesize copper nanoparticles starting from copper chloride as a salt precursor in the presence of diethanol amine as a ligand and benzophenone as a radical photoinitiator. However, from the Figure 54, we can notice that the intensity of the absorption begins to decrease after the maximum irradiation time mainly because of the continued aggregation of the particles. To address the problem of aggregation of the obtained copper particles, different surfactants are being employed to coat these particles by a protective layer

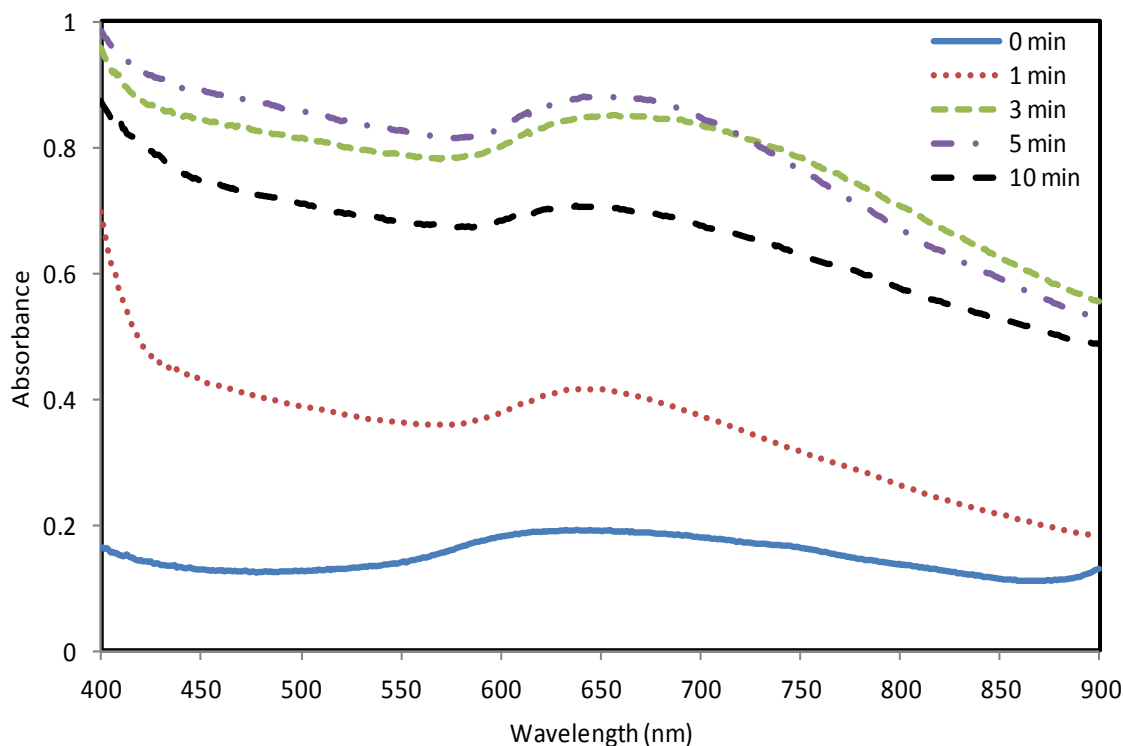


Figure 56 UV-visible spectra of CuSO₄-amine coordination complex under UV-irradiation at different times.

The experimental work to stabilize copper particles with the help of polymers as capping agents is discussed in the next Section.

5.4.7 Stabilization of Cu-NPs against aggregation

A real challenge to synthesize and to employ copper nanoparticles in different application areas is their tendency towards aggregation and oxidation in an ambient atmosphere.²⁹⁴ The most commonly used technique to stabilize copper nanoparticles against aggregation is with the help of polymeric stabilizers.²³³ Already discussed in detail in Section 2.6, among all the polymers the most commonly used polymer to stabilize copper particles is Poly-vinyl pyrrolidone (PVP). A lot of data on the use of PVP as a capping agent is available in the literature.^{50,256-257,238,241} Jeong *et*

al²⁵⁶.determined oxidation resistance accompanied by high conductivity of the copper particles that can be achieved by adding PVP as a polymeric capping agent at different molecular weights (10,000, 29,000 and 40,000 g/mol) and also found out the effect of the molecular weight on the size of NPs obtained. Apart from using PVP as a stabilizer, there is another convincing study carried out by Kobayashi *et al.*²³⁴ in which they used polypyrrole (a conductive polymer) to stabilize Cu-NPs through the polymerization of pyrrole by chemical reduction method. The copper particles obtained by this method were chemically stable in air for a number of days.

We report the stabilization of copper nanoparticles against oxidation and aggregation by photoreducing CuCl₂-amine coordination complex in the presence of these two capping agents i.e. pyrrole and PVP.

5.4.7.1 Effect of pyrrole as a stabilizer on Cu-NPs

In order to observe the effect of the addition of pyrrole on the CuCl₂-amine coordination complex, first of all, CuCl₂-amine was prepared by dissolving 0.01M CuCl₂ in 10ml ethanol, then 0.02M photoinitiator (benzophenone) was added and mixed them for 3 minutes in an ultrasonic bath, 0.04M diethanol amine (DEA) was added to the CuCl₂-ethanol solution. As soon as diethanol amine was added to the CuCl₂-ethanol solution, color of the solution turns blue from green (*shown in Figure 53*). At the end, 0.2% (w/v) pyrrole was added in the CuCl₂-amine coordination complex. Afterwards the solution was deaerated in a quartz cuvette by bubbling nitrogen for 10 minutes, and then the cuvette was sealed with a rubber plug. The further details on the synthesis can be found from Section 4.4.2. Process was monitored during UV-irradiation by using UV-vis spectra analysis, while the solution was diluted (1:30 times) to obtain the UV-vis spectra in a desired range.

UV-vis spectra were recorded after different intervals of irradiation time (1min, 3min, 5min, and 10min). The change in color after irradiating CuCl₂-amine coordination complex in the presence of pyrrole after different intervals of time is noticed to be same as it was observed for the CuCl₂-amine coordination complex without the presence of pyrrole. (*Figure 53*). While the UV-vis spectra shown in

Figure 57 shows almost no change even after 3 mins of irradiation. This is mainly because of the high amount of dilution done in order to obtain UV-vis spectra in a desired range. However, after irradiating this solution for 5 mins, a characteristic peak appears at around 580nm which confirmed the formation of Cu nanoparticles in the presence of polypyrrole²³⁴. Absorption increases with the further increase in irradiation time to 10mins, and the absorption peak at 580 nm shift to a larger wavelength (580nm to 610nm). As per literature²⁹⁵, this shift in the absorption wavelength shows an increment in size of the copper particles obtained.

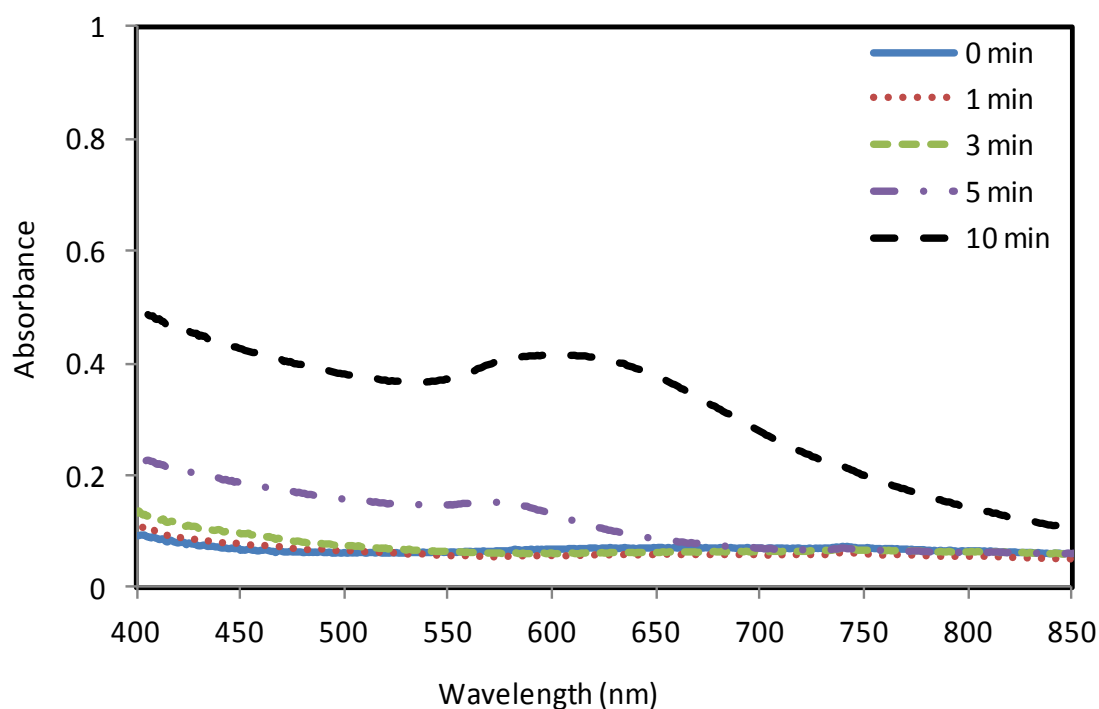


Figure 57 UV-visible spectra of CuCl_2 -amine coordination complex in the presence of 0.2% (w/v) pyrrole under UV-irradiation at different times of irradiation.

The primary motive behind the use of polymer capping agents is to prevent the agglomeration of the particles, by keeping them physically isolated from each other. This feature of the protective molecules also provides a mean to control the size and size distribution of the obtained particles: by adsorbing on to the surface of the particles and thus preventing the coalescence of the particles. To investigate the role of pyrrole as a size controller in photochemical synthesis of copper nanoparticles, particle size and the size distribution of the obtained particles with and without the presence of 0.2 % (w/v) of pyrrole was determined with the help of DLS analysis.

When there was no stabilizing agent added to the CuCl_2 -amine coordination complex, mean particle size of the particles is calculated to be 516nm with a very broad spectrum of size distribution ranging from almost 340 to 800 nm.

Whereas, with the addition of 0.2 % (w/v) pyrrole in the CuCl_2 -amine coordination complex only a slight decrease in the mean size of the copper colloids was observed i.e. 435 nm. Similarly, no profound effect was found on the particle size distribution of the particles which ranges almost from 255-800 nm (Figure 58-b). It is noteworthy, that a shift in absorption towards higher wavelength was observed after 10 mins of UV-irradiation in CuCl_2 -amine coordination complex in the presence of 0.2 % (w/v) of pyrrole. According to literature,²⁶⁰ this shift in the absorbance towards higher wavelength is due to the increase in particle size of the particles. Thus, DLS data supports the theoretical implication once deduced from the UV-vis spectra of the CuCl_2 -amine coordination complex in the presence of pyrrole.

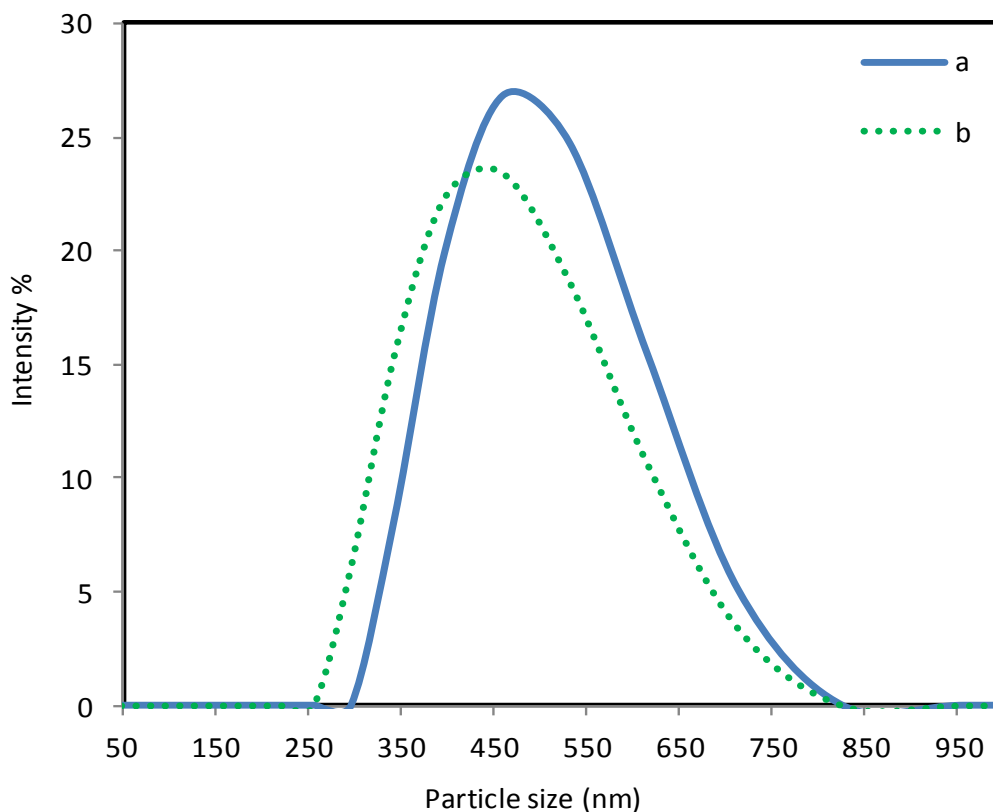


Figure 58 DLS images of diameter distribution by intensity of copper colloids (a) CuCl_2 -amine coordination complex (b) CuCl_2 -amine coordination complex in the presence of 0.2 % (w/v) pyrrole

5.4.7.2 Effect of PVP as a stabilizer on Cu-NPs

To optimize the particle size and size distribution of the copper particles obtained by the photoreduction of CuCl_2 -amine coordination complex, 0.5 % (w/v) PVP was used as a polymer capping agent. For this purpose, CuCl_2 -amine coordination complex was first formed by dissolving 0.01M CuCl_2 in 10ml ethanol in the presence of 0.02M photoinitiator (benzophenone) and mixing them for 3 minutes in an ultrasonic bath and at the end 0.04M diethanol amine (DEA) was added. 0.5% (w/v) PVP was added in the CuCl_2 -amine coordination complex which serves as a polymer capping agent.

Afterwards, the obtained solution was deaerated in a UV cuvette by bubbling nitrogen for 10 minutes. By using UV-vis spectra analyses, process was then monitored during UV-irradiation, while the solution was diluted (1:30 times) to obtain the UV-vis spectra in a desired range.

The absorbance spectra of CuCl_2 -amine coordination complex in the presence of 0.5wt%PVP is shown in Figure 59. A deep red colored solution was observed after irradiating CuCl_2 -amine coordination complex in the presence of 0.5%w/v PVP for 10 mins. While the UV-vis spectra shown in Figure 59 shows almost no change even after 3 mins of irradiation. This is because of the dilution of the solution to a larger extent as compared to the UV-vis spectra without the presence of PVP. After 5mins UV-irradiation a characteristic plasmon band appears at about 575nm which is the same absorbance band observed for copper nanoparticles in literature²⁶¹.

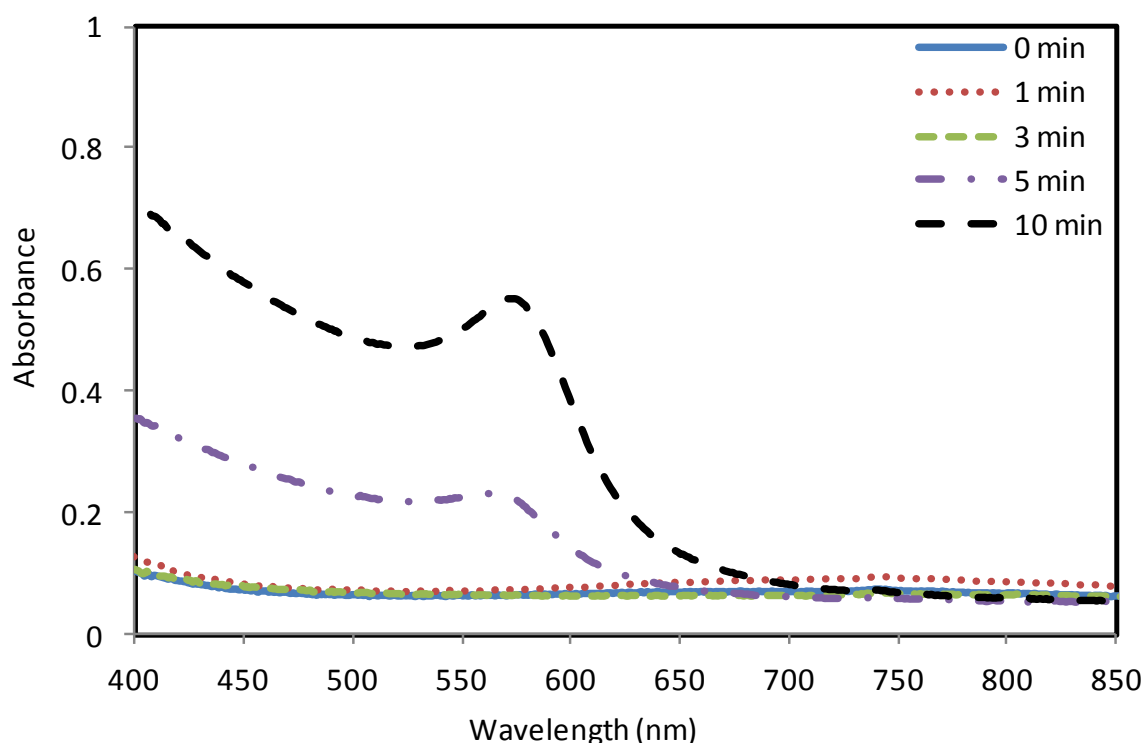


Figure 59 UV-visible spectra of CuCl_2 -amine coordination complex in the presence of 0.5 % (w/v) PVP under UV-irradiation at different times of irradiation

Absorbance increases with the increase in irradiation time to 10 mins, a very sharp peak is observed after the maximum irradiation time and no shift change is observed

in this case. The stable position of absorbance peak observed in Figure 59 with the increase in irradiation time indicates that there is no aggregation of the particles.

On the basis of experimental results obtained with the help of UV-vis spectra, we can state that PVP works efficiently in stabilizing copper particles. The UV-vis spectra of copper nanoparticles in the presence of PVP shows a very sharp peak at 575nm with no shift in wavelength with the increase in irradiation time unlikely as observed for the other two studies held before i.e. CuCl_2 -amine coordination complex with and without the presence of 0.2%(w/v) pyrrole (Figure 54 & Figure 57). This may lead to the assumption that PVP serves its role efficiently not only to prevent the particles from aggregation but also to control the size of the copper particles prepared in this study.

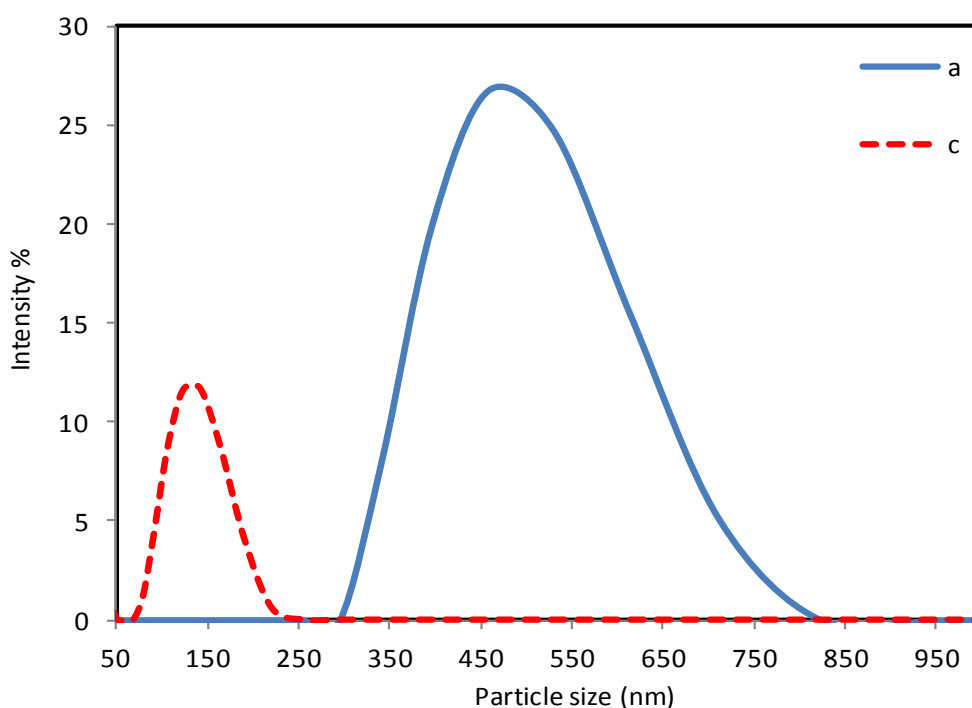


Figure 60 DLS images of diameter distribution by intensity of copper colloids (a) CuCl_2 -amine coordination complex (c) CuCl_2 -amine coordination complex in the presence of 0.5 % (w/v) PVP

We performed DLS analyses to check the effect of the stabilizing agent PVP on the particle size and size distribution of the copper particles.

A drastic change in the particle size and size distribution of the copper particles with the addition of 0.5 % (w/v) PVP can be observed in Figure 60-c. The DLS results

show that the particle size of copper obtained in the presence of 0.5% (w/v) PVP is about 120 nm, while the size distribution ranges from under 100nm i.e. in the range of 70-120 nm i.e. almost 3 times lesser than those without PVP addition(Figure 60-a). This is due to the adsorption of PVP on the surface of copper particles which prevents the coalescence and therefore the aggregation of the particles.

Based on the results obtained by UV-vis spectra and DLS analysis, the fact is established that PVP served not only to stabilize the copper particles against aggregation but also to reduce the particle size of copper particles to a great extent. PVP works both as a size controller and as a polymeric capping agent as it protects the nuclei and impedes it from the aggregation with the help of the polar groups, which are strongly adsorbed at the surface of the copper particles on the surface of copper particles with coordination bonds.²⁸⁶

The purpose of the addition of these polymers is to keep the Cu-NPs physically isolated from each other and to prevent agglomeration. The polymers used in this work qualify to stabilize the copper particles against aggregation or precipitation. But, the oxidative stability was not achieved with the help of these polymers. Although, Y.Kobayashi *et al.*²³⁴ proposed a chemical reduction method to stabilize Cu-NPs by coating them with polypyrrole and claimed to achieve oxidative stability for 50 days after their preparation. Different studies^{50, 238,241,256-256} are available on the use of PVP as a protective molecule to stabilize these Cu-NPs against oxidation. But, the CuCl₂-amine complex containing both the polymeric stabilizers i.e. 0.2%(w/v) pyrrole and 0.5%(w/v) of PVP in it exposed to air, nanoparticles started to oxidize, leading to a drastic change in the color of the solution from deep red to colorless.

5.4.8 Stabilization of Cu-NPs against oxidation

To protect copper nanoparticles against oxidation during preparation and storage, ascorbic acid is often used as an anti-oxidant^{91, 297}. A novel chemical reduction method is introduced by Dang *et al.*²⁵¹ to protect these nanoparticles against oxidation by employing ascorbic acid as a protective agent. Furthermore, to prevent

the agglomeration of the obtained particles, PVP was employed as a polymeric capping agent. In their work,²⁵¹ they reported ascorbic acid as a strong antioxidant for colloidal copper, claimed to obtain very small sized particles in the range of 10-20 nm and stability was achieved for almost 2 months.

In this work we used sodium L-ascorbate and PVP in couple to achieve stabilization against oxidation and aggregation. To prepare the copper-amine coordination complex in the presence of sodium L-ascorbate and PVP, we had to change the scheme being followed till now for all the solutions. The medium of solvent was changed due to the reason that sodium L-ascorbate is highly soluble in water as compared to ethanol. The photoinitiator used for this formulation was Darocur 1173, because benzophenone is totally insoluble in H₂O. The course of action remains the same. First, of all, copper-amine coordination complex was prepared by dissolving 0.01M CuCl₂ in 10 ml H₂O and after this 0.02M photoinitiator (Darocur 1173) and 0.04M diethanol amine (DEA) was added. To this, CuCl₂-amine coordination complex 0.02M sodium L-ascorbate was added followed by adding 0.5% (w/v) PVP and mixed them in an ultrasonic bath for 3-5mins. The obtained solution was diluted (1:30 times) to obtain the UV-vis spectra in a desired range. We do not use rubber capped air tight cuvettes which were used in all the formulations made till now. The solutions were irradiated for different times under an inert atmosphere at intensity of 45mW.cm⁻².

As seen in Figure 61, a change in color is obvious of the irradiated complex with the increase in irradiation time starting from 1min to 10 mins.

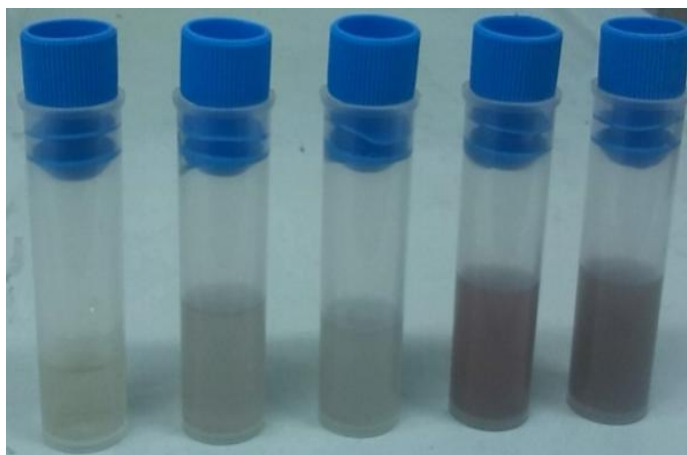


Figure 61 Color change observed after different times of UV-irradiation.

The UV-vis absorption spectra of copper nanoparticles in water before and after irradiation are shown in Figure 62-a. As is clear from the spectra, a sharp peak at around 575 nm is observed after maximum irradiation time which confirms the formation of Cu-NPs. When the same complex irradiated for 10 mins came into contact with air, the color of the solution sustained for almost 20 mins. And the spectra measured after 20 mins of opening the container, it shows a peak at around 576 nm with the decreased intensity as measured earlier for the same solution before coming into contact with air (Figure 62-b). The measured absorption spectra show no such shift change in the wavelength, and proved to achieve stability although for very small time period i.e. for almost 20 minutes in an open atmosphere. The oxidation resistance may become possible due to the ability of sodium L-ascorbate to scavenge free radicals and reactive oxygen molecules. The particle size distribution of the nanosized copper particles obtained in the presence of sodium L-ascorbate and PVP was determined with the help of DLS analysis. An evident change in the particle size and size distribution of the copper particles can be observed in Figure 63

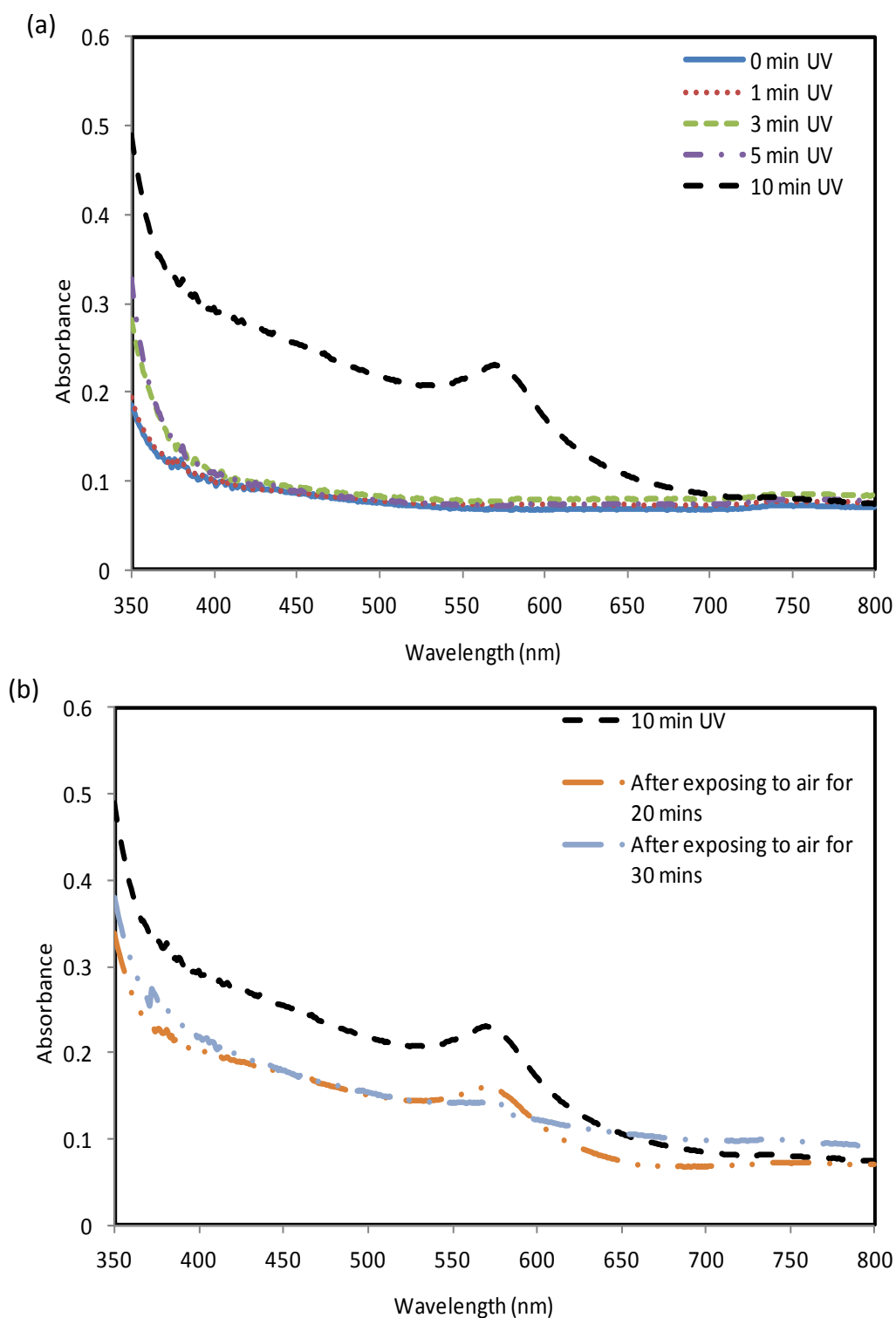


Figure 62(a) UV-vis spectra of CuCl₂-diethanol amine coordination complex in the presence of 0.02M Sodium L-ascorbate and 0.5%(w/v) PVP for different intervals of time.(b) same solution after exposing to open air.

The DLS results show that the size distribution of copper particles obtained in the presence of sodium L-ascorbate and PVP ranges from 70-530 nm, having mean

particle size to be about 230nm. Shift in the particle size and size distribution is so evident as compared to the one having no stabilizing agent (shown in Figure 63-a).

But, the particle size and size distribution is broader as compared to the CuCl_2 -amine coordination complex in the presence of PVP (Figure 60-c). This increase may be due to the increase in the thickness of the particles due to the coating of sodium L-ascorbate around them, as it covers the surface of the particles and protects them from oxidation. It is evident that PVP works efficiently not only to stabilize the particles against aggregation but also to reduce the particle size of copper particles to a great extent.

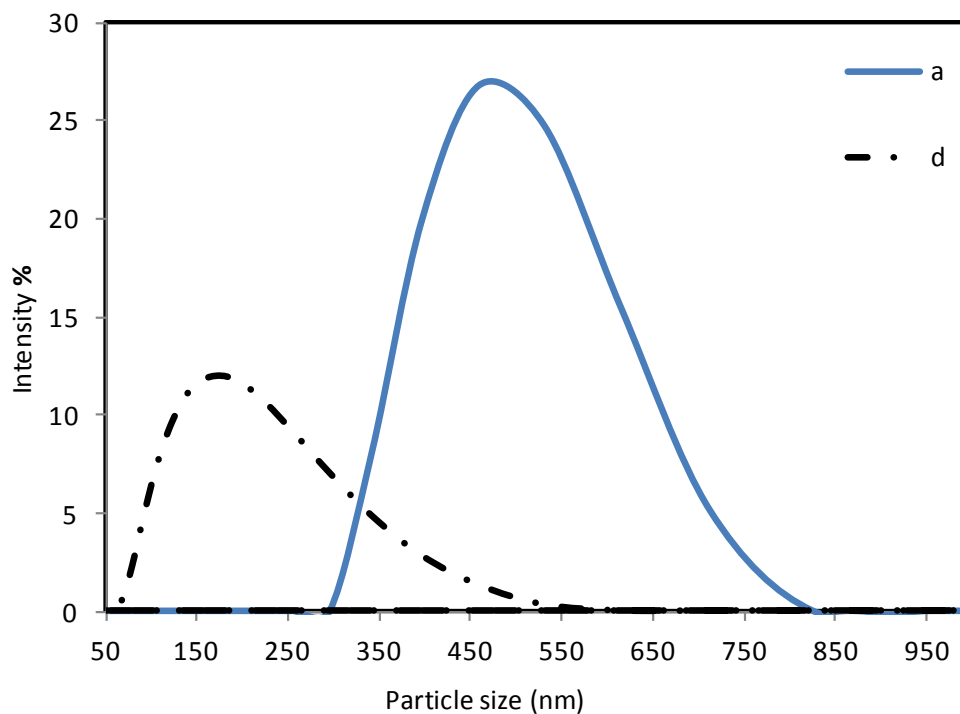


Figure 63 DLS images of diameter distribution by intensity of copper colloids (a) CuCl_2 -amine coordination complex (d) CuCl_2 -amine coordination complex in the presence of 0.02M Sodium L-ascorbate and 0.5%(w/v) PVP

5.4.9 DLS Analysis

Particle size distribution was estimated with the help of DLS technique. DLS analysis was performed on the copper-amine coordination complex, and also on upon adding pyrrole and PVP to check the effect of these polymers on the size distribution of the particles obtained after subjected to UV-irradiation 10 mins. The size distribution of the complex containing sodium ascorbate was also calculated.

It can be observed by looking at Figure 64 that when there is no other polymer added particle size has a broad distribution ranging from almost 340 to 800 nm, and the mean particle size is calculated to be 516nm. Whereas in the presence of pyrrole, there is no profound change observed in the particle size distribution, it ranges from almost 255 to 800 nm. The mean particle size in this case is found to be 435 nm. However, with the addition of PVP in the same Cu-amine complex, one can observe a drastic change in the particles size distribution of the particles which ranges from almost 70 to 200 nm. And the mean particles size of the Cu particles obtained is about 120 nm. And the particle size distribution of the solution containing copper particles in the presence of PVP and sodium ascorbate ranges from 70-530 nm, having mean particle size 230nm.

After looking at the results obtained by DLS, one can conclude that addition of pyrrole has almost no effect on the size of the particles.

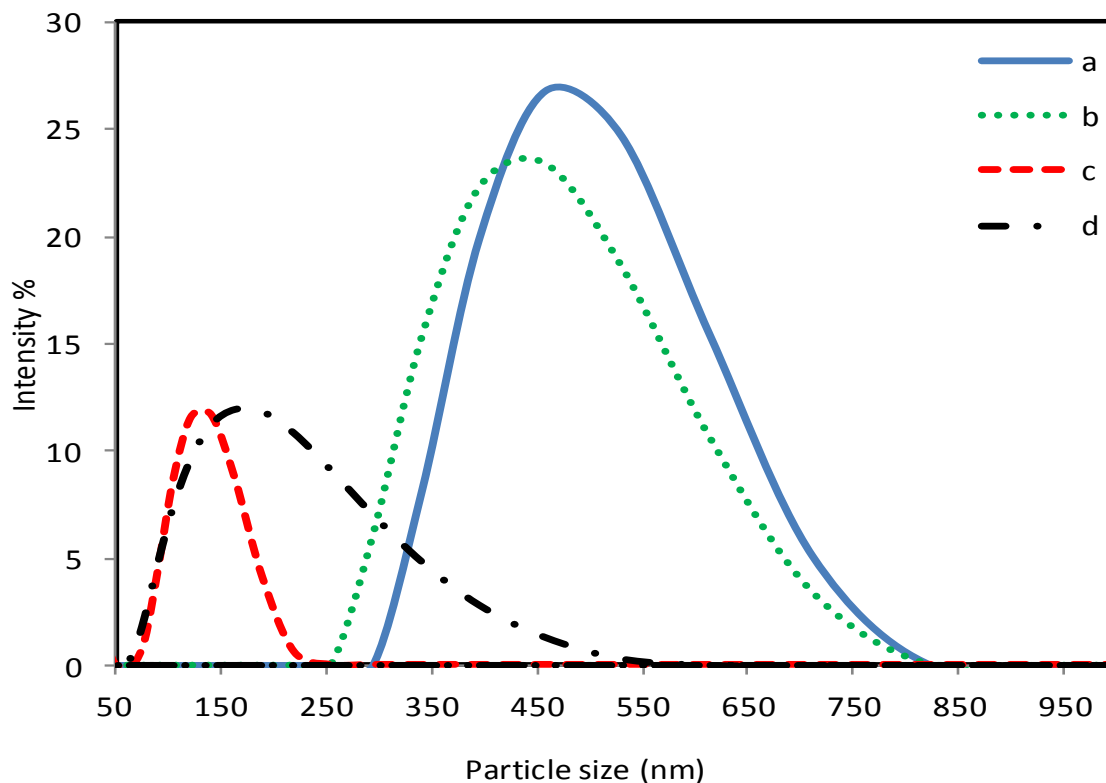


Figure 64 Particle size distribution from DLS (a) CuCl_2 -amine coordination complex (b) CuCl_2 -amine coordination complex in presence of 0.2wt%Py (c) CuCl_2 -amine coordination complex in presence of 0.5wt%PVP. (d). CuCl_2 -amine coordination complex in presence of 0.5wt%PVP in the presence of 0.4% Na-ascorbate

5.5 Photopolymerization of acrylic oligomers in the presence of CuCl_2 and diethanol amine

The copper nanoparticles were successfully prepared by photoreducing CuCl_2 -amine coordination complex in the presence of benzophenone as a radical photoinitiator in an ethanol solution. The stability of the obtained particles against aggregation or precipitation was achieved with the help of polymeric capping agents. While, the

oxidative stability in an open atmosphere was improved by using an antioxidant i.e. sodium L-ascorbate.

The next step was to investigate the contemporary acrylic resin crosslinking reaction and in-situ formation of copper metal particles. In order to obtain UV-cured acrylic crosslinked films, formulations were prepared by adding increasing concentrations of copper chloride in the range between 5wt%-20wt% while keeping the diethanol amine constant at 2wt%, and PI (benzophenone) was used in higher amount i.e. 5wt%, to a di acrylate resin i.e. PEGDA-700 in order to guarantee the curing. The UV-crosslinked films were prepared by subjected to UV-irradiation under an inert atmosphere at intensity 45 mW.cm^{-2} for 10 minutes. The details of the formulation and synthesis procedure are discussed already in Section 4.4.2.

A problem was faced when the polymeric formulations contained higher concentrations of copper precursors (5-20wt %), as it was done in case of silver particles: they were not able to be UV-crosslinked under an inert atmosphere at intensity of 45 mW.cm^{-2} .

In order to figure out this problem, we studied the UV-vis spectra of CuCl_2 -amine complex before irradiation and found it to be highly absorbing both in the visible region ranges from 500-900 nm and below 400 nm, with a maximum of absorption at 350 nm shown in Figure 65. On the other hand, the photoinitiator benzophenone being employed in this work absorbs light at about 280 nm i.e. in the UV-B range. So, we decided to choose a photoinitiator that have an absorption range extending to the visible region of the spectrum, in particular at around 400-480 nm where the minimum in the CuCl_2 absorption spectrum is observed.

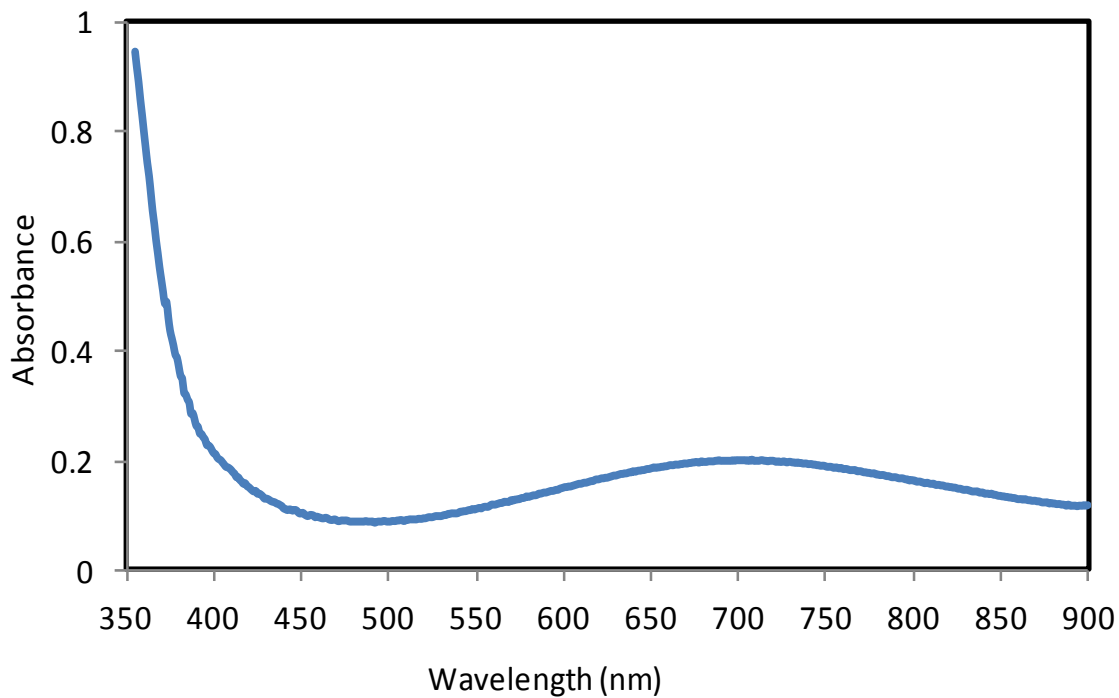


Figure 65 UV-vis absorption spectra of CuCl_2 -amine complex before UV-irradiation

Most commonly used radical photoinitiators to cure acrylate formulations absorb in the region from 300-400 nm. But, photoinitiators that extend to the visible region are also available these days. Recently very strong photoinitiators absorbing at 400 nm is introduced i.e. bis(acyl)phosphane oxide BAPO.²⁹⁸ Muller et al. claimed^{298-a} to make a new photoinitiator by combining Lucirin TPO and Irgacure 819(BAPO) together and successfully photoreduced copper particles in their presence. So, we collect different photoinitiators that can absorb light in the UV-A as well as in visible range to crosslink our system. Pacioni et al.²⁶⁴ used water soluble benzoin Irgacure 2959 and Irgacure 907 as photoinitiators to photochemically reduce copper nanoparticles by employing different copper salts i.e. CuCl_2 , CuSO_4 , $\text{Cu}(\text{NO}_3)_2$. Different photoinitiators listed in Table 5.4 along with their UV-vis absorption peaks were tried to crosslink our system containing 5wt% CuCl_2 , 2wt% diethanol amine with respect to 1g PEGDA.

All these photoinitiators when added 2%(w/w) in PEGDA in the absence of copper precursor can cross-link the system within 3 minutes of UV-irradiation under nitrogen at the same intensity of light used before i.e. 45 mW.cm^{-2} .

Table 5.4 List of photoinitiators with their UV-vis absorption peaks

Sr. No.	Photoinitiators	Chemical Identity	UV-vis absorption peaks in nm
1	Camphorquinone	4,7,7-trimethylbicyclo[2.2.1]heptane-2,3-dione	400-500
2	Darocure 1173	2-Hydroxy-2-methyl-1 phenyl-1-propanone	245, 280, 331
3	Darocure TPO	Diphenyl (2,4,6-trimethylbenzoyl)-phosphine oxide	295, 368, 380, 393
5	Irgacure 2959	2-Hydroxy-1-[4-(2-hydroxyethoxy) phenyl]-2-methyl-1-propanone	276
6	Irgacure 907	2-Methyl-1-[4-(methylthio)phenyl]-2-(4-morpholinyl)-1-propanone	230, 304
7	Irgacure 819	Phosphine oxide, phenyl bi 2,4,6-trimethyl benzoyl)	295, 370
8	ITX	Thioxanthen-9-one	250, 380

The absorption spectrum of camphorquinone (CQ) lies in the visible region i.e. 400-500 nm. So, at first we investigated the effects of the different percentages of camphorquinone CQ with and without the presence of benzophenone on the crosslinking behavior of our polymeric formulation. Different percentages of

camphorquinone (CQ) along with the varying concentrations of benzophenone with respect to 1 gm PEGDA employed to cross-link the required formulation is given in Table 5.5

Table 5.5 Amounts of photoinitiators used

Sr. No.	CuCl ₂ (Wt %)	Diethanol amine (Wt %)	Benzophenone (Wt %)	Camphorquinone (Wt %)
1.	5	2	5	0
2.	5	5	0	5
3.	5	2	5	2
4.	5	2	2	5
5.	5	2	1	2
6.	5	2	2	2
7.	5	2	3	2
8.	5	2	4	2
9.	5	2	1	5
10.	5	2	2	5
11.	5	2	3	5
12.	5	2	4	5

We did not observe any cross-linking effect by UV-irradiating our sample in the presence of the given concentrations of benzophenone and camphorquinone.

The different types of photoinitiators used in different concentrations listed in Table 5.6 were added to the formulation containing 5wt% CuCl₂, 2 wt% diethanol amine in 1 g PEGDA respectively.

Table 5.6 Amounts of photoinitiators used in wt%

Sr.No.	Irgacure 819	Thioxanthone (ITX)	Lucirin TPO	Darocur 1173	Benzophenone
1.	1	-	-	-	2
2.	-	1	-	-	2
3.	-	-	1	-	2
4.	-	-	-	1	2
5.	2	-	-	-	-
6.	-	2	-	-	-
7.	-	-	2	-	-
8.	-	-	-	2	-
9.	1	-	2	-	-
10.	2	-	1	-	-
11.	1	2	-	-	-
12.	2	1	-	-	-
13.	1	1	-	-	-

In order to UV-cross link the polymeric formulation, we employed static as well as dynamic lamp to observe the changes happening during UV-irradiation. But, this photoinitiating system did not work as well.

We tried to use 2wt% of these photoinitiators I-2959 and I-907 respectively by emulating the same system used by Pacioni et. al.²⁹⁹ to photo cure the polymeric formulation. But, in our case these photoinitiators did not serve the purpose to UV-crosslink the polymeric formulation.

After carrying out all these trials, we came to a conclusion that in the presence of copper chloride content in a polymeric formulation, it is not possible to crosslink it with the help of UV-irradiation in the presence of different photoinitiator systems having absorption spectra ranging in UV as well as in visible region.

5.5.1 DSC Analysis

DSC analysis is a thermo analytical technique in which the difference in the amount of heat required to increase the temperature of a sample and reference are measured as a function of temperature.

In order to study the kinetics of the reaction this analysis was undertaken to determine the effect of the addition of copper chloride on inhibition of the crosslinking reaction as discussed in previous section.

In order to observe the exothermicity of the polymerization reaction with and without the presence of copper salt, formulations were prepared by adding 2wt% of thermal initiator AIBN (azo-bis isobutyronitrile) in the presence of 2wt% diethanol amine without the presence of CuCl_2 and by adding 5wt% of CuCl_2 . Here, we prepared another sample by adding 1wt% CuCl_2 under the same conditions to check whether the crosslinking reaction happens in the presence of a lower concentration of CuCl_2 .

The DSC spectra are reported in Figure 66. As the temperature increase no change in all the samples is observed till 60°C , when AIBN decomposes and starts the polymerization, an exothermic peak is appeared for the sample containing no copper salt. For the sample containing 1wt% CuCl_2 the exothermic peak is shifted up to 90°C . The curve for the sample containing 5% copper chloride appears to be straight and no exothermicity has shown in the temperature range $25\text{-}100^\circ\text{C}$. This confirms our observation that the addition of 5% CuCl_2 inhibits the crosslinking reaction. While, the appearance of an exothermic peak in the presence of lower concentration of CuCl_2 shows that polymerization is being done.

No thermal change in the sample containing 5wt% CuCl_2 on the contrary to the ones containing 0% and 1% CuCl_2 therefore proves that the crosslinking reaction may take place in the presence of lower concentration of copper chloride but with the increase in its concentration, there will be no chemical reaction taking place.

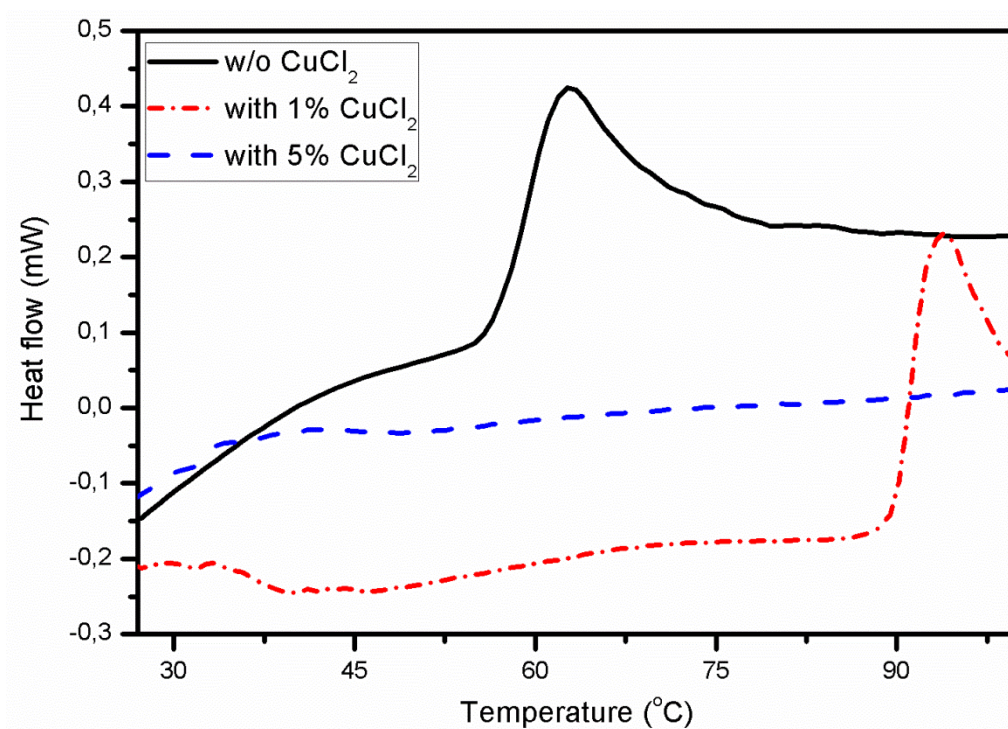


Figure 66 DSC curves of samples without CuCl_2 and the samples containing 1wt% and 5wt% CuCl_2 .

5.5.2 Optical characterization of UV-cured films embedding Cu particles

Interestingly, polymeric formulations containing lower concentrations of copper precursor can be crosslinked as determined with the help of DLS analysis. In order to obtain UV-cured acrylic crosslinked films, formulations were prepared by adding different concentrations of copper chloride i.e. 1wt% and 0.5wt% while keeping the diethanol amine constant at 2wt% and PI (benzophenone) was added at higher concentration i.e. 5wt%. The films of 100 μ thickness were subjected to UV-irradiation under nitrogen at an intensity of 45mW.cm⁻² respectively; the resulting UV-crosslinked films obtained were red in color. The crosslinked films in the presence of higher amount of CuCl_2 have deep red color as compared to the one having lesser percentage 0.5% CuCl_2 as shown in Figure 67.

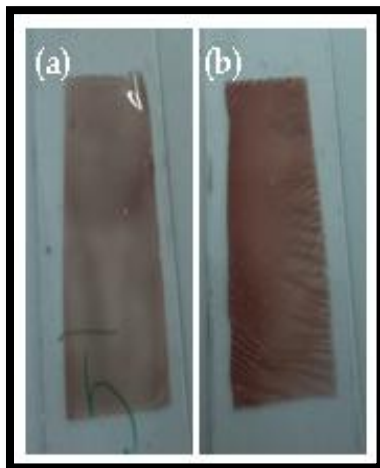


Figure 67 Color change observed in a freshly prepared film containing a) 0.5wt%CuCl₂, b) 1wt%CuCl₂

The absorption spectra of UV-cross linked films in the presence of 1wt % and 0.5 wt% CuCl₂ measured immediately after their preparation is shown in Figure 68. A clear and strong absorption band centered at around 574nm was observed in the presence 1 wt% CuCl₂ and absorption spectra of very low intensity and at about 576nm is observed for 0.5wt% CuCl₂ respectively. It is clear from the Figure 68, the intensity of the surface plasmon absorbance increases with the increase in the concentration of copper salt in the photocurable formulation. The strong absorption peak at 574 nm can be attributed to the formation of copper particles, as previously recorded for the UV-irradiation of ethanol solution containing the copper precursor.

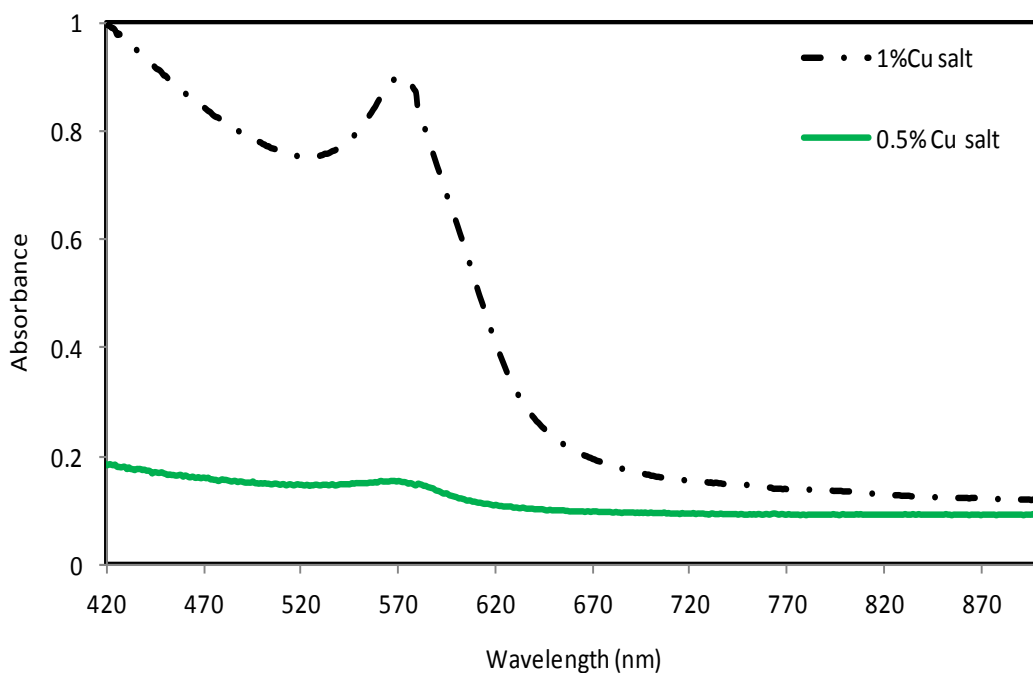


Figure 68 UV-Vis absorption spectra of the crosslinked film freshly prepared containing 0.5wt% and 1wt%CuCl₂, 5wt%PI, 2wt%DEA

The UV-cross linked polymeric films were exposed to an ambient atmosphere and the red color of the film starts tarnishing as soon exposed to air. The change in color observed in the films after two hours is shown in Figure 69, where we can observe that the film containing 0.5% CuCl₂ becomes almost transparent and the film containing 1% CuCl₂ still has some redness on its one side. However, the UV-vis spectra of the same films after being exposed for 2 hours to the open atmosphere are shown in Figure 70.

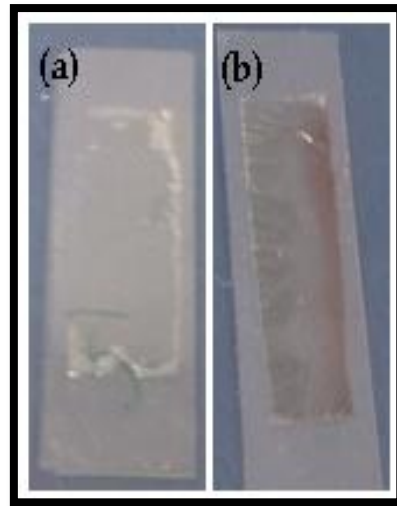


Figure 69 Color change observed in a film after 2 hrs containing a) 1wt%CuCl₂, b) 0.5wt%CuCl₂

A decrease in the intensity of the absorption spectra is quite obvious. A shift towards higher wavelength for the peak containing 0.5% Cu salt content leads to the fact that the copper particles starts to aggregate and starts oxidizing back to copper oxide state when added to a very low concentration. Although the intensity of the absorbance spectra decreases for the peak containing 1% of CuCl₂ salt concentration, but no such shift in wavelength is observed.

The work was carried out in our laboratory to in-situ generate copper particles along with the crosslinking of the acrylic resin. In conclusion, it is stated that it is possible to obtain copper particles by carefully selecting experimental conditions in the presence of very low concentration of copper precursor, i.e. in this case the best results were produced in the presence of 1wt% CuCl₂.

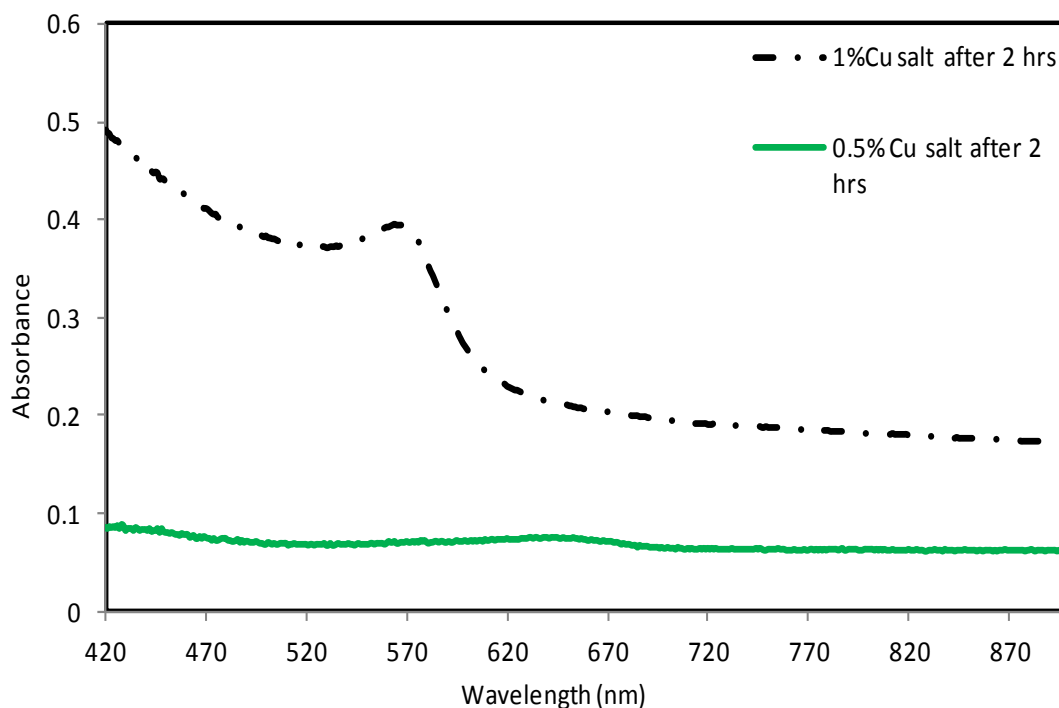


Figure 70 UV-Vis absorption spectra of the crosslinked film containing 1%CuCl₂ and 0.5wt% CuCl₂, 5%PI, 2%DEA after 2 hrs in an open atmosphere

5.5.3 Stabilization of UV-cross linked films against oxidation

In order to achieve oxidation stability of the copper particles embedded in a UV-cured acrylic crosslinked films. Based on the data available in literature^{15, 50,238,241,256,257} we have tried to in-situ synthesized copper metal particles in the presence of polymer capping agents. In this work, 0.5%(w/w) PVP and 0.2%(w/w) pyrrole were used as the polymeric capping agents and added to the polymeric formulation containing 1wt% CuCl₂, 5wt% benzophenone and 2wt% diethanol amine. We investigated the effect of the presence of pyrrole and PVP on the photochemical formation of copper particles, their stability against oxidation with the help of UV-vis spectra.

5.5.3.1 *Effect of pyrrole on the stabilization of Cu-NPs embedded in a polymer matrix*

For the stabilization of metal colloids in a polymeric matrix, the UV-crosslinked films were prepared by dissolving 1wt% CuCl₂ and 5wt% benzophenone in a few drops of ethanol, 1g PEGDA was added and 2wt% diethanol amine was added at the end. 0.2 % (w/w) pyrrole with respect to PEGDA was added and mixed well with the help of ultraturax for 2mins. With the addition of pyrrole in a CuCl₂-amine complex, green color turns to black as shown in Figure 71(a-b). The films of 100 μ were subjected to UV irradiation under nitrogen at intensity of 45mW.cm⁻² for the necessary time to get cured.

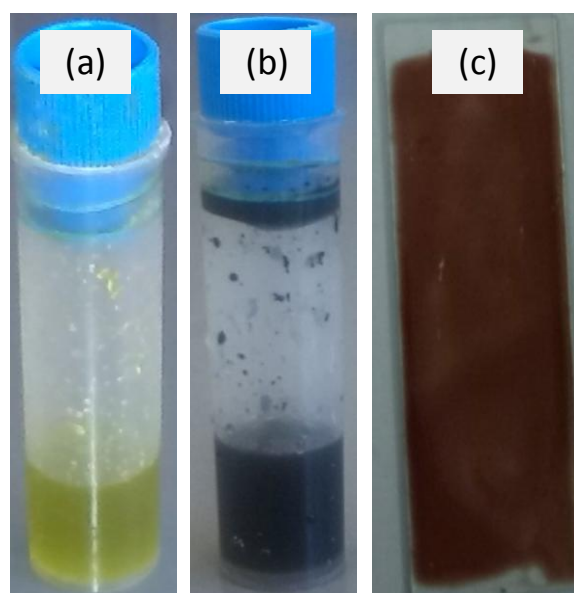


Figure 71 Change in color observed (a) CuCl₂-amine coordination complex in PEGDA, (b) in the presence of 0.2 % (w/w) pyrrole, (c) Freshly prepared crosslinked film in the presence of 0.2 % (w/w) pyrrole

The crosslinked film obtained after UV-irradiation was red in color as shown in Figure 71-c. The deep red color of the film can be attributed to the formation of copper particles, as previously observed for the UV-irradiation CuCl₂-amine coordination complex. However, for the confirmation of the formation of copper nanoparticles, UV-crosslinked films were subjected to the UV-vis spectra. Spectra in Figure 72 show a single absorption peak at around 575 nm.

To monitor the stability of copper particles in air, we measured the absorption of the cross-linked film embedded with Cu-NPs after regular intervals of time. The UV-vis spectra of freshly prepared film and after exposing it to ambient atmosphere for different intervals of time are shown in Figure 72. The decrease in intensity can be easily observed with the increase in time of exposure to open atmosphere. A red shift in wavelength was observed from 575 nm for the freshly prepared film, to 578 nm after exposure in air for 1 hr. After being exposed to air for 2 and 3 hrs respectively, absorption spectrum was shifted towards 579 nm. Usually with the increase in particle size, absorption peak shifts towards higher wavelength.

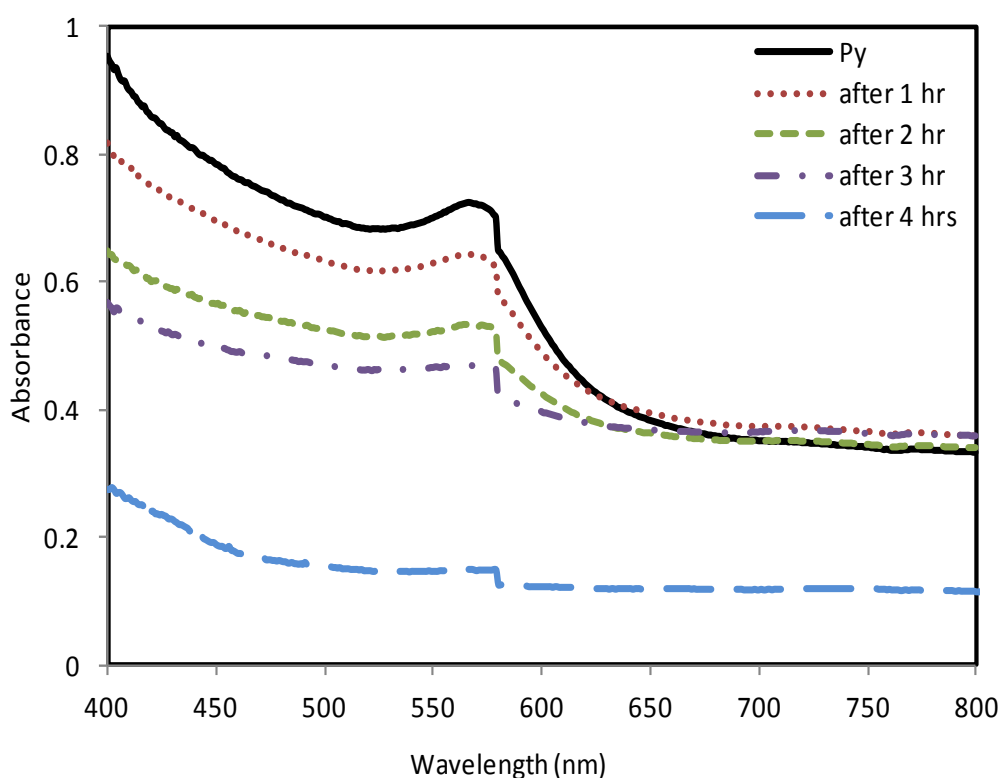


Figure 72 UV-vis spectra of the cross linked films containing 1%CuCl₂, 5%PI, and 2% DEA in the presence of 0.2% pyrrole after regular intervals of time

However, after being exposed to air for 4 hrs, no peak observed. This could be due to the oxidation of copper particles to copper oxide (I) nanoparticles since the similar optical behavior of copper oxide (I) nanoparticles have been reported by Halin et al.³⁰⁰

5.5.3.2 Effect of PVP on the stabilization of Cu-NPs embedded in a polymer matrix

Investigation of the contemporary acrylic resin crosslinking reaction and in-situ preparation of copper particles was carried out in the presence of PVP as a polymer capping agent. In order to obtain UV-cured acrylic crosslinked films, 1wt% CuCl₂ and 5wt% benzophenone were dissolved in a few drops of ethanol, 1g PEGDA was added and 2wt% diethanol amine was added at the end. 0.5 % (w/w) PVP with respect to PEGDA was added and mixed well with the help of ultraturax for 5 mins. With the addition of PVP in a CuCl₂-amine complex, green color turns to blue as shown in Figure 73(a-b)

The films of 100 μ were subjected to UV irradiation under nitrogen at intensity of 45mW.cm⁻². A deep red colored film was obtained after irradiating the sample for 10mins. In a similar way, stability of copper particles obtained in the presence of 0.5 % (w/w) PVP was measured after regular intervals of time. The UV-vis spectra in

Figure 74 clearly show a strong absorption band at around 575 nm for the freshly prepared film, which confirms the formation of copper particles. However, the intensity of absorption band decreases with the increase in time of contact with air. The UV-cross linked film containing PVP as a stabilizer show a stable position of absorbance peak at around 575 nm even after 2 hrs of exposure. However, a red shift to 576 nm and 578 nm was observed after exposing for 3 hrs and 4 hrs respectively.

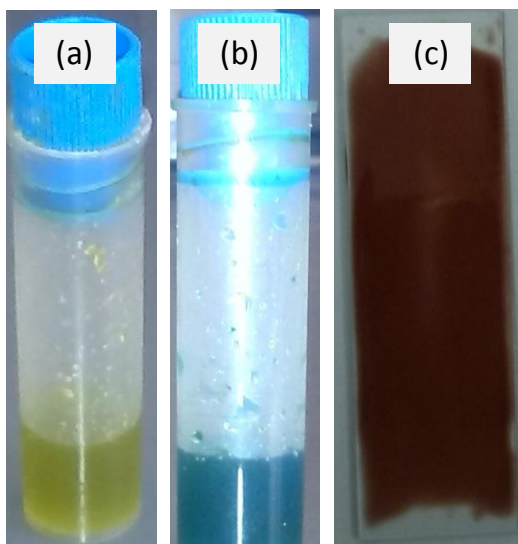


Figure 73 Change in color observed (a) CuCl_2 -amine coordination complex in PEGDA, (b) in the presence of 0.5% (w/w) PVP, (c) Crosslinked film in the presence of 0.5% (w/w) PVP,

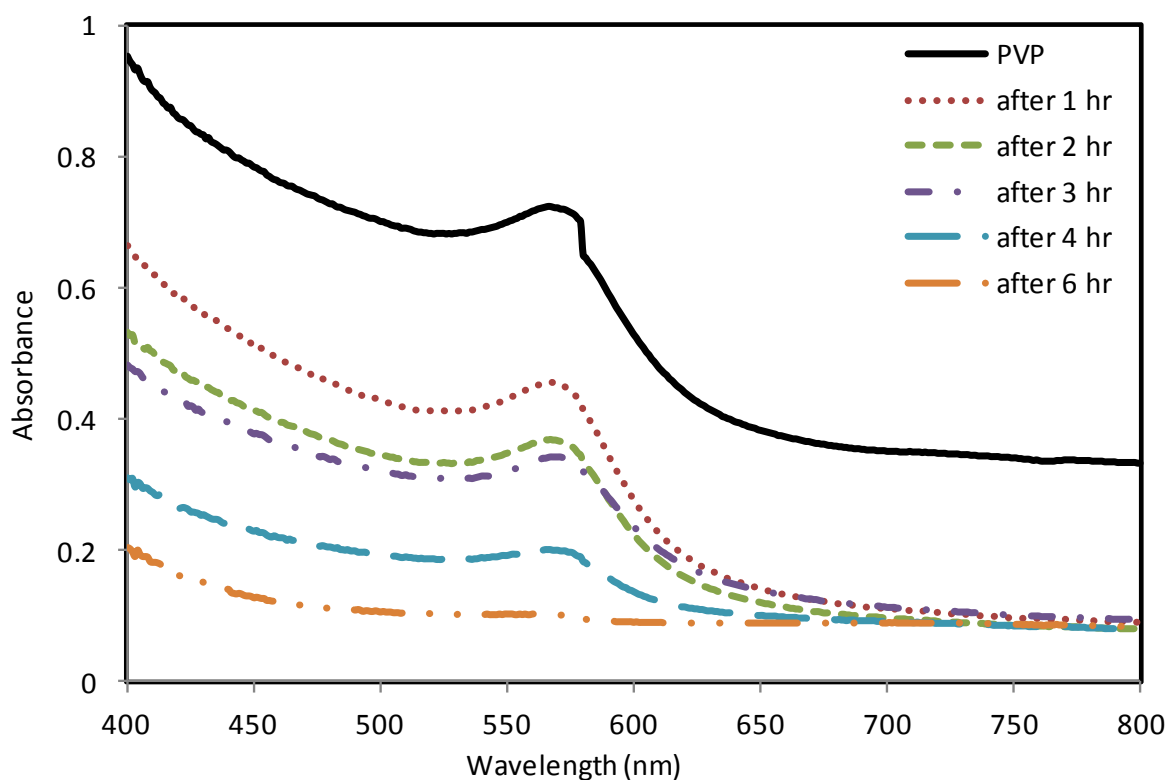


Figure 74 UV-vis spectra of the cross linked films containing 1% CuCl_2 , 5% PI, and 2% DEA in the presence of 0.5% PVP after regular intervals of time

After being exposed to air for 6 hrs no absorption spectra was recorded. This straight line after observed after few hours of exposure to air could be due to the oxidation of copper particles to copper oxide (I) nanoparticles since the similar optical behavior of copper oxide (I) nanoparticles have been reported by Halin et al.³⁰⁰

The absorption spectra shown in Figure 68 and Figure 70 clearly indicates that the photochemical formation of copper nanoparticles is possible independent of the presence of stabilizers and also the obtained Cu-NPs are only stable for an hour in an ambient atmosphere. In-situ formation of copper nanoparticles along with the cross-linking of the acrylic resin in the presence of pyrrole and PVP can be observed clearly from the absorption spectra shown in Figure 72 and Figure 74 respectively.

The results show that copper nanoparticles can be successfully prepared and stabilized against oxidation by photoreducing copper precursor in an acrylic resin in the presence of stabilizers by one step photochemical method. Although Cu particles obtained in the presence of 0.2wt%pyrrole and 0.5wt% PVP persisted against oxidation, but for only few hours in an atmospheric condition.

Chapter 6

Conclusions

And

Future Work

6.1 Conclusions

Electrically conductive polymeric composites have been synthesized by reducing silver nitrate by one step free radical photopolymerization (UV-curing) in the presence of pyrrole without any other reducing agent. The evaluation of the photochemical processes was made monitoring the effect of irradiation on ethanol solutions containing the salt and pyrrole. By UV-Visible absorption spectroscopy, it was confirmed the reduction of silver salt to silver metal and the contemporary UV-induced pyrrole polymerization. It was also made possible by TEM analyses to assess the interesting morphology of the particles: it was ascertained that spherical silver particles coated with pyrrole were obtained. However, silver particles obtained in the ethanol solution were highly agglomerated. In order to overcome this problem, PVP was added in different concentrations to protect the particles from the aggregation: the function of stabilizer was to facilitate the reaction between its functional groups and nanoparticles due to which the collision and coalescence in between the particles decreases. The effect of the addition of different concentrations of the stabilizer PVP was studied with the help of UV-vis spectra, DLS, STEM and XRD analysis. Based on the experimental results obtained already it can be concluded that in all samples silver nanoparticles were formed independent of the presence of PVP. However, by adding different amounts of stabilizer, a change in the absorption spectra of the particles was observed. It was noticed that the band position depends on the particles size and on the amount of stabilizer added to the solution. Therefore, with the PVP concentration in the range of 1 wt% and 2 wt%, strong plasmon absorbance band was observed and it was expected that the particle size and particle size distribution would be narrowest for this range of PVP. This assumption was later confirmed with the help of DLS and STEM analysis. The PVP concentration of 1wt% may be not sufficient enough to prevent the agglomeration of all the obtained nanoparticles. However, PVP concentration of 2wt% leads to the formation of the smallest particle size and narrow size distribution.

The samples containing PVP concentration more than 2wt% have very broad absorbance peaks as observed through UV-vis spectra, while the particle size and size distribution was observed with the help of DLS.

When silver salt and pyrrole are added to acrylic monomer, in the presence of radical photoinitiator, the concomitant formation of acrylic polymer network and the silver in situ reduction and pyrrole polymerization take place. When embedded in the polymer matrix, the metal particles show a size in the range of 50–80 nm. A decrease of resistivity by increasing silver precursor content was observed and the addition of pyrrole to the formulations induced always a further decrease of resistivity in comparison with the films obtained only in the presence of silver salt. The composite materials are conductive and therefore proved to be good candidates as polymeric materials for resistors. However, the expected behavior in the reduction of particle size of the silver particles upon adding PVP in the range of 1 and 2wt% was observed with the help of FESEM analysis.

Since copper is much cheaper, but possesses a very high conductivity (only 6% less than that of Ag)¹⁹⁸, for industrial or bulk usage Cu NPs can be considered as a replacement for silver NPs. However, synthesis of metallic copper nanoparticles is a challenging task as they undergo rapid oxidation in air or in aqueous media.²⁴⁸

In this work, a facile method for the preparation of copper NPs was developed by photo reduction of CuCl_2 in the presence of benzophenone as a photoinitiator and diethanol amine which assists in the conversion of Cu^+ ions to Cu^0 state. The course of action carried out for the synthesis and characterization of silver nanoparticles was followed in the same way. The effect of irradiation on the ethanol solution containing CuCl_2 and diethanol amine was observed by UV-vis spectra, which therefore confirmed the photoreduction of Cu-amine coordination complex to copper particles. The appearance of a film on the wall of cuvette shows the heterogeneous nucleation of the copper particles which was further confirmed with the help of UV-vis spectra. However, exposure of these particles to air results in an extensive oxidation. In order to address these two problems, we tried to coat obtained copper nanoparticles with the help of polymer capping agents, two polymers were used for this cause i.e. PVP and polypyrrole. With the addition of these polymers in an ethanol based solution of copper nanoparticles no heterogeneous nucleation was observed which was confirmed with the help of UV-vis spectra. And stability of the Cu NPs against aggregation was obtained. However, as soon as the cuvette containing these particles was opened, a drastic change in the

color appeared, followed by the aggregation of the particles, and no absorption spectra was observed. In order to prevent oxidation of copper nanoparticles in solution form, sodium ascorbate was used in couple with PVP, and copper nanoparticles were stable up to 20 minutes in an open atmosphere. The particle size and particle size distribution was estimated with the help of DLS analysis, and the experimental results showed copper nanoparticles are smaller in the presence of PVP as a stabilizing agent as contrast to the other stabilizers.

In order to investigate the photochemical formation of copper nanoparticles along with the acrylic crosslinking reaction. The polymeric formulation were prepared by adding higher concentration of copper chloride (5wt %) in the presence of 2wt% diethanol amine and higher amount of photoinitiator was added to guarantee the curing (5wt); it was observed that no reaction took place. We tried different photoinitiating systems but, there was an inhibition to the crosslinking reaction of the polymer in the presence of stated amount of copper chloride.

However, with the decrease in copper salt concentration to 1wt%, in-situ copper nanoparticles formed along with the formation of acrylic polymer network.

These obtained particles were stabilized against oxidation just for two hours in an open atmosphere. So, to increase the stability of obtained Cu-NPs in a polymeric matrix, the same capping agents were employed as were used in an ethanol solution i.e. polypyrrole and PVP. In the presence of these polymer capping agents, the obtained polymeric films embedded with the copper nanoparticles were stable against oxidation for almost 4hrs and 6 hrs respectively.

6.2 Future work

Following are the recommendations based on the work carried out for the doctorate studies.

- The ultimate goal to achieve is to make copper particles embedded polymer composites electrically conductive.
 - a. In order to achieve this goal, we have to work on different issues regarding copper particles. The first and most obvious is to increase the oxidative

stability. To the best of our knowledge, no study is available on the stability achieved for the copper nanoparticles produced by the photoreduction of copper chloride. However, in this work copper particles embedded in a polymer network were stabilized in an open atmosphere for about 6 hours. But, this value is not sufficient to make use of the obtained films in different applications.

- b. The next point is to increase the amount of copper chloride salt in the polymer matrix. As it was done previously while using silver salt, the concentration of silver nitrate was increased up to 20wt% which instantly resulted in decreasing the resistivity of the polymer films. Although, trials were done to increase the copper concentration in an acrylic resin by following the same route as was followed for lesser percentages of copper salt (i.e. 0.5 wt% and 1wt %). But, the acrylic monomer was not polymerized in the presence of higher amount of copper chloride in it.

REFERENCES

1. Hanemann, T. & Szabó, D. V. Polymer-Nanoparticle Composites: From Synthesis to Modern Applications. *Materials* **3**, 3468–3517 (2010).
2. Shameli, K. *et al.* Green biosynthesis of silver nanoparticles using *Callicarpa maingayi* stem bark extraction. *Molecules* **17**, 8506–8517 (2012).
3. Preparation, Characterization and Stabilization of Nanosized Copper Particles.
at
<http://www.academia.edu/6716662/Preparation_Characterization_and_Stabilization_of_Nanosized_Copper_Particles>
4. Biswas, A. *et al.* Advances in top–down and bottom–up surface nanofabrication: Techniques, applications & future prospects. *Advances in Colloid and Interface Science* **170**, 2–27 (2012).
5. Albin, A. & Fagnoni, M. Green chemistry and photochemistry were born at the same time. *Green Chem.* **6**, 1–6 (2004).
- 5-a Lüdersdorff FW. Verh. Verein. Beförderung Gewerbefleiss. Preussen. 1833;12:224.
6. Gul, V. E. *Structure and Properties of Conducting Polymer Composites*. (VSP, 1996).
7. Nanoscale Materials. *Scribd* at
<<http://www.scribd.com/doc/13694200/Nanoscale-Materials>>
8. Henzler, M., Lüer, T. & Burdach, A. Nonmetallic conductivity of epitaxial monolayers of Ag at low temperatures. *Physical Review B* **58**, 10046–10053 (1998).
- 8-a (G. Mie, *Annalen der Physik* **330**(3), 377 (1908))

9. Belloni, J., Mostafavi, M., Remita, H., Marignier, J.-L. & Delcourt, M.-O. Radiation-induced synthesis of mono- and multi-metallic clusters and nanocolloids. *New J. Chem.* **22**, 1239–1255 (1998).
10. Ozin, G. A. & Arsenault, A. C. *Nanochemistry: A Chemical Approach to Nanomaterials*. (Royal Society of Chemistry, 2005).
11. Liang, H.-P., Wan, L.-J., Bai, C.-L. & Jiang, L. Gold hollow nanospheres: tunable surface plasmon resonance controlled by interior-cavity sizes. *J Phys Chem B* **109**, 7795–7800 (2005).
12. Brudny, V. L., Mendoza, B. S. & Luis Mochán, W. Second-harmonic generation from spherical particles. *Phys. Rev. B* **62**, 11152–11162 (2000).
13. Narayanan, R. & El-Sayed, M. A. Raman Studies on the Interaction of the Reactants with the Platinum Nanoparticle Surface during the Nanocatalyzed Electron Transfer Reaction. *J. Phys. Chem. B* **109**, 18460–18464 (2005).
14. Abid, J.-P., Nappa, J., Girault, H. H. & Brevet, P.-F. Pure surface plasmon resonance enhancement of the first hyperpolarizability of gold core-silver shell nanoparticles. *J Chem Phys* **121**, 12577–12582 (2004).
15. Renaud, G. *et al.* Real-Time Monitoring of Growing Nanoparticles. *Science* **300**, 1416–1419 (2003).
16. Nepijko, S. A., Ievlev, D. N., Schulze, W., Urban, J. & Ertl, G. Growth of Rodlike Silver Nanoparticles by Vapor Deposition of Small Clusters. *ChemPhysChem* **1**, 140–142 (2000).
17. Andersson, M., Pedersen, J. S. & Palmqvist, A. E. C. Silver Nanoparticle Formation in Microemulsions Acting Both as Template and Reducing Agent. *Langmuir* **21**, 11387–11396 (2005).

18. Henglein, A. Small-particle research: physicochemical properties of extremely small colloidal metal and semiconductor particles. *Chem. Rev.* **89**, 1861–1873 (1989).
19. Belloni, J. Nucleation, growth and properties of nanoclusters studied by radiation chemistry: Application to catalysis. *Catalysis Today* **113**, 141–156 (2006).
20. Ling, Q.-D. *et al.* Polymer electronic memories: Materials, devices and mechanisms. *Progress in Polymer Science* **33**, 917–978 (2008).
21. Esumi, K., Suzuki, A., Aihara, N., Usui, K. & Torigoe, K. Preparation of Gold Colloids with UV Irradiation Using Dendrimers as Stabilizer. *Langmuir* **14**, 3157–3159 (1998).
22. Yang, X. & Lu, Y. Preparation of polypyrrole-coated silver nanoparticles by one-step UV-induced polymerization. *Materials Letters* **59**, 2484–2487 (2005).
23. Liao, H., Nehl, C. L. & Hafner, J. H. Biomedical applications of plasmon resonant metal nanoparticles. *Nanomedicine (Lond)* **1**, 201–208 (2006).
24. Foster, E. W., Kearns, G. J., Goto, S. & Hutchison, J. E. Patterned Gold-Nanoparticle Monolayers Assembled on the Oxide of Silicon. *Advanced Materials* **17**, 1542–1545 (2005).
25. Tang, S., Vongehr, S. & Meng, X. Carbon Spheres with Controllable Silver Nanoparticle Doping. *J. Phys. Chem. C* **114**, 977–982 (2010).
26. Nanotechnology in the Roman Empire. at <http://newundersol.blogspot.it/2013/09/nanotechnology-in-roman-empire.html>

27. Barber, D. J. & Freestone, I. C. An Investigation of the Origin of the Colour of the Lycurgus Cup by Analytical Transmission Electron Microscopy. *Archaeometry* **32**, 33–45 (1990).
28. Hornyak, G. L., Patrissi, C. J. & Martin, C. R. Fabrication, Characterization, and Optical Properties of Gold Nanoparticle/Porous Alumina Composites: The Nonscattering Maxwell–Garnett Limit. *Journal of Physical Chemistry B* **101**, 1548–1555 (1997).
29. Schmid, G. & Fenske, D. Metal clusters and nanoparticles. *Phil. Trans. R. Soc. A* **368**, 1207–1210 (2010).
30. Lok, C. Nanotechnology: Small wonders. *Nature News* **467**, 18–21 (2010).
31. Meyers, M. A., Mishra, A. & Benson, D. J. Mechanical properties of nanocrystalline materials. *Progress in Materials Science* **51**, 427–556 (2006).
- 31-b. European Commission, nanotechnology innovation for tomorrow world EUR 21151EN 2004 [Online]
32. Nanotechnology risks - the real issues. at <http://www.nanowerk.com/spotlight/spotid=1781.php>
33. Nass, R., Remškar, M., Žumer, M. & Luthar, W. *Industrial application of nanomaterials - chances and risks: technology analysis*. (Future Technologies Division of VDI Technologiezentrum, 2004).
34. Oberdörster, G., Oberdörster, E. & Oberdörster, J. Nanotoxicology: an emerging discipline evolving from studies of ultrafine particles. *Environ. Health Perspect.* **113**, 823–839 (2005).
35. Domenech, B. *et al.* in *Ion Exchange Technologies* (ed. Kilislioglu, A.) (InTech, 2012). at <http://www.intechopen.com/books/ion-exchange->

technologies/bifunctional-polymer-metal-nanocomposite-ion-exchange-materials>

36. Petit, C., Lixon, P. & Pileni, M. P. In situ synthesis of silver nanocluster in AOT reverse micelles. *J. Phys. Chem.* **97**, 12974–12983 (1993).
37. Gates, B. D. *et al.* New approaches to nanofabrication: molding, printing, and other techniques. *Chem. Rev.* **105**, 1171–1196 (2005).
38. Sakakibara, K., Hill, J. P. & Ariga, K. Thin-Film-Based Nanoarchitectures for Soft Matter: Controlled Assemblies into Two-Dimensional Worlds. *Small* **7**, 1288–1308 (2011).
39. ITA Nanotrust Dossiers. at <<http://epub.oeaw.ac.at/?arp=0x002544e3>>
40. Uekawa, N., Kajiwara, J., Kakegawa, K. & Sasaki, Y. Low Temperature Synthesis and Characterization of Porous Anatase TiO₂ Nanoparticles. *Journal of Colloid and Interface Science* **250**, 285–290 (2002).
41. Maira, A. J. *et al.* Gas-phase photo-oxidation of toluene using nanometer-size TiO₂ catalysts. *Applied Catalysis B: Environmental* **29**, 327–336 (2001).
42. Parala, H., Devi, A., Bhakta, R. & Fischer, R. A. Synthesis of nano-scale TiO₂ particles by a nonhydrolytic approach. *J. Mater. Chem.* **12**, 1625–1627 (2002).
43. Brinker, C. J. & Scherer, G. W. *Sol-gel Science: The Physics and Chemistry of Sol-gel Processing*. (Gulf Professional Publishing, 1990).
44. Li, Y., White, T. . & Lim, S. . Low-temperature synthesis and microstructural control of titania nano-particles. *Journal of Solid State Chemistry* **177**, 1372–1381 (2004).
45. Chen, S. & Carroll, D. L. Synthesis and Characterization of Truncated Triangular Silver Nanoplates. *Nano Lett.* **2**, 1003–1007 (2002).

46. Lu, L., Kobayashi, A., Tawa, K. & Ozaki, Y. Silver Nanoplates with Special Shapes: Controlled Synthesis and Their Surface Plasmon Resonance and Surface-Enhanced Raman Scattering Properties. *Chem. Mater.* **18**, 4894–4901 (2006).
47. Ijeri, V. S. *et al.* An elegant and facile single-step UV-curing approach to surface nano-silvering of polymer composites. *Soft Matter* **6**, 4666–4668 (2010).
48. Henglein, A. Colloidal Silver Nanoparticles: Photochemical Preparation and Interaction with O₂, CCl₄, and Some Metal Ions. *Chem. Mater.* **10**, 444–450 (1998).
49. Balan, L., Schneider, R., Turck, C., Lougnot, D. & Morlet-Savary, F. Photogenerating Silver Nanoparticles and Polymer Nanocomposites by Direct Activation in the Near Infrared. *Journal of Nanomaterials* **2012**, (2011).
50. Zhu, X., Wang, B., Shi, F. & Nie, J. Direct, Rapid, Facile Photochemical Method for Preparing Copper Nanoparticles and Copper Patterns. *Langmuir* **28**, 14461–14469 (2012).
- 50-K. Mallick*, M.J. Witcomb, M.S. Scurrall, In situ synthesis of copper nanoparticles and poly(o-toluidine):A metal–polymer composite material. *Available online 8 November 2005*
51. Kurihara, K. (Clarkson C. of T., Kizling, J., Stenius, P. & Fendler, J. H. Laser and Pulse Radiolytically Induced Colloidal Gold Formation in Water and in Water-in-Oil Microemulsions. *J. Am. Chem. Soc.; (United States)* **105:9**, (1983).
52. Bronstein, L. *et al.* Laser Photolysis Formation of Gold Colloids in Block Copolymer Micelles. *Langmuir* **15**, 83–91 (1999).

53. Sakamoto, M., Tachikawa, T., Fujitsuka, M. & Majima, T. Photochemical Formation of Au/Cu Bimetallic Nanoparticles with Different Shapes and Sizes in a Poly(vinyl alcohol) Film. *Advanced Functional Materials* **17**, 857–862 (2007).
54. Eustis, S., Hsu, H.-Y. & El-Sayed, M. A. Gold Nanoparticle Formation from Photochemical Reduction of Au³⁺ by Continuous Excitation in Colloidal Solutions. A Proposed Molecular Mechanism. *J. Phys. Chem. B* **109**, 4811–4815 (2005).
55. Yonezawa, Y., Sato, T., Kuroda, S. & Kuge, K. Photochemical formation of colloidal silver: peptizing action of acetone ketyl radical. *J. Chem. Soc., Faraday Trans.* **87**, 1905–1910 (1991).
56. Kapoor, S. & Mukherjee, T. Photochemical formation of copper nanoparticles in poly(N-vinylpyrrolidone). *Chemical Physics Letters* **370**, 83–87 (2003).
57. Boyd, J. E. Silver and Sunlight: The Science of Early Photography | Chemical Heritage Foundation. at <http://www.chemheritage.org/discover/media/magazine/articles/28-2-silver-and-sunlight.aspx?page=2>
58. Faraday, M. *The Bakerian Lecture: Experimental Relations of Gold (and Other Metals) to Light.* (Royal Society of London, 1857). at <http://archive.org/details/philtrans01816596>
59. Deng, T., Arias, F., Ismagilov, R. F., Kenis, P. J. A. & Whitesides, G. M. Fabrication of Metallic Microstructures Using Exposed, Developed Silver Halide-Based Photographic Film. *Anal. Chem.* **72**, 645–651 (2000).
60. Sakamoto, M., Tachikawa, T., Kim, S. S., Fujitsuka, M. & Majima, T. Association Behavior of a Nitrilotriacetic-Acid-Modified Dye in a Poly(Vinyl Alcohol) Film

- Containing Ni(II)-Adsorbed Gold Nanoparticles. *ChemPhysChem* **8**, 1701–1706 (2007).
61. Sakamoto, M., Fujistuka, M. & Majima, T. Light as a construction tool of metal nanoparticles: Synthesis and mechanism. *Journal of Photochemistry and Photobiology C: Photochemistry Reviews* **10**, 33–56 (2009).
 62. Stellacci, F. *et al.* Laser and Electron-Beam Induced Growth of Nanoparticles for 2D and 3D Metal Patterning. *Advanced Materials* **14**, 194–198 (2002).
 63. Sakamoto, M. & Majima, T. Photochemistry for the Synthesis of Noble Metal Nanoparticles. *Bulletin of the Chemical Society of Japan* **83**, 1133–1154 (2010).
 64. Hada, H., Yonezawa, Y., Yoshida Akio & Kurakake, A. Photoreduction of silver ion in aqueous and alcoholic solutions. *J. Phys. Chem.* **80**, 2728–2731 (1976).
 65. Sato, T., Onaka, H. & Yonezawa, Y. Sensitized photoreduction of silver ions in the presence of acetophenone. *Journal of Photochemistry and Photobiology A: Chemistry* **127**, 83–87 (1999).
 66. Eustis, S. Structure and spectra of photochemically obtained nanosized silver particles in presence of modified porous silica. at https://www.academia.edu/4627629/Structure_and_spectra_of_photochemically_obtained_nanosized_silver_particles_in_presence_of_modified_porous_silica
 67. Scaiano, J. C. *et al.* Photochemical routes to silver and gold nanoparticles. *Pure and Applied Chemistry* **81**, 635–647 (2009).
 68. Jockusch, S., Landis, M. S., Freiermuth, B. & Turro, N. J. Photochemistry and Photophysics of α -Hydroxy Ketones. *Macromolecules* **34**, 1619–1626 (2001).

69. Temel, G., Enginol, B., Aydin, M., Balta, D. K. & Arsu, N. Photopolymerization and photophysical properties of amine linked benzophenone photoinitiator for free radical polymerization. *Journal of Photochemistry and Photobiology A: Chemistry* **219**, 26–31 (2011).
70. Eichler, J., Herz, C. P. & Schnabel, W. On the photolysis of hydroxy alkylphenones and o-substituted derivatives. Laser flash photolysis and photocuring studies. *Die Angewandte Makromolekulare Chemie* **91**, 39–54 (1980).
71. Wu, P.-W. *et al.* Two-Photon Photographic Production of Three-Dimensional Metallic Structures within a Dielectric Matrix. *Advanced Materials* **12**, 1438–1441 (2000).
72. Qiu, J. *et al.* Manipulation of Gold Nanoparticles inside Transparent Materials. *Angewandte Chemie International Edition* **43**, 2230–2234 (2004).
73. Shimotsuma, Y., Hirao, K., Kazansky, P. G. & Qiu, J. Three-Dimensional Micro- and Nano-Fabrication in Transparent Materials by Femtosecond Laser. *Japanese Journal of Applied Physics* **44**, 4735–4748 (2005).
74. Tanaka, T., Ishikawa, A. & Kawata, S. Two-photon-induced reduction of metal ions for fabricating three-dimensional electrically conductive metallic microstructure. *Applied Physics Letters* **88**, 081107 (2006).
75. Maruo, S. & Saeki, T. Femtosecond laser direct writing of metallic microstructures by photoreduction of silver nitrate in a polymer matrix. *Opt. Express* **16**, 1174–1179 (2008).

76. Sakamoto, M., Tachikawa, T., Fujitsuka, M. & Majima, T. Three-Dimensional Writing of Copper Nanoparticles in a Polymer Matrix with Two-Color Laser Beams. *Chem. Mater.* **20**, 2060–2062 (2008).
77. Sakamoto, M., Tachikawa, T., Fujitsuka, M. & Majima, T. Two-Laser-Guided Three-Dimensional Microfabrication and Processing in a Flexible Polymer Matrix. *Advanced Materials* **20**, 3427–3432 (2008).
78. Berti, L., Alessandrini, A. & Facci, P. DNA-Templated Photoinduced Silver Deposition. *J. Am. Chem. Soc.* **127**, 11216–11217 (2005).
79. De Cremer, G. *et al.* Photoactivation of Silver-Exchanged Zeolite A. *Angewandte Chemie International Edition* **47**, 2813–2816 (2008).
80. Mishra, M. K. Radical Photopolymerization of Vinyl Monomers. *Journal of Macromolecular Science, Part C: Polymer Reviews* **22**, 409–470 (1982).
81. Free Radical Vinyl Polymerization. at <http://www.pslc.ws/macrog/radical.htm>
82. Zhu, Y. *et al.* Conductive polymer nanocomposites containing in situ ultra-fine metal particles. *Chin J Polym Sci* **31**, 1061–1065 (2013).
83. Pothukuchi, S., Li, Y. & Wong, C. P. Development of a novel polymer–metal nanocomposite obtained through the route of in situ reduction for integral capacitor application. *J. Appl. Polym. Sci.* **93**, 1531–1538 (2004).
84. Kelly, K. L., Coronado, E., Zhao, L. L. & Schatz, G. C. The Optical Properties of Metal Nanoparticles: The Influence of Size, Shape, and Dielectric Environment. *J. Phys. Chem. B* **107**, 668–677 (2003).

85. Prieto-Simón, B., Macanás, J., Muñoz, M. & Fàbregas, E. Evaluation of different mediator-modified screen-printed electrodes used in a flow system as amperometric sensors for NADH. *Talanta* **71**, 2102–2107 (2007).
86. Muraviev, D. N. *et al.* Simple route for intermatrix synthesis of polymer stabilized core-shell metal nanoparticles for sensor applications. *Physica Status Solidi (A) Applications and Materials Science* **204**, 1686–1692 (2007).
87. Muraviev, D. N., Macanás, J., Ruiz, P. & Munoz, M. Synthesis, stability and electrocatalytic activity of polymer-stabilized monometallic Pt and bimetallic Pt/Cu core-shell nanoparticles. *Physica Status Solidi (A) Applications and Materials Science* **205**, 1460–1464 (2008).
88. Uygun, M., Kahveci, M. U., Odaci, D., Timur, S. & Yagci, Y. Antibacterial Acrylamide Hydrogels Containing Silver Nanoparticles by Simultaneous Photoinduced Free Radical Polymerization and Electron Transfer Processes. *Macromol. Chem. Phys.* **210**, 1867–1875 (2009).
89. Dallas, P., Sharma, V. K. & Zboril, R. Silver polymeric nanocomposites as advanced antimicrobial agents: classification, synthetic paths, applications, and perspectives. *Adv Colloid Interface Sci* **166**, 119–135 (2011).
90. Li, S., Meng Lin, M., Toprak, M. S., Kim, D. K. & Muhammed, M. Nanocomposites of polymer and inorganic nanoparticles for optical and magnetic applications. *Nano Rev* **1**, (2010).
91. Usman, M. S., Ibrahim, N. A., Shameli, K., Zainuddin, N. & Yunus, W. M. Z. W. Copper nanoparticles mediated by chitosan: synthesis and characterization via chemical methods. *Molecules* **17**, 14928–14936 (2012).

92. O'Mullane, A. P., Dale, S. E., Macpherson, J. V. & Unwin, P. R. Fabrication and electrocatalytic properties of polyaniline/Pt nanoparticle composites. *Chem. Commun.* 1606–1607 (2004). doi:10.1039/B404636F
93. Wang, J., Neoh, K. G. & Kang, E. T. Preparation of Nanosized Metallic Particles in Polyaniline. *Journal of Colloid and Interface Science* **239**, 78–86 (2001).
94. Zhou, Y., Itoh, H., Uemura, T., Naka, K. & Chujo, Y. Synthesis of Novel Stable Nanometer-Sized Metal (M = Pd, Au, Pt) Colloids Protected by a π -Conjugated Polymer. *Langmuir* **18**, 277–283 (2002).
95. Lu, J., Moon, K.-S. & Wong, C. P. Development of novel silver nanoparticles/polymer composites as high K polymer matrix by in-situ photochemical method. in *Electronic Components and Technology Conference, 2006. Proceedings. 56th* 6 pp.– (2006). doi:10.1109/ECTC.2006.1645910
96. Breimer, M. A., Yevgeny, G., Sy, S. & Sadik, O. A. Incorporation of Metal Nanoparticles in Photopolymerized Organic Conducting Polymers: A Mechanistic Insight. *Nano Lett.* **1**, 305–308 (2001).
- 96-a Khan, A. A. & Paquiza, L. Electrical behavior of conducting polymer based 'polymeric–inorganic' nanocomposite: Polyaniline and polypyrrole zirconium titanium phosphate. *Synthetic Metals* **161**, 899–905 (2011).
- 96-b Akamatu, H. & Inokuchi, H. On the Electrical Conductivity of Violanthrone, Iso-Violanthrone, and Pyranthrone. *The Journal of Chemical Physics* **18**, 810–811 (1950).
- 96-c Fink, J. *et al.* Electronic structure of pyrrole-based conducting polymers: An electron-energy-loss-spectroscopy study. *Phys. Rev. B* **34**, 1101–1115 (1986).

97. Yagci, Y., Sangermano, M. & Rizza, G. A visible light photochemical route to silver–epoxy nanocomposites by simultaneous polymerization–reduction approach. *Polymer* **49**, 5195–5198 (2008).
- 97-a Chitte, H. K. Synthesis of Polypyrrole Using Ferric Chloride as Oxidant Together with Some Dopants for Use in Gas Sensors. *Journal of Sensor Technology* **01**, 47–56 (2011).
- 97-b Malhotra, B. D. *Handbook of Polymers in Electronics*. (iSmithers Rapra Publishing, 2001).
98. Zhang, Z. & Han, M. One-step preparation of size-selected and well-dispersed silver nanocrystals in polyacrylonitrile by simultaneous reduction and polymerization. *J. Mater. Chem.* **13**, 641–643 (2003).
99. Wang, Y. *et al.* A convenient route to polyvinyl pyrrolidone/silver nanocomposite by electrospinning. *Nanotechnology* **17**, 3304 (2006).
100. Chan, Y. N. C., Craig, G. S. W., Schrock, R. R. & Cohen, R. E. Synthesis of palladium and platinum nanoclusters within microphase-separated diblock copolymers. *Chem. Mater.* **4**, 885–894 (1992).
101. Krasia Theodora & Schlaad Helmut. in *Metal-Containing and Metallosupramolecular Polymers and Materials* **928**, 157–167 (American Chemical Society, 2006).
102. Antonietti, M., Förster, S., Hartmann, J. & Oestreich, S. Novel Amphiphilic Block Copolymers by Polymer Reactions and Their Use for Solubilization of Metal Salts and Metal Colloids. *Macromolecules* **29**, 3800–3806 (1996).

103. Antonietti, M., Wenz, E., Bronstein, L. & Seregina, M. Synthesis and characterization of noble metal colloids in block copolymer micelles. *Adv. Mater.* **7**, 1000–1005 (1995).
104. Selvan, T., Spatz, J. P., Klok, H.-A. & Möller, M. Gold–Polypyrrole Core–Shell Particles in Diblock Copolymer Micelles. *Adv. Mater.* **10**, 132–134 (1998).
105. Selvan, T., Spatz, J. P., Klok, H.-A. & Möller, M. Gold–Polypyrrole Core–Shell Particles in Diblock Copolymer Micelles. *Adv. Mater.* **10**, 132–134 (1998).
106. Zhang, J. *et al.* A Novel Method to Synthesize Polystyrene Nanospheres Immobilized with Silver Nanoparticles by Using Compressed CO₂. *Chem. Eur. J.* **10**, 3531–3536 (2004).
107. Pileni, M.-P., Zemb, T. & Petit, C. Solubilization by reverse micelles: Solute localization and structure perturbation. *Chemical Physics Letters* **118**, 414–420 (1985).
- 107-a. Zhu, Y. J.; Qian, Y. T.; Li, X. J.; Zhang, M. W. Chem. Gamma-Radiation synthesis and characterization of polyacrylamide-silver Nanocomposites *Commun.* 1997, 1081)
- 107-b. Yin, Y. D.; Xu, X. L.; Xia, C. J.; Ge, X. W.; Zhang, Z. C. *Chem. Commun.* 1998, 941.
108. Zhang, J. *et al.* A new method to recover the nanoparticles from reverse micelles: recovery of ZnS nanoparticles synthesized in reverse micelles by compressed CO₂. *Chem. Commun.* 2724–2725 (2001). doi:10.1039/B109802K
109. Zhang, J. *et al.* Recovery of Silver Nanoparticles Synthesized in AOT/C12E4 Mixed Reverse Micelles by Antisolvent CO₂. *Chem. Eur. J.* **8**, 3879–3883 (2002).

110. Malinauskas, A., Malinauskiene, J. & Ramanavičius, A. Conducting polymer-based nanostructured materials: electrochemical aspects. *Nanotechnology* **16**, R51 (2005).
111. Zhu, Y., Qian, Y., Li, X. & Zhang, M. A nonaqueous solution route to synthesis of polyacrylamide-silver nanocomposites at room temperature. *Nanostructured Materials* **10**, 673–678 (1998).
112. Zhu, J.-F. & Zhu, Y.-J. Microwave-assisted one-step synthesis of polyacrylamide-metal (M = Ag, Pt, Cu) nanocomposites in ethylene glycol. *J Phys Chem B* **110**, 8593–8597 (2006).
113. Mehdizadeh Taheri, S., Fischer, S. & Förster, S. Routes to Nanoparticle-Polymer Superlattices. *Polymers* **3**, 662–673 (2011).
114. Althues, H., Henle, J. & Kaskel, S. Functional inorganic nanofillers for transparent polymers. *Chem Soc Rev* **36**, 1454–1465 (2007).
115. Kickelbick, G. Concepts for the incorporation of inorganic building blocks into organic polymers on a nanoscale. *Progress in Polymer Science* **28**, 83–114 (2003).
116. Smith, G. D. & Bedrov, D. Dispersing Nanoparticles in a Polymer Matrix: Are Long, Dense Polymer Tethers Really Necessary? *Langmuir* **25**, 11239–11243 (2009).
117. Oliveira, M. M. *et al.* A simple two-phase route to silver nanoparticles/polyaniline structures. *J Phys Chem B* **110**, 17063–17069 (2006).
118. Brust, M., Walker, M., Bethell, D., Schiffrin, D. J. & Whyman, R. Synthesis of thiol-derivatised gold nanoparticles in a two-phase Liquid–Liquid system. *J. Chem. Soc., Chem. Commun.* 801–802 (1994). doi:10.1039/C39940000801

119. *Hybrid Organic-Inorganic Composites*. **585**, (American Chemical Society, 1995).
120. Lee, D. C. & Jang, L. W. Preparation and characterization of PMMA–Clay hybrid composite by emulsion polymerization. *J. Appl. Polym. Sci.* **61**, 1117–1122 (1996).
121. Kim, T. H., Jang, L. W., Lee, D. C., Choi, H. J. & Jhon, M. S. Synthesis and Rheology of Intercalated Polystyrene/Na⁺-Montmorillonite Nanocomposites. *Macromol. Rapid Commun.* **23**, 191–195 (2002).
122. Hergeth, W.-D., Peller, M. & Hauptmann, P. Polymerizations in the presence of seeds. II. Monitoring the emulsion polymerization in the presence of fillers by means of ultrasound. *Acta Polym.* **37**, 468–469 (1986).
123. Hergeth, W.-D., Starre, P., Schmutzler, K. & Wartewig, S. Polymerizations in the presence of seeds: 3. Emulsion polymerization of vinyl acetate in the presence of quartz powder. *Polymer* **29**, 1323–1328 (1988).
124. W HERGETH, U. S. Polymerization in the presence of seeds. Part IV: Emulsion polymers containing inorganic filler particles. *Polymer* **30**, 254–258 (1989).
125. Veinot, J. G. C., Galloro, J., Pugliese, L., Pestrin, R. & Pietro, W. J. Surface Functionalization of Cadmium Sulfide Quantum-Confined Nanoclusters. 5. Evidence of Facile Surface-Core Electronic Communication in the Photodecomposition Mechanism of Functionalized Quantum Dots†. *Chem. Mater.* **11**, 642–648 (1999).
126. Park, J. *et al.* Ultra-large-scale syntheses of monodisperse nanocrystals. *Nat Mater* **3**, 891–895 (2004).
127. Li, S. *et al.* Synthesis and magnetic properties of bulk transparent PMMA/Fe-oxide nanocomposites. *Nanotechnology* **20**, 185607 (2009).

128. Guo, Z. *et al.* Fabrication and characterization of iron oxide nanoparticles reinforced vinyl-ester resin nanocomposites. *Composites Science and Technology* **68**, 1513–1520 (2008).
129. Avella, M., Errico, M. E., Martelli, S. & Martuscelli, E. Preparation methodologies of polymer matrix nanocomposites. *Appl. Organometal. Chem.* **15**, 435–439 (2001).
130. Avella, M., Errico, M. E. & Martuscelli, E. Novel PMMA/CaCO₃ Nanocomposites Abrasion Resistant Prepared by an in Situ Polymerization Process. *Nano Lett.* **1**, 213–217 (2001).
131. Luca Quaroni, G. C. Preparation of Polymer-Coated Functionalized Silver Nanoparticles. *Journal of the American Chemical Society* (1999). doi:10.1021/ja992088q
132. Dirix, Y., Bastiaansen, C., Caseri, W. & Smith, P. Preparation, structure and properties of uniaxially oriented polyethylene-silver nanocomposites. *Journal of Materials Science* **34**, 3859–3866 (1999).
133. Dirix, Y. *et al.* Optically anisotropic polyethylene-gold nanocomposites. *Appl Opt* **38**, 6581–6586 (1999).
134. Mirkin, C. A., Letsinger, R. L., Mucic, R. C. & Storhoff, J. J. A DNA-based method for rationally assembling nanoparticles into macroscopic materials. *Nature* **382**, 607–609 (1996).
135. Bourgeat-Lami, E. Organic-inorganic nanostructured colloids. *J Nanosci Nanotechnol* **2**, 1–24 (2002).

136. Caseri, W. Nanocomposites of polymers and metals or semiconductors: Historical background and optical properties. *Macromol. Rapid Commun.* **21**, 705–722 (2000).
137. Landfester, K. Polyreactions in Miniemulsions. *Macromol. Rapid Commun.* **22**, 896–936 (2001).
138. Erdem, B., Sudol, E. D., Dimonie, V. L. & El-Aasser, M. S. Encapsulation of inorganic particles via miniemulsion polymerization. III. Characterization of encapsulation. *J. Polym. Sci. A Polym. Chem.* **38**, 4441–4450 (2000).
139. Song, X., Yin, G., Zhao, Y., Wang, H. & Du, Q. Effect of an anionic monomer on the pickering emulsion polymerization stabilized by titania hydrosol. *J. Polym. Sci. A Polym. Chem.* **47**, 5728–5736 (2009).
140. Al-Ghamdi, G. H., Sudol, E. D., Dimonie, V. L. & El-Aasser, M. S. Encapsulation of titanium dioxide in styrene/n-butyl acrylate copolymer by miniemulsion polymerization. *J. Appl. Polym. Sci.* **101**, 3479–3486 (2006).
141. Bechthold, N., Tiarks, F., Willert, M., Landfester, K. & Antonietti, M. Miniemulsion polymerization: applications and new materials. *Macromol. Symp.* **151**, 549–555 (2000).
142. Joumaa, N., Toussay, P., Lansalot, M. & Elaissari, A. Surface modification of iron oxide nanoparticles by a phosphate-based macromonomer and further encapsulation into submicrometer polystyrene particles by miniemulsion polymerization. *J. Polym. Sci. A Polym. Chem.* **46**, 327–340 (2008).
143. Van Berkel, K. Y. & Hawker, C. J. Tailored Composite Polymer-Metal Nanoparticles by Miniemulsion Polymerization and Thiol-ene Functionalization. *J Polym Sci A Polym Chem* **48**, 1594–1606 (2010).

144. Spagnoli, D., Banfield, J. F. & Parker, S. C. Free Energy Change of Aggregation of Nanoparticles. *J. Phys. Chem. C* **112**, 14731–14736 (2008).
145. Rozenberg, B. A. & Tenne, R. Polymer-assisted fabrication of nanoparticles and nanocomposites. *Progress in Polymer Science* **33**, 40–112 (2008).
146. Cao, G. *Nanostructures & Nanomaterials: Synthesis, Properties & Applications*. (Imperial College Press, 2004).
147. Carotenuto, G., Nicolais, L., Martorana, B. & Perlo, P. in *Metal–Polymer Nanocomposites* (eds. Nicolais, L. & Carotenuto, G.) 155–181 (John Wiley & Sons, Inc., 2004). at <http://onlinelibrary.wiley.com/doi/10.1002/0471695432.ch5/summary>
148. Luckham, P. F. Manipulating forces between surfaces: applications in colloid science and biophysics. *Adv Colloid Interface Sci* **111**, 29–47 (2004).
149. Isabel Pastoriza-Santos, L. M. L.-M. Formation of PVP-Protected Metal Nanoparticles in DMF. (2002). doi:10.1021/la015578g
150. Toshima, N. & Yonezawa, T. Bimetallic nanoparticles—novel materials for chemical and physical applications. *New J. Chem.* **22**, 1179–1201 (1998).
151. El Badawy, A. M., Scheckel, K. G., Suidan, M. & Tolaymat, T. The impact of stabilization mechanism on the aggregation kinetics of silver nanoparticles. *Science of The Total Environment* **429**, 325–331 (2012).
152. Henglein, A. & Giersig, M. Formation of Colloidal Silver Nanoparticles: Capping Action of Citrate. *J. Phys. Chem. B* **103**, 9533–9539 (1999).
153. Badawy, A. M. E. *et al.* Impact of Environmental Conditions (pH, Ionic Strength, and Electrolyte Type) on the Surface Charge and Aggregation of Silver Nanoparticles Suspensions. *Environ. Sci. Technol.* **44**, 1260–1266 (2010).

154. Song, K. C., Lee, S. M., Park, T. S. & Lee, B. S. Preparation of colloidal silver nanoparticles by chemical reduction method. *Korean J. Chem. Eng.* **26**, 153–155 (2009).
155. Liu, J.-K., Yang, X.-H. & Tian, X.-G. Preparation of silver/hydroxyapatite nanocomposite spheres. *Powder Technology* **184**, 21–24 (2008).
156. Wang, H., Qiao, X., Chen, J., Wang, X. & Ding, S. Mechanisms of PVP in the preparation of silver nanoparticles. *Materials Chemistry and Physics* **94**, 449–453 (2005).
157. Zhang, Z., Zhao, B. & Hu, L. PVP Protective Mechanism of Ultrafine Silver Powder Synthesized by Chemical Reduction Processes. *Journal of Solid State Chemistry* **121**, 105–110 (1996).
158. Contents: Macromol. Rapid Commun. 24/2005. *Macromol. Rapid Commun.* **26**, 1887–1891 (2005).
159. Kittler, S., Greulich, C., Köller, M. & Epple, M. Synthesis of PVP-coated silver nanoparticles and their biological activity towards human mesenchymal stem cells. *Mat.-wiss. u. Werkstofftech.* **40**, 258–264 (2009).
160. Carotenuto, G. Synthesis and characterization of poly(N-vinylpyrrolidone) filled by monodispersed silver clusters with controlled size. *Appl. Organometal. Chem.* **15**, 344–351 (2001).
161. Bera, T. & Ramachandrarao, P. Morphological changes in biomimetically synthesized hydroxyapatite and silver nanoparticles for medical applications. *J Mater Sci* **44**, 2264–2270 (2009).

162. Xu, X., Wang, Q., Choi, H. C. & Kim, Y. H. Encapsulation of iron nanoparticles with PVP nanofibrous membranes to maintain their catalytic activity. *Journal of Membrane Science* **348**, 231–237 (2010).
163. Xia, X., Xie, C., Cai, S., Yang, Z. & Yang, X. Corrosion characteristics of copper microparticles and copper nanoparticles in distilled water. *Corrosion Science* **48**, 3924–3932 (2006).
164. Liz-Marzán, L. M., Giersig, M. & Mulvaney, P. Synthesis of Nanosized Gold–Silica Core–Shell Particles. *Langmuir* **12**, 4329–4335 (1996).
165. Marinakos, S. M., Shultz, D. A. & Feldheim, D. L. Gold Nanoparticles as Templates for the Synthesis of Hollow Nanometer-Sized Conductive Polymer Capsules. *Adv. Mater.* **11**, 34–37 (1999).
166. Vishwas V. Hardikar, E. M. Coating of Nanosize Silver Particles with Silica. *Journal of Colloid and Interface Science* 133–136 (2000).
doi:10.1006/jcis.1999.6579
167. Thearith Ung, L. M. L.-M. Controlled Method for Silica Coating of Silver Colloids. Influence of Coating on the Rate of Chemical Reactions. *Langmuir* **14**, (1998).
168. Kobayashi, Y., Correa-Duarte, M. A. & Liz-Marzán, L. M. Sol–Gel Processing of Silica-Coated Gold Nanoparticles. *Langmuir* **17**, 6375–6379 (2001).
169. Kobayashi, Y. & Sakuraba, T. Silica-coating of metallic copper nanoparticles in aqueous solution. *Colloids and Surfaces A: Physicochemical and Engineering Aspects* **317**, 756–759 (2008).
170. Mott, D., Galkowski, J., Wang, L., Luo, J. & Zhong, C.-J. Synthesis of Size-Controlled and Shaped Copper Nanoparticles. *Langmuir* **23**, 5740–5745 (2007).

171. Ang, T. P., Wee, T. S. A. & Chin, W. S. Three-Dimensional Self-Assembled Monolayer (3D SAM) of n-Alkanethiols on Copper Nanoclusters. *J. Phys. Chem. B* **108**, 11001–11010 (2004).
172. Lisiecki, I., Billoudet, F. & Pileni, M. P. Control of the Shape and the Size of Copper Metallic Particles. *J. Phys. Chem.* **100**, 4160–4166 (1996).
173. Wu, S.-H. & Chen, D.-H. Synthesis of high-concentration Cu nanoparticles in aqueous CTAB solutions. *Journal of Colloid and Interface Science* **273**, 165–169 (2004).
174. Giuffrida, S., Costanzo, L. L., Ventimiglia, G. & Bongiorno, C. Photochemical synthesis of copper nanoparticles incorporated in poly(vinyl pyrrolidone). *J Nanopart Res* **10**, 1183–1192 (2008).
175. Kapoor, S. & Mukherjee, T. Photochemical formation of copper nanoparticles in poly(N-vinylpyrrolidone). *Chemical Physics Letters* **370**, 83–87 (2003).
176. Xiong, Y. *et al.* Poly(vinyl pyrrolidone): a dual functional reductant and stabilizer for the facile synthesis of noble metal nanoplates in aqueous solutions. *Langmuir* **22**, 8563–8570 (2006).
177. Huang, H. H. *et al.* Synthesis, Characterization, and Nonlinear Optical Properties of Copper Nanoparticles. *Langmuir* **13**, 172–175 (1997).
- 177-a. Mie, G., Beitrage zur Optik truber Medien, speziell kolloidaler Metallosungen. *Ann. Phys.* **1908**, 25, 377-445.
178. Jeong, S. *et al.* Controlling the Thickness of the Surface Oxide Layer on Cu Nanoparticles for the Fabrication of Conductive Structures by Ink-Jet Printing. *Adv. Funct. Mater.* **18**, 679–686 (2008).

179. Kobayashi, Y. *et al.* Synthesis of metallic copper nanoparticles coated with polypyrrole. *Colloid Polym Sci* **287**, 877–880 (2009).
180. Ng, K. H. & Penner, R. M. Electrodeposition of silver–copper bimetallic particles having two archetypes by facilitated nucleation. *Journal of Electroanalytical Chemistry* **522**, 86–94 (2002).
181. M. Cazayous, C. L. Cu-Ag core-shell nanoparticles: A direct correlation between micro-Raman and electron microscopy. *Phys. Rev. B* **73**, (2006).
182. Lee, W. *et al.* Redox–Transmetalation Process as a Generalized Synthetic Strategy for Core–Shell Magnetic Nanoparticles. *J. Am. Chem. Soc.* **127**, 16090–16097 (2005).
183. Magdassi, S., Grouchko, M. & Kamyshny, A. Copper Nanoparticles for Printed Electronics: Routes Towards Achieving Oxidation Stability. *Materials* **3**, 4626–4638 (2010).
184. Zhu, X., Wang, B., Shi, F. & Nie, J. Direct, Rapid, Facile Photochemical Method for Preparing Copper Nanoparticles and Copper Patterns. *Langmuir* **28**, 14461–14469 (2012).
185. Kapoor, S., Palit, D. K. & Mukherjee, T. Preparation, characterization and surface modification of Cu metal nanoparticles. *Chemical Physics Letters* **355**, 383–387 (2002).
- 186 Xia, Y., Xiong, Y., Lim, B. & Skrabalak, S. E. Shape-controlled synthesis of metal nanocrystals: simple chemistry meets complex physics? *Angew. Chem. Int. Ed. Engl.* **48**, 60–103 (2009).
- 187 Lee, H. Utilization of Shape-Controlled Nanoparticles as Catalysts with Enhanced Activity and Selectivity. *RSC Adv.* (2014). doi:10.1039/C4RA05958A

- 188 Jorge Macanás, Patricia Ruiz, Amanda Alonso, María Muñoz & DmitriN Muraviev. in *Ion Exchange and Solvent Extraction* 1–44 (CRC Press, 2011). at <<http://www.crcnetbase.com/doi/abs/10.1201/b10813-2>>
- 189 Kamat, P. V. Photophysical, Photochemical and Photocatalytic Aspects of Metal Nanoparticles. *J. Phys. Chem. B* **106**, 7729–7744 (2002).
- 190 Baptista, P. V. *et al.* Nanoparticles in molecular diagnostics. *Prog Mol Biol Transl Sci* **104**, 427–488 (2011).
- 191 Radwan, S. H. & Azzazy, H. M. E. Gold nanoparticles for molecular diagnostics. *Expert Rev. Mol. Diagn.* **9**, 511–524 (2009).
- 192 Azzazy, H. M. E. & Mansour, M. M. H. In vitro diagnostic prospects of nanoparticles. *Clin. Chim. Acta* **403**, 1–8 (2009).
193. Larginho, M. & Baptista, P. V. Gold and silver nanoparticles for clinical diagnostics - From genomics to proteomics. *J Proteomics* **75**, 2811–2823 (2012).
194. Conde, J., o, Doria, G., alo & Baptista, P. Noble Metal Nanoparticles Applications in Cancer. *Journal of Drug Delivery* **2012**, (2011).
195. Jain, P. K., El-Sayed, I. H. & El-Sayed, M. A. Au nanoparticles target cancer. *Nano Today* **2**, 18–29 (2007).
196. Huang, X., Jain, P. K., El-Sayed, I. H. & El-Sayed, M. A. Gold nanoparticles: interesting optical properties and recent applications in cancer diagnostics and therapy. *Nanomedicine* **2**, 681–693 (2007).
197. Jain, P. K., Huang, X., El-Sayed, I. H. & El-Sayed, M. A. Review of Some Interesting Surface Plasmon Resonance-enhanced Properties of Noble Metal Nanoparticles and Their Applications to Biosystems. *Plasmonics* **2**, 107–118 (2007).

- 197-a . Xia, N. Halas, MRS Bull. 30, 338 (2005)
198. Khatua, S. *et al.* Plasmonic Nanoparticles–Liquid Crystal Composites †. *The Journal of Physical Chemistry C* **114**, 7251–7257 (2010).
199. Haes, A. J. & Van Duyne, R. P. A Nanoscale Optical Biosensor: Sensitivity and Selectivity of an Approach Based on the Localized Surface Plasmon Resonance Spectroscopy of Triangular Silver Nanoparticles. *J. Am. Chem. Soc.* **124**, 10596–10604 (2002).
200. Duval Malinsky, M., Kelly, K. L., Schatz, G. C. & Van Duyne, R. P. Nanosphere Lithography: Effect of Substrate on the Localized Surface Plasmon Resonance Spectrum of Silver Nanoparticles. *J. Phys. Chem. B* **105**, 2343–2350 (2001).
201. Haynes, C. L. & Van Duyne, R. P. Nanosphere Lithography: A Versatile Nanofabrication Tool for Studies of Size-Dependent Nanoparticle Optics. *J. Phys. Chem. B* **105**, 5599–5611 (2001).
202. Zhang, Y., Huang, R., Zhu, X., Wang, L. & Wu, C. Synthesis, properties, and optical applications of noble metal nanoparticle-biomolecule conjugates. *Chin. Sci. Bull.* **57**, 238–246 (2012).
203. Mortazavi, D., Kouzani, A. Z., Kaynak, A. & Duan, W. Nano-plasmonic biosensors: A review. in *2011 IEEE/ICME International Conference on Complex Medical Engineering (CME)* 31–36 (2011). doi:10.1109/ICCME.2011.5876700
204. Barnes, W. L., Dereux, A. & Ebbesen, T. W. Surface plasmon subwavelength optics. *Nature* **424**, 824–830 (2003).
205. Zijlstra, P. & Orrit, M. Single metal nanoparticles: optical detection, spectroscopy and applications. *Rep. Prog. Phys.* **74**, 106401 (2011).

206. Willets, K. A. & Van Duyne, R. P. Localized Surface Plasmon Resonance Spectroscopy and Sensing. *Annual Review of Physical Chemistry* **58**, 267–297 (2007).
- 207 Wilcoxon, J. Optical Absorption Properties of Dispersed Gold and Silver Alloy Nanoparticles†. *J. Phys. Chem. B* **113**, 2647–2656 (2009).
208. Jain, P. K., Lee, K. S., El-Sayed, I. H. & El-Sayed, M. A. Calculated Absorption and Scattering Properties of Gold Nanoparticles of Different Size, Shape, and Composition: Applications in Biological Imaging and Biomedicine. *J. Phys. Chem. B* **110**, 7238–7248 (2006).
209. Murphy, C. J. *et al.* Anisotropic Metal Nanoparticles: Synthesis, Assembly, and Optical Applications. *J. Phys. Chem. B* **109**, 13857–13870 (2005).
210. Liz-Marzán, L. M. Tailoring Surface Plasmons through the Morphology and Assembly of Metal Nanoparticles. *Langmuir* **22**, 32–41 (2006).
211. Doria, G. *et al.* Gold-silver-alloy nanoprobe for one-pot multiplex DNA detection. *Nanotechnology* **21**, 255101 (2010).
- 211-a S. S. Joshi, S.F. Pat, V. Iyer and S. Mahumuni, Radiation induced synthesis and characterization of copper nanoparticles. (411007) 1998
212. Baptista, P. V., Doria, G. & Conde, J. Alloy metal nanoparticles for multicolor cancer diagnostics. in **7909**, 79090K–79090K–10 (2011).
- 213 .*Optical Properties of Metal Clusters.* at
<<http://www.springer.com/materials/book/978-3-540-57836-9>>
214. Hulst, H. C. van de. *Light Scattering by Small Particles.* (Dover Publications, 1981).
215. Link, S. & El-Sayed, M. A. Optical properties and ultrafast dynamics of metallic nanocrystals. *Annu Rev Phys Chem* **54**, 331–366 (2003).

216. Mulvaney, P. Surface Plasmon Spectroscopy of Nanosized Metal Particles. *Langmuir* **12**, 788–800 (1996).
217. Hao, E., Schatz, G. C. & Hupp, J. T. Synthesis and optical properties of anisotropic metal nanoparticles. *J Fluoresc* **14**, 331–341 (2004).
218. Brioude, A., Jiang, X. C. & Pileni, M. P. Optical Properties of Gold Nanorods: DDA Simulations Supported by Experiments. *J. Phys. Chem. B* **109**, 13138–13142 (2005).
219. Mayer, A. B. R. Colloidal metal nanoparticles dispersed in amphiphilic polymers. *Polym. Adv. Technol.* **12**, 96–106 (2001).
220. Hervés, P. *et al.* Catalysis by metallic nanoparticles in aqueous solution: model reactions. *Chem. Soc. Rev.* **41**, 5577–5587 (2012).
221. Kuppan, B. & Selvam, P. Platinum-supported mesoporous carbon (Pt/CMK-3) as anodic catalyst for direct methanol fuel cell applications: The effect of preparation and deposition methods. *Progress in Natural Science: Materials International* **22**, 616–623 (2012).
222. Chen, M. S. & Goodman, D. W. The Structure of Catalytically Active Gold on Titania. *Science* **306**, 252–255 (2004).
223. Narayanan, R. & El-Sayed, M. A. Catalysis with Transition Metal Nanoparticles in Colloidal Solution: Nanoparticle Shape Dependence and Stability. *J. Phys. Chem. B* **109**, 12663–12676 (2005).
224. Valden, M., Lai, X. & Goodman, D. W. Onset of Catalytic Activity of Gold Clusters on Titania with the Appearance of Nonmetallic Properties. *Science* **281**, 1647–1650 (1998).

225. Mishra, M. K. Radical Photopolymerization of Vinyl Monomers. *Journal of Macromolecular Science, Part C: Polymer Reviews* **22**, 409–470 (1982).
226. Vescovo, L., Sangermano, M., Scarazzini, R., Kortaberria, G. & Mondragon, I. In-situ-Synthesized Silver/Epoxy Nanocomposites: Electrical Characterization by Means of Dielectric Spectroscopy. *Macromol. Chem. Phys.* **211**, 1933–1939 (2010).
227. Yonezawa, Y., Sato, T., Ohno, M. & Hada, H. Photochemical formation of colloidal metals. *J. Chem. Soc., Faraday Trans. 1* **83**, 1559–1567 (1987).
228. Park, H.-H., Zhang, X., Choi, Y.-J., Park, H.-H. & Hill, R. H. Synthesis of Ag Nanostructures by Photochemical Reduction Using Citrate-Capped Pt Seeds. *Journal of Nanomaterials* **2011**, (2010).
229. Kshirsagar, P., Sangaru, S. S., Brunetti, V., Malvindi, M. A. & Pompa, P. P. Synthesis of fluorescent metal nanoparticles in aqueous solution by photochemical reduction. *Nanotechnology* **25**, 045601 (2014).
230. Itakura, T., Torigoe, K. & Esumi, K. Preparation and Characterization of Ultrafine Metal Particles in Ethanol by UV Irradiation Using a Photoinitiator. *Langmuir* **11**, 4129–4134 (1995).
231. Maretti, L., Billone, P. S., Liu, Y. & Scaiano, J. C. Facile Photochemical Synthesis and Characterization of Highly Fluorescent Silver Nanoparticles. *J. Am. Chem. Soc.* **131**, 13972–13980 (2009).
232. Król-Gracz, A., Michalak, E., Nowak, P. M. & Dyonizy, A. Photo-induced chemical reduction of silver bromide to silver nanoparticles. *cent.eur.j.chem.* **9**, 982–989 (2011).

233. Magdassi, S., Grouchko, M. & Kamyshny, A. Copper Nanoparticles for Printed Electronics: Routes Towards Achieving Oxidation Stability. *Materials* **3**, 4626–4638 (2010).
234. Kobayashi, Y. *et al.* Synthesis of metallic copper nanoparticles coated with polypyrrole. *Colloid Polym Sci* **287**, 877–880 (2009).
235. Kim, H.-S., Dhage, S. R., Shim, D.-E. & Hahn, H. T. Intense pulsed light sintering of copper nanoink for printed electronics. *Appl. Phys. A* **97**, 791–798 (2009).
236. Huang, Z. *et al.* Highly Dispersed Silica-Supported Copper Nanoparticles Prepared by Precipitation–Gel Method: A Simple but Efficient and Stable Catalyst for Glycerol Hydrogenolysis. *Chem. Mater.* **20**, 5090–5099 (2008).
237. Cioffi, N. *et al.* Copper Nanoparticle/Polymer Composites with Antifungal and Bacteriostatic Properties. *Chem. Mater.* **17**, 5255–5262 (2005).
238. Huang, H. H. *et al.* Synthesis, Characterization, and Nonlinear Optical Properties of Copper Nanoparticles. *Langmuir* **13**, 172–175 (1997).
239. Wu, S.-H. & Chen, D.-H. Synthesis of high-concentration Cu nanoparticles in aqueous CTAB solutions. *Journal of Colloid and Interface Science* **273**, 165–169 (2004).
240. Mott, D., Galkowski, J., Wang, L., Luo, J. & Zhong, C.-J. Synthesis of Size-Controlled and Shaped Copper Nanoparticles. *Langmuir* **23**, 5740–5745 (2007).
241. Giuffrida, S., Costanzo, L. L., Ventimiglia, G. & Bongiorno, C. Photochemical synthesis of copper nanoparticles incorporated in poly(vinyl pyrrolidone). *J Nanopart Res* **10**, 1183–1192 (2008).

242. Brege, J. J., Hamilton, C. E., Crouse, C. A. & Barron, A. R. Ultrasmall copper nanoparticles from a hydrophobically immobilized surfactant template. *Nano Lett.* **9**, 2239–2242 (2009).
243. Park, B. K. *et al.* Synthesis and size control of monodisperse copper nanoparticles by polyol method. *Journal of Colloid and Interface Science* **311**, 417–424 (2007).
244. Qi, L., Ma, J. & Shen, J. Synthesis of Copper Nanoparticles in Nonionic Water-in-Oil Microemulsions. *Journal of Colloid and Interface Science* **186**, 498–500 (1997).
245. Raja, M. Production of copper nanoparticles by electrochemical process. *Powder Metall Met Ceram* **47**, 402–405 (2008).
246. Condorelli, G. G., Costanzo, L. L., Fragalà, I. L., Giuffrida, S. & Ventimiglia, G. A single photochemical route for the formation of both copper nanoparticles and patterned nanostructured films. *J. Mater. Chem.* **13**, 2409–2411 (2003).
247. Liz-Marzán, L. M., Giersig, M. & Mulvaney, P. Synthesis of Nanosized Gold–Silica Core–Shell Particles. *Langmuir* **12**, 4329–4335 (1996).
248. Marinakos, S. M., Shultz, D. A. & Feldheim, D. L. Gold Nanoparticles as Templates for the Synthesis of Hollow Nanometer-Sized Conductive Polymer Capsules. *Adv. Mater.* **11**, 34–37 (1999).
249. Vishwas V. Hardikar, E. M. Coating of Nanosize Silver Particles with Silica. *Journal of Colloid and Interface Science* 133–136 (2000).
doi:10.1006/jcis.1999.6579
250. Thearith Ung, L. M. L.-M. Controlled Method for Silica Coating of Silver Colloids. Influence of Coating on the Rate of Chemical Reactions. *Langmuir* **14**, (1998).

251. Kobayashi, Y., Correa-Duarte, M. A. & Liz-Marzán, L. M. Sol–Gel Processing of Silica-Coated Gold Nanoparticles. *Langmuir* **17**, 6375–6379 (2001).
252. Kobayashi, Y. & Sakuraba, T. Silica-coating of metallic copper nanoparticles in aqueous solution. *Colloids and Surfaces A: Physicochemical and Engineering Aspects* **317**, 756–759 (2008).
253. Ang, T. P., Wee, T. S. A. & Chin, W. S. Three-Dimensional Self-Assembled Monolayer (3D SAM) of n-Alkanethiols on Copper Nanoclusters. *J. Phys. Chem. B* **108**, 11001–11010 (2004).
254. Lisiecki, I., Billoudet, F. & Pileni, M. P. Control of the Shape and the Size of Copper Metallic Particles. *J. Phys. Chem.* **100**, 4160–4166 (1996).
255. Xiong, Y. *et al.* Poly(vinyl pyrrolidone): a dual functional reductant and stabilizer for the facile synthesis of noble metal nanoplates in aqueous solutions. *Langmuir* **22**, 8563–8570 (2006).
256. Jeong, S. *et al.* Controlling the Thickness of the Surface Oxide Layer on Cu Nanoparticles for the Fabrication of Conductive Structures by Ink-Jet Printing. *Adv. Funct. Mater.* **18**, 679–686 (2008).
257. Kapoor, S., Palit, D. K. & Mukherjee, T. Preparation, characterization and surface modification of Cu metal nanoparticles. *Chemical Physics Letters* **355**, 383–387 (2002).
258. De Lima, R., Seabra, A. B. & Durán, N. Silver nanoparticles: a brief review of cytotoxicity and genotoxicity of chemically and biogenically synthesized nanoparticles. *J Appl Toxicol* **32**, 867–879 (2012).
259. Reidy, B., Haase, A., Luch, A., Dawson, K. A. & Lynch, I. Mechanisms of Silver Nanoparticle Release, Transformation and Toxicity: A Critical Review of

- Current Knowledge and Recommendations for Future Studies and Applications. *Materials* **6**, 2295–2350 (2013).
260. in *Metal–Polymer Nanocomposites* (eds. Nicolais, L. & Carotenuto, G.) i–xiv (John Wiley & Sons, Inc., 2004). at <http://onlinelibrary.wiley.com/doi/10.1002/0471695432.fmatter/summary>
>
261. Balazs, A. C., Emrick, T. & Russell, T. P. Nanoparticle polymer composites: where two small worlds meet. *Science* **314**, 1107–1110 (2006).
262. Chapman, R. & Mulvaney, P. Electro-optical shifts in silver nanoparticle films. *Chemical Physics Letters* **349**, 358–362 (2001).
263. Karttunen, M., Ruuskanen, P., Pitkänen, V. & Albers, W. M. Electrically Conductive Metal Polymer Nanocomposites for Electronics Applications. *Journal of Elec Materi* **37**, 951–954 (2008).
264. Chiolerio, A. & Sangermano, M. In situ synthesis of Ag-acrylic nanocomposites: Tomography-based percolation model, irreversible photoinduced electromigration and reversible electromigration. *Materials Science and Engineering: B* **177**, 373–380 (2012).
265. Chiolerio, A., Vescovo, L. & Sangermano, M. Conductive UV-Cured Acrylic Inks for Resistor Fabrication: Models for their Electrical Properties. *Macromol. Chem. Phys.* **211**, 2008–2016 (2010).
266. Yağci, Y. & Reetz, I. Externally stimulated initiator systems for cationic polymerization. *Progress in Polymer Science* **23**, 1485–1538 (1998).

267. Sangermano, M., Pegel, S., Pötschke, P. & Voit, B. Antistatic Epoxy Coatings With Carbon Nanotubes Obtained by Cationic Photopolymerization. *Macromol. Rapid Commun.* **29**, 396–400 (2008).
268. Chiolerio, A. *et al.* Preparation of polymer-based composite with magnetic anisotropy by oriented carbon nanotube dispersion. *Diamond and Related Materials* **17**, 1590–1595 (2008).
269. Sangermano, M., Tagci, Y. & Rizza, G. In situ synthesis of silver-epoxy nanocomposites by photoinduced electron transfer and cationic polymerization processes. *MACROMOLECULES* **40**, 8827–8829 (2007).
270. Sangermano, M. *et al.* Polysulfone/Metal Nanocomposites by Simultaneous Photoinduced Crosslinking and Redox Reaction. *Macromolecular Materials and Engineering* **296**, 820–825 (2011).
271. Günes, S., Neugebauer, H. & Sariciftci, N. S. Conjugated polymer-based organic solar cells. *Chem. Rev.* **107**, 1324–1338 (2007).
272. McQuade, D. T., Pullen, A. E. & Swager, T. M. Conjugated polymer-based chemical sensors. *Chem. Rev.* **100**, 2537–2574 (2000).
273. Yagci, Y., Yilmaz, F., Kiralp, S. & Toppare, L. Photoinduced Polymerization of Thiophene Using Iodonium Salt. *Macromol. Chem. Phys.* **206**, 1178–1182 (2005).
274. Sangermano, M., Sordo, F., Chiolerio, A. & Yagci, Y. One-pot photoinduced synthesis of conductive polythiophene-epoxy network films. *Polymer* **54**, 2077–2080 (2013).
275. Kortaberria, G., Sangermano, M. & Mondragon, I. In Situ Synthetized Silver/Epoxy Nanocomposites: Electrical Characterization in Terms of

- Dielectric Relaxation Spectroscopy. *Macromolecular Symposia* **321-322**, 112–117 (2012).
276. Giuffrida, S. *et al.* Photochemical Mechanism of the Formation of Nanometer-Sized Copper by UV Irradiation of Ethanol Bis(2,4-pentandionato)copper(II) Solutions. *Chem. Mater.* **16**, 1260–1266 (2004).
277. Chitte, H. K. Synthesis and Characterization of Polymeric Composites Embedded with Silver Nanoparticles. *World Journal of Nano Science and Engineering* **02**, 19–24 (2012).
278. Chiolerio, A., Roppolo, I. & Sangermano, M. Radical diffusion engineering: tailored nanocomposite materials for piezoresistive inkjet printed strain measurement. *RSC Adv.* **3**, 3446–3452 (2013).
- 278-b “Pyrrole Polymerization with wood derivatives and compositeconducting films obtained thereof” Sasso C. Ph.DThesis, University of Grenoble (F), 12, 2010.)
279. Folarin, O. M., Sadiku, E. R. & Maity, A. Polymer-noble metal nanocomposites: Review. (2011). at
<<http://researchspace.csir.co.za/dspace/handle/10204/5625>>
280. Kerker, M., Wang, D. S. & Chew, H. Surface enhanced Raman scattering (SERS) by molecules adsorbed at spherical particles. *Appl Opt* **19**, 3373–3388 (1980).
281. Mallick, K., Witcomb, M. J. & Scurrall, M. S. In situ synthesis of copper nanoparticles and poly(o-toluidine): A metal–polymer composite material. *European Polymer Journal* **42**, 670–675 (2006).
282. B. T.MESHESHA, N. B. Polyol mediated synthesis & characterization of Cu nanoparticles: Effect of 1-hexadecylamine as stabilizing agent. (2009).

283. Chatterjee, A. K. *et al.* A simple robust method for synthesis of metallic copper nanoparticles of high antibacterial potency against *E. coli*. *Nanotechnology* **23**, 085103 (2012).
284. Datta, K. K. R., Kulkarni, C. & Eswaramoorthy, M. Aminoclay: a permselective matrix to stabilize copper nanoparticles. *Chem. Commun.* **46**, 616–618 (2010).
285. Sierra-*et al.* Synthesis of Copper Nanoparticles Coated with Nitrogen Ligands. *Journal of Nanomaterials* **2014**, e361791 (2014).
286. Dang, T. M. D., Le, T. T. T., Fribourg-Blanc, E. & Dang, M. C. The influence of solvents and surfactants on the preparation of copper nanoparticles by a chemical reduction method. *Adv. Nat. Sci: Nanosci. Nanotechnol.* **2**, 025004 (2011).
287. Pflaum, R. T. & Brandt, W. W. Metal-Amine Coördination Compounds. I. Copper(II) Complexes. *J. Am. Chem. Soc.* **76**, 6215–6219 (1954).
288. Meshesha, B. T., Barrabés, N., Medina, F. & Sueiras, J. E. Polyol Mediated Synthesis & Characterization of Cu Nanoparticles: Effect of 1-hexadecylamine As Stabilizing Agent. in *Proceedings of the 1st WSEAS International Conference on Nanotechnology* 87–91 (World Scientific and Engineering Academy and Society (WSEAS), 2009). at <http://dl.acm.org/citation.cfm?id=1561831.1561849>
289. Majid, K., Mushtaq, R. & Ahmad, S. Synthesis, Characterization and Coordinating Behaviour of Aminoalcohol Complexes with Transition Metals. *Journal of Chemistry* **5**, S969–S979 (2008).
290. Karadag, A., Yilmaz, V. T. & Thoene, C. Di- and triethanolamine complexes of Co(II), Ni(II), Cu(II) and Zn(II) with thiocyanate: synthesis, spectral and thermal

- studies. Crystal structure of dimeric Cu(II) complex with deprotonated diethanolamine, $[\text{Cu}_2(\mu\text{-dea})_2(\text{NCS})_2]$. *Polyhedron* **20**, 635–641 (2001).
291. Yin, M. *et al.* Copper Oxide Nanocrystals. *J. Am. Chem. Soc.* **127**, 9506–9511 (2005).
292. Pileni, M. P. Optical properties of nanosized particles dispersed in colloidal solutions or arranged in 2D or 3D superlattices. *New J. Chem.* **22**, 693–702 (1998).
293. Yanase, A. & Komiyama, H. In situ observation of oxidation and reduction of small supported copper particles using optical absorption and X-ray diffraction. *Surface Science* **248**, 11–19 (1991).
294. Tauran, Y., Brioude, A., Coleman, A. W., Rhimi, M. & Kim, B. Molecular recognition by gold, silver and copper nanoparticles. *World J Biol Chem* **4**, 35–63 (2013).
295. Dang, T. M. D., Le, T. T. T., Fribourg-Blanc, E. & Dang, M. C. Synthesis and optical properties of copper nanoparticles prepared by a chemical reduction method. *Adv. Nat. Sci: Nanosci. Nanotechnol.* **2**, 015009 (2011).
296. Lisiecki, I. & Pileni, M. P. Synthesis of copper metallic clusters using reverse micelles as microreactors. *J. Am. Chem. Soc.* **115**, 3887–3896 (1993).
297. Yu, W., Xie, H., Chen, L., Li, Y. & Zhang, C. Synthesis and Characterization of Monodispersed Copper Colloids in Polar Solvents. *Nanoscale Res Lett* **4**, 465–470 (2009).
298. Gloeckner, P. *Radiation Curing: Coatings and Printing Inks* ; *Technical Basics, Applications and Trouble Shooting.* (Vincentz Network GmbH & Co KG, 2008).

299. Pacioni, N. L., Pardoe, A., McGilvray, K. L., Chrétien, M. N. & Scaiano, J. C. Synthesis of copper nanoparticles mediated by photogenerated free radicals: catalytic role of chloride anions. *Photochem. Photobiol. Sci.* **9**, 766–774 (2010).
300. Halin, D. S. C., Talib, I. A., Daud, A. R. & Abd Hamid, M. A. Cuprous Oxide Thin Films for a Photoelectrochemical Cell of ITO/Cu< and graphite *Advanced Materials Research* **501**, 247–251 (2012).